The Impact of Microbial Interactions and Hydrogen Peroxide on Western Lake Erie Cyanobacterial Blooms

by

Derek J. Smith

A dissertation submitted in partial fulfillment
of the requirements for the degree of
Doctor of Philosophy
(Earth and Environmental Sciences)
in the University of Michigan
2021

Doctoral Committee:

Associate Professor Timothy W. Davis, Co-Chair
Professor Gregory J. Dick, Co-Chair
Associate Professor Rose M. Cory
Professor Ursula Jakob
Professor George W. Kling

Derek J. Smith

smitdere@umich.edu

ORCID iD: 0000-0002-0895-5712

Dedication

To my family, who supported and encouraged me, especially Chris, who I often relied on to vent about my frustrations. To my friends in Toledo, who were probably more excited about my "impending doctorate" than I was. To Sarah, who was an early source of support, even though things didn't work out. And to Erin, who kept me grounded, helped put my lack of self-confidence into perspective, and listened when I was at my lowest.

Acknowledgements

The work presented in this dissertation was a large, collaborative effort, and it would have been impossible to complete this work without the help of many other people. I thank my advisors, Greg Dick and Tim Davis, who guided me through the many issues and headaches that occurred throughout my graduate career and encouraged me to press forward during my low points. I thank my other committee members Rose Cory, George Kling, and Ursula Jakob for providing feedback and being invested in improving my research and writing, and Vincent Denef, Melissa Duhaime, and the rest of the D^3 and geomicrobiology groups for providing honest feedback and support. In particular, Sunit Jain and Robert Hein provided bioinformatic and computational support and McKenzie Powers, Colleen Yancey, Will James, Claire Zwiers, and Katie Polik have provided field and lab support. Jason Dobkowski and Lija Treibergs also provided valuable lab support. Nina Lin and James Tan designed the high-throughput colony sampling procedure for sampling *Microcystis* colonies. Jenan Kharbush advised me on metabolite extraction and ran LC-MS analyses, and Roland Kersten provided lab space and LC-MS time.

This work would not have been possible without invitations to participate in NOAA GLERL and Environment and Climate Change Canada harmful algal bloom monitoring programs to collect samples, and the Cooperative Institute for Great Lakes Research (CIGLR) for helping with nutrient and chlorophyll *a* sample analysis. In particular, Steve Ruberg, Dack Stuart, Kent Baker, Kevin Meyer, Duane Gossiaux, and Paul Den Uyl for field work support, and Christine Kitchens, Ashley Burtner, Dana Palladino, and Tom Johengen for nutrient and

chlorophyll *a* analysis, and Arthur Zastepa for inviting me to participate in Environment Canada cruises. Tom Johengen and Dave Fanslow generously provided materials for incubating bottles during experimental work. I thank Tom Bridgeman for supporting this work by allocating space for bottle experiments and allowing use of the University of Toledo Lake Erie Center resources for additional sample collection. The help of other staff and students at the Lake Erie Center were also essential for this work; I particularly thank Brenda Snyder, Rachel Lohner, and Pam Struffolino for helping orient me in the Lake Erie Center labs and being willing to answer questions, Chris Mayer for providing an aquaculture tank, and Alex Lytten for operating research vessels, going on extra sampling trips and offering personal dock space specifically for this work. I additionally thank Frank Schemenaur from BGSU for aiding in sampling collection.

Finally, thanks to Jason Dobkowski, Adrianna Trusiak, Kevin Meyer, Sharon Grim, Dack Stuart, and Jenny Bowen for the hikes, movie and game nights, odes to haggises, and their friendship.

Table of Contents

Dedication ..... **ii**

Acknowledgements ..... **iii**

List of Tables ..... **ix**

List of Figures ..... **xii**

List of Appendices ..... **xx**

Abstract ..... **xxi**

Chapter 1 Introduction **1**

1.1 Causes and Impacts of Cyanobacterial Blooms 3

1.2 The Issue of Variable Microcystin Production Among *Microcystis* Strains and the Ecological and Physiological Role of Microcystin Production 5

1.3 Reactive Oxygen Species and Their Impacts on Microbial Growth and Population Dynamics 9

1.4 Microbial Interactions Determine Responses to Hydrogen Peroxide 12

1.5 The *Microcystis* Phycosphere 13

1.6 Dissertation Outline and Research Questions 16

1.7 References 17

Chapter 2 Heterotrophic Bacteria Dominate Catalase Expression During *Microcystis* Blooms **30**

2.1 Abstract 30

2.2 Introduction 31

2.3 Results 34

2.3.1 Dynamics in Pigments, Microcystin Concentrations, Toxic Microcystis Abundance, and H_2O_2 34

2.3.2 Catalase and Peroxidase Gene Abundance and Taxonomy 36

2.3.3 Catalase and Peroxidase Transcript Abundance 40

2.3.4 Axenic Culturing Experiments 42

2.4 Discussion 43

2.4.1 Microcystin Production Does not Determine the Response of a Microcystis Strain to an Exogenous H_2O_2 Scavenger 43

2.4.2 The Ability of Microcystis to Degrade H_2O_2 Does not Preclude Benefit From an Exogenous H_2O_2 Scavenger 47

2.4.3 The Relative Contribution of Attached Bacteria to H_2O_2 Decomposition in Phytoplankton Assemblages....49
2.5 Conclusions....50
2.6 Methods....51
2.6.1 Field Sampling and Water Chemistry....51
2.6.2 DNA and RNA Extraction and Sequencing....53
2.6.3 qPCR and Toxic:nontoxic Microcystis Ratio....54
2.6.4 Metagenomic Assembly....55
2.6.5 Read Mapping, Contig Binning, and MAG Quality Assessment....57
2.6.6 Gene Annotations and Abundance....59
2.6.7 Culturing Experiments....61
2.6.8 Scripts and Data Availability....63
2.7 Figures and Tables....64
2.8 References....91
Chapter 3 Individual *Microcystis* Colonies Harbor Distinct Bacterial Communities That Differ by *Microcystis* Oligotype and With Time....100
3.1 Abstract....100
3.2 Introduction....101
3.3 Methods....104
3.3.1 Field Sampling....104
3.3.2 Individual Colony Isolation via Droplet Encapsulation....104
3.3.3 DNA Extraction and Sequencing....106
3.3.4 Bioinformatic and Statistical Analyses....108
3.4 Results and Discussion....110
3.4.1 Microcystis Colony Oligotype Assignment....110
3.4.2 Microcystis Phycosphere Community Diversity....111
3.4.3 Microcystis Phycosphere Communities are Dissimilar From Bulk Community Samples....112
3.4.4 The Microcystis Phycosphere Lacks a Core Community....114
3.4.5 Microcystis Phycosphere Communities Vary With Time and Microcystis Oligotype....115
3.4.6 Potential Mechanisms to Explain Clustering by Microcystis Oligotype....118
3.4.7 Potential Mechanisms to Explain Clustering by Sampling Date....120
3.4.8 Interactions Between Cyanobacteria in the Phycosphere....122
3.5 Conclusions....124
3.6 Figures and Tables....125
3.7 References....148
Chapter 4 Metagenomic and Metatranscriptomic Evidence for Uptake of Phytoplankton-Derived Carbon by Novel Acidobacteria Genera in *Microcystis* Blooms....157
4.1 Abstract....157

4.2 Introduction 158
4.3 Methods 160
4.3.1 Genome Assembly and Gene Annotation 160
4.3.2 16S rRNA Phylogenetic Analysis 162
4.3.3 Amplicon Dataset Mining 162
4.3.4 Identification of Pseudocobalamin in Microcystis Cultures 163
4.4 Results and Discussion 165
4.4.1 The MAGs From Western Lake Erie are Novel Species of Subdivision 3 Acidobacteria 165
4.4.2 Evidence for Expression of Genes Involved in Biofilm Adhesion and Respiration of Exopolysaccharides and Phytoplankton Exudates 166
4.4.3 Evidence for Uptake of Low Molecular Weight Organics in Phytoplankton Exudates 168
4.4.4 Evidence for Regeneration of Nitrogen From Peptides and Amino Acids 170
4.4.5 Evidence for Vitamin B_{12} Auxotrophy and Uptake 171
4.4.6 Presence and Relative Abundance in Amplicon Datasets 174
4.5 Conclusions 176
4.6 Figures and Tables 177
4.7 References 192
Chapter 5 Characterization of Biological H_2O_2 Production and Decay During Lake Erie Cyanobacterial Blooms 201
5.1 Abstract 201
5.2 Introduction 202
5.3 Methods 206
5.3.1 Field Sampling 206
5.3.2 H_2O_2 Bottle Experiments and H_2O_2 Measurements 207
5.3.3 Calculations of Experimental Light Conditions and In Situ Profiling 210
5.3.4 Chlorophyll a, CDOM, DIC, Nutrient, Respiration, and Primary Production Measurements 212
5.3.5 DNA Extraction, Sequencing, and Bioinformatics Analysis 214
5.3.6 Statistical Analyses 216
5.4 Results 217
5.4.1 H_2O_2 Concentrations, Net H_2O_2 Production, and Modeled Gross H_2O_2 Production 217
5.4.2 Failed Model Assumptions and Uncertainty in Gross H_2O_2 Production Rates 219
5.4.3 Correlations Between H_2O_2 Production and Chemical and Biological Parameters 220
5.4.4 Correlations Between H_2O_2 Production and Microbial Community Dissimilarity and OTU Abundances 221
5.5 Discussion 222
5.5.1 Biological Production was a Major Source of H_2O_2 During the Experiments 222
5.5.2 Biological H_2O_2 Production is Light-Dependent but not Directly Attributed to Large Phytoplankton and Microcystis Colonies 225
5.5.3 H_2O_2 Production is Related to Microbial Community Composition 228

5.5.4 Absolute Decay Rate Constants are Correlated With Gross H_2O_2 Production 230
5.6 Conclusions 231
5.7 Figures and Tables.....233
5.8 References 254
Chapter 6 Conclusions 264
6.1 Overview and Summary.....264
6.2 Variable *katG* Distribution Across *Microcystis* Strains and its Importance for H_2O_2 Resistance.....267
6.3 Increased H_2O_2 Concentrations do not Favor Microcystin-Producing *Microcystis* Strains *per se* 270
6.4 The Impact of Community Wide H_2O_2 Decomposition on the Composition of *Microcystis* Strains During Blooms 271
6.5 *Microcystis* Phycosphere Bacterial Communities are Distinct From Bacterial Communities in Bulk Whole Water and Phytoplankton Seston.....273
6.6 *Microcystis* Phycosphere Community Composition Varies With Sampling Date and *Microcystis* Oligotype 273
6.7 Genomic Analysis Highlights Potential Peptide, Amino Acid, and Vitamin Exchange Within the *Microcystis* Phycosphere.....275
6.8 Biotic H_2O_2 Production can be an Important Source of H_2O_2 During *Microcystis* Blooms 276
6.9 Biotic H_2O_2 Production in Western Lake Erie is Related to Photosynthesis but not Attributed to Large Phytoplankton Assemblages and *Microcystis* Colonies.....277
6.10 Phytoplankton Assemblages do not Impact Whole Water H_2O_2 Decomposition Rates .278
6.11 H_2O_2 Production Rates are Correlated With Microbial Community Composition and OTU Abundances.....279
6.12 Future Directions.....280
6.13 References 282
Appendices 289

List of Tables

Table 2.1: *Microcystis* 16S rRNA and *mcyD* gene copy numbers and percentage of *Microcystis* population with the potential to produce the toxin microcystin as determined by qPCR analysis. 83

Table 2.2: Coordinates of 16S rRNA genes in closed *Microcystis* genomes available in the NCBI genome database. 84

Table 2.3: Taxonomy of MAGs containing genes encoding the catalase and peroxidase genes of interest. 85

Table 2.4: Modified BG-11 recipe used in backwash solution for collecting biomass retentate on 100 μm filter mesh. 89

Table 2.5: A list of primers (Integrated DNA Technologies, IA, USA) and probes (Applied Biosystems, Foster City, CA, USA) used in the qPCR analysis. 90

Table 3.1: The number and position of nucleotide variations between 16S rRNA gene copies found within each closed *Microcystis* genome. 145

Table 3.2: OTUs identified as significant diagnostic OTUs for either sampling date or oligotype along with their Indval g statistics. 145

Table 3.3: Maximum and mean percent abundance for each OTU with observation frequency between 50 and 18% or lower than 18% with maximum abundance higher than 5%. 146

Table 3.4: Maximum and mean percent abundance of each frequent OTU (observation frequency greater than 50%). 147

Table 3.5: Mantel test results. 147

Table 4.1: Description of public datasets mined for Acidobacteria 16S rRNA sequences in this study. 190

Table 4.2: Quality information for Acidobacteria MAGs from western Lake Erie cyanobacterial blooms. 191

Table 4.3: Expression of B_{12} dependent genes in Acidobacteria CoA2 C42 MAG. 192

Table 5.1: Comparison of total gross H_2O_2 production and net H_2O_2 production in experiments where gross H_2O_2 production rates could be calculated.. 250

Table 5.2: Bootstrap support and p-values of chemical and biological variables (rows) in stepwise linear regression models generated with ordination of microbial community dissimilarities on PCoA axes (columns).....251

Table 5.3: Bootstrap support and p-values of variables in stepwise linear regression models generated with stepAIC of chemical and biological parameters (rows) vs ordination of microbial community dissimilarities on PCoA axes (columns). 251

Table 5.4: Comparison of R^2 values and mean absolute errors (MAE) in models for predicting gross biotic and net H_2O_2 production rates.....252

Table 5.5: OTUs in the random forest model for gross biotic H_2O_2 production with importance lower bounds above 0.01. 253

Table 5.6: OTUs in the random forest model for net H_2O_2 production with importance lower bounds above 0.01. 254

Appendix Table 1: Blastn Results of Acidobacteria Hypothetical Protein Sequences Against NCBI nr Database.....290

Appendix Table 2: Total Gross H_2O_2 Production, Absolute Decay Constants, Maximum H_2O_2 Concentrations, and Model Fit in H_2O_2 Production and Decay Experiments 291

Appendix Table 3: Time Point When $[H_2O_2]_{spike} \approx [H_2O_2]_{unamended}$ in Light-Exposed H_2O_2 Production and Decay Experiments 296

Appendix Table 4: Correlation and Regression Statistics Between Gross Biotic H_2O_2 Production in Dark Bottles and Measured Biological and Chemical Parameters. 298

Appendix Table 5: Welch's T-Test Results Testing the Hypothesis That the Mean Abundance of Important OTUs in Random Forest Models in Whole Water and 105 µm Filtered Water are Significantly Different. 299

Appendix Table 6: Estimates of Biotic O_2^- Production in Western Lake Erie From Literature Values 302

List of Figures

Figure 2.1: Temporal dynamics in algal pigments, toxic:nontoxic *Microcystis*, hydrogen peroxide, and catalase and peroxidase gene abundance in the 2014 western Lake Erie cyanobacterial bloom.....65

Figure 2.2: Temporal and spatial variation in the relative abundance of transcripts encoding catalases and peroxidases (excluding *ahpC*) in Lake Erie metatranscriptomes from the 100 μm particle size fraction collected during the 2014 western Lake Erie cyanobacterial bloom. 65

Figure 2.3: Relative abundance and taxonomic composition of *ahpC* transcripts from the 2014 western Lake Erie cyanobacterial bloom.....66

Figure 2.4: Taxonomic composition of *katG* transcripts from the 2014 western Lake Erie cyanobacterial bloom.....68

Figure 2.5: Impact of sodium pyruvate on maximum growth rates of *Microcystis* strains.....68

Figure 2.6: H_2O_2 concentrations in axenic *Microcystis* cultures.....70

Figure 2.7: Conceptual diagram of H_2O_2 production, concentrations, and decomposition by the microbial community influencing *Microcystis* population structure.....70

Figure S 2.1: Sampling sites in western Lake Erie.....71

Figure S 2.2: Comparison of normalization strategy for determining the percentage of toxic *Microcystis* strains in metagenomic reads. 72

Figure S 2.3: Temporal and spatial variation in the relative abundance of catalase and peroxidase genes in Lake Erie metagenomes from the total community size fraction.. 73

Figure S 2.4: Spatial and temporal variation in the relative abundance of *ccpA* and *mauG* homologs in metagenomes (A) and metatranscriptomes (B). 74

Figure S 2.5: Taxonomic composition of *katG* in >100 μm particle attached fraction and total community metagenomes from the 2014 western Lake Erie cyanobacterial bloom. 75

Figure S 2.6: Temporal and spatial variation in the fraction of *Microcystis* cells with *katG*, estimated by normalizing *Microcystis katG* read counts to counts of the single-copy housekeeping genes *rpoB* and *recA* from *Microcystis*. 76

Figure S 2.7: Temporal and spatial variation in *Microcystis katG* relative transcript abundance 77

Figure S 2.8: Taxonomic composition of *ahpC* in >100 μm particle attached fraction and total community metagenomes from the 2014 western Lake Erie cyanobacterial bloom. 78

Figure S 2.9: Distribution of catalase and peroxidase genes of interest among publicly available genomes of targeted cyanobacteria 79

Figure S 2.10: Growth curves of seven axenic *Microcystis* strains cultured with and without 1 mM sodium pyruvate supplemented to the growth medium. 80

Figure S 2.11: Decay of 500 nM H_2O_2 standard in the filtrates of *Microcystis* cultures supplemented with1 mM sodium pyruvate. 81

Figure S 2.12: Relative expression of *katG* (top) and *ahpC* (bottom) using read counts normalized by total library size. 82

Figure 3.1: Description of individual *Microcystis* colony sampling via droplet encapsulation. 125

Figure 3.2: Example black and white micrographs of *Microcystis* colonies in bulk phytoplankton seston collected from western Lake Erie blooms. 126

Figure 3.3: Maximum and mean relative abundance of all non-*Microcystis* OTUs identified in the *Microcystis* phycosphere plotted against their observation frequency 127

Figure 3.4: NMDS ordination and hierarchical clustering of bacterial communities in the *Microcystis* phycosphere, 100 µm retentate, whole water communities from western Lake Erie. 128

Figure 3.5: Changes in the relative abundance of OTUs that are frequently present or indicators of date and *Microcystis* oligotype in *Microcystis* phycosphere communities. 129

Figure 3.6: NMDS ordination of bacterial communities in the *Microcystis* phycosphere. 130

Figure 3.7: Hierarchical clustering of bacterial communities in the *Microcystis* phycosphere. 131

Figure S 3.1: Sampling sites in western Lake Erie. 132

Figure S 3.2: Weekly changes in bloom pigments and microcystin concentrations over time at the sites sampled. 133

Figure S 3.3: The relative proportions of each *Microcystis* MED node identified in *Microcystis* colonies. 134

Figure S 3.4: Distribution of observed richness, estimated richness, and Shannon diversity index of *Microcystis* colony phycosphere communities (A), whole water field samples (B), and 105 µm filtered field samples (C). 136

Figure S 3.5: Temporal change of alpha diversity metrics. 136

Figure S 3.6: Mean alpha diversity metrics of phycosphere communities associated with different *Microcystis* oligotypes. 137

Figure S 3.7: Linear regression between Shannon Index (A) and Chao1 estimated species richness (B) and colony area. 138

Figure S 3.8: NMDS ordination of whole water bacterial communities in western Lake Erie over four years colored by month. 139

Figure S 3.9: NMDS ordination of whole water bacterial communities in western Lake Erie over four years colored by the natural log of chlorophyll *a* concentration. 140

Figure S 3.10: Dendogram of Bray-Curtis dissimilarity in bacterial communities in the *Microcystis* phycosphere, 100 µm retentate, whole water communities from Lake Erie. 141

Figure S 3.11: Absolute abundances of *Microcystis* MED nodes in whole water communities collected in 2019.....142

Figure S 3.12: Correlation in Bray-Curtis dissimilarity between *Microcystis* phycosphere communities and Euclidean distance in CDOM absorbance (A), total PAR in top 0.5 m (B), temperature (C), and nitrate concentration (D) at the time of colony collection.....143

Figure S 3.13: Representative colony droplet micrographs.. 144

Figure 4.1: Taxonomic assignment of novel Acidobacteria MAGs based on 16S rRNA phylogeny and whole genome alignments (gANI).....177

Figure 4.2: Relative abundance of low molecular weight organic carbon transporters and enzymes related to their metabolism by Bryobacter CoA8 C33 (blue) and Acidobacterium CoA2 C42 (red) associated with phytoplankton seston in the August 4th metatranscriptome from nearshore western Lake Erie station WE12.....178

Figure 4.3: Relative abundance of transcripts from Bryobacter CoA8 C33 genes involved in cobalamin transport (A), cobalamin remodeling (B), and cobalamin-dependent genes and their independent counterparts (C) in the August 4th metatranscriptome from western Lake Erie nearshore station WE12.....179

Figure 4.4: MS2 spectra of pseudocobalamin forms in *Microcystis* cultures and *Spirulina* powder, which served as a positive control.....181

Figure 4.5: Percent abundance of *Bryobacter* and Acidobacterium CoA2 C42 as a function of *Microcystis* percent abundance in whole water microbial community rRNA amplicon datasets from freshwaters. 181

Figure 4.6: Percent abundance of *Bryobacter* and Acidobacterium CoA2 C42 OTUs in size fractionated samples from a western Lake Erie time series collected in the summer-fall of 2014. 182

Figure 4.7: Percent abundance of Acidobacteria of interest and major Cyanobacteria taxa, *Anabaena / Dolichospermum* and *Microcystis* in size fractionated samples from a time series of Lake Taihu cyanobacterial blooms. 183

Figure S 4.1: Histogram of shared amino acid identity between protein coding genes in Acidobacteria MAGs and NCBI non-redundant database. 183

Figure S 4.2: Total number of metatranscriptomic reads mapped to each Acidobacterium MAG. 184

Figure S 4.3: Ranked relative abundance plot of top 50 most abundant genes from the Acidobacterium CoA2 C42 MAG in the 2014 western Lake Erie metatranscriptome collected from > 100 µm size fraction during August phycocyanin peaks (nearshore station WE12, August 4th). 185

Figure S 4.4: Ranked relative abundance plot of top 50 most abundant genes from the *Bryobacter* CoA8 C33 MAG in the 2014 western Lake Erie metatranscriptome collected from > 100 µm size fraction during August phycocyanin peaks (nearshore station WE12, August 4th). 186

Figure S 4.5: Putative central carbon metabolism and sugar degradation pathways in *Bryobacter* CoA8 C33 and Acidobacterium CoA2 C42. 187

Figure S 4.6: Ranked relative abundance plot of top 50 most abundant genes encoding transporters from the Acidobacterium CoA2 C42 MAG in the 2014 western Lake Erie metatranscriptome collected from > 100 μm size fraction during August phycocyanin peaks (nearshore station WE12, August 4th). 188

Figure S 4.7: Ranked relative abundance plot of top 50 most abundant genes encoding transporters from the *Bryobacter* CoA8 C33 MAG in the 2014 western Lake Erie metatranscriptome collected from > 100 μm size fraction during August phycocyanin peaks (nearshore station WE12, August 4th). 189

Figure S 4.8: Percent abundance of Acidobacterium CoA2 C42 in free-living microbial communities in the Great Lakes. 190

Figure 5.1: Net H_2O_2 production and decay rates in whole (blue) and 0.22 μm filtered water (red) exposed to light. 233

Figure 5.2: H_2O_2 production in whole water incubated in light (blue) and dark (red) bottles. 234

Figure 5.3: H_2O_2 production in whole (blue) and 105 μm filtered (red) water. 235

Figure 5.4: Linear regressions with net H_2O_2 production and net H_2O_2 decay rates (A) and with absolute decay constants and total gross H_2O_2 production (B). 235

Figure 5.5: Significant differences in chlorophyll *a*, $H_2CO_3^*$, CDOM concentrations, pH, and day integrated UVA were detected between experiments on dates where the model did and did not fit the data. 236

Figure 5.6: Linear regressions of gross biotic H_2O_2 production rates and chlorophyll *a* concentration, respiration rate, primary production rates, and CDOM absorbance. 237

Figure 5.7: Linear regressions of net H_2O_2 production rates and chlorophyll *a* concentration, respiration rate, primary production rate, CDOM absorbance, and DOC concentration. 238

Figure 5.8: Reductions in *Microcystis* abundance and chlorophyll *a* concentration in 105 µm filtered water compared to whole water. 238

Figure 5.9: Linear regression of gross biotic H_2O_2 production rate and abundance of important OTUs in random forest models. 239

Figure 5.10: The 12 OTUs with the highest negative correlation with net H_2O_2 production rate according to a Spearman's rank-order correlation. 240

Figure S 5.1: Sites of water collection in western Lake Erie. 241

Figure S 5.2: Light attenuation in Lake Erie water column and bottle experiments. 242

Figure S 5.3: Histogram of the time of maximum H_2O_2 in unamended whole water bottles. 243

Figure S 5.4: Measured and modeled H_2O_2 concentrations from experiments with poor fit on 22-Aug-2017 with whole water. 243

Figure S 5.5: Measured and modeled H_2O_2 concentrations from experiments with poor fit on 30-Aug-2017 with whole water. 244

Figure S 5.6: Measured and modeled H_2O_2 concentrations from experiments with poor fit on 23-Jul-2019 with whole water. 244

Figure S 5.7: Measured and modeled H_2O_2 concentrations from experiments with poor fit on 6-Aug-2019 with whole water. 245

Figure S 5.8: Measured and modeled H_2O_2 concentrations from experiments with poor fit on 6-Aug-2019 with 105 µm filtered water. 245

Figure S 5.9: Measured and modeled H_2O_2 concentrations from experiments with poor fit on 24-Aug-2019 with whole water. 246

Figure S 5.10: Measured and modeled H_2O_2 concentrations from experiments with poor fit on 24-Aug-2019 with 105 µm filtered water. 246

Figure S 5.11: Correlation with model error sum of squares and chlorophyll *a* concentrations and primary production rates. 247

Figure S 5.12: Significant correlations between net H_2O_2 production, total phosphorus (P), total dissolved phosphorus (TDP), soluble reactive phosphorus (SRP), and nitrate (NO_3) concentrations in bottle experiments. 248

Figure S 5.13: Correlations between the difference in whole water gross biotic H_2O_2 production rate in the light and dark and respiration rates, primary production rates, and CDOM absorbance. 249

Figure S 5.14: Correlations between *Microcystis* abundance and gross biotic H_2O_2 production rates (A) and net H_2O_2 production rates (B). 249

List of Appendices

Appendix 1 Blastn Results of Acidobacteria Hypothetical Protein Sequences Against NCBI nr 290

Appendix 2 Total Gross H_2O_2 Production, Absolute Decay Constants, Maximum H_2O_2 Concentrations, and Model Fit in H_2O_2 Production and Decay Experiments 291

Appendix 3 Time Point When $[H_2O_2]_{spike} \approx [H_2O_2]_{unamended}$ in Light-Exposed H_2O_2 Production and Decay Experiments 296

Appendix 4 Correlation and Regression Statistics Between Gross Biotic H_2O_2 Production in Dark Bottles and Measured Biological and Chemical Parameters. 298

Appendix 5 Welch's T-Test Results Testing the Hypothesis That the Mean Abundance of Important OTUs in Random Forest Models in Whole Water and 105 µm Filtered Water are Significantly Different. 299

Appendix 6 Estimates of Biotic O_2^- Production in Western Lake Erie From Literature Values 302

Abstract

Cyanobacterial harmful algal blooms (CHABs) are threats to freshwaters globally. Some strains of the harmful cyanobacterium, *Microcystis*, produce microcystins, toxins that sicken animals and people. The proportions of microcystin-producing (toxic) and non-microcystin-producing (nontoxic) strains of *Microcystis* are an important determinant of bloom microcystin concentrations. Microcystins may protect cyanobacteria from hydrogen peroxide (H_2O_2), which is ubiquitous in surface waters and can stress microbes. Therefore, H_2O_2 concentrations may impact the proportions of toxic and nontoxic *Microcystis* during blooms by favoring toxic strains, but the current literature conflicts in supporting this hypothesis.

Sources and sinks of H_2O_2 during CHABs are not well characterized. Some microorganisms produce enzymes to decompose H_2O_2, and microbial decomposition is the dominant sink for H_2O_2 in surface waters. However, H_2O_2 decomposition varies across microbial taxa. Some microbes lack enzymes for H_2O_2 decomposition and rely on other community members for H_2O_2 decomposition. In addition, microbial production is an important source of H_2O_2 in surface waters and may be greater than known chemical sources of H_2O_2. Thus, impacts from H_2O_2 depend on community wide H_2O_2 production. Microorganisms likely affect *Microcystis* growth, as CHABs contain diverse communities of microbes, some of which physically attach to *Microcystis* colonies. However, which organisms degrade and produce H_2O_2 during CHABs and the microbial communities that specifically associate with *Microcystis* are unknown.

To address the above knowledge gaps, a combination of cultivation experiments, field incubations, and cultivation-independent approaches were used. *Microcystis* strains were cultured with an exogenous H_2O_2 scavenger to investigate how H_2O_2 impacts *Microcystis* growth. Several toxic and nontoxic strains were unaffected, but one toxic strain had improved growth rates with the H_2O_2 scavenger, which suggests that microcystin production alone does not determine the impact of H_2O_2 exposure on *Microcystis* strains. The microbes that contain and express genes for H_2O_2 decomposition during western Lake Erie CHABs were identified using multi-omics approaches. Key genes for H_2O_2 decomposition were absent in many *Microcystis* strains, and the expression of these genes in phytoplankton seston was dominated by particle-attached bacteria, implicating the bacteria as major H_2O_2 sinks. These results suggest that bacterial decomposition of H_2O_2 affects growth rates of some *Microcystis* strains.

To characterize the importance of colony-attached bacteria for H_2O_2 dynamics in CHABs, H_2O_2 production and decay rates in western Lake Erie were measured with and without filtering out all microbes or phytoplankton aggregates >105 μm diameter. Biotic H_2O_2 production was the dominant source of H_2O_2 on average and was related to photosynthesis and microbial community composition. H_2O_2 production and decay were not affected by *Microcystis* colonies, implicating other free-living microbes as main sources and sinks. Colony-attached bacteria may protect *Microcystis* when H_2O_2 production outpaces decay in free-living communities.

Bacterial communities associated with *Microcystis* were characterized with 16S rRNA amplicon sequencing of individual colonies. *Microcystis* microbiomes lacked universal members, yet colonies with shared *Microcystis* oligotype and sampling date had more similar microbiomes. Therefore, H_2O_2 decomposition may vary across strains and colonies over time.

Genomes of bacteria identified as key catalase producers were further analyzed to investigate potential metabolic interactions with phytoplankton. Evidence for uptake of vitamins, peptides, and algal exudates suggests that the bacteria use organic nitrogen and carbon in phytoplankton exudates for growth. Furthermore, use of oligopeptide exudates may be associated with efflux and deamination of amino acids by the bacteria, which perhaps regenerates nitrogen for phytoplankton growth.

Chapter 1 Introduction

Harmful cyanobacterial blooms are a growing threat to freshwater ecosystems globally (Huisman *et al.*, 2018). One of the most cosmopolitan bloom-forming cyanobacteria is *Microcystis* (Harke *et al.*, 2016), some of which can produce microcystins, a class of potent liver toxins that can lead to illness and water shortages when they contaminate drinking water (Roegner *et al.*, 2014; Steffen *et al.*, 2017). However, microcystin production varies widely between bloom-forming cyanobacteria strains, as some strains and species lack the ability to produce microcystins (Meiβner *et al.*, 1996; Christiansen *et al.*, 2008), and the relative proportion of toxic and nontoxic cyanobacteria is an important determinant of microcystin concentrations in blooms (Kardinaal *et al.*, 2007; Briand *et al.*, 2009; Davis *et al.*, 2009). While the cause of cyanobacteria bloom formation is linked to anthropogenic eutrophication and climate change (Carpenter *et al.*, 1998; Paerl & Huisman, 2009; Huisman *et al.*, 2018), the ecological factors that favor toxic over nontoxic cyanobacteria are unknown. Because microcystins are thought to protect cyanobacteria from stress caused by hydrogen peroxide (H_2O_2), increasing concentrations of H_2O_2 during cyanobacteria blooms have been hypothesized to favor toxic strains over nontoxic strains (Paerl & Otten, 2013).

Hydrogen peroxide (H_2O_2) is a ubiquitous stressor in aquatic ecosystems (Zinser, 2018b), where it can rapidly oxidize and damage cell structures when H_2O_2 accumulates inside cell membranes (Imlay, 2003; Imlay, 2019). Because of its harmful impacts on microbial growth, microbes produce enzymes to degrade and detoxify H_2O_2 (Mishra & Imlay, 2012), but these enzymes are not universally distributed across microbial taxa (Passardi *et al.*, 2007; Morris *et al.*,

2008; Kim *et al.*, 2019a). However, because H_2O_2 rapidly diffuses across cell membranes (Seaver & Imlay, 2001), decomposition of H_2O_2 by one microbe reduces environmental H_2O_2 concentrations for the surrounding community members (Morris *et al.*, 2011; Morris *et al.*, 2012). Thus, H_2O_2 detoxification is underpinned by interactions between microorganisms. Because *Microcystis* grows in colonies containing other non-cyanobacteria (Worm & Søndergaard, 1998; Parveen *et al.*, 2013), interactions between these bacteria and *Microcystis* may have important implications in bloom development and *Microcystis* physiology. For example, interactions with bacteria can influence growth and toxin production in phytoplankton (Morris *et al.*, 2011; Amin *et al.*, 2015; Durham *et al.*, 2017; Jackrel *et al.*, 2020), however the nature of the interactions between *Microcystis* and its associated bacteria is relatively understudied.

The research presented in this dissertation focuses on the role of microbial interactions and hydrogen peroxide in western Lake Erie *Microcystis* blooms. Specifically, this work aims to answer the following major knowledge gaps: How does H_2O_2 impact the growth of different *Microcystis* strains, and how does H_2O_2 decomposition by associated bacteria impact *Microcystis* strains? What is the taxonomic composition of the microbial communities associated with *Microcystis*, and does the community composition change across multiple *Microcystis* colonies? Third, what is the biological contribution to H_2O_2 production during blooms, and how does H_2O_2 production relate to bacterial community composition and *Microcystis* growth during blooms? In the remainder of the introduction, background information is provided to better put these major knowledge gaps into perspective. Specifically, information on the causes and impacts of cyanobacteria blooms, the issue of variable microcystin-production by *Microcystis* strains and the hypothesized role of microcystin production in the cell, the importance of H_2O_2 in aquatic

environments and microbial communities, how microbial interactions determine responses to H_2O_2 and impact phytoplankton fitness generally.

1.1 Causes and Impacts of Cyanobacterial Blooms

Cyanobacteria are an ancient group of oxygen-producing photosynthetic bacteria that have important effects on the global environment. As the first oxygen-producing organisms, cyanobacteria were responsible for the oxygenation of Earth's atmosphere (Knoll, 2003). Oxygenic photosynthesis was transferred to plants and algae through multiple endosymbioses of cyanobacteria (Delwiche *et al.*, 1995; Delwiche, 1999). Cyanobacteria play important roles in the modern global carbon (Campbell *et al.*, 1994; Liu *et al.*, 1997) and nitrogen cycles (Capone *et al.*, 1997; Ohlendieck *et al.*, 2000). However, some cyanobacterial species can cause cyanobacterial harmful algal blooms (CHABs), which often cause discoloration of the water due to the proliferation of cyanobacterial biomass, that threaten ecosystem and human health (Huisman *et al.*, 2018).

CHABs have many harmful impacts on aquatic ecosystems and water quality. The accumulation of cyanobacteria scums in surface waters can shade and prevent growth of benthic vegetation (Scheffer *et al.*, 1993; McGowan *et al.*, 2005), and the decomposition of senescent cyanobacterial biomass can lead to hypoxic bottom waters in lake systems where the stratification regime is suitable (Rao *et al.*, 2014; Watson *et al.*, 2016). The resulting low oxygen waters can lead to fish kills (Rao *et al.*, 2014), and may negatively impact benthic macroinvertebrates (Modig & Ólafsson, 1998; Bridgeman *et al.*, 2006). Bloom-forming cyanobacteria also produce a variety of taste and odor compounds, which interfere with the recreational use of lakes and impact palatability of drinking water (Jüttner & Watson, 2007), as well as toxic secondary metabolites that can sicken birds, livestock, and humans (Carmichael,

2001; Stewart *et al.*, 2008; Huisman *et al.*, 2018). The combined negative effects that CHABs have on ecosystems also impart substantial socioeconomic costs. For example, algal and cyanobacteria blooms have been estimated to cost the USA $82 million – $4.8 billion US dollars annually and the Canadian Lake Erie Basin $86 - $164 million Canadian dollars annually (Smith *et al.*, 2019).

While CHABs have occurred during pre-industrial times, the frequency and severity of CHABs are increasing globally due to increasing anthropogenic stressors on aquatic ecosystems (Huisman *et al.*, 2018; Ho *et al.*, 2019). Since the 1800s, cyanobacteria abundance has increased in lakes globally at rates disproportionate to increases in other phytoplankton groups (Taranu *et al.*, 2015), and CHABs are now regular events in some of the largest lakes and seas in the world, including: western Lake Erie (Steffen *et al.*, 2014; Watson *et al.*, 2016), Lake Taihu (Chen *et al.*, 2003; Duan *et al.*, 2009), Lake Victoria (Olokotum *et al.*, 2020), and the Baltic Sea (Kahru & Elmgren, 2014).The increasing frequency of cyanobacterial blooms are largely attributed to cultural eutrophication, or increasing inputs of the growth limiting nutrients nitrogen (N) and phosphorus (P) from agricultural and urban activity (Carpenter *et al.*, 1998). P inputs are thought to be the main driver of CHABs in freshwaters (Schindler, 1974; Schindler *et al.*, 2008), and have been used to predict total biomass of cyanobacteria blooms in Lake Erie (Scavia *et al.*, 2016). However, N inputs may stimulate bloom formation in some systems (Gobler *et al.*, 2016; Paerl *et al.*, 2016) or be important in favoring growth and toxin production in non-nitrogen fixing cyanobacteria (Davis *et al.*, 2015; Gobler *et al.*, 2016; Chaffin *et al.*, 2018). Furthermore, the fate of N inputs into freshwaters is likely important for the development of marine algal blooms downstream in coastal systems (Paerl *et al.*, 2016; Paerl *et al.*, 2018), where N is considered the primary limiting nutrient (Howarth & Marino, 2006; Paerl, 2018).

While the main cause of CHABs is eutrophication, climate change is expected to exacerbate CHAB frequency and severity (Huisman *et al.*, 2018; Paerl & Barnard, 2020). With the increasing severity of storm events due to climate change, nutrient inputs from runoff are projected to increase (Sinha *et al.*, 2017), thus increasing eutrophication and potentially CHAB frequency and severity (Reichwaldt & Ghadouani, 2012; Michalak *et al.*, 2013). The irregularity of these events interspersed with increasingly common droughts (Groisman & Knight, 2008) will result in larger pulses of nutrients (Kleinman *et al.*, 2006) and decreased water residence times, thus allowing cyanobacteria blooms to remain in nutrient enriched waters for longer periods of time (Reichwaldt & Ghadouani, 2012). Furthermore, more frequent droughts and warmer waters will favor prolonged lake stratification (Paerl & Huisman, 2009). Many cyanobacteria are well equipped to take advantage of calm, stratified waters via buoyancy regulation with gas vesicles, which allows them to reach high light levels at the water surface (Walsby *et al.*, 1997; Joehnk *et al.*, 2008), and with the production of photoprotective pigments (Paerl *et al.*, 1983). In addition, because cyanobacteria reach maximum growth rates at higher temperatures compared to other phytoplankton, warmer waters are expected to favor cyanobacteria over other phytoplankton groups (Joehnk *et al.*, 2008; Paerl & Huisman, 2009).

1.2 The Issue of Variable Microcystin Production Among *Microcystis* Strains and the Ecological and Physiological Role of Microcystin Production

While a variety of cyanobacterial species form blooms (Steffen *et al.*, 2014; Huisman *et al.*, 2018), one of the most globally widespread and dominant cyanobacteria genera in freshwaters is *Microcystis* (Harke *et al.*, 2016). Some *Microcystis* strains and species can produce microcystins, a class of liver toxins that are produced nonribosomally with a series of six polyketide synthetase and nonribosomal peptide synthetase enzymes in addition to four tailoring enzymes that are all encoded by the *mcy* gene cluster (Dittmann *et al.*, 1997; Tillett *et al.*, 2000). There are over 200

different chemical variants (congeners) of microcystin that differ in the amino acid at two variable positions in the peptide chain (Spoof & Catherine, 2016; Díez-Quijada *et al.*, 2019). Microcystins are potent toxins, having originally been named fast-death factor due to the rapid onset of poisoning symptoms and death in mice experiments (Hughes *et al.*, 1958; Bishop *et al.*, 1959). Ingestion of the toxin results in liver hemorrhaging and death in extreme cases, and livestock and pet deaths due to microcystin ingestion are common (Carmichael, 2001; Roegner *et al.*, 2014). While human illness and death due to acute microcystin exposure is rarer, it can occur when microcystins contaminate finished municipal water supplies (Carmichael, 2001; Roegner *et al.*, 2014). *Microcystis* blooms in Lakes Taihu and Erie have caused drinking water shutdowns for the cities of Wuxi, China (Qin *et al.*, 2010) and Toledo, OH, USA (Steffen *et al.*, 2017) due to microcystin contamination of drinking water. Some evidence suggests that chronic exposure to low concentrations of microcystins may increase the risk of liver disease in humans (Svirčev *et al.*, 2009; Li *et al.*, 2011). For these reasons, *Microcystis* blooms are threats to human health and drinking water availability.

Microcystin concentrations during *Microcystis* blooms vary both temporally and spatially within and across bloom events (Vaitomaa *et al.*, 2003; Kardinaal *et al.*, 2007; Davis *et al.*, 2009; Berry *et al.*, 2017b). This is due in part to variations in the rate of microcystin production under different growth conditions (Sivonen, 1990; Orr & Jones, 1998; Kaebernick *et al.*, 2000; Jähnichen *et al.*, 2007; Zilliges *et al.*, 2011). However, not all species and strains of *Microcystis* produce microcystins, as some lack a complete *mcy* gene cluster (Meiβner *et al.*, 1996; Dittmann *et al.*, 1997; Christiansen *et al.*, 2008). Microcystin-producing (referred to here as "toxic") and non-producing strains (referred to here as "nontoxic") of *Microcystis* often coexist during blooms, and the relative proportions of these different species and strains is an important

determinant of microcystin concentrations during CHABs (Vaitomaa *et al.*, 2003; Kardinaal *et al.*, 2007; Briand *et al.*, 2009; Davis *et al.*, 2009). Therefore, understanding the ecological drivers of successions in *Microcystis* strains and species is important for understanding bloom development and variations in bloom microcystin concentrations and will perhaps aid in future management decisions and designing novel bloom treatment strategies (Hellweger *et al.*, 2019).

The ecological role of microcystin production is contested. It is unlikely that it has evolved as a grazing deterrent, as the genes for microcystin production predate the evolution of metazoan grazers (Rantala *et al.*, 2004). Rather, it is likely related to central metabolic processes, as microcystin production is strongly correlated with cell division rates (Orr & Jones, 1998). While nutrient availability is known to impact microcystin biosynthesis (Sivonen, 1990; Orr & Jones, 1998; Long *et al.*, 2001; Vézie *et al.*, 2002; Downing *et al.*, 2005; Ginn *et al.*, 2010), it has been argued that the impact of nutrients on microcystin production within a given strain is an indirect effect of nutrient availability on cellular growth rates (Orr & Jones, 1998; Long *et al.*, 2001; Neilan *et al.*, 2013). Current evidence suggests that microcystin production is related to central carbon-nitrogen metabolism and photosynthesis, as microcystin is localized in the thylakoids, the membranes where the photosystem proteins are located (Young *et al.*, 2005), and microcystin production increases with light intensity (Kaebernick *et al.*, 2000; Zilliges *et al.*, 2011) and inorganic carbon deficiency (Jähnichen *et al.*, 2007). Microcystins also bind to key enzymes involved in photosynthesis (Zilliges *et al.*, 2011; Meissner *et al.*, 2013; Barchewitz *et al.*, 2019), and influence the cellular localization of Rubisco, the carbon-fixing enzyme in photosynthesis (Barchewitz *et al.*, 2019). There is evidence suggesting a role of microcystin in intercell signaling (Schatz *et al.*, 2007), however the localization of microcystin within the thylakoid membranes may conflict with this hypothesis. Because microcystin binds to proteins at areas

sensitive to oxidative damage (Zilliges *et al.*, 2011), and expression of the *mcy* operon is regulated by promoters involved in N starvation (Ginn *et al.*, 2010) and iron starvation (Martin-Luna *et al.*, 2006; Alexova *et al.*, 2011a), microcystin may play a role in the overall cellular stress response. Further supporting that microcystin is involved in stress responses, a mutant strain incapable of microcystin production was more sensitive to high light and hydrogen peroxide (Zilliges *et al.*, 2011), expressed different amounts of proteins involved in redox control (Alexova *et al.*, 2011b), and had a different metabolome composition under increased light exposure (Meissner *et al.*, 2015) when compared to the wild-type.

The uncertainty around the ecological and physiological function of microcystin production makes predicting the environmental factors that favor toxic over nontoxic *Microcystis* difficult. However, several observations support that some environmental conditions may favor toxic over nontoxic *Microcystis*, although the number of different *Microcystis* strains tested is limited in most cases. Toxic *Microcystis* strains tend to have higher nutrient demands than nontoxic strains (Vézie *et al.*, 2002), suggesting that increased nitrogen availability may favor growth of toxic *Microcystis.* Supporting that nitrogen availability favors toxic *Microcystis,* growth of toxic strains increased with inorganic nitrogen additions in bottle experiments (Davis *et al.*, 2009; Davis *et al.*, 2010). However, additions of organic N forms tend to favor nontoxic *Microcystis* (Davis et al., 2010), complicating the relationship between the dominance of toxic strains and total N availability. Iron deficiency may also favor toxic strains, as toxic *Microcystis* were found to better tolerate iron starvation than nontoxic *Microcystis* in laboratory experiments (Alexova *et al.*, 2011a).

Although there appear to be some traits that separate toxic and nontoxic *Microcystis*, some phenotypic and genotypic variation between strains of *Microcystis* do not correlate or cluster

along a toxic versus nontoxic dichotomy. One example is the effect of temperature; increasing temperatures favored toxic *Microcystis* over nontoxic *Microcystis* in some studies (Dziallas & Grossart, 2011), but a nontoxic *Microcystis* strain was found to have a higher optimum growth temperature than toxic *Microcystis* in another study (Thomas & Litchman, 2016). Furthermore, the proteomes of some toxic *Microcystis* were more similar to those of nontoxic *Microcystis* (Alexova *et al.*, 2011b). In addition, some studies with natural toxic and nontoxic *Microcystis* strains have supported that increasing concentrations of reactive oxygen species may favor toxic *Microcystis* (Dziallas & Grossart, 2011). However, another study found that nontoxic *Microcystis* had improved recovery from large H_2O_2 additions when compared to a toxic strain (Schuurmans *et al.*, 2018). These conflicting results may indicate that some of the competitive advantages or disadvantages of toxic strains previously reported are not necessarily due to the production of microcystin, which complicates relating variations in *Microcystis* strain traits to outcomes for bloom microcystin concentrations.

1.3 Reactive Oxygen Species and Their Impacts on Microbial Growth and Population Dynamics

As discussed above, one proposed physiological function of microcystins is to protect the cell from damage from reactive oxygen species (ROS). The ROS superoxide radical anion (O_2^-), hydrogen peroxide (H_2O_2), and hydroxyl radical (•OH) are one-electron reduction products in the sequential four electron reduction of molecular oxygen to water. ROS are produced both via photochemical reactions with chromophoric dissolved organic matter (CDOM) (Cooper & Zika, 1983; Cooper *et al.*, 1989b) and biological enzymes and metabolisms (Diaz *et al.*, 2013; Diaz & Plummer, 2018; Zinser, 2018b) and are ubiquitous in oxygenated aquatic ecosystems. ROS can rapidly oxidize and damage cell structures when they accumulate inside cell membranes (Imlay, 2003; Imlay, 2019). Of the three, H_2O_2 is thought to be the most significant as an exogenous

stressor to microbial growth and populations because the very short half-life of •OH (Brezonik & Fulkerson-Brekken, 1998) likely causes it to react with dissolved molecules before it can cross cell membranes (Zinser, 2018b), and O_2^- is impermeable to cell membranes at pH above 6 (Korshunov & Imlay, 2002), which is in contrast to the rapid rate of diffusion across cell membranes by H_2O_2 (Seaver & Imlay, 2001). However, exogenous O_2^- is likely important as an indirect exogenous stressor because it can form H_2O_2 via reactions with dissolved organic matter and metals (Voelker *et al.*, 2000; Rose & Waite, 2006; Heller & Croot, 2010) and spontaneous dismutation (Zafiriou, 1990).

ROS can play an important role in structuring microbial communities because of varying sensitivities to oxidative stress among taxa (Perelman *et al.*, 2003; Morris *et al.*, 2008; Morris *et al.*, 2011; Kim *et al.*, 2016). Differences in the sensitivity of microbial taxa to H_2O_2 are determined in part by the collection of enzymes in a given organism that decompose H_2O_2 into harmless products (Morris *et al.*, 2008; Morris *et al.*, 2012; Kim *et al.*, 2016; Kim *et al.*, 2019a). Microbes produce catalase and peroxidase enzymes that respectively dismutate H_2O_2 into water and molecular oxygen or reduce H_2O_2 to water with an electron donor (Mishra & Imlay, 2012). However, the distribution of these enzymes across microbial taxa is not uniform (Passardi *et al.*, 2007; Bernroitner *et al.*, 2009). This can lead to large differences in H_2O_2 sensitivity between genera (Ostrowski *et al.*, 2001; Morris *et al.*, 2008; Morris *et al.*, 2011; Kim *et al.*, 2016; Ma *et al.*, 2018; Kim *et al.*, 2019a). However, differences in H_2O_2 sensitivity among different strains of the same genus or species with the same catalase and peroxidase gene content also occur (Morris *et al.*, 2011; Bayer *et al.*, 2019). Differences in H_2O_2 sensitivity between microbial taxa suggest that ROS may affect community composition at multiple taxonomic levels. Cyanobacteria are particularly sensitive, enabling treatment of cyanobacterial blooms with H_2O_2, which can be

dosed at levels that eliminate cyanobacteria while most algae remain unaffected (Matthijs *et al.*, 2012). Other bacterial groups are also suppressed by H_2O_2 concentrations used during cyanobacteria bloom treatment (Lin *et al.*, 2018; Lusty & Gobler, 2020), and amendments of lower H_2O_2 concentrations can inhibit respiration and secondary production in natural communities (Xenopoulos & Bird, 1997; Weinbauer & Suttle, 1999; Anesio *et al.*, 2005). Natural changes in H_2O_2 concentrations can also impact microbial communities. For example, an absence of H_2O_2-producing species can lead to the proliferation of H_2O_2-sensitive pathogens in human microbiomes (Eschenbach *et al.*, 1989), and *Prochlorococcus* cannot tolerate H_2O_2 production rates typical of the open ocean without the presence of "helper" microbes that degrade H_2O_2 (Morris *et al.*, 2011; Ma *et al.*, 2018; Zinser, 2018a). However, the importance of natural H_2O_2 production and decay dynamics in structuring entire microbial communities, and how H_2O_2 production and decay rates vary with microbial community composition in aquatic environments, is largely unknown (Zinser, 2018b). This is particularly true for freshwaters, where the enzymes and organisms involved in H_2O_2 decomposition have not been characterized to the same extent as in marine systems (Morris *et al.*, 2011; Morris *et al.*, 2016).

Natural variations in H_2O_2 are hypothesized to impact the relative proportion of *Microcystis* strains in the environment (Dziallas & Grossart, 2011; Paerl & Otten, 2013). To date, the differential impact of H_2O_2 on the growth of *Microcystis* strains has only been explored along the toxic vs. nontoxic dichotomy (Dziallas & Grossart, 2011; Zilliges *et al.*, 2011; Schuurmans *et al.*, 2018), yielding conflicting results. In one study, three toxic strains had lower reductions in chlorophyll *a* content than two nontoxic strains when treated with H_2O_2 (Dziallas & Grossart, 2011), which is congruent with the hypothesis that microcystins protect the cell from ROS (Zilliges *et al.*, 2011). However, the opposite result was found in another study, where a

mutant strain incapable of microcystin biosynthesis degraded H_2O_2 faster than the wild type, and the mutant and a natural nontoxic strain could recover from large additions of H_2O_2 while a toxic strain could not (Schuurmans *et al.*, 2018). These conflicting results could be an artifact of the lack of standardized conditions between the experiments. The toxicity of H_2O_2 toward cyanobacteria is dependent on light intensity (Drábková *et al.*, 2007; Morris *et al.*, 2011; Piel *et al.*, 2020) and wavelength (Piel *et al.*, 2020), deviation from optimal growth temperature (Ma *et al.*, 2018), cell density (Morris *et al.*, 2008; Morris *et al.*, 2011), and the presence of H_2O_2-degrading bacteria (Morris *et al.*, 2008; Morris *et al.*, 2011; Kim *et al.*, 2019a). Therefore, it is difficult to determine if the discrepancies in these results are due to differences in the sensitivities of the strains to H_2O_2, different culturing conditions, or some combination. In addition, Schuurmans et al. 2018 largely measured growth inhibition at large H_2O_2 doses, orders of magnitude above concentrations observed in natural waters (Cooper *et al.*, 1989a; Cory *et al.*, 2016), and used light levels far below those typical of natural sunlight in summer surface waters (Sagert & Schubert, 2000). The Dziallas and Grossart and Zilliges et al. studies did not measure background H_2O_2 concentrations of the growth media during their experiment, so the total H_2O_2 exposure in their experiments is unknown. Therefore, the extent to which naturally occurring H_2O_2 concentrations impact the growth of different Microcystis strains is still uncertain.

1.4 Microbial Interactions Determine Responses to Hydrogen Peroxide

The response of a given microorganism to H_2O_2 is determined by interactions with other community members. Because H_2O_2 diffuses through cell membranes at rates similar to water (Seaver & Imlay, 2001), intracellular H_2O_2 decomposition by microbes can rapidly reduce environmental H_2O_2 concentrations and in the process protect other sensitive organisms that lack the enzymatic pathways to decompose H_2O_2 themselves (Morris *et al.*, 2012; Zinser, 2018a). For

example, some strains of *Prochlorococcus* (Morris *et al.*, 2008; Morris *et al.*, 2011), ammonia-oxidizing archaea (AOA) (Kim *et al.*, 2016; Bayer *et al.*, 2019), and acI clade actinobacteria (Kim *et al.*, 2019b), all require supplementation of an exogenous H_2O_2 scavenger in culture media to grow when exposed to environmentally relevant H_2O_2 concentrations. In *Prochlorococcus* and AOA, H_2O_2 sensitivity is thought to be due to the absence of catalase genes in the genomes (Morris *et al.*, 2008; Kim *et al.*, 2016), while in acI actinobacteria, H_2O_2 sensitivity is due to either the absence of catalase in some strains or the presence of catalase with low specific activity and catalytic efficiency in others (Kim *et al.*, 2019b). Co-cultivation with catalase-producing "helper" bacteria abolishes the H_2O_2 sensitive phenotype in both *Prochlorococcus* (Morris *et al.*, 2008; Morris *et al.*, 2011) and AOA (Bayer *et al.*, 2019). Such interactions demonstrate that the impact of environmental H_2O_2 on a given microbial species or strain depends on both the sensitivity of the species or strain to H_2O_2 and the rate of H_2O_2 decomposition by the surrounding community members. *Microcystis* may be especially impacted by the activity of the surrounding bacterial community because it grows in buoyant aggregates or "colonies" surrounded by an exopolysaccharide mucilage layer that other bacteria often adhere to (Worm & Søndergaard, 1998; Brunberg, 1999; Parveen *et al.*, 2013; Agha *et al.*, 2016). This suggests that traits in the associated bacteria may impact the response of *Microcystis* strains to H_2O_2 and other environmental gradients.

1.5 The *Microcystis* Phycosphere

While *Microcystis* is the causative organism of many CHABs, blooms are complex communities of interacting microorganisms (Parveen *et al.*, 2013; Louati *et al.*, 2015; Berry *et al.*, 2017a; Chun *et al.*, 2019; Zhu *et al.*, 2019; Chun *et al.*, 2020). The microbial community composition of *Microcystis* blooms varies temporally (Parveen *et al.*, 2013; Berry *et al.*, 2017a;

Chun *et al.*, 2020; Jankowiak & Gobler, 2020), by location (Cook *et al.*, 2020; Jankowiak & Gobler, 2020), and with the dominating *Microcystis* genotype (Chun *et al.*, 2020), but some taxa appear regularly in *Microcystis* blooms (Cook *et al.*, 2020). *Microcystis* and other phytoplankton harbor microbial communities within the phycosphere, a zone of close physical proximity to the phytoplankton cell(s) enriched in organic matter exuded by the phytoplankton (Bell & Mitchell, 1972; Seymour *et al.*, 2017). Many of the bacteria that occupy the phycosphere are beneficial, improving phytoplankton growth through a variety of mechanisms (Amin *et al.*, 2009; Van Mooy *et al.*, 2012; Amin *et al.*, 2015; Christie-Oleza *et al.*, 2017; Durham *et al.*, 2017), while others are parasitic (Caiola & Pellegrini, 1984; Seyedsayamdost *et al.*, 2011; Agha *et al.*, 2016). Some organisms can be either beneficial or harmful to phytoplankton, depending on growth conditions (Grossart & Simon, 2007; Seyedsayamdost *et al.*, 2011; Hennon *et al.*, 2017).

The phycosphere communities associated with *Microcystis* are distinct from both surrounding free-living communities (Parveen *et al.*, 2013; Louati *et al.*, 2015; Jankowiak & Gobler, 2020) and the phycosphere communities of other cyanobacteria (Louati *et al.*, 2015; Zhu *et al.*, 2019). This indicates that *Microcystis* interacts with specific bacterial populations. Despite this, the phycosphere communities among *Microcystis* strains and colonies vary taxonomically, with more closely related *Microcystis* genomes having more similar phycosphere microbiomes in both enrichment cultures established from single colonies and colonies isolated and immediately sequenced (Jackrel *et al.*, 2019; Pérez-Carrascal *et al.*, 2020). However, the degree to which strain-specific interactions, neutral effects, and temporal changes in either the environment or free-living communities that may seed the phycosphere structure *Microcystis* phycosphere communities is currently unknown.

The functional significance of distinct microbiomes across *Microcystis* colonies is largely unknown. Although the microbiomes between *Microcystis* strains are taxonomically distinct, the functional potential of communities (as defined by metagenomics) in established enrichment cultures were relatively similar (Jackrel *et al.*, 2019). There are currently no data that can distinguish whether this is the result of cultivation bias, or if functional converge of strain-specific microbiomes also occurs in natural *Microcystis* colonies. In bulk phytoplankton aggregates dominated by Microcystis, functional dissimilarity was lower than taxonomic dissimilarity (Cook *et al.*, 2020), although how the relatively smaller functional dissimilarity translates into observed functional outcomes is still unknown. However, in other phytoplankton species, taxonomically distinct microbiomes also have strain specific growth-impacts. For example, growth and toxin production in species of the diatom *Pseudo-nitschiza* was improved only by their co-isolated bacteria, not bacteria co-isolated from other *Pseudo-nitschiza* species (Sison-Mangus *et al.*, 2014). These results in *Pseudo-nitschiza* support that some strain-specific outcomes also would arise from distinct *Microcystis* phycosphere microbiomes. Additionally, microbiome members shared between multiple *Microcystis* strains may have strain-specific outcomes on *Microcystis* growth. For example, one strain of *Pseudanabaena* can colonize the mucilage of multiple *Microcystis* strains, but the impact on *Microcystis* growth was either neutral or harmful, depending on the *Microcystis* strain (Agha *et al.*, 2016). Together, this supports that *Microcystis* microbiomes are likely to differ both in terms of the members present and the impact of shared members on *Microcystis* growth. For this reason, not only could differences in the traits of *Microcystis* strains account for successions in their relative abundance, but differences in the traits of other bacteria associated with particular *Microcystis* strains may also impact *Microcystis* relative abundance.

1.6 Dissertation Outline and Research Questions

In Chapter 2 of this dissertation, two research questions are addressed. Which enzymes and organisms are involved in H_2O_2 decomposition during western Lake Erie cyanobacterial blooms, and how does the presence of an H_2O_2 scavenger impact different toxic and nontoxic *Microcystis* strains. The work in this chapter improves our understanding of how microbial interactions impact how different *Microcystis* strains respond to H_2O_2 and helps reconcile conflicting evidence in the current literature on whether elevated H_2O_2 concentrations during blooms favor toxic or nontoxic *Microcystis* strains.

In Chapter 3, bacterial communities in the phycospheres of individual *Microcystis* colonies were examined in order to separate the communities specifically associated with *Microcystis* from those associated with other phytoplankton or large particles. As the first time series dataset of individual *Microcystis* colony microbiomes, this chapter also characterized how phycosphere bacterial community composition changes over time and between colonies of different oligotypes. This is an important first step in our understanding for how functions provided by associated bacteria may change over a bloom and potentially impact the relative proportions of different *Microcystis* strains.

In Chapter 4, the genome sequences of two novel Acidobacteria that had high catalase transcript abundance relative to their metagenomic abundance in Chapter 2 were examined in order to characterize their uptake of organic carbon and nitrogen compounds. One of these bacteria was also identified in *Microcystis* phycosphere communities in Chapter 4. The genome and metatranscriptomic sequences were mined for evidence of uptake of cyanobacterial and phytoplankton derived compounds, and this research begins to characterize the complete interactions between phytoplankton associated bacteria in western Lake Erie cyanobacteria blooms.

In Chapter 5, the knowledge gap of how microbial communities in western Lake Erie are related to microbial community composition and *Microcystis* growth was addressed by measuring H_2O_2 production rates in western Lake Erie as a function of chlorophyll *a* concentration, respiration rates, primary production rates, the abundances of bacteria species, and microbial community dissimilarity, with and without light exposure, and with and without large phytoplankton assemblages (including *Microcystis* colonies >105 μm).

In Chapter 6, the conclusions of Chapters 2-5 are synthesized, and avenues for future research to address shortcomings of the experimental and sampling approaches as well as new research questions formed from the research results are discussed.

1.7 References

Agha, R., del Mar Labrador, M., de los Ríos, A., & Quesada, A. (2016). Selectivity and detrimental effects of epiphytic *Pseudanabaena* on *Microcystis* colonies. *Hydrobiologia, 777*(1): 139-148.

Alexova, R., Fujii, M., Birch, D., Cheng, J., Waite, T. D., Ferrari, B. C., & Neilan, B. A. (2011a). Iron uptake and toxin synthesis in the bloom-forming *Microcystis aeruginosa* under iron limitation. *Environ Microbiol, 13*(4): 1064-1077.

Alexova, R., Haynes, P. A., Ferrari, B. C., & Neilan, B. A. (2011b). Comparative protein expression in different strains of the bloom-forming cyanobacterium *Microcystis aeruginosa*. *Mol Cell Proteomics, 10*(9).

Amin, S. A., Green, D. H., Hart, M. C., Krüpper, F. C., Sunda, W. G., & Carrano, C. J. (2009). Photolysis of iron-siderophore chelates promotes bacterial-algal mutualism. *Proc Natl Acad Sci, 106*(40): 17071-17076. doi:10.1073 pnas.0905512106

Amin, S. A., Hmelo, L. R., van Tol, H. M., Durham, B. P., Carlson, L. T., Heal, K. R. *et al.* (2015). Interaction and signalling between a cosmopolitan phytoplankton and associated bacteria. *Nature, 522*(7554): 98-101. doi:10.1038/nature14488

Anesio, A. M., Granéli, W., Aiken, G. R., Kieber, D. J., & Mopper, K. (2005). Effect of humic substance photodegradation on bacterial growth and respiration in lake water. *Appl Environ Microbiol, 71*(10): 6267-6275.

Barchewitz, T., Guljamow, A., Meissner, S., Timm, S., Henneberg, M., Baumann, O. *et al.* (2019). Non-canonical localization of RubisCO under high-light conditions in the toxic

cyanobacterium Microcystis aeruginosa PCC7806. *Environ Microbiol, 21*(12): 4836-4851.

Bayer, B., Pelikan, C., Bittner, M. J., Reinthaler, T., Könneke, M., Herndl, G. J., & Offre, P. (2019). Proteomic Response of Three Marine Ammonia-Oxidizing Archaea to Hydrogen Peroxide and Their Metabolic Interactions with a Heterotrophic Alphaproteobacterium. *mSystems, 4*(4): e00181-00119.

Bell, W., & Mitchell, R. (1972). Chemotactic and growth responses of marine bacteria to algal extracellular products. *Biol. Bull, 143*(2): 265-277.

Bernroitner, M., Zamocky, M., Furtmüller, P. G., Peschek, G. A., & Obinger, C. (2009). Occurrence, phylogeny, structure, and function of catalases and peroxidases in cyanobacteria. *J Exp Bot, 60*(2): 423-440.

Berry, M. A., Davis, T. W., Cory, R. M., Duhaime, M. B., Johengen, T. H., Kling, G. W. *et al.* (2017a). Cyanobacterial harmful algal blooms are a biological disturbance to Western Lake Erie bacterial communities. *Environ Microbiol, 19*(3): 1149-1162.

Berry, M. A., White, J. D., Davis, T. W., Jain, S., Johengen, T. H., Dick, G. J. *et al.* (2017b). Are oligotypes meaningful ecological and phylogenetic units? A case study of *Microcystis* in freshwater lakes. *Front Microbiol, 8*: 365.

Bishop, C., Anet, E., & Gorham, P. (1959). Isolation and identification of the fast-death factor in *Microcystis aeruginosa* NRC-1. *Can J Biochem Physiol, 37*(3): 453-471.

Brezonik, P. L., & Fulkerson-Brekken, J. (1998). Nitrate-induced photolysis in natural waters: controls on concentrations of hydroxyl radical photo-intermediates by natural scavenging agents. *Environ Sci Technol, 32*(19): 3004-3010.

Briand, E., Escoffier, N., Straub, C., Sabart, M., Quiblier, C., & Humbert, J.-F. (2009). Spatiotemporal changes in the genetic diversity of a bloom-forming Microcystis aeruginosa (cyanobacteria) population. *ISME J, 3*(4): 419-429.

Bridgeman, T. B., Schloesser, D. W., & Krause, A. E. (2006). Recruitment of *Hexagenia* mayfly nymphs in western Lake Erie linked to environmental variability. *Ecological Applications, 16*(2): 601-611.

Brunberg, A.-K. (1999). Contribution of bacteria in the mucilage of *Microcystis* spp.(Cyanobacteria) to benthic and pelagic bacterial production in a hypereutrophic lake. *FEMS Microbiol Ecol, 29*(1): 13-22.

Caiola, M. G., & Pellegrini, S. (1984). Lysis of *Microcystis aeruginosa* (KÜTZ.) By *Bdellovibrio*-like Bacteria. *J Phycol, 20*(4): 471-475.

Campbell, L., Nolla, H., & Vaulot, D. (1994). The importance of *Prochlorococcus* to community structure in the central North Pacific Ocean. *Limnol Oceanogr, 39*(4): 954-961.

Capone, D. G., Zehr, J. P., Paerl, H. W., Bergman, B., & Carpenter, E. J. (1997). *Trichodesmium*, a globally significant marine cyanobacterium. *Science, 276*(5316): 1221-1229.

Carmichael, W. W. (2001). Health effects of toxin-producing cyanobacteria:"The CyanoHABs". *Human and ecological risk assessment: An International Journal, 7*(5): 1393-1407.

Carpenter, S. R., Caraco, N. F., Correll, D. L., Howarth, R. W., Sharpley, A. N., & Smith, V. H. (1998). Nonpoint pollution of surface waters with phosphorus and nitrogen. *Ecological applications, 8*(3): 559-568.

Chaffin, J. D., Davis, T. W., Smith, D. J., Baer, M. M., & Dick, G. J. (2018). Interactions between nitrogen form, loading rate, and light intensity on *Microcystis* and *Planktothrix* growth and microcystin production. *Harmful Algae, 73*: 84-97.

Chen, Y., Qin, B., Teubner, K., & Dokulil, M. T. (2003). Long-term dynamics of phytoplankton assemblages: *Microcystis*-domination in Lake Taihu, a large shallow lake in China. *J Plankton Res, 25*(4): 445-453.

Christiansen, G., Molitor, C., Philmus, B., & Kurmayer, R. (2008). Nontoxic strains of cyanobacteria are the result of major gene deletion events induced by a transposable element. *Mol Biol Evol, 25*(8): 1695-1704.

Christie-Oleza, J. A., Sousoni, D., Lloyd, M., Armengaud, J., & Scanlan, D. J. (2017). Nutrient recycling facilitates long-term stability of marine microbial phototroph-heterotroph interactions. *Nat Microbiol, 2*(17100): 1-10.

Chun, S.-J., Cui, Y., Lee, C. S., Cho, A. R., Baek, K., Choi, A. *et al.* (2019). Characterization of distinct cyanoHABs-related modules in microbial recurrent association network. *Front Microbiol, 10*: 1637.

Chun, S.-J., Cui, Y., Lee, J. J., Choi, I.-C., Oh, H.-M., & Ahn, C.-Y. (2020). Network analysis reveals succession of Microcystis genotypes accompanying distinctive microbial modules with recurrent patterns. *Water Res, 170*: 115326.

Cook, K. V., Li, C., Cai, H., Krumholz, L. R., Hambright, K. D., Paerl, H. W. *et al.* (2020). The global *Microcystis* interactome. *Limnol Oceanogr, 65*(S1): S194-S207. doi:10.1002/lno.11361

Cooper, W. J., & Zika, R. G. (1983). Photochemical formation of hydrogen peroxide in surface and ground waters exposed to sunlight. *Science, 220*(4598): 711-712.

Cooper, W. J., Lean, D., & Carey, J. (1989a). Spatial and temporal patterns of hydrogen peroxide in lake waters. *Can J Fish Aquat Sci, 46*(7): 1227-1231.

Cooper, W. J., Zika, R. G., Petasne, R. G., & Fischer, A. M. (1989b). Sunlight-Induced Photochemistry of Humic Substances in Natural Waters: Major Reactive Species. In I. H. Suffet & P. MacCarthy (Eds.), *Aquatic Humic Substances* (pp. 333-362). Washington, DC: American Chemical Society.

Cory, R. M., Davis, T. W., Dick, G. J., Johengen, T., Denef, V. J., Berry, M. A. *et al.* (2016). Seasonal dynamics in dissolved organic matter, hydrogen peroxide, and cyanobacterial blooms in Lake Erie. *Front Mar Sci, 3*: 54.

Davis, T. W., Berry, D. L., Boyer, G. L., & Gobler, C. J. (2009). The effects of temperature and nutrients on the growth and dynamics of toxic and non-toxic strains of *Microcystis* during cyanobacteria blooms. *Harmful Algae, 8*(5): 715-725.

Davis, T. W., Harke, M. J., Marcoval, M. A., Goleski, J., Orano-Dawson, C., Berry, D. L., & Gobler, C. J. (2010). Effects of nitrogenous compounds and phosphorus on the growth of toxic and non-toxic strains of *Microcystis* during cyanobacterial blooms. *Aquat Microb Ecol, 61*(2): 149-162.

Davis, T. W., Bullerjahn, G. S., Tuttle, T., McKay, R. M., & Watson, S. B. (2015). Effects of increasing nitrogen and phosphorus concentrations on phytoplankton community growth and toxicity during *Planktothrix* blooms in Sandusky Bay, Lake Erie. *Environ Sci Technol, 49*(12): 7197-7207.

Delwiche, C. F., Kushell, M., & Palmer, J. D. (1995). Phylogenetic analysis of *tufA* sequences indicates a cyanobacterial origin of all plastids. *Mol Phylogenetics Evol, 4*(2): 110-128.

Delwiche, C. F. (1999). Tracing the thread of plastid diversity through the tapestry of life. *Am Nat, 154*(S4): S164-S177.

Diaz, J. M., Hansel, C. M., Voelker, B. M., Mendes, C. M., Andeer, P. F., & Zhang, T. (2013). Widespread production of extracellular superoxide by heterotrophic bacteria. *Science, 340*(6137): 1223-1226.

Diaz, J. M., & Plummer, S. (2018). Production of extracellular reactive oxygen species by phytoplankton: past and future directions. *J Plankton Res, 40*(6): 655-666.

Díez-Quijada, L., Prieto, A. I., Guzmán-Guillén, R., Jos, A., & Cameán, A. M. (2019). Occurrence and toxicity of microcystin congeners other than MC-LR and MC-RR: A review. *Food Chem Toxicol, 125*: 106-132.

Dittmann, E., Neilan, B. A., Erhard, M., Von Döhren, H., & Börner, T. (1997). Insertional mutagenesis of a peptide synthetase gene that is responsible for hepatotoxin production in the cyanobacterium *Microcystis aeruginosa* PCC 7806. *Mol Microbiol, 26*(4): 779-787.

Downing, T., Meyer, C., Gehringer, M., & Van de Venter, M. (2005). Microcystin content of *Microcystis aeruginosa* is modulated by nitrogen uptake rate relative to specific growth rate or carbon fixation rate. *Environ Toxicol, 20*(3): 257-262.

Drábková, M., Admiraal, W., & Maršálek, B. (2007). Combined exposure to hydrogen peroxide and light selective effects on cyanobacteria, green algae, and diatoms. *Environ Sci Technol, 41*(1): 309-314.

Duan, H., Ma, R., Xu, X., Kong, F., Zhang, S., Kong, W. *et al.* (2009). Two-decade reconstruction of algal blooms in China's Lake Taihu. *Environ Sci Technol, 43*(10): 3522-3528.

Durham, B. P., Dearth, S. P., Sharma, S., Amin, S. A., Smith, C. B., Campagna, S. R. *et al.* (2017). Recognition cascade and metabolite transfer in a marine bacteria-phytoplankton model system. *Environ Microbiol, 19*(9): 3500-3513. doi:10.1111/1462-2920.13834

Dziallas, C., & Grossart, H.-P. (2011). Increasing oxygen radicals and water temperature select for toxic *Microcystis* sp. *PLoS One, 6*(9): e25569.

Eschenbach, D. A., Davick, P. R., Williams, B. L., Klebanoff, S. J., Young-Smith, K., Critchlow, C., & Holmes, K. K. (1989). Prevalence of hydrogen peroxide-producing *Lactobacillus* species in normal women and women with bacterial vaginosis. *J Clin Microbiol, 27*(2): 251-256.

Ginn, H., Pearson, L., & Neilan, B. (2010). NtcA from Microcystis aeruginosa PCC 7806 is autoregulatory and binds to the microcystin promoter. *Appl Environ Microbiol, 76*(13): 4362-4368. Retrieved from https://www.ncbi.nlm.nih.gov/pmc/articles/PMC2897459/pdf/1862-09.pdf

Gobler, C. J., Burkholder, J. M., Davis, T. W., Harke, M. J., Johengen, T., Stow, C. A., & Van de Waal, D. B. (2016). The dual role of nitrogen supply in controlling the growth and toxicity of cyanobacterial blooms. *Harmful Algae, 54*: 87-97.

Groisman, P. Y., & Knight, R. W. (2008). Prolonged dry episodes over the conterminous United States: New tendencies emerging during the last 40 years. *J Clim, 21*(9): 1850-1862.

Grossart, H.-P., & Simon, M. (2007). Interactions of planktonic algae and bacteria: effects on algal growth and organic matter dynamics. *Aquat Microb Ecol, 47*(2): 163-176.

Harke, M. J., Steffen, M. M., Gobler, C. J., Otten, T. G., Wilhelm, S. W., Wood, S. A., & Paerl, H. W. (2016). A review of the global ecology, genomics, and biogeography of the toxic cyanobacterium, *Microcystis* spp. *Harmful Algae, 54*: 4-20.

Heller, M., & Croot, P. (2010). Kinetics of superoxide reactions with dissolved organic matter in tropical Atlantic surface waters near Cape Verde (TENATSO). *J Geophys Res Oceans, 115*(C12).

Hellweger, F. L., Vick, C., Rückbeil, F., & Bucci, V. (2019). Fresh Ideas Bloom in Gut Healthcare to Cross-Fertilize Lake Management. *Environ Sci Technol, 53*(24): 14099-14112.

Hennon, G. M., Morris, J. J., Haley, S. T., Zinser, E. R., Durrant, A. R., Entwistle, E. *et al.* (2017). The impact of elevated CO 2 on *Prochlorococcus* and microbial interactions with 'helper' bacterium *Alteromonas*. *ISME J, 12*(2): 520.

Ho, J. C., Michalak, A. M., & Pahlevan, N. (2019). Widespread global increase in intense lake phytoplankton blooms since the 1980s. *Nature, 574*(7780): 667-670.

Howarth, R. W., & Marino, R. (2006). Nitrogen as the limiting nutrient for eutrophication in coastal marine ecosystems: evolving views over three decades. *Limnol Oceanogr, 51*(1part2): 364-376.

Hughes, E. O., Gorham, P., & Zehnder, A. (1958). Toxicity of a unialgal culture of *Microcystis aeruginosa*. *Can J Microbiol, 4*(3): 225-236.

Huisman, J., Codd, G. A., Paerl, H. W., Ibelings, B. W., Verspagen, J. M., & Visser, P. M. (2018). Cyanobacterial blooms. *Nat Rev Microbiol, 16*: 471-483.

Imlay, J. A. (2003). Pathways of oxidative damage. *Annu Rev Microbiol, 57*(1): 395-418.

Imlay, J. A. (2019). Where in the world do bacteria experience oxidative stress? *Environ Microbiol, 21*(2): 521-530.

Jackrel, S. L., White, J. D., Evans, J. T., Buffin, K., Hayden, K., Sarnelle, O., & Denef, V. J. (2019). Genome Evolution and Host Microbiome Shifts Correspond with Intraspecific Niche Divergence within Harmful Algal Bloom-Forming *Microcystis aeruginosa*. *Mol Ecol, 28*(17): 3994-4011.

Jackrel, S. L., Yang, J. W., Schmidt, K. C., & Denef, V. J. (2020). Host specificity of microbiome assembly and its fitness effects in phytoplankton. *ISME J*: 1-15.

Jähnichen, S., Ihle, T., Petzoldt, T., & Benndorf, J. (2007). Impact of inorganic carbon availability on microcystin production by *Microcystis aeruginosa* PCC 7806. *Appl Environ Microbiol, 73*(21): 6994-7002.

Jankowiak, J. G., & Gobler, C. J. (2020). The composition and function of microbiomes within *Microcystis* colonies are significantly different than native bacterial assemblages in two North American lakes. *Front Microbiol, 11*: 1016.

Joehnk, K. D., Huisman, J., Sharples, J., Sommeijer, B., Visser, P. M., & Stroom, J. M. (2008). Summer heatwaves promote blooms of harmful cyanobacteria. *Global Change Biol, 14*(3): 495-512.

Jüttner, F., & Watson, S. B. (2007). Biochemical and ecological control of geosmin and 2-methylisoborneol in source waters. *Appl Environ Microbiol, 73*(14): 4395-4406.

Kaebernick, M., Neilan, B. A., Börner, T., & Dittmann, E. (2000). Light and the transcriptional response of the microcystin biosynthesis gene cluster. *Appl Environ Microbiol, 66*(8): 3387-3392.

Kahru, M., & Elmgren, R. (2014). Multidecadal time series of satellite-detected accumulations of cyanobacteria in the Baltic Sea. *Biogeosciences, 11*(13): 3619.

Kardinaal, W. E. A., Janse, I., Kamst-van Agterveld, M., Meima, M., Snoek, J., Mur, L. R. *et al.* (2007). *Microcystis* genotype succession in relation to microcystin concentrations in freshwater lakes. *Aquat Microb Ecol, 48*(1): 1-12.

Kim, J.-G., Park, S.-J., Damsté, J. S. S., Schouten, S., Rijpstra, W. I. C., Jung, M.-Y. *et al.* (2016). Hydrogen peroxide detoxification is a key mechanism for growth of ammonia-oxidizing archaea. *Proc Natl Acad Sci, 113*(28): 7888-7893.

Kim, M., Shin, B., Lee, J., Park, H. Y., & Park, W. (2019a). Culture-independent and culture-dependent analyses of the bacterial community in the phycosphere of cyanobloom-forming *Microcystis aeruginosa*. *Sci Rep, 9*(1): 1-13.

Kim, S., Kang, I., Seo, J.-H., & Cho, J.-C. (2019b). Culturing the ubiquitous freshwater actinobacterial acI lineage by supplying a biochemical 'helper' catalase. *ISME J, 13*: 2252-2263.

Kleinman, P. J., Srinivasan, M., Dell, C. J., Schmidt, J. P., Sharpley, A. N., & Bryant, R. B. (2006). Role of rainfall intensity and hydrology in nutrient transport via surface runoff. *J Environ Qual, 35*(4): 1248-1259.

Knoll, A. H. (2003). The geological consequences of evolution. *Geobiology, 1*(1): 3-14.

Korshunov, S. S., & Imlay, J. A. (2002). A potential role for periplasmic superoxide dismutase in blocking the penetration of external superoxide into the cytosol of Gram-negative bacteria. *Mol Microbiol, 43*(1): 95-106.

Li, Y., Chen, J.-a., Zhao, Q., Pu, C., Qiu, Z., Zhang, R., & Shu, W. (2011). A cross-sectional investigation of chronic exposure to microcystin in relationship to childhood liver damage in the Three Gorges Reservoir Region, China. *Environ Health Perspect, 119*(10): 1483-1488.

Lin, L., Shan, K., Xiong, Q., Zhou, Q., Li, L., Gan, N., & Song, L. (2018). The ecological risks of hydrogen peroxide as a cyanocide: its effect on the community structure of bacterioplankton. *J Oceanol Limnol, 36*(6): 2231-2242.

Liu, H., Nolla, H. A., & Campbell, L. (1997). *Prochlorococcus* growth rate and contribution to primary production in the equatorial and subtropical North Pacific Ocean. *Aquat Microb Ecol, 12*(1): 39-47.

Long, B. M., Jones, G. J., & Orr, P. T. (2001). Cellular microcystin content in N-limited *Microcystis aeruginosa* can be predicted from growth rate. *Appl Environ Microbiol, 67*(1): 278-283.

Louati, I., Pascault, N., Debroas, D., Bernard, C., Humbert, J.-F., & Leloup, J. (2015). Structural diversity of bacterial communities associated with bloom-forming freshwater cyanobacteria differs according to the cyanobacterial genus. *PloS one, 10*(11): e0140614.

Lusty, M. W., & Gobler, C. J. (2020). The Efficacy of Hydrogen Peroxide in Mitigating Cyanobacterial Blooms and Altering Microbial Communities across Four Lakes in NY, USA. *Toxins, 12*(7): 428.

Ma, L., Calfee, B. C., Morris, J. J., Johnson, Z. I., & Zinser, E. R. (2018). Degradation of hydrogen peroxide at the ocean's surface: the influence of the microbial community on the realized thermal niche of *Prochlorococcus*. *ISME J, 12*(2): 473-484.

Martin-Luna, B., Sevilla, E., Hernandez, J. A., Bes, M. T., Fillat, M. F., & Peleato, M. L. (2006). Fur from *Microcystis aeruginosa* binds in vitro promoter regions of the microcystin biosynthesis gene cluster. *Phytochemistry, 67*(9): 876-881.

Matthijs, H. C., Visser, P. M., Reeze, B., Meeuse, J., Slot, P. C., Wijn, G. *et al.* (2012). Selective suppression of harmful cyanobacteria in an entire lake with hydrogen peroxide. *Water Res, 46*(5): 1460-1472.

McGowan, S., Leavitt, P. R., Hall, R. I., Anderson, N. J., Jeppesen, E., & Odgaard, B. V. (2005). Controls of algal abundance and community composition during ecosystem state change. *Ecology, 86*(8): 2200-2211.

Meissner, S., Fastner, J., & Dittmann, E. (2013). Microcystin production revisited: conjugate formation makes a major contribution. *Environ Microbiol, 15*(6): 1810-1820.

Meissner, S., Steinhauser, D., & Dittmann, E. (2015). Metabolomic analysis indicates a pivotal role of the hepatotoxin microcystin in high light adaptation of *Microcystis*. *Environ Microbiol, 17*(5): 1497-1509.

Meiβner, K., Dittmann, E., & Börner, T. (1996). Toxic and non-toxic strains of the cyanobacterium *Microcystis aeruginosa* contain sequences homologous to peptide synthetase genes. *FEMS Microbiol Lett, 135*(2-3): 295-303.

Michalak, A. M., Anderson, E. J., Beletsky, D., Boland, S., Bosch, N. S., Bridgeman, T. B. *et al.* (2013). Record-setting algal bloom in Lake Erie caused by agricultural and meteorological trends consistent with expected future conditions. *Proc Natl Acad Sci, 110*(16): 6448-6452.

Mishra, S., & Imlay, J. (2012). Why do bacteria use so many enzymes to scavenge hydrogen peroxide? *Arch Biochem Biophys, 525*(2): 145-160.

Modig, H., & Ólafsson, E. (1998). Responses of Baltic benthic invertebrates to hypoxic events. *Journal of Experimental Marine Biology and Ecology, 229*(1): 133-148.

Morris, J. J., Kirkegaard, R., Szul, M. J., Johnson, Z. I., & Zinser, E. R. (2008). Facilitation of robust growth of *Prochlorococcus* colonies and dilute liquid cultures by "helper" heterotrophic bacteria. *Appl Environ Microbiol, 74*(14): 4530-4534.

Morris, J. J., Johnson, Z. I., Szul, M. J., Keller, M., & Zinser, E. R. (2011). Dependence of the cyanobacterium *Prochlorococcus* on hydrogen peroxide scavenging microbes for growth at the ocean's surface. *PloS one, 6*(2): e16805.

Morris, J. J., Lenski, R. E., & Zinser, E. R. (2012). The Black Queen Hypothesis: evolution of dependencies through adaptive gene loss. *MBio, 3*(2): e00036-00012.

Morris, J. J., Johnson, Z. I., Wilhelm, S. W., & Zinser, E. R. (2016). Diel regulation of hydrogen peroxide defenses by open ocean microbial communities. *J Plankton Res, 38*(4): 1103-1114.

Neilan, B. A., Pearson, L. A., Muenchhoff, J., Moffitt, M. C., & Dittmann, E. (2013). Environmental conditions that influence toxin biosynthesis in cyanobacteria. *Environ Microbiol, 15*(5): 1239-1253.

Ohlendieck, U., Stuhr, A., & Siegmund, H. (2000). Nitrogen fixation by diazotrophic cyanobacteria in the Baltic Sea and transfer of the newly fixed nitrogen to picoplankton organisms. *J Mar Syst, 25*(3-4): 213-219.

Olokotum, M., Mitroi, V., Troussellier, M., Semyalo, R., Bernard, C., Montuelle, B. *et al.* (2020). A review of the socioecological causes and consequences of cyanobacterial blooms in Lake Victoria. *Harmful Algae, 96*: 101829.

Orr, P. T., & Jones, G. J. (1998). Relationship between microcystin production and cell division rates in nitrogen-limited Microcystis aeruginosa cultures. *Limnol Oceanogr, 43*(7): 1604-1614.

Ostrowski, M., Cavicchioli, R., Blaauw, M., & Gottschal, J. C. (2001). Specific Growth Rate Plays a Critical Role in Hydrogen Peroxide Resistance of the Marine Oligotrophic Ultramicrobacterium *Sphingomonas alaskensis* Strain RB2256. *Appl Environ Microbiol, 67*(3): 1292-1299.

Paerl, H., Otten, T., & Kudela, R. (2018). Mitigating the expansion of harmful algal blooms across the freshwater-to-marine continuum. *Environ Sci Technol, 52*(10): 5519-5529.

Paerl, H. W., Tucker, J., & Bland, P. T. (1983). Carotenoid enhancement and its role in maintaining blue-green algal (*Microcystis aeruginosa*) surface blooms. *Limnol Oceanogr, 28*(5): 847-857.

Paerl, H. W., & Huisman, J. (2009). Climate change: a catalyst for global expansion of harmful cyanobacterial blooms. *Environ Microbiol Rep, 1*(1): 27-37.

Paerl, H. W., & Otten, T. G. (2013). Blooms bite the hand that feeds them. *Science, 342*(6157): 433-434.

Paerl, H. W., Scott, J. T., McCarthy, M. J., Newell, S. E., Gardner, W. S., Havens, K. E. *et al.* (2016). It takes two to tango: When and where dual nutrient (N & P) reductions are

needed to protect lakes and downstream ecosystems. *Environ Sci Technol, 50*(20): 10805-10813.

Paerl, H. W. (2018). Why does N-limitation persist in the world's marine waters? *Mar Chem*.

Paerl, H. W., & Barnard, M. A. (2020). Mitigating the global expansion of harmful cyanobacterial blooms: Moving targets in a human-and climatically-altered world. *Harmful Algae, 96*(101845).

Parveen, B., Ravet, V., Djediat, C., Mary, I., Quiblier, C., Debroas, D., & Humbert, J. F. (2013). Bacterial communities associated with *Microcystis* colonies differ from free-living communities living in the same ecosystem. *Environ Microbiol Rep, 5*(5): 716-724.

Passardi, F., Zamocky, M., Favet, J., Jakopitsch, C., Penel, C., Obinger, C., & Dunand, C. (2007). Phylogenetic distribution of catalase-peroxidases: are there patches of order in chaos? *Gene, 397*(1): 101-113.

Perelman, A., Uzan, A., Hacohen, D., & Schwarz, R. (2003). Oxidative stress in *Synechococcus* sp. strain PCC 7942: various mechanisms for H_2O_2 detoxification with different physiological roles. *J Bacteriol, 185*(12): 3654-3660.

Pérez-Carrascal, O. M., Tromas, N., Terrat, Y., Moreno, E., Giani, A., Marques, L. C. B. *et al.* (2020). Single-colony sequencing reveals phylosymbiosis, co-phylogeny, and horizontal gene transfer between the cyanobacterium *Microcystis* and its microbiome. *bioRxiv*.

Piel, T., Sandrini, G., White, E., Xu, T., Schuurmans, J. M., Huisman, J., & Visser, P. M. (2020). Suppressing Cyanobacteria with Hydrogen Peroxide Is More Effective at High Light Intensities. *Toxins, 12*(18): 2-20. doi:10.3390/toxins12010018

Qin, B., Zhu, G., Gao, G., Zhang, Y., Li, W., Paerl, H. W., & Carmichael, W. W. (2010). A drinking water crisis in Lake Taihu, China: linkage to climatic variability and lake management. *Environ Manage, 45*(1): 105-112.

Rantala, A., Fewer, D. P., Hisbergues, M., Rouhiainen, L., Vaitomaa, J., Börner, T., & Sivonen, K. (2004). Phylogenetic evidence for the early evolution of microcystin synthesis. *Proc Natl Acad Sci, 101*(2): 568-573.

Rao, Y. R., Howell, T., Watson, S. B., & Abernethy, S. (2014). On hypoxia and fish kills along the north shore of Lake Erie. *J Great Lakes Res, 40*(1): 187-191.

Reichwaldt, E. S., & Ghadouani, A. (2012). Effects of rainfall patterns on toxic cyanobacterial blooms in a changing climate: between simplistic scenarios and complex dynamics. *Water Res, 46*(5): 1372-1393.

Roegner, A. F., Brena, B., González-Sapienza, G., & Puschner, B. (2014). Microcystins in potable surface waters: toxic effects and removal strategies. *J Appl Toxicol, 34*(5): 441-457.

Rose, A. L., & Waite, T. D. (2006). Role of superoxide in the photochemical reduction of iron in seawater. *Geochim Cosmochim Acta, 70*(15): 3869-3882.

Sagert, S., & Schubert, H. (2000). Acclimation of *Palmaria palmata* (Rhodophyta) to light intensity: comparison between artificial and natural light fields. *J Phycol, 36*(6): 1119-1128.

Scavia, D., DePinto, J. V., & Bertani, I. (2016). A multi-model approach to evaluating target phosphorus loads for Lake Erie. *J Great Lakes Res, 42*(6): 1139-1150.

Schatz, D., Keren, Y., Vardi, A., Sukenik, A., Carmeli, S., Börner, T. *et al.* (2007). Towards clarification of the biological role of microcystins, a family of cyanobacterial toxins. *Environ Microbiol, 9*(4): 965-970.

Scheffer, M., Hosper, S. H., Meijer, M. L., Moss, B., & Jeppesen, E. (1993). Alternative equilibria in shallow lakes. *Trends Ecol Evol, 8*(8): 275-279.

Schindler, D. W. (1974). Eutrophication and recovery in experimental lakes: implications for lake management. *Science, 184*(4139): 897-899.

Schindler, D. W., Hecky, R. E., Findlay, D., Stainton, M., Parker, B., Paterson, M. *et al.* (2008). Eutrophication of lakes cannot be controlled by reducing nitrogen input: results of a 37-year whole-ecosystem experiment. *Proc Natl Acad Sci, 105*(32): 11254-11258.

Schuurmans, J. M., Brinkmann, B. W., Makower, A. K., Dittmann, E., Huisman, J., & Matthijs, H. C. (2018). Microcystin interferes with defense against high oxidative stress in harmful cyanobacteria. *Harmful Algae, 78*: 47-55.

Seaver, L. C., & Imlay, J. A. (2001). Hydrogen peroxide fluxes and compartmentalization inside growing *Escherichia coli*. *J Bacteriol, 183*(24): 7182-7189.

Seyedsayamdost, M. R., Case, R. J., Kolter, R., & Clardy, J. (2011). The Jekyll-and-Hyde chemistry of *Phaeobacter gallaeciensis*. *Nat Chem, 3*(4): 331-335. Retrieved from https://www.nature.com/articles/nchem.1002.pdf

Seymour, J. R., Amin, S. A., Raina, J.-B., & Stocker, R. (2017). Zooming in on the phycosphere: the ecological interface for phytoplankton-bacteria interactions. *Nat Microbiol, 2*(17065): 1-12. doi:10.1038/nmicrobiol.2017.65

Sinha, E., Michalak, A., & Balaji, V. (2017). Eutrophication will increase during the 21st century as a result of precipitation changes. *Science, 357*(6349): 405-408.

Sison-Mangus, M. P., Jiang, S., Tran, K. N., & Kudela, R. M. (2014). Host-specific adaptation governs the interaction of the marine diatom, *Pseudo-nitzschia* and their microbiota. *ISME J, 8*(1): 63-76.

Sivonen, K. (1990). Effects of light, temperature, nitrate, orthophosphate, and bacteria on growth of and hepatotoxin production by *Oscillatoria agardhii* strains. *Appl Environ Microbiol, 56*(9): 2658-2666.

Smith, R. B., Bass, B., Sawyer, D., Depew, D., & Watson, S. B. (2019). Estimating the economic costs of algal blooms in the Canadian Lake Erie Basin. *Harmful algae, 87*: 101624.

Spoof, L., & Catherine, A. (2016). Appendix 3: Tables of microcystins and nodularins. In J. Meriluoto, L. Spoof, & G. A. Codd (Eds.), *Handbook of cyanobacterial monitoring and cyanotoxin analysis* (pp. 526-537): John Wiley & Sons, Ltd.

Steffen, M. M., Belisle, B. S., Watson, S. B., Boyer, G. L., & Wilhelm, S. W. (2014). Status, causes and controls of cyanobacterial blooms in Lake Erie. *J Great Lakes Res, 40*(2): 215-225.

Steffen, M. M., Davis, T. W., McKay, R. M. L., Bullerjahn, G. S., Krausfeldt, L. E., Stough, J. M. *et al.* (2017). Ecophysiological Examination of the Lake Erie *Microcystis* Bloom in 2014: Linkages between Biology and the Water Supply Shutdown of Toledo, OH. *Environ Sci Technol, 51*(12): 6745-6755.

Stewart, I., Seawright, A. A., & Shaw, G. R. (2008). Cyanobacterial poisoning in livestock, wild mammals, and birds — an overview. In *Cyanobacterial Harmful Algal Blooms: State of the Science and Research Needs* (pp. 613-637): Springer.

Svirčev, Z., Krstič, S., Miladinov-Mikov, M., Baltič, V., & Vidovič, M. (2009). Freshwater cyanobacterial blooms and primary liver cancer epidemiological studies in Serbia. *J Environ Sci Health C, 27*(1): 36-55.

Taranu, Z. E., Gregory-Eaves, I., Leavitt, P. R., Bunting, L., Buchaca, T., Catalan, J. *et al.* (2015). Acceleration of cyanobacterial dominance in north temperate-subarctic lakes during the Anthropocene. *Ecol Lett, 18*(4): 375-384.

Thomas, M. K., & Litchman, E. (2016). Effects of temperature and nitrogen availability on the growth of invasive and native cyanobacteria. *Hydrobiologia, 763*(1): 357-369.

Tillett, D., Dittmann, E., Erhard, M., von Döhren, H., Börner, T., & Neilan, B. A. (2000). Structural organization of microcystin biosynthesis in *Microcystis aeruginosa* PCC7806: an integrated peptide–polyketide synthetase system. *Chem Biol, 7*(10): 753-764.

Vaitomaa, J., Rantala, A., Halinen, K., Rouhiainen, L., Tallberg, P., Mokelke, L., & Sivonen, K. (2003). Quantitative real-time PCR for determination of microcystin synthetase E copy numbers for *Microcystis* and *Anabaena* in lakes. *Appl Environ Microbiol, 69*(12): 7289-7297.

Van Mooy, B. A., Hmelo, L. R., Sofen, L. E., Campagna, S. R., May, A. L., Dyhrman, S. T. *et al.* (2012). Quorum sensing control of phosphorus acquisition in *Trichodesmium* consortia. *ISME J, 6*(2): 422-429.

Vézie, C., Rapala, J., Vaitomaa, J., Seitsonen, J., & Sivonen, K. (2002). Effect of nitrogen and phosphorus on growth of toxic and nontoxic *Microcystis* strains and on intracellular microcystin concentrations. *Microb Ecol, 43*(4): 443-454.

Voelker, B. M., Sedlak, D. L., & Zafiriou, O. C. (2000). Chemistry of superoxide radical in seawater: Reactions with organic Cu complexes. *Environ Sci Technol, 34*(6): 1036-1042.

Walsby, A. E., Hayes, P. K., Boje, R., & Stal, L. J. (1997). The selective advantage of buoyancy provided by gas vesicles for planktonic cyanobacteria in the Baltic Sea. *New Phytol, 136*(3): 407-417.

Watson, S. B., Miller, C., Arhonditsis, G., Boyer, G. L., Carmichael, W., Charlton, M. N. *et al.* (2016). The re-eutrophication of Lake Erie: harmful algal blooms and hypoxia. *Harmful Algae, 56*: 44-66.

Weinbauer, M. G., & Suttle, C. A. (1999). Lysogeny and prophage induction in coastal and offshore bacterial communities. *Aquat Microb Ecol, 18*(3): 217-225.

Worm, J., & Søndergaard, M. (1998). Dynamics of heterotrophic bacteria attached to *Microcystis* spp.(Cyanobacteria). *Aquat Microb Ecol, 14*(1): 19-28.

Xenopoulos, M. A., & Bird, D. F. (1997). Effect of acute exposure to hydrogen peroxide on the production of phytoplankton and bacterioplankton in a mesohumic lake. *Photochem Photobiol, 66*(4): 471-478.

Young, F. M., Thomson, C., Metcalf, J. S., Lucocq, J. M., & Codd, G. A. (2005). Immunogold localisation of microcystins in cryosectioned cells of *Microcystis*. *J Struct Biol, 151*(2): 208-214.

Zafiriou, O. (1990). Chemistry of superoxide ion-radical (O_2^-) in seawater. I. pK_{asw}^*(HOO) and uncatalyzed dismutation kinetics studied by pulse radiolysis. *Mar Chem, 30*: 31-43.

Zhu, C.-M., Zhang, J.-Y., Guan, R., Hale, L., Chen, N., Li, M. *et al.* (2019). Alternate succession of aggregate-forming cyanobacterial genera correlated with their attached bacteria by co-pathways. *Sci Total Environ, 688*: 867-879.

Zilliges, Y., Kehr, J.-C., Meissner, S., Ishida, K., Mikkat, S., Hagemann, M. *et al.* (2011). The cyanobacterial hepatotoxin microcystin binds to proteins and increases the fitness of *Microcystis* under oxidative stress conditions. *PloS one, 6*(3): e17615.

Zinser, E. R. (2018a). Cross-protection from hydrogen peroxide by helper microbes: the impacts on the cyanobacterium *Prochlorococcus* and other beneficiaries in marine communities. *Environ Microbiol Rep, 10*(4): 399-411.

Zinser, E. R. (2018b). The microbial contribution to reactive oxygen species dynamics in marine ecosystems. *Environ Microbiol Rep, 10*(4): 412-427.

Chapter 2 Heterotrophic Bacteria Dominate Catalase Expression During *Microcystis* Blooms

2.1 Abstract

In the oligotrophic oceans, key autotrophs depend on "helper" bacteria to reduce oxidative stress from hydrogen peroxide (H_2O_2) in the extracellular environment. H_2O_2 is also a ubiquitous stressor in freshwaters, but the effects of H_2O_2 on autotrophs and their interactions with bacteria is less well understood in freshwaters. Naturally occurring H_2O_2 in freshwater systems is proposed to impact the proportion of microcystin-producing (toxic) and non-microcystin-producing (nontoxic) *Microcystis* in blooms, which determines toxin concentrations and human health impacts. However, how different strains of *Microcystis* respond to naturally occurring H_2O_2 concentrations and the microbes responsible for H_2O_2 decomposition in freshwater cyanobacterial blooms are unknown. To address these knowledge gaps, we used metagenomics and metatranscriptomics to track the presence and expression of genes for H_2O_2 decomposition by microbes during the 2014 western Lake Erie cyanobacterial bloom. We found that *katG*, encoding the key enzyme for decomposing extracellular H_2O_2, was absent in most *Microcystis* cells, and that *katG* expression was dominated by heterotrophic bacteria. The H_2O_2 scavenger pyruvate was added to axenic *Microcystis* cultures to assess how exogenous H_2O_2 decomposition impacts the growth of toxic and nontoxic *Microcystis* strains. Pyruvate significantly improved growth rates of one toxic strain while other toxic and nontoxic strains were unaffected. These results indicate that heterotrophic bacteria play a key role in H_2O_2 decomposition in *Microcystis* blooms and suggest that this activity may affect the fitness of some

Microcystis strains and thus the strain composition of *Microcystis* blooms, but not along a toxic versus nontoxic dichotomy.

2.2 Introduction

Interactions between microorganisms are pervasive in aquatic ecosystems, with potentially far-reaching implications for system productivity, the cycling of nutrients, and the toxin production of harmful algal blooms (Seymour *et al.*, 2017). The importance of interactions between microorganisms is illustrated by the detoxification of hydrogen peroxide (H_2O_2). H_2O_2 is a ubiquitous oxidative stressor on microorganisms in natural waters (Imlay, 2003; Latifi *et al.*, 2009; Imlay, 2019) that can shape microbial community composition and function (Morris, 2015; Mas *et al.*, 2016; Zinser, 2018b). In oligotrophic marine environments, dominant primary producers such as *Prochlorococcus,* heterotrophs such as *Pelagibacter* (SAR11), and nitrifiers such as ammonia-oxidizing Thaumarchaeota lack enzymatic defense against H_2O_2 and cannot grow in the presence of H_2O_2 concentrations typical of natural waters (concentrations between 200 nM to ~1 μM) unless associated with organisms that produce catalases to detoxify the H_2O_2 (Morris *et al.*, 2008; Scanlan *et al.*, 2009; Morris *et al.*, 2011; Kim *et al.*, 2016; Zinser, 2018b; Bayer *et al.*, 2019). Because H_2O_2 rapidly diffuses across membranes (Seaver & Imlay, 2001a), decomposition of H_2O_2 by catalase and peroxidase enzymes produced by these heterotrophic "helpers" reduces environmental H_2O_2 concentrations to tolerable levels and provides community-wide protection to the sensitive "beneficiaries" (Morris *et al.*, 2008; Scanlan *et al.*, 2009; Morris *et al.*, 2012; Kim *et al.*, 2016; Bayer *et al.*, 2019). As long as some "helper" bacteria maintain low environmental H_2O_2 levels, other microbes can lose catalase genes in order to conserve resources in the nutrient-scarce open ocean (Morris *et al.*, 2012; Morris, 2015).

In eutrophic systems, H_2O_2 has been implicated as a potential factor influencing the toxin concentrations of cyanobacterial harmful algal blooms (CHABs) (Paerl & Otten, 2013), which are a growing worldwide threat to freshwater ecosystems and associated ecosystem services, including drinking water supplies (Paerl & Paul, 2012; Roegner *et al.*, 2014; Huisman *et al.*, 2018). Globally, freshwater CHABs are often dominated by *Microcystis* spp. that can produce microcystins, which are a class of potent liver toxins (Harke *et al.*, 2016). Microcystins have been shown to increase the resistance of *Microcystis* to H_2O_2 by binding and protecting proteins from oxidative damage (Zilliges *et al.*, 2011), leading to the hypothesis that transiently high concentrations of H_2O_2 in the water column may favor microcystin-producing ("toxic") strains of *Microcystis* over non-microcystin-producing ("nontoxic") strains (Paerl & Otten, 2013). Indeed, through photochemical reduction of O_2 by chromophoric dissolved organic matter and aerobic microbial metabolisms, H_2O_2 often reaches high concentrations in freshwaters (Cooper *et al.*, 1989; Häkkinen *et al.*, 2004; Marsico *et al.*, 2015) that can have negative effects on cyanobacterial growth (Morris *et al.*, 2008; Morris *et al.*, 2011; Zilliges *et al.*, 2011; Ma *et al.*, 2018). The highest concentrations of H_2O_2 in Lake Erie CHABs occur during bloom phases with high microcystin concentrations (Cory *et al.*, 2016; Cory *et al.*, 2017), supporting the idea that high H_2O_2 concentrations favor the proliferation of toxic *Microcystis* strains. Some laboratory experiments in cell culture also support this hypothesis by showing that H_2O_2 disproportionately inhibits the growth of nontoxic *Microcystis* strains (Dziallas & Grossart, 2011). However, a more recent study also suggested the opposite, that microcystin interferes with the *Microcystis* defense against H_2O_2 (Schuurmans *et al.*, 2018).

These contrasting conclusions on the role of H_2O_2 on *Microcystis* strains may be due to differences in H_2O_2 exposure of the cells in the lab or field. For example, laboratory studies of

cell cultures generally have not measured background concentrations of H_2O_2 in the growth medium (Dziallas & Grossart, 2011; Zilliges *et al.*, 2011). Without such H_2O_2 quantification, the effect of H_2O_2 on the growth of *Microcystis* strains remains uncertain. In addition, most studies to date have measured the response of *Microcystis* to single, large doses of H_2O_2 that exceed natural concentrations by 3-6 orders of magnitude, but are typical for doses of H_2O_2 used to control CHABs (Ding *et al.*, 2012; Mikula *et al.*, 2012; Lürling *et al.*, 2014; Gao *et al.*, 2015; Schuurmans *et al.*, 2018; Daniel *et al.*, 2019; Kim *et al.*, 2019a; Piel *et al.*, 2020). Thus, the responses of different *Microcystis* strains to naturally occurring H_2O_2 concentrations are unknown.

Despite the hypothesized role of H_2O_2 in influencing *Microcystis* population dynamics, the microbes responsible for H_2O_2 decomposition in eutrophic systems or during CHABs have not been studied. The distribution of catalase and peroxidase genes in *Microcystis* mirrors that of *Prochlorococcus* and ammonia-oxidizing archaea in that *Microcystis* lacks catalases and heme peroxidases but has multiple peroxiredoxin genes, suggesting that it may benefit from H_2O_2 decomposition by other community members (Kim *et al.*, 2019a). Such interactions could potentially improve the fitness of *Microcystis* strains more sensitive to H_2O_2, thus influencing the relative proportions of *Microcystis* strains in the environment and, by extension, microcystin concentrations during blooms. However, there are currently no data showing the impacts of community wide H_2O_2 detoxification on *Microcystis* growth at naturally occurring H_2O_2 concentrations.

Here, the following research questions are addressed: 1) What is the impact of H_2O_2 on the growth of various toxic and nontoxic *Microcystis* strains? 2) Which genes encoding proteins that detoxify H_2O_2 are expressed in *Microcystis* bloom communities, and how does the expression of

these genes relate to the proportion of toxic and nontoxic *Microcystis* strains? 3) Which community members express H_2O_2 detoxification genes? We analyzed the relative abundance of toxic and nontoxic *Microcystis* populations and the expression of genes encoding enzymes that are responsible for H_2O_2 decay in aquatic ecosystems (catalases and peroxidases) (Moffett & Zafiriou, 1990; Zinser, 2018a) during the 2014 western Lake Erie *Microcystis* bloom, which led to a drinking water ban for the city of Toledo (Steffen *et al.*, 2017). Our results show that catalase transcripts are dominated by heterotrophic bacteria, but that only some cultured *Microcystis* strains benefit from an H_2O_2 scavenger, suggesting that the impact of catalase activity from heterotrophic bacteria on *Microcystis* growth varies between strains and thus may impact *in situ Microcystis* strain and species composition.

2.3 Results

2.3.1 Dynamics in Pigments, Microcystin Concentrations, Toxic Microcystis Abundance, and H_2O_2

Changes in concentrations of H_2O_2, pigments, and microcystin concentrations at three stations (two nearshore and one offshore, Figure S 2.1) during the 2014 western Lake Erie CHAB show that the cyanobacteria bloom more heavily impacted nearshore stations (WE2 and WE12) than the offshore station (WE4, Figure 2.1). This pattern is discussed in detail in Cory et al. (Cory *et al.*, 2016) and Berry et al. (Berry *et al.*, 2017). Phycocyanin (a pigment found in cyanobacteria) and chlorophyll *a* were highly correlated at all stations, confirming that the blooms were dominated by cyanobacteria (Berry *et al.*, 2017). Phycocyanin concentrations peaked in early August, with a second peak in late September at the nearshore stations (Figure 2.1A).

Concentrations of particulate microcystins correlated with phycocyanin in July through early August, with the highest microcystin concentrations occurring at the nearshore stations

(Figures 2.1A, 2.1B). Biomass captured in the >100 μm particle size fraction is responsible for most of the microcystin production and contains 93-99% of the total *Microcystis* biomass during *Microcystis* blooms (Kurmayer *et al.*, 2003; Chaffin *et al.*, 2011). In this particle size fraction, peak microcystin concentrations at the nearshore stations coincided with a *Microcystis* population that was dominated by toxic strains (60-100% of the *Microcystis* cells; Figure 2.1B) as determined by the ratio of the relative abundance of the *mcyD* and 16S rRNA genes in *Microcystis* (Davis *et al.*, 2009). At the nearshore stations, microcystin concentrations decreased substantially starting in mid-August and remained low, despite high cyanobacterial biomass and *Microcystis* abundance (Berry *et al.*, 2017). This reduced microcystin concentration coincided with a *Microcystis* population shift towards dominance of nontoxic cells (25% to less than 1% of *Microcystis* cells contained *mcyD*; Figures 2.1B, S 2.2). At nearshore station WE2, a smaller second peak in microcystin concentrations and the percentage of toxic *Microcystis* occurred with the increase in phycocyanin in September, although microcystin concentrations and percent toxic *Microcystis* were lower than levels detected in July. At the offshore station, microcystins and phycocyanin concentrations both decreased, suggesting a decline in overall *Microcystis* abundance rather than a compositional change in the population as observed at the nearshore stations (Figure 2.1B). Consistent with this interpretation, *Microcystis* 16S copy number was substantially lower at the offshore station (Table 2.1) and the proportion of toxic *Microcystis* cells (40-60%) was more consistent over time than at the nearshore stations (Figure 2.1B).

The percentage of toxic *Microcystis* determined by metagenomic mapping and qPCR generally agreed for samples analyzed by both methods (Figure 2.1B). The exception was a sample collected on August 25th at nearshore station WE12, where the qPCR ratio was higher than that determined by the metagenome by 85% (Figure 2.1B). However, the overall trends in

the percentage of toxic *Microcystis* agree between the two methods. The percentage of toxic *Microcystis* determined in the metagenomic samples was generally higher when normalizing to the single-copy housekeeping gene *rpoB* rather than the 16S rRNA gene (Figure S 2.2). This is likely due to the presence of multiple 16S rRNA gene copies per *Microcystis* cell, which would inflate estimates of total *Microcystis* cells. Indeed, many bacteria have multiple rRNA operons (Roller *et al.*, 2016), and all closed *Microcystis* genomes in the NCBI database (Pruitt *et al.*, 2007) have two 16S rRNA gene copies (Table 2.2). However, estimates of percent toxic *Microcystis* were not doubled when normalizing to *rpoB* (Figure S 2.2), suggesting variable 16S rRNA gene copy numbers between *Microcystis* strains. This prevents accurately correcting estimates of percent toxic *Microcystis* in the qPCR. However, the overall trends in percent toxic *Microcystis* agree when normalizing to both *rpoB* and the 16S rRNA gene in the metagenomic samples (Figure S 2.2), which suggests that the trends in the qPCR data are robust despite potentially underestimating the percentage of toxic *Microcystis*.

H_2O_2 ranged from 20 ± 36 to 590 ± 4 nM (standard error (SE) of technical replicates) in the surface waters of Lake Erie over the course of the bloom (Cory *et al.*, 2016; Cory *et al.*, 2017). The highest concentrations of H_2O_2 were observed at each nearshore station in late July, the week prior to peaks in both microcystins and pigments. At nearshore station WE2, a smaller second peak in H_2O_2 (260 ± 51 nM) coincided with the smaller, second peak in microcystin concentrations in September. Peaks in H_2O_2 concentrations at offshore station WE4 were lower than those nearshore, reaching a maximum of 210 ± 94 nM (Figure 2.1C).

2.3.2 Catalase and Peroxidase Gene Abundance and Taxonomy

Metagenomes were obtained from the > 0.22 μm size fraction (targeting the whole microbial community) and from the > 100 μm particle-attached fraction (targeting *Microcystis*

colonies, microplankton and attached bacteria). Assembly and binning of sequence reads produced metagenome-assembled genomes (MAGs) of the dominant cyanobacteria (*Microcystis, Synechococcus, Pseudanabaena,* and *Anabaena/Dolichospermum*) and other bacteria (Supplemental File 1 & 2), allowing us to assess the distribution and expression of genes encoding catalases and peroxidases among specific microbial taxa during the bloom (see methods). The taxonomy of MAGs that contained the following genes were determined, and the abundances of these genes were quantified: monofunctional heme catalase (*katE*), catalase-peroxidase (*katG*), manganese catalase (MnCAT), ascorbate peroxidase (APX), and alkyl hydroperoxide reductase subunit C (*ahpC*) (Table 2.3, see methods). These genes were targeted because there is biochemical evidence supporting that they scavenge H_2O_2 as a defense against H_2O_2 toxicity (Mishra & Imlay, 2012), or use of H_2O_2 as a terminal electron acceptor, as in the case of *ccpA* (Khademian & Imlay, 2017). We targeted APX because it can be abundant in marine metatranscriptomes (Morris *et al.*, 2016). Of these genes, the periplasmic *katG* has the primary function to decompose *extracellular* H_2O_2 while the primary role of cytoplasmic *ahpC* is to decompose *intracellularly* produced H_2O_2 and organic peroxides (Tichy & Vermaas, 1999; Seaver & Imlay, 2001a; Seaver & Imlay, 2001b; Perelman *et al.*, 2003; Cosgrove *et al.*, 2007). However, both can compensate for each other under certain physiological conditions (Tichy & Vermaas, 1999; Seaver & Imlay, 2001b; Cosgrove *et al.*, 2007).

Genes encoding the catalase-peroxidase *katG* and the peroxiredoxin *ahpC* had the highest abundance relative to bacterial *rpoB* (Figures 2.1C, S 2.3). In most cases, *ahpC* was the more abundant of the two genes. *KatG* was equally abundant in both the particle-attached and total community size fractions, while *ahpC* had a higher relative abundance in the particle-attached fraction (Figures 2.1C, S 2.3). Neither *katG* nor *ahpC* gene relative abundances were

significantly correlated with microcystins, pigment, or H_2O_2 concentrations in the lake ($p > 0.05$, ANOVA). Genes encoding *katE* and *ccpA* were consistently present at low relative abundance and comprised an average of 0.06 ± 0.08 % and 3 ± 1 % (95% confidence interval on mean of all samples) of the total catalase and peroxidase reads, respectively. However, the cytochrome *c* peroxidases share many structural similarities with the methylamine-utilization protein *mauG*, and many of the genes identified as *ccpA* hit equally well to *mauG* genes in NCBI and paperBLAST (Price & Arkin, 2017). Therefore, their role in H_2O_2 decomposition is uncertain, and we report their abundances separately in Figure S 2.4. Genes encoding MnCat and APX were rare. MnCat was only detectable in the September 29th sample from the particle size fraction, while APX comprised 0 - 0.4 % of the total catalase and peroxidase reads.

In the metagenomes of the particle-attached fraction from all bloom samples, *katG* was present in MAGs from diverse groups of bacteria (Figure S 2.5). Of the genes that could be assigned a taxonomy in the particle-attached fraction, *katG* from *Microcystis*, *Phenylobacterium,* Flammeovirgaceae bins 42896 C11 and 42896 E20, Burkholderiaceae bin 53603 E6, and Rhodobacteraceae bin 49625 E6 were most abundant in the particle-attached fraction (Figure S 2.5). *Microcystis katG* comprised 0.1 – 47 % (mean 14 ± 8 %) of the total *katG* reads in the particle-attached metagenomes whenever present. While no *katG* from a single organism dominated, *Microcystis* was often the most abundant of the *katG* that could be assigned a taxonomy in the metagenomes (Figure S5). The ratio of *Microcystis katG* to *Microcystis* housekeeping genes (estimated by dividing *Microcystis katG* reads to *Microcystis rpoB* and *recA* reads) ranged from 0.4 – 26 % (mean 9 ± 4 %) but was relatively consistent throughout most of the bloom season in the particle-attached fraction (Figure S6). The fraction of the *Microcystis* population with *katG* was consistent whether normalizing to *rpoB* or *recA,* with the exception of

two samples (8 July nearshore and 4 August offshore total community samples). *KatG* was also detected in *Cyanobium/Synechococcus* MAGs, another abundant cyanobacterium in the bloom (Berry *et al.*, 2017), but was only occasionally present at low relative abundance (Table 2.3, Figure S 2.5). *AhpC* from *Microcystis* was also the most abundant in the particle-attached fraction; however, *Microcystis* accounted for a larger proportion of the total *ahpC* reads than for *katG* (2 – 80 %, mean 40 ± 15 %, Figure S8). The percentage of the *Microcystis* population with *ahpC* ranged from 60 – 140 % (mean 100 ± 15 %).

The dominant organisms with *katG* and *ahpC* in the whole community were distinct from those in the particle-attached fraction. In the whole community, *katG* from *Candidatus Fonsibacter* and unclassified Chloroflexi had the highest abundance consistently throughout the bloom (Figure S 2.5), but they were largely absent in the particle-attached fraction. Similarly, the most abundant taxa containing *katG* in the particle-attached fraction were rare in the total community fraction, with *Microcystis* only accounting for < 0.01 – 0.5 % of the total *katG* in this size fraction (mean 0.2 ± 0.1 %) (Figure S 2.5). The fraction of the *Microcystis* population with *katG* was highest in early July and decreased into the fall (Figure S 2.6). *Microcystis ahpC* was also less abundant in the whole community fraction, comprising an average of 8 ± 6 % of the total *ahpC* reads (Figure S 2.8). No single organism dominated *ahpC* reads in the total community, but, in addition to *Microcystis, ahpC* from *Clavibacter,* Pelagibacterales, *Limnohabitans,* and *Candidatus Methylopumilus* were the most abundant (Figure S8).

To confirm the presence/absence of catalases in dominant bloom-forming cyanobacteria, we surveyed publicly available cyanobacterial genomes (Figure S 2.9, see methods). The genomes of *Microcystis, Anabaena/Dolichospermum, Pseudanabaena, Planktothrix,* and *Synechococcus* were targeted because they are regular members of cyanobacterial blooms,

especially in Lake Erie and its surrounding bays and tributaries, with *Microcystis* and *Planktothrix* being the dominant potential microcystin-producers (Ouellette *et al.*, 2006; Davis *et al.*, 2014; Davis *et al.*, 2015; Berry *et al.*, 2017). We also compared the distribution of catalases and peroxidases in these genomes to that of *Prochlorococcus*, a dominant cyanobacterium in the open ocean that has been shown to be dependent on other community members for detoxification of H_2O_2 (Morris *et al.*, 2011). In total, 343 public genomes were analyzed, and 99 % of the genomes had a gene encoding the peroxiredoxin *ahpC*. Nearly all of the 150 *Microcystis* genomes lack genes encoding catalases, with the exception of four *Microcystis* genomes that have *katG*. Similarly, catalase genes were absent in all published *Prochlorococcus* genomes, consistent with previous genomic studies and the low tolerance of H_2O_2 by this genus (Morris *et al.*, 2008; Bernroitner *et al.*, 2009). In contrast, 57 % of *Pseudanabaena* genomes possess catalases, while 43% of *Anabaena-Dolichospermum* genomes contain manganese catalases. All the *Anabaena-Dolichospermum* genomes lack heme catalases. A majority of *Synechococcus* genomes have either or both *katE* and *katG*, which is consistent with previous observations of the relatively high H_2O_2 tolerance of this genus as well as previous intergenomic comparisons (Bernroitner *et al.*, 2009; Morris *et al.*, 2011).

2.3.3 Catalase and Peroxidase Transcript Abundance

To focus on *Microcystis* and their particle-associated bacteria, metatranscriptomes were obtained from the particle-attached fraction. *AhpC* transcripts were the most abundant, followed by *katG*. While no significant correlations were observed between the relative abundance of *ahpC* or *katG* with H_2O_2, phycocyanin, or chlorophyll *a* concentration throughout the entire field season ($p > 0.05$, F-test), qualitative patterns were observed with H_2O_2. The highest *katG* transcript relative abundance was observed at the nearshore station WE12, shortly after the

highest concentrations of H_2O_2 and during peak bloom microcystin concentrations (Figure 2.2). The highest *ahpC* transcript abundance occurred in late August and September when concentrations of H_2O_2 were within the lower range of measured concentrations (Figures 2.3A, 2.3B). Genes encoding *katE* were sporadically expressed at low levels. Genes encoding *ccpA*/*mauG* were expressed at low levels with no apparent patterns with any bloom parameters, with the exception of one sample collected on 23 September at WE12, where expression of *ccpA/mauG* relative to total bacterial *rpoB* expression was closer to the lower range of *katG* transcript abundance. No transcripts for MnCAT encoding genes were found in the metatranscriptomes (Figure 2.2). APX transcripts were rare (< 0.01 relative to bacterial *rpoB*) or absent in most samples. The exception was one sample collected on 8 September at the offshore station and 23 September at nearshore station WE12. On 8 September, unbinned APX was the most abundant gene in the metatranscriptome apart from *ahpC*, but on 23 September unbinned APX was 10-fold less abundant than *katG* (Figure 2.2).

Heterotrophic bacteria dominated *katG* transcripts in all samples (Figure 2.4A), while *Microcystis* dominated the *ahpC* transcript pool in five of the seven samples (Figure 2.3C). *Microcystis katG* transcripts comprised only 0 - 17 % (mean 7 ± 3 %) of the total *katG* reads, despite being the most abundant in the metagenome, and only accounted for 0.8 % of *katG* reads during peak *katG* expression. Highly abundant *katG* transcripts were often from organisms present at low relative abundance in the metagenomic reads (Figure 2.4B). The most striking example of this result was observed on 4 August, when total *katG* transcript relative abundance was the highest; *katG* in *Paludibaculum* (Acidobacteria) and *Bryobacter* (Acidobacteria) comprised ~40% and ~6% of the total *katG* RNA reads, respectively (Figure 2.4B). *Bryobacter* and *Paludibaculum* comprised a lower proportion of the total *katG* transcripts in other samples,

but the relative abundance of transcripts from both organisms was consistently enriched relative to gene abundance when present. *KatG* expression by an uncultured Flammeovirgaceae (Bin 42896 E20, Bacteroidetes) was also a significant portion of total *katG* expression during peak *katG* expression (17.8 %), and was a major proportion of total *katG* transcripts for all dates, with the exception of 21 July. Throughout the bloom, *katG* transcripts from *Phenylobacterium* (Alphaproteobacteria) and Rhodobacteraceae (Alphaproteobacteria) were less abundant but present in nearly all samples except at the offshore station WE4, which lacked Rhodobacteraceae *katG* transcripts.

2.3.4 Axenic Culturing Experiments

To assess how bacterial cross-protection from natural H_2O_2 concentrations impacts the growth of toxic and nontoxic *Microcystis* strains, we grew axenic *Microcystis* cultures for 12-13 days in the presence and absence of sodium pyruvate, a rapid scavenger of H_2O_2 that is used to remove H_2O_2 in cell cultures (Kim *et al.*, 2016; Lopalco *et al.*, 2016; Kawasaki & Kamagata, 2017; Ma *et al.*, 2018). We found that one strain had a significant improvement in maximum specific growth rate (μ_{max}) when cultured with sodium pyruvate, while the remaining strains showed no differences in maximum specific growth rate (Figure 2.5). The potential benefit of sodium pyruvate for a *Microcystis* strain was unrelated to the presence or absence of the *mcy* gene cluster or catalase and peroxidase genes in its genome. Although there were slight increases in the cell densities of four strains when cultured with sodium pyruvate, final cell densities at the end of the experiment were not significantly different in the majority of strains when cultured with pyruvate ($p > 0.05$, Welch's T-test, Figure S 2.10). One strain had significantly lower mean final cell densities when cultured with sodium pyruvate ($p = 0.01102$, Welch's T-test, Figure S 2.10).

In the pyruvate treated cultures, H_2O_2 concentrations could not be quantified because pyruvate decayed the H_2O_2 standard 10-25 % during the flow injection analysis (Figure S 2.11, see methods). However, the rapid decay of the standard suggests that H_2O_2 concentrations were maintained at very low levels in the pyruvate treatments. The initial H_2O_2 concentrations of the control treatments ranged from 910 – 1330 nM (mean 1000 ± 148 nM, 95% confidence interval; Figure 2.6). In four strains, H_2O_2 concentrations subsequently declined to 170 ± 40 nM. Three strains did not decay H_2O_2 as efficiently; H_2O_2 concentrations in these cultures declined to 370 ± 70 nM. In sterile BG-11 2N media, H_2O_2 concentrations showed complex dynamics, decreasing to 580 ± 50 nM within 2 days and subsequently increasing to 1700 ± 100 nM; therefore, declines in H_2O_2 below ~580 nM were attributed to the presence of the strain.

2.4 Discussion

2.4.1 Microcystin Production Does not Determine the Response of a Microcystis Strain to an Exogenous H_2O_2 Scavenger

Variations in H_2O_2 concentrations have been hypothesized to impact the relative proportions of toxic and nontoxic *Microcystis* strains in the environment. However, there is conflicting evidence on whether the growth of toxic *Microcystis* is either less (Schuurmans *et al.*, 2018) or more (Dziallas & Grossart, 2011; Zilliges *et al.*, 2011) favored than nontoxic *Microcystis* when exposed to elevated H_2O_2 concentrations. The *Microcystis* strains tested here (3 naturally toxic, 3 naturally nontoxic, and 1 nontoxic mutant) showed different impacts of H_2O_2 on growth. The maximum growth rate of most strains was not significantly impacted by pyruvate, an external scavenger of H_2O_2, suggesting no fitness benefit from the removal of H_2O_2 from the growth medium (Figure 2.5). However, strain PCC 7806 (toxic) showed a significantly higher maximum growth rate when cultured with pyruvate (Figure 2.5), indicating that H_2O_2 in the growth media imposed oxidative stress on this strain despite its ability to decompose H_2O_2.

Reductions in PCC 7806 growth rate by H_2O_2 is consistent with other laboratory culture experiments with this strain that showed growth of PCC 7806 was inhibited by higher H_2O_2 concentrations than those used in this study (Schuurmans *et al.*, 2018). However, final maximum cell densities in this strain were not significantly higher when cultured with the H_2O_2 scavenger relative to controls (Figure S 2.10), suggesting that growth benefits of H_2O_2 removal were limited to when growth rates were highest. Such reduced growth rate may be important during competition with other *Microcystis* strains and phytoplankton taxa in communities.

The mutant strain of PCC 7806, incapable of microcystin biosynthesis (Dittmann *et al.*, 1997), did not display significantly different growth rates in the presence or absence of pyruvate as observed in the wild type strain (Figure 2.5), indicating that the environmentally relevant concentrations of H_2O_2 in the medium have no detectable effect on growth of the mutant. The lack of any effect of the H_2O_2 scavenger on the mutant suggests that it does not benefit from help decomposing H_2O_2. The lack of change in maximum growth rates with H_2O_2 exposure in the microcystin knockout mutant contrasts with the hypothesized protection provided by microcystins and with previous results showing higher growth impairments of H_2O_2 additions to the mutant strain when compared to the wildtype (Dziallas & Grossart, 2011; Zilliges *et al.*, 2011). However, the data are inconsistent with the idea that production of microcystins directly impairs the response of *Microcystis* to H_2O_2 (Schuurmans *et al.*, 2018), because growth rates in the wild-type and mutant are not significantly different when exposed to naturally relevant H_2O_2 concentrations, and both strains degraded H_2O_2 similarly (Figure 2.6).

In the absence of H_2O_2, wild type PCC 7806 had significantly higher maximum growth rates than the mutant strain (Figure 5, $p < 0.05$, Welch's two-sided T-test). This indicates that growth rates of the mutant strain of PCC 7806 are reduced compared to those of the wild-type

under these experimental conditions, but the reduced growth rates are unrelated to H_2O_2 exposure. This growth rate reduction may be related to other changes in the mutant due to the absence of microcystins. For example, previous studies have shown that the mutant PCC 7806 strain has an altered metabolome (Meissner *et al.*, 2015; Barchewitz *et al.*, 2019), proteome content (Dittmann *et al.*, 2001), assembly and subcellular localization of the RubisCO enzyme (Barchewitz *et al.*, 2019), and has higher relative expression of peroxiredoxins and other genes involved in oxidative stress response (Schuurmans *et al.*, 2018) when compared to the wild type. Such metabolic differences between the wild-type and mutant PCC 7806 may also explain how the two strains differ in whether or not they benefit from an exogenous H_2O_2 scavenger despite having similar growth rates in the presence of naturally occurring H_2O_2 concentrations. Furthermore, these differences in the effect of H_2O_2 scavengers may suggest that metabolic differences between *Microcystis* strains may lead to tradeoffs between growth rates when exposed to H_2O_2 and potential maximum growth rates under reduced H_2O_2 exposure. However, with the data and experimental design here, the mechanism of growth rate reduction in the mutant strain of PCC 7806 cannot be confirmed.

While cultivation with an H_2O_2 scavenger had different impacts on the growth of wild-type strain PCC 7806 and the nontoxic knockout mutant, other strains that varied in their ability to produce microcystin (2 toxic, 3 nontoxic), showed no significant differences in maximum growth rate when cultured with or without sodium pyruvate (Figure 2.5). All of the tested strains have *ahpC*, lack *katG*, and could degrade H_2O_2 in the growth medium (Figure 2.6), which suggests that the presence or absence of microcystin biosynthesis, catalases, and peroxidases alone does not determine whether or not a given strain will benefit from help decomposing H_2O_2.

Therefore, other traits must also determine the overall impact of H_2O_2 on the growth of a given *Microcystis* strain.

Several mechanisms could potentially explain the differences in the response of the *Microcystis* strains to H_2O_2. Previous studies with H_2O_2-sensitive *Nitrosopumilus* found that cell surface proteins rather than canonical H_2O_2 scavengers were differentially expressed based on H_2O_2 exposure, suggesting that alteration of the cell wall and membrane make it less permeable to H_2O_2 at higher concentrations (Bayer *et al.*, 2019). These findings suggest that differences in the cell surface structures of the *Microcystis* strains tested could explain their different responses to pyruvate. Supporting this hypothesis, *Microcystis* cells excrete exopolysaccharide that can degrade H_2O_2 (Gao *et al.*, 2015), and the exopolysaccharide composition varies between *Microcystis* strains (Forni *et al.*, 1997). However, how changes in exopolysaccharide chemistry impact H_2O_2 resistance in *Microcystis* have not been measured.

In addition, light intensity determines whether or not *Prochlorococcus* strains benefit from H_2O_2 decomposition by a "helper" bacterium (Morris *et al.*, 2011); some *Prochlorococcus* strains benefitted at low light intensity, while other strains benefitted at high light intensity. Deviation from optimal growth temperature also determines the toxicity of H_2O_2 to *Prochlorococcus* (Ma *et al.*, 2018). Therefore, *Microcystis* strains may only benefit from H_2O_2 removal at certain temperatures. Because the optimal growth temperatures of *Microcystis* strains vary (Xiao *et al.*, 2017; Bui *et al.*, 2018), the temperature at which a given strain becomes sensitive to H_2O_2 should also vary if the same temperature dependent response to H_2O_2 observed in *Prochlorococcus* also occurs in *Microcystis*. Some evidence suggests that nutrient limitation impacts the sensitivity of *Microcystis* to H_2O_2 (Sandrini *et al.*, 2020), so differences in the nutrient quotas between *Microcystis* strains may also create differences in H_2O_2 sensitivity under

different nutrient regimes. Finally, the sensitivity of a given strain to H_2O_2 may be determined by the susceptibility of its cellular components in addition to its mechanism for H_2O_2 decomposition. Some *Microcystis* strains may have more proteins in their proteomes that are sensitive to H_2O_2 damage, as H_2O_2 damage is limited to specific protein structures in the absence of free iron (Imlay, 2003). *Microcystis* proteomes do vary between strains (Alexova *et al.*, 2011), however the number and variation of H_2O_2 sensitive structures within *Microcystis* proteomes has not been measured.

2.4.2 The Ability of Microcystis to Degrade H_2O_2 Does not Preclude Benefit From an Exogenous H_2O_2 Scavenger

Bloom-forming cyanobacteria in eutrophic lakes may benefit from helper bacteria in a manner similar to *Prochlorococcus* in the oligotrophic oceans. The presence of alkyl hydroperoxide reductase (*ahpC*) and absence of catalases (*katG* and *katE*) in most published *Microcystis* genomes is the same as the case of some *Prochlorococcus* (Morris *et al.*, 2008; Morris *et al.*, 2011; Morris, 2015; Kim *et al.*, 2019a) and some species of Thaumarchaeota (Kim *et al.*, 2016; Bayer *et al.*, 2019), which are completely inhibited by sub-micromolar H_2O_2 concentrations. The presence of *ahpC* and the lack of *katG* in these marine organisms means that they must depend on other microorganisms to scavenge H_2O_2. In this study, we found that most *Microcystis* cells in Lake Erie blooms also lack *katG,* and that community *katG* expression is dominated by heterotrophic bacteria. However, in contrast to *Prochlorococcus* and some Thaumarchaeota, all of the *Microcystis* strains tested could degrade and tolerate H_2O_2 concentrations within the range of some of the highest concentrations observed in Lake Erie blooms (Cory *et al.*, 2016) and that inhibit *Prochlorococcus* (Morris *et al.*, 2011).

Despite degrading H_2O_2 in the growth medium, one *Microcystis* strain had significantly higher maximum growth rates when cultured with sodium pyruvate (Figure 2.5). Because the

cultured *Microcystis* strains in our experiment all lack *katG*, the decomposition of H_2O_2 is presumably from *ahpC*, which is known to compensate for the loss of *katG* in some bacteria at the sub-micromolar concentrations typically observed in natural waters (Tichy & Vermaas, 1999; Seaver & Imlay, 2001b; Perelman *et al.*, 2003; Cosgrove *et al.*, 2007). These results support that AhpC protein can scavenge extracellular H_2O_2 for some organisms and suggest that *Microcystis* can lower environmental H_2O_2 to some extent even without *katG*. However, the presence of an exogenous H_2O_2 scavenger still improved growth rates in one *Microcystis* strain, suggesting that H_2O_2 caused stress despite H_2O_2 degradation by the cells. Growth impairment from H_2O_2 despite its decomposition has also been observed in other *Microcystis* strains (Daniel *et al.*, 2019). This may indicate that a portion of H_2O_2 decay comes from reactions that damage cellular structures, or that there is a fitness cost to H_2O_2 decomposition in some *Microcystis* strains. Indeed, AhpC activity requires thioredoxin or glutathione and NADH as electron donors (Nogoceke *et al.*, 1997; Tichy & Vermaas, 1999; Hosoya-Matsuda *et al.*, 2005; Mishra & Imlay, 2012); thus, H_2O_2 decomposition in *Microcystis* may impart a cost to growth in conditions under which electron donors limit growth. For example, the form and concentration of nitrogen in the environment changes the intracellular concentrations of NAD(P)H in *Microcystis* (Steffen et al., 2014) which may impact H_2O_2 decomposition by AhpC. Additionally, if the environmental conditions that cause electron donor limitation vary between *Microcystis* strains, electron donor availability could be another factor that determines differences in the sensitivity of H_2O_2 between strains.

Given that the toxicity of H_2O_2 toward cyanobacteria is dependent on temperature (Ma *et al.*, 2018), nutrient availability (Robles-Rengel *et al.*, 2019; Sandrini *et al.*, 2020), and light wavelength (Piel *et al.*, 2020), and that H_2O_2 concentrations during the growth phase of our cultures (Figure 2.6) were lower than peak H_2O_2 concentrations during *Microcystis* blooms

(Figure 2.1) we cannot rule out that H_2O_2 may inhibit growth of the *Microcystis* strains tested here more broadly or severely than shown by our lab experiments. Ultimately, additional experiments over a range of culturing conditions are required to fully characterize the response of each *Microcystis* strain to H_2O_2. We also note that H_2O_2 present at high concentrations in culturing media (Morris & Zinser, 2013; Kawasaki & Kamagata, 2017), exerts strong bias on the cultivation of bacteria from the environment (Tanaka *et al.*, 2014), and may even inhibit successful cultivation of some cyanobacterial strains but not others (Morris *et al.*, 2008; Morris *et al.*, 2011). Thus, cultured strains of *Microcystis*, especially those that have been in culture for years like those used here, may have higher tolerance of H_2O_2 than natural populations. Unfortunately, axenic cultures of *Microcystis* strains from Lake Erie are not currently available to our knowledge.

2.4.3 The Relative Contribution of Attached Bacteria to H_2O_2 Decomposition in Phytoplankton Assemblages

Metatranscriptomics revealed that *Microcystis katG* comprised very few total *katG* transcripts (<1 % of total transcripts during peak expression) in the particle-attached fraction, and a small fraction of *Microcystis* cells in Lake Erie had *katG*. The most highly expressed *katG* genes in the particle-attached fraction were from heterotrophic bacteria, suggesting that they may be responsible for most of the H_2O_2 degradation in phytoplankton assemblages and thus provide protection from H_2O_2 to other community members. However, *katG* expression may not necessarily be indicative of efficient H_2O_2 decomposition in some bacteria because some organisms have *katG* with low specific activity and catalytic efficiency (k_{cat}/K_m) and still require helpers in order to tolerate naturally-relevant H_2O_2 concentrations (Kim *et al.*, 2019b). As the organisms responsible for the majority of *katG* expression are uncultured, and no axenic isolates of *Microcystis* with *katG* are currently available, it is unclear how *katG* expression of these

organisms relates to rates of H_2O_2 decomposition in the environment. However, *Microcystis* colonies are encapsulated by exopolysaccharide slimes (Plude *et al.*, 1991; Forni *et al.*, 1997; Gao *et al.*, 2015) that can impart resistance to oxidative stress (Gao *et al.*, 2015) and are colonized by heterotrophic bacteria (Worm & Søndergaard, 1998; Brunberg, 1999; Parveen *et al.*, 2013). Thus, bacterial cells attached to the colony perimeter are likely exposed to more exogenous H_2O_2 than *Microcystis* cells in the colony interior, perhaps making them larger sinks for H_2O_2 than *Microcystis* cells in the colony interior. However, cultivation of the *katG*-containing organisms and measurements of their H_2O_2 decomposition rates are required to understand their roles in H_2O_2 decomposition during cyanobacterial blooms.

2.5 Conclusions

In summary, the *Microcystis* strains tested here all decompose H_2O_2, yet differ in their sensitivity to H_2O_2. One strain of *Microcystis* benefited from the presence of a scavenger of H_2O_2. Whether a strain benefitted or was unaffected by an exogenous H_2O_2 scavenger was not related to its ability to produce microcystins. This suggests that H_2O_2 is a stressor during natural bloom development that can impair growth of some *Microcystis* strains *in situ* but does not necessarily favor toxic over nontoxic *Microcystis*. There is some evidence that the sensitivity of a given strain may change with environmental conditions, suggesting whether or not H_2O_2 impairs the growth of a given strain may change with environmental conditions.

H_2O_2 concentrations are determined by the relative strength of its sources and sinks in the environment, and the main sink for H_2O_2 in aquatic environments are microbial catalases (Moffett & Zafiriou, 1990). Thus, taken together with the differential sensitivity of *Microcystis* strains toward H_2O_2, the drawdown of H_2O_2 via catalase production by heterotrophic bacteria may shape temporal changes in the relative proportion of *Microcystis* strains. When

heterotrophic catalase and peroxidase activity is low and H_2O_2 production rates are high, H_2O_2 would accumulate to higher concentrations and may give a competitive advantage to *Microcystis* strains that are more resistant to H_2O_2 (Figure 2.7). Indeed, we observed a succession of strains during the 2014 bloom event, reflected by a transition in the proportion of *Microcystis* containing the *mcy* genes (Figure 2.1B). While our results do not support the idea that H_2O_2 favors microcystin-producing strains *per se*, it is possible that the strains present during the early phase of the bloom dominated, in part, due to a higher resistance to the elevated H_2O_2 concentrations. How changes in H_2O_2 production and decay influence *Microcystis* strain composition remains to be tested directly, and how the sensitivity of *Microcystis* strains to H_2O_2 varies with environmental conditions is unknown. However, the interactive effect of stress from H_2O_2 with other factors such as temperature, light intensity, and nutrient form and availability could perhaps explain strain succession patterns during bloom events and may improve our understanding of the widely observed transition (65) from high to low microcystin concentrations during early to late phases of *Microcystis* blooms.

2.6 Methods

2.6.1 Field Sampling and Water Chemistry

Weekly sampling was conducted at three locations in the western basin of Lake Erie in conjunction with the NOAA Great Lakes Environmental Research Laboratory long-term HABs monitoring program. These sites correspond to NOAA stations WE2, WE12, and WE4 (Figure S 2.1). The average depth at nearshore stations WE2 and WE12 is 4.8 ± 0.1 m and 5.9 ± 0.1 m, respectively, while the average depth at offshore station WE4 is 7.8 ± 0.1 m. Water chemistry measurements (pH, conductivity, nutrients) are detailed elsewhere (Berry *et al.*, 2017). At all stations, pH ranged from 7.80-9.29 (mean=8.55 ± 0.06), conductivity ranged from 175.5-314.6

µS/cm (mean=250.6 ± 5.2 µS/cm), water temperature ranged from 25.0 °C (mid-August) to 12.5 °C (mid-October) with a mean of 20.6 ± 0.6 °C from June-October. Total N as nitrite/nitrate and ammonium ranged from 0-1.1 mg/L and 0.1-36.4 µg/L while soluble reactive phosphorus and total phosphorus ranged from 0.04-21.2 and 9.9-132.7 µg/L, respectively. These values are typical of Lake Erie (Winter *et al.*, 2015; Gobler *et al.*, 2016) and other eutrophic lakes impacted by CHABs (Jensen & Andersen, 1992; Paerl *et al.*, 2011). Water quality data were collected by the NOAA Great Lakes Research Lab as are available under NCEI accession 0187718.

In-situ hyperspectral light profiles were collected at each sampling site using a Sea-Bird HyperPro II© (Sea-Brid Scientific, Philomath, OR) profiler equipped with up- and down-facing HyperOCR radiometers measuring wavelengths 348 – 801 nm (bin size = 3.3 nm), plus an identical fixed surface radiometer to record sky conditions. The profiler was deployed on the sunny side of the vessel and allowed to free-fall through the water column to avoid the vessel shadow. A duplicate cast was collected as soon as the profiler was returned to the surface to capture identical light conditions. Profiles were collected after the vessel had been drifting without power for several minutes, so the water column through which the profiler traveled had as little artificial disturbance as possible. Light profile data were processed using ProSoft (Sea-Brid Scientific, Philomath, OR). Output spectral light intensities in power units (W/m^2) were converted to photon flux units (µmol photons/m^2/s) by dividing by the photon energy, which was calculated using the following equation:

$$E_{ph} = hc/\lambda$$

where h is Planck's constant (6.626×10^{-34} J/s), c is the speed of light (per m), and λ is the wavelength of light in meters. Total photon flux was calculated as the sum of the spectral photon fluxes from a single Sea-Bird cast.

Microbial samples were obtained from a 20L depth-integrated water sample collected from the surface to 1 meter above the lake bottom. To collect the whole community fraction, 150 mL of depth-integrated sample was filtered onto a 47 mm Millipore Express® PLUS membrane with a 0.22 μm pore size, placed into 2 mL cyrovials with 1 mL RNAlater, and kept on ice during cruise transit. To collect the colony-associated fraction, 2 L of depth-integrated sample was filtered through a 100 μm pore-size mesh, and the retentate was backwashed into a falcon tube using altered BG-11 medium (Table 2.4). RNAlater was added in a 2:1 ratio with the backwash. The backwash was filtered onto a 1.6 μm pore size Glass Fiber Filter with a syringe. After filtration, all filters were placed into 2 mL cryovials with 1mL of RNAlater and kept on ice during cruise transit. Upon arrival at the lab, all filters were frozen at -80 °C until extraction. H_2O_2, chlorophyll, and microcystin measurements were conducted as described in (Cory *et al.*, 2016), and phycocyanin measurements were conducted as described in (Berry *et al.*, 2017).

2.6.2 DNA and RNA Extraction and Sequencing

Filters with collected biomass were thawed, folded with biomass facing inwards, and rinsed with sterile PBS to remove RNAlater preservative. Filters were incubated in 100 μL Qiagen ATL tissue lysis buffer, 300 μL Qiagen AL lysis buffer, and 30 μL proteinase K for 1 hour at 56 °C on a rotisserie (Qiagen, Hilden, Germany). Cells were further lysed by vortexing in this lysis buffer for 10 minutes. Lysates were homogenized using a Qiashredder column, and DNA was purified from the filtrate using the Qiagen DNeasy Blood and Tissue kit according to the manufacturer's standard protocol. The quantity and quality of DNA in each sample were determined using a NanoDrop Lite Spectrophotometer (Thermo Scientific). DNA extracts were frozen at -80 °C until analysis.

For RNA extraction, the filters were incubated in 600 µL Qiagen RLT+ buffer and 6 µL β-mercaptoethanol for 90 minutes on a rotisserie. The filters were then vortexed for 10 minutes and homogenized using a Qiashredder column. RNA was purified from the homogenized solution using the RNeasy kit according to the manufacturer's standard protocol.

All sequencing was performed at the University of Michigan Sequencing Core. Paired-end DNA sequencing (2 x 125) was conducted on Illumina Hiseq 2000 with V4 chemistry reagents with "low-input prep" using the Rubicon ThruPlex kit. RNA single-read sequencing (1 x 50) was performed on Illumina HiSeq 2000 with V4 chemistry reagents. Before sequencing, RNA libraries were prepared with a 50/50 mix of plant and bacterial ribo-zero kits to remove rRNA sequences. In total, 23 metagenomes and 7 metatranscriptomes were sequenced, and the 7 metatranscriptomes were paired with 7 of the metagenomes collected at the same date and sampling location. Of these, 15 metagenomes are from the 100 µm fraction and 8 are from the total community fraction. All metatranscriptomes are from the 100 µm fraction.

2.6.3 qPCR and Toxic:nontoxic Microcystis Ratio

Two *Microcystis*-specific gene targets for qPCR were used during this study, the 16S rRNA gene and *mcyD* gene. Targeting the 16S rRNA gene allowed for quantification of the total *Microcystis* population. The *mcyD* gene is found within the microcystin synthetase gene operon, which is responsible for the production of microcystin and is only found in toxic strains of *Microcystis* (Tillett *et al.*, 2000). Quantitative polymerase chain reaction (qPCR) was executed using an Applied Biosystems 7500 Fast Instrument using TaqMan® labeled probes (Applied Biosystems) and Microcystis-specific *mcyD* and 16S rRNA primers (Table 2.5)(Kaebernick *et al.*, 2000; Rinta-Kanto *et al.*, 2005; Ouellette *et al.*, 2006). Standard curves for the *Microcystis* 16S rRNA and *mcyD* were composed using a double-stranded synthetic DNA construct (gBlock;

Integrated DNA Technologies, IA, USA) that can be tailored to contain any sequence of interest. The sequence tested was identical to the PCR product obtained from the qPCR process for the *Microcystis* 16S rRNA and *mcyD* genes. Ten-fold serial dilutions of the gBlock ranging in concentration from 10^2-10^8 copies were run in duplicate 25 µL reactions using the cycling conditions described below. For amplification of the 16S targets, the cycling conditions were 95 °C for 10 minutes, followed by 45 cycles of 95 °C for 15 sec and 60 °C for 1 minute. For amplification of the *mcyD* gene, the cycling conditions were 95 °C for 10 min, followed by 45 cycles of 95 °C for 15 sec, 50 °C for 1 min, and 60 °C for 1 min. For dates that we had a corresponding metagenomic sample, we also assessed the toxic:nontoxic *Microcystis* ratio by mapping quality-checked, dereplicated metagenomic reads to the *mcyD* and 16S rRNA gene sequences of the V4 region from all publicly available *Microcystis* genomes in the Integrated Microbial Genomes database (IMG) using the blastn function of the Basic Local Alignment Search Tool (BLAST, version 2.2.28+) (Altschul *et al.*, 1990). Because the 16S rRNA gene can be present in two identical copies in some strains of *Microcystis*, we also checked that the values for percent toxic *Microcystis* strains were similar when normalizing to the single-copy housekeeping gene *rpoB* in *Microcystis* rather than the 16S rRNA gene. All blast hits against the reference genes were filtered to exclude hits with a bit score less than 50 and an e-value greater than $1x10^{-5}$ for all genes using the postBlast.pl script. Reads were only counted if they had a percent identity of at least 99% for the 16S rRNA gene, 95% for *mcyD*, and 97% for *rpoB*. All final read counts for each gene target were normalized by the length of the reference gene.

2.6.4 Metagenomic Assembly

Metagenomic short reads from each sample were individually processed and assembled *de novo*. Before assembly, metagenomic short reads from each sample were dereplicated at

100% length and identity using a custom made dereplicate.pl script, and sequencing adaptors were removed with Scythe (https://github.com/vsbuffalo/scythe). Sickle was then used to remove low quality reads (Joshi & Fass, 2011), and the forward and reverse reads were interleaved using the custom script interleave.pl. The *de novo* assembly for each sample was constructed using IDBA-UD with the following parameters: min kmer = 55, max kmer = 115, kmer step size = 10 (Peng *et al.*, 2012).

Because the quality of the assembly of a genome from a metagenome can be reduced when its read coverage exceeds 20X (Hug *et al.*, 2016), we performed a subsampling approach to optimize *Microcystis* coverage, which could be as high as 1200X in some samples. *Microcystis* coverage in each sample was estimated by mapping the unprocessed reads to the complete *Microcystis aeruginosa* NIES-843 genome using the Burrows-Wheeler Aligner version 0.7.9a (Li & Durbin, 2009). Our results confirmed that the longest contigs containing *Microcystis* housekeeping genes were obtained when *Microcystis* coverage was between 20-35X. Therefore, for each sample in which the *Microcystis* coverage was greater than 35X, an additional *de novo* assembly was constructed by obtaining a randomized subset of the reads to normalize the *Microcystis* coverage to 35X using IDBA-UD with the following parameters: min kmer = 52, max kmer = 92, kmer step = 8 (Peng *et al.*, 2012). In total, 42 assemblies were constructed from the metagenomic reads.

To improve the assembly of lower abundance bacteria, combined-sample assemblies (co-assemblies) were generated with MEGAHIT (Li *et al.*, 2015) using kmin 21, kmax 141, and kmer step size of 12. We performed 3 co-assemblies in total: one from the two samples with highest *Paludibaculum* abundance (Aug-4 and Aug-25 particle metagenomes from WE12), another containing all the samples in which *Paludibaculum* was present (8 samples total), and

another with the same 8 samples, but the read kmer coverage was normalized to 20X prior to assembly with BBnorm in the BBtools package (Bushnell, 2018). Paired-end short reads were quality and adapter screened and dereplicated with BBtools prior to co-assembly (Bushnell, 2018). An additional single sample MEGAHIT assembly was constructed on the particle size fraction sample from August 4th at WE12 following the same pipeline.

2.6.5 Read Mapping, Contig Binning, and MAG Quality Assessment

The metagenomic read coverage of contigs in each assembly was obtained by mapping reads to their corresponding assembly using bowtie2 (Langmead & Salzberg, 2012). Differential coverage across samples was determined by iteratively mapping reads from each sample used in the assembly to the co-assembled contigs. Binning of contigs in single sample IDBA-UD assemblies was iteratively performed by clustering assembled contigs by the Euclidean distance of tetranucleotide frequencies and visualized in Databionics Emergent Self-Organizing Maps (ESOMs) (Dick *et al.*, 2009). Genome sequences of *Microcystis aeruginosa* NIES-843, *Rhizobiales* bacterium AUSA02, and *Brevundimonas subvibrioides* were included in all ESOM maps as reference genomes. Each sample received its own ESOM, but contigs generated from full and subsampled reads were binned together in the same ESOM map. For most 100 μm fraction samples, contigs greater than 5000 bp in length were split into 5000 bp pieces, while contigs below 2500 bp in length were not included in the binning process. For the total community fraction and the 100 μm sample from Sept. 29 at WE4, a contig size window of 4000-10,000 bp was used because the larger number of contigs above 2500 bp became computationally unmanageable.

In the co-assemblies, contigs were binned using a multi-algorithm binning approach. Contigs were binned using differential coverage and tetranucleotide frequencies in CONCOCCT

(Alneberg *et al.*, 2014) and Metabat2 (Kang *et al.*, 2019) and with tetranucleotide frequencies alone using VizBin (Laczny *et al.*, 2015) and ESOMs. The contig size window for ESOM was 4-10 kbp and 2.5-10 kbp for the other binners. The resulting redundant bin datasets from each assembly were dereplicated using DASTool (Sieber *et al.*, 2018). The single-sample MEGAHIT assembly was binned using the above co-assembly workflow. For this assembly, differential coverage was estimated by mapping reads from August 4th WE12 and August 25th WE12 to the contigs.

The completeness, contamination, and redundancy estimates of each genomic bin were generated using the lineage workflow in CheckM (Parks *et al.*, 2015). The bins from single sample IDBA-UD assemblies with contamination metrics greater than or equal to 5%, which is the established benchmark for a draft genome of low contamination (Parks *et al.*, 2015), were refined by plotting GC content versus the read coverage of all scaffolds within the target bin, and removing outlier contigs. Coverage and tetranucleotide frequencies of the co-assembly bins were visualized for manual refinement in Anvio (Eren *et al.*, 2015). Refined bins were reanalyzed using the lineage workflow in CheckM (Parks *et al.*, 2015). All bins with contamination scores greater than 5% after refinement were eliminated from downstream analysis. Contamination scores of the final bins were considered while ignoring the amount of contamination due to strain heterogeneity. Redundant marker genes were considered to be from closely related strains if their shared amino acid identity was greater than 90% (CheckM default). In total, 315 MAGs were generated with low contamination (< 5%), and varying levels of completeness (Supplemental File 1). This redundant bin dataset was dereplicated using dRep (Olm *et al.*, 2017) with 97 % ANI and 60 % alignment coverage cutoffs and skipping the MASH pre-clustering step. Only

MAGs with completeness above 75% were included in the final dereplicated MAG dataset, leaving a total of 136 MAGs (Supplemental File 2).

The taxonomy of each dereplicated bin was obtained with CheckM's tree qa function and GhoastKoala taxonomy annotations of gene calls (Kanehisa *et al.*, 2016). Taxonomic classification with these methods remained coarse in many cases, so EMIRGE was used to assemble 16S rRNA genes (Miller *et al.*, 2011), which were then assigned to bins by matching fragments of the 16S at the ends of contigs via the blastn function of the Basic Local Alignment Search Tool (BLAST, version 2.2.28+) (Altschul *et al.*, 1990). The mean insert size and accompanying standard deviation input used in the EMIRGE 16S assemblies were estimated from the mapping results of the raw metagenomic reads to their corresponding assembled contigs. The SILVA SSU 16S rRNA database version 128 was curated by the emirge_makedb.py script provided in the EMIRGE package then used as the reference in EMIRGE to map short reads for assembly (Pruesse *et al.*, 2007). The final assembled 16S rRNA sequences were compared to the original reference database via BLAST version 2.2.28+ and taxonomy was assigned with the Wang method (Wang *et al.*, 2007) in MOTHUR v. 1.43.0 (Schloss *et al.*, 2009). An EMIRGE sequence was only considered as belonging to a bin if the percent match to a bin 16S fragment covered greater than 10% of the assembled 16S rRNA gene, had a bit score of at least 50 and an E-value of at most $1x10^{-5}$, and did not conflict with taxonomy as determined by CheckM and GhostKoala. Final bin taxonomy was assigned using EMIRGE whenever available, otherwise the CheckM and GhostKoala taxonomy was used.

2.6.6 Gene Annotations and Abundance

Gene calls and functional annotations of metagenome assembled contigs were obtained using IMG annotation pipeline (Huntemann *et al.*, 2015). Genes of interest were obtained from

the IMG database by conducting a KEGG orthology search of bacterial genomes in the IMG online interface (Markowitz *et al.*, 2011). The following KEGG Orthology IDs were used to target our specific genes of interest: K03781 (*katE/katA/catB,* herein listed collectively as *katE*), K07217 (*katN/ydbDA/cotG/yjqC* herein listed collectively as MnCAT), K03782 (*katG*), K00428 (*ccpA/yhjA/mauG* herein listed collectively as *ccpA*), K03386 (*ahpC*), K00434 (ascorbate peroxidase, APX), K03043 (*rpoB*), and K03553 (*recA*). Custom BLAST databases were constructed from the gene calls with KEGG orthology annotations of interest if their final IMG annotation matched that of the KEGG Orthology ID. The taxonomy of genes was assigned to match the taxonomic assignments of the dRep bin cluster in which they were found. Unbinned genes were assigned a taxonomy if they had a ≥ 95% match to a protein in NCBI nr (as of October 17th, 2018) with blastx (Altschul *et al.*, 1990). All other unbinned genes were included as unassigned. Genes in the custom databases were sorted by gene length (longest to shortest) and clustered at 95 % identity with vsearch (Rognes *et al.*, 2016).

To determine the abundance of catalases and peroxidases in the metagenomes and metatranscriptomes, BBtool screened short reads were mapped to the assembled gene databases with BLAST version 2.2.31+ (Altschul *et al.*, 1990). The quality-screening pipeline for metatranscriptomic reads did not include a dereplication step. The alignments to the assembled genes were filtered to exclude hits with a percent identity less than 95 % and an e-value greater than $1x10^{-5}$ using the postBlast.pl script. To avoid double counting reads, only the best matches were counted for each read using the top5.pl script. Only read counts to genes with at least 70% AAI and alignment coverage to other proteins with the same functional annotation in the NCBI nr protein database with blastx version 2.2.31+ (Altschul *et al.*, 1990) were included. Because

more reads inherently map to longer genes, the read counts of each gene were normalized by gene length.

In order to correct for varying library and genome sizes between samples, the gene abundances were reported as ratios to the number of reads that mapped to a custom database of the single-copy housekeeping gene *rpoB*, encoding the beta-subunit of the bacterial RNA polymerase. BLAST mappings against *rpoB* were filtered and quality checked as described above for the catalase and peroxidase blasts. We chose to normalize to bacterial *rpoB* rather than total library size to reduce the impact of eukaryotic genomes on the abundance and expression values for the bacterial community. However, we checked the assumption that *rpoB* is constitutively expressed and a good normalization strategy by normalizing metatranscriptomic read counts via total library size, expressed as reads per kilobase of transcript per million mapped reads (RPKM). We found that the expression patterns were generally the same, with the exception of the two early samples that showed much lower gene expression overall due to the dominance of eukaryotic genomes (Figure S 2.12).

2.6.7 Culturing Experiments

The growth of seven axenic *Microcystis* cultures was assessed with and without the presence of 1 mM sodium pyruvate, a scavenger of extracellular H_2O_2 (Kim *et al.*, 2016; Ma *et al.*, 2018). Six strains were purchased axenic from the Pasteur Culture Collection of Cyanobacteria (PCC 7806, PCC 7806 ΔmcyB, PCC 7941, PCC 9806, PCC 9701, PCC 7005). Strain NIES 843 was generously provided by Dr. Steve Wilhelm at the University of Tennessee. The cultures were maintained at room temperature under cool white fluorescent lights (30-60 μmol photons/m^2/sec) in BG-11 2N, a variant of standard BG-11 media (Allen & Stanier, 1968) with the sodium nitrate concentration reduced to 2 mM. Axenicity was monitored by light

microscopy, DAPI fluorescence microscopy, and inoculating *Microcystis* cultures into LB and TSB media and monitoring for the development of turbidity after 3-4 weeks.

The experimental cultures were grown in 1 L glass pyrex bottles at 24.4 °C (average in July-August of 2014-2017) and 330 µmol photons/m^2/sec (average PAR intensity at 0.5 m depth in Lake Erie during July-August of 2017 as determined from approximately biweekly hyperspectral profiles) for 12-14 days in a Caron Plant Growth Chamber (model 7311-50, Caron Marietta, OH). The growth medium was BG-11 2N. The positions of the bottles were randomized to correct for potential differences in light intensity across incubator shelving. Cell densities and H_2O_2 concentrations were monitored every other day. Cell density was measured via cell counts under a compound microscope using a Reichert Bright-Line™ Hemacytometer (Hausser Scientific, Horsham, PA). Maximum growth rates were determined by taking the 1st derivative of a spline curve fit to the cell density data of each biological replicate (average R^2 = 0.994 ± 0.006, 95% confidence interval).

H_2O_2 concentration was measured using the chemiluminescent reaction of the conjugate base of hydrogen peroxide with 10-methyl-9-(*p*-formylphenyl)acridinium carboxylate trifluoromethanesulfonate in a FeLume flow-injection analysis (King *et al.*, 2007). Standard additions of a nominal 200 µM H_2O_2 solution were added to each sample to correct for matrix effects (final nominal concentrations of added standard were 0, 500, 750 nM). The concentration of the H_2O_2 standard solution was measured from its absorbance at 240 nm in a 5 cm quartz cuvette and the molar absorptivity of H_2O_2 (38.1 $M^{-1}s^{-1}$) (King *et al.*, 2007). A new standard solution was prepared from a 30% H_2O_2 stock solution on each day measurements were performed. Decay of the standard additions during the flow-injection analysis was used to confirm H_2O_2 degradation by sodium pyruvate treated samples. Signal decay was monitored by

taking 4 replicate injections of each sample, and the normalized signal decay was calculated as the difference in the peak integrals of the chemiluminescent signal in the first and final replicate injections divided by the peak integral of the first injection.

2.6.8 Scripts and Data Availability

All custom bioinformatics scripts and pipelines used in this study can be found on our github page: https://github.com/Geo-omics/scripts. All read datasets are publicly available in NCBI SRA under BioSample accession numbers: SAMN09102072-87. All metagenomic assemblies are submitted to IMG and publicly available (IMG assembly IDs: 3300005044-3300021599, 3300028428- 3300028430 and 3300034010). The R package growthrates v. 0.8.1 (https://github.com/tpetzoldt/growthrates) was used to calculate growth rates, and Welch's T-tests were computed with base R v. 4.0.2.

2.7 Figures and Tables

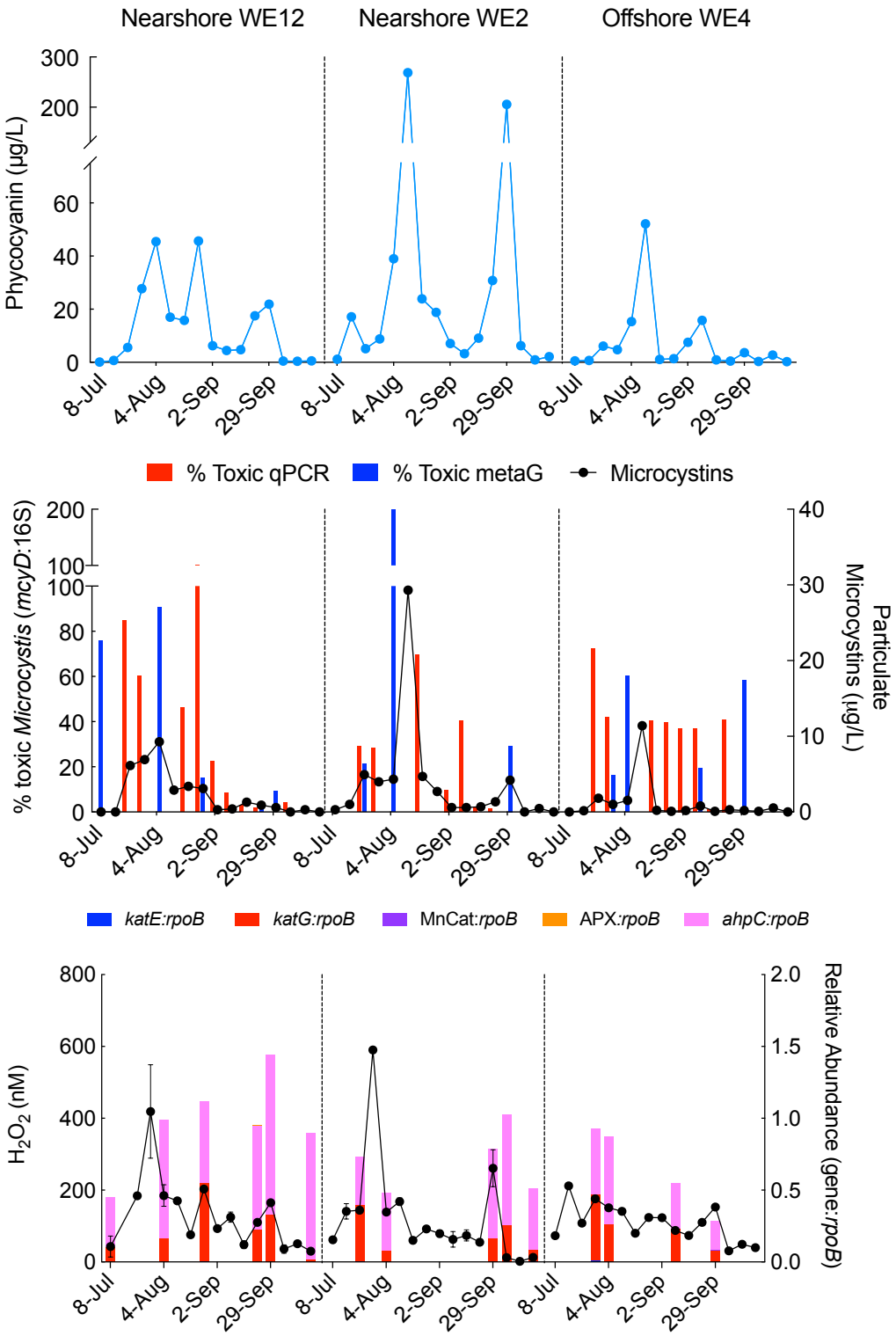

Figure 2.1: Temporal dynamics in algal pigments, toxic:nontoxic *Microcystis*, hydrogen peroxide, and catalase and peroxidase gene abundance in the 2014 western Lake Erie cyanobacterial bloom. Dotted lines separate data from each station. **A:** Changes in phycocyanin concentrations at each station. **B**: Percentage of *Microcystis* population containing the *mcyD* gene required for microcystin production as determined by qPCR (red) and BLAST against metagenomic reads (blue) at each station. BDL = below detection limit. **C**: Relative abundance of catalase and peroxidase genes from all organisms in Lake Erie metagenomes from the 100 µm particle size fraction at each station. Read counts in C are normalized to the length of the matching gene in the database and to the number of reads that mapped to bacterial *rpoB*, encoding the beta-subunit of RNA polymerases. Error bars on H_2O_2 concentrations show the standard error of technical replicates measurements (n=3).

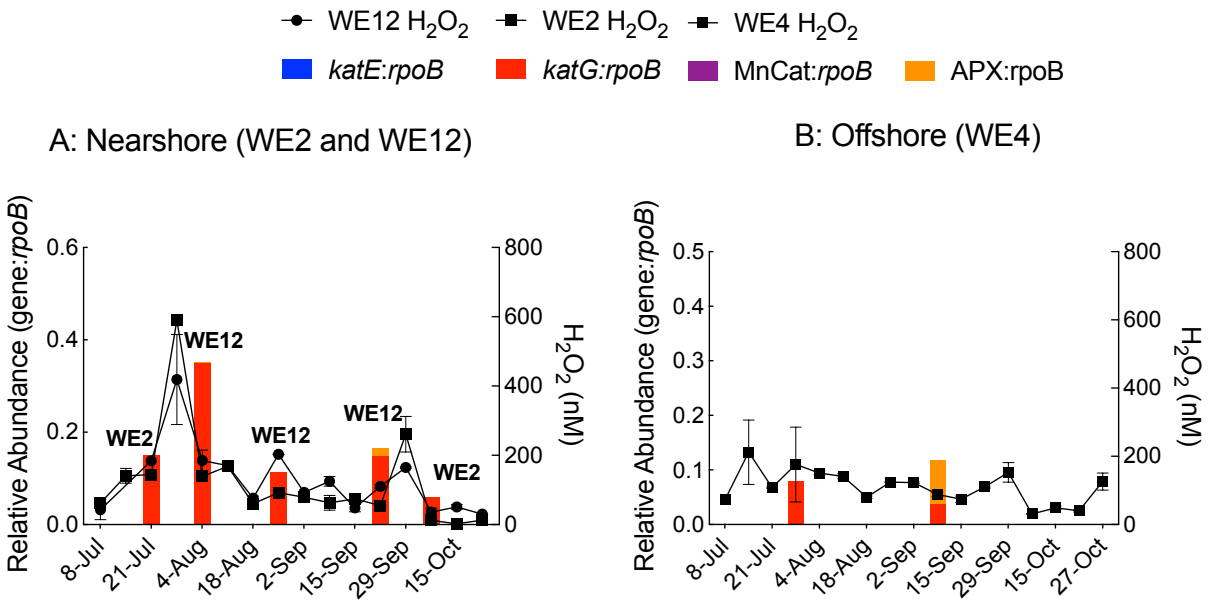

Figure 2.2: Temporal and spatial variation in the relative abundance of transcripts encoding catalases and peroxidases (excluding *ahpC*) in Lake Erie metatranscriptomes from the 100 µm particle size fraction collected during the 2014 western Lake Erie cyanobacterial bloom. Read counts were normalized to the length of each gene and to the number of reads that mapped to bacterial *rpoB*, encoding the beta-subunit of RNA polymerases. Error bars on H_2O_2 concentrations show the standard error of technical replicates measurements (n=3). **A:** Abundance of genes at nearshore stations WE2 and WE12. Square symbols show WE2 H_2O_2. Circles show WE12 H_2O_2. **B:** Abundance of genes at offshore station WE4.

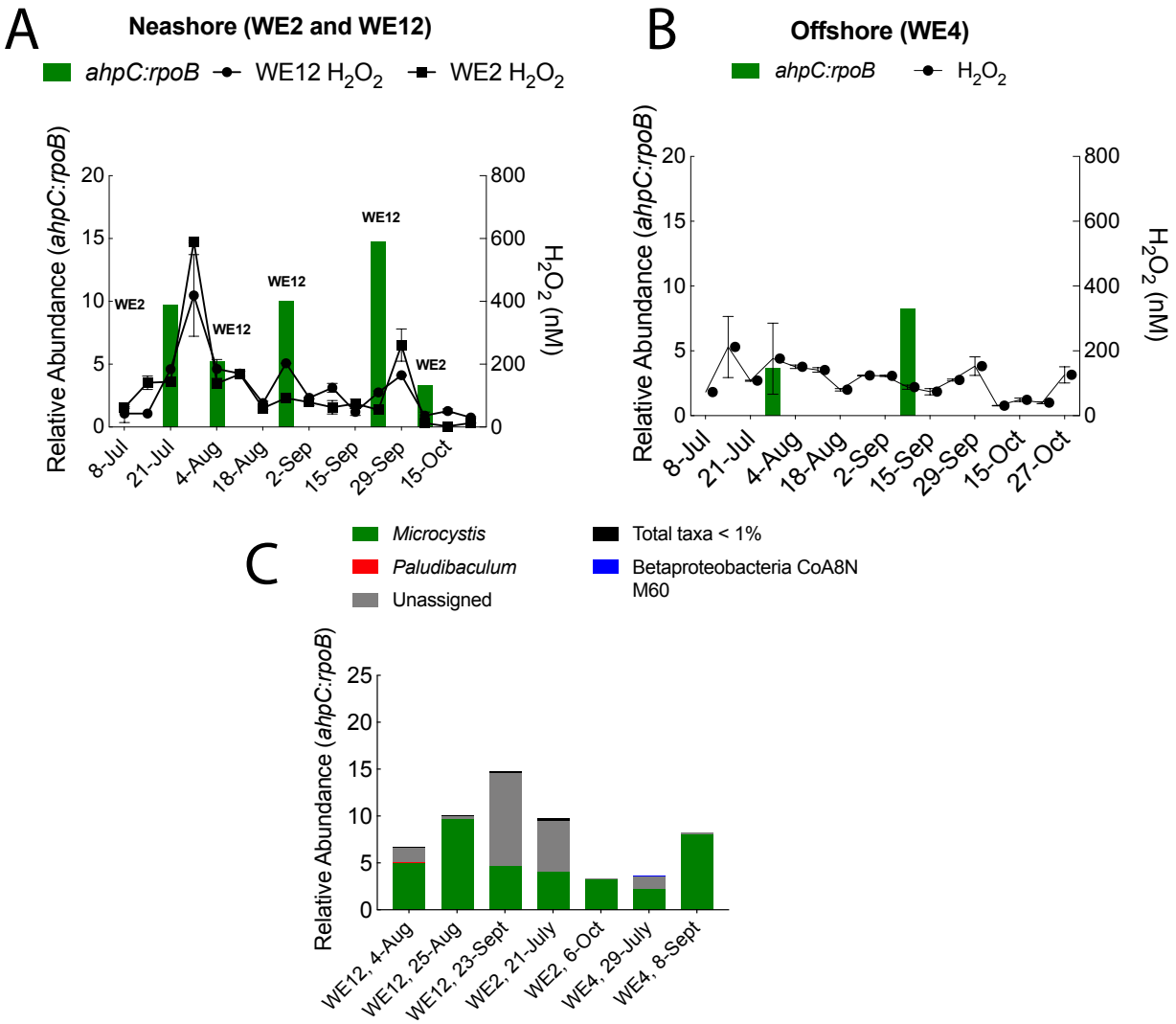

Figure 2.3: Relative abundance and taxonomic composition of *ahpC* transcripts from the 2014 western Lake Erie cyanobacterial bloom. **A:** Relative abundance of *ahpC* in Lake Erie metatranscriptomes of the 100 µm size fraction from nearshore stations WE2 and WE12. **B:** Relative abundance of *ahpC* in Lake Erie metatranscriptomes of the 100 µm size fraction from offshore station WE4. **C:** Taxonomic composition of *ahpC* in metatranscriptomes of the >100 µm size fraction.

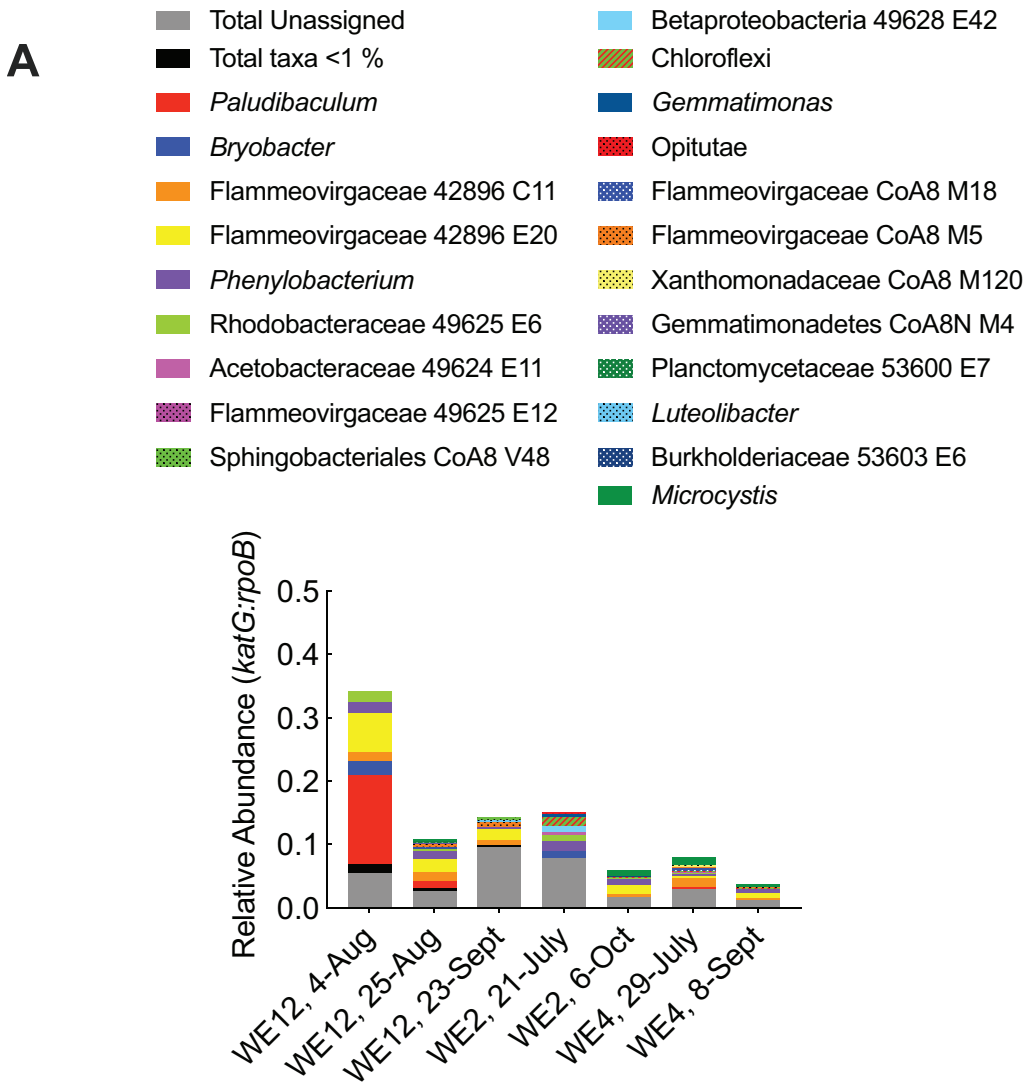
A
Total Unassigned
Total taxa <1 %
Paludibaculum
Bryobacter
Flammeovirgaceae 42896 C11
Flammeovirgaceae 42896 E20
Phenylobacterium
Rhodobacteraceae 49625 E6
Acetobacteraceae 49624 E11
Flammeovirgaceae 49625 E12
Sphingobacteriales CoA8 V48
Betaproteobacteria 49628 E42
Chloroflexi
Gemmatimonas
Opitutae
Flammeovirgaceae CoA8 M18
Flammeovirgaceae CoA8 M5
Xanthomonadaceae CoA8 M120
Gemmatimonadetes CoA8N M4
Planctomycetaceae 53600 E7
Luteolibacter
Burkholderiaceae 53603 E6
Microcystis
Relative Abundance (katG:rpoB)
0.5
0.4
0.3
0.2
0.1
0.0
WE12, 4-Aug
WE12, 25-Aug
WE12, 23-Sept
WE2, 21-July
WE2, 6-Oct
WE4, 29-July
WE4, 8-Sept

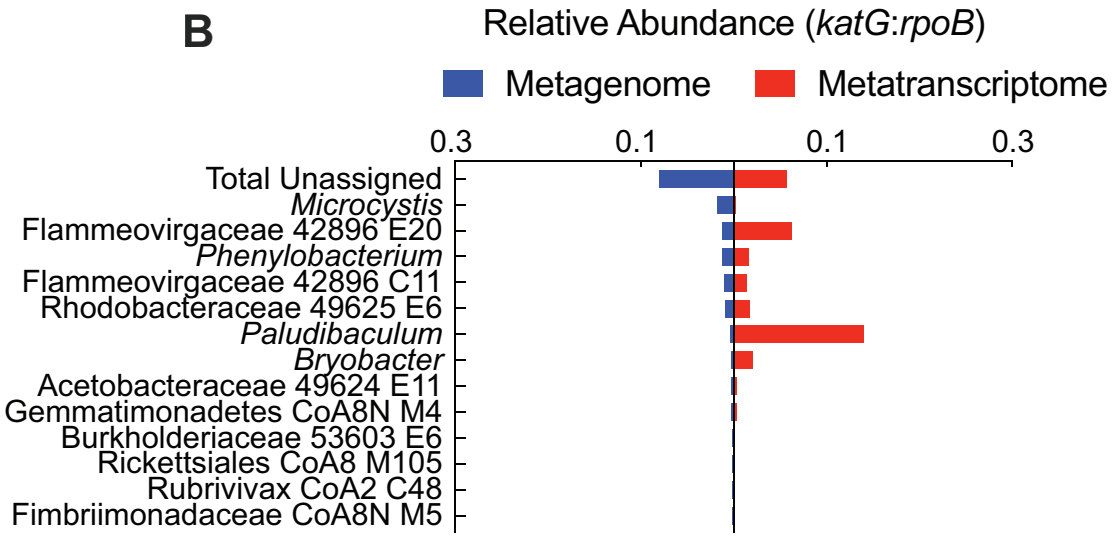
B
Relative Abundance (katG:rpoB)
Metagenome
Metatranscriptome
0.3
0.1
0.1
0.3
Total Unassigned
Microcystis
Flammeovirgaceae 42896 E20
Phenylobacterium
Flammeovirgaceae 42896 C11
Rhodobacteraceae 49625 E6
Paludibaculum
Bryobacter
Acetobacteraceae 49624 E11
Gemmatimonadetes CoA8N M4
Burkholderiaceae 53603 E6
Rickettsiales CoA8 M105
Rubrivivax CoA2 C48
Fimbriimonadaceae CoA8N M5

Figure 2.4: Taxonomic composition of *katG* transcripts from the 2014 western Lake Erie cyanobacterial bloom. **A:** Taxonomic composition of *katG* in Lake Erie metatranscriptomes from the >100 μm particle size fraction. **B:** Comparison of the abundance of *katG* in the metagenome and metatranscriptome collected when overall *katG* expression was highest (August 4th, WE12). Taxa are ranked by their abundance in the metagenome. All gene abundances are normalized to the abundance of *rpoB* gene, encoding the beta-subunit of bacterial RNA polymerases.

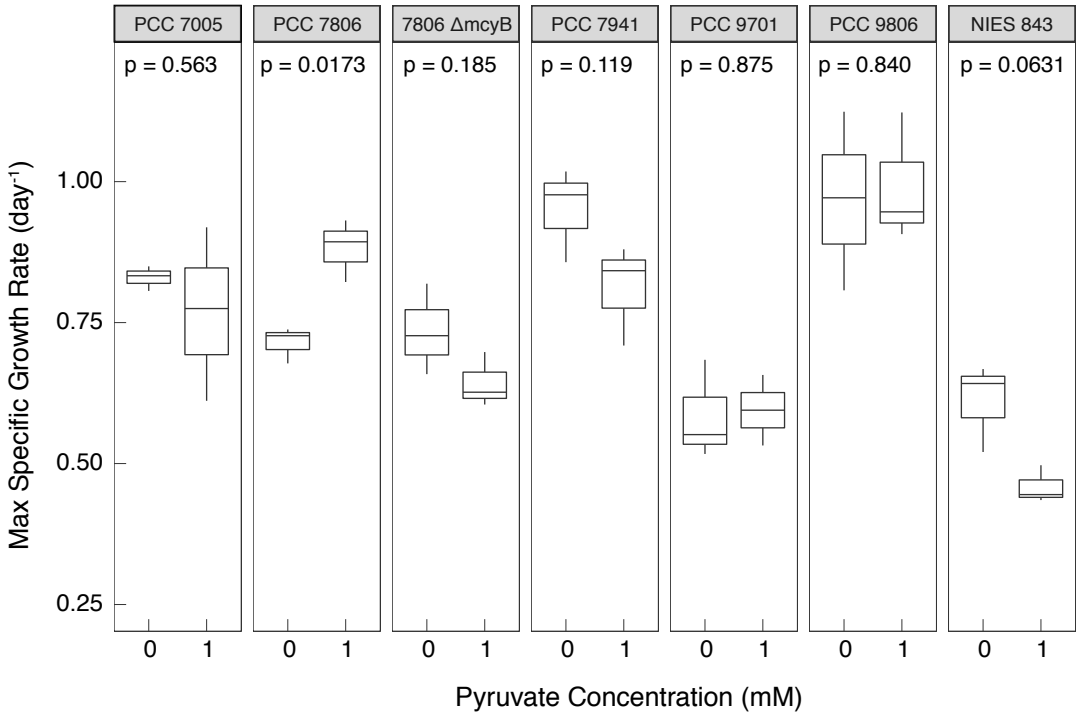

Figure 2.5: Impact of sodium pyruvate on maximum growth rates of *Microcystis* strains. Maximum specific growth rates of seven *Microcystis* strains with and without 1 mM sodium pyruvate supplemented to the growth medium. Treatment groups for each strain contained three biological replicates. P-values were calculated with a Welch's two-sided T-test.

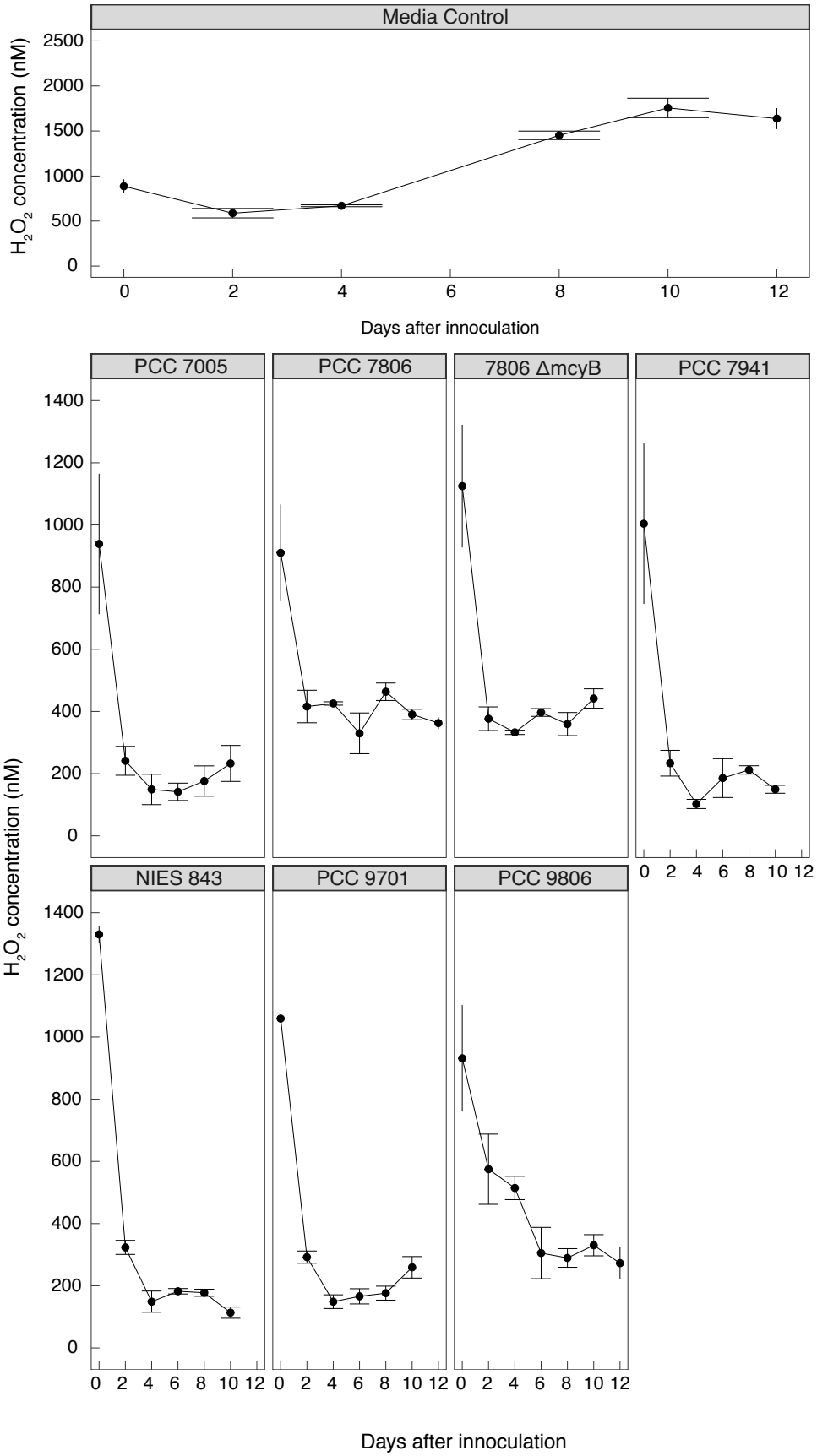
Media Control
PCC 7005
PCC 7806
7806 ΔmcyB
PCC 7941
NIES 843
PCC 9701
PCC 9806
H_2O_2 concentration (nM)
Days after innoculation

Figure 2.6: H_2O_2 concentrations in axenic *Microcystis* cultures. Mean H_2O_2 concentrations observed in axenic *Microcystis* cultures and sterile BG-11 2N media without sodium pyruvate. Error bars show 95% confidence intervals of three biological replicates for the *Microcystis* strains and 95% confidence interval of the standard addition slope for sterile BG-11 2N media.

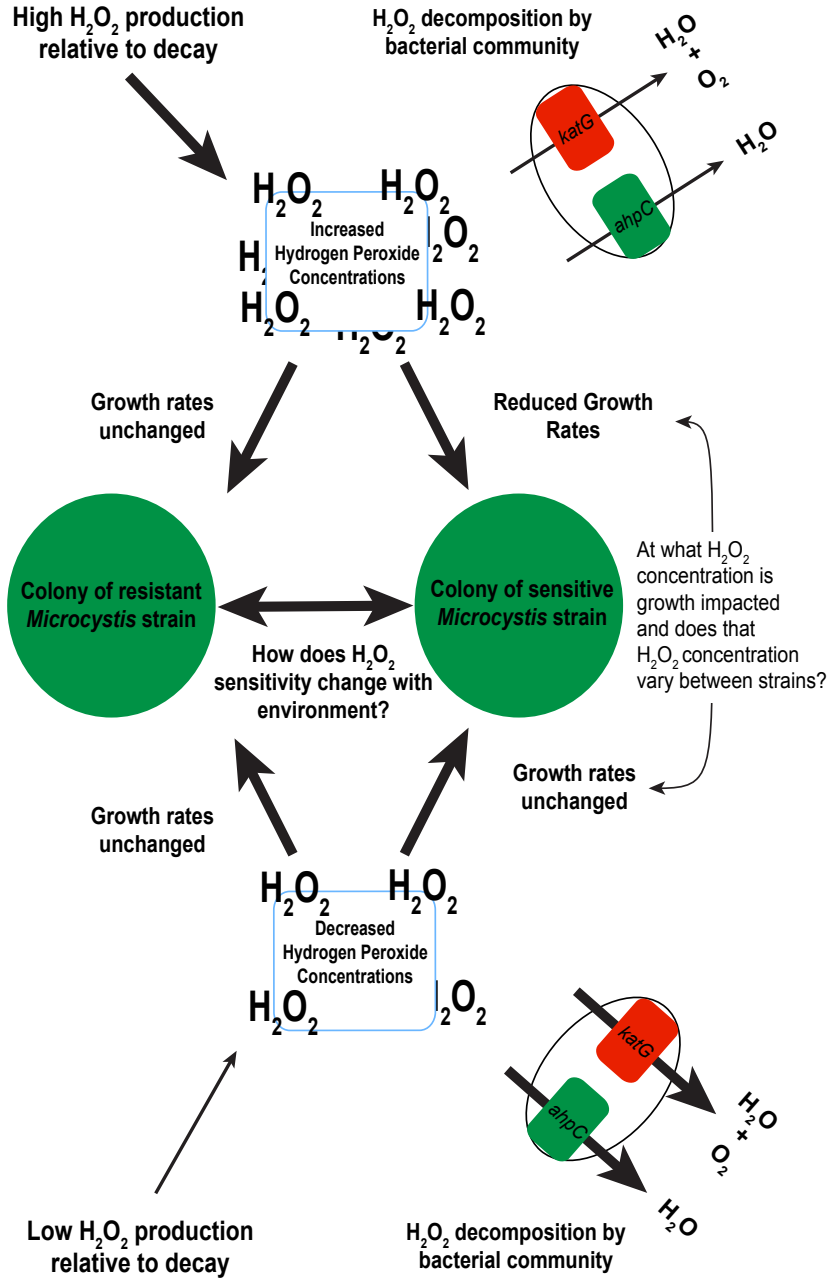

Figure 2.7: Conceptual diagram of H_2O_2 production, concentrations, and decomposition by the microbial community influencing *Microcystis* population structure.

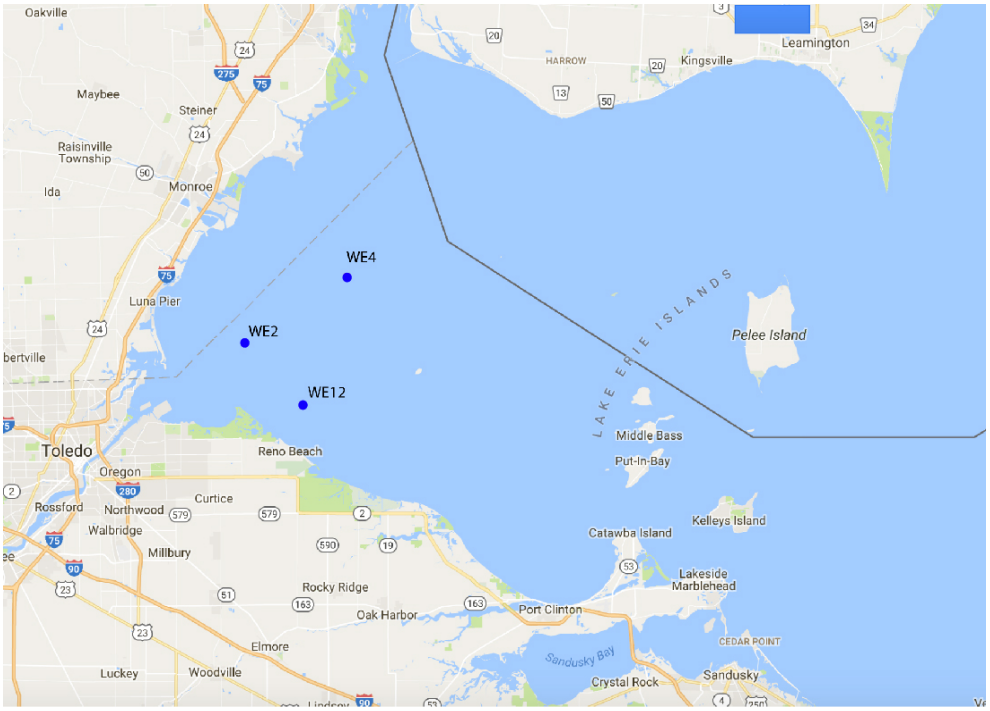

Figure S 2.1: Sampling sites in western Lake Erie.

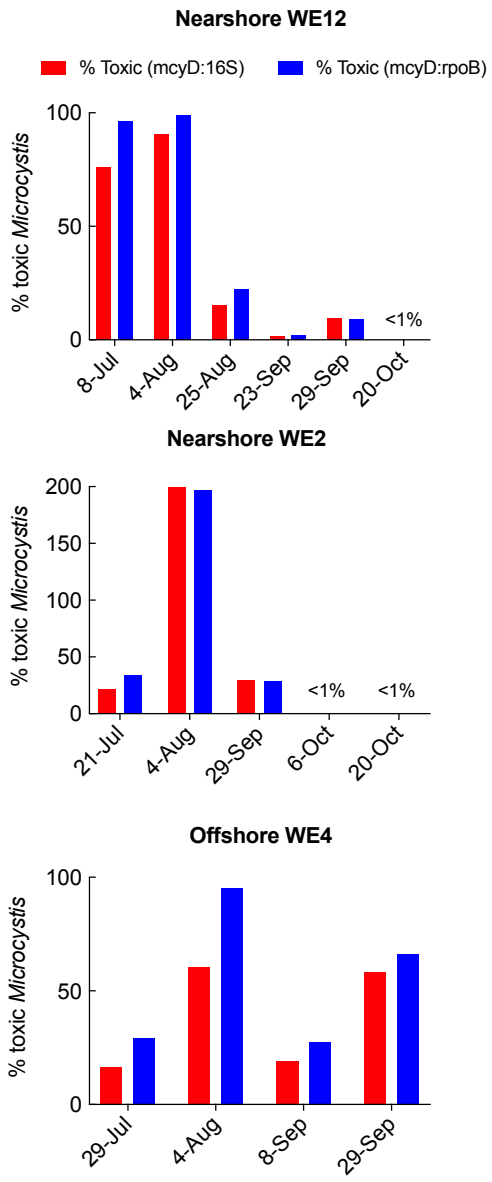

Figure S 2.2: Comparison of normalization strategy for determining the percentage of toxic *Microcystis* strains in metagenomic reads. Red bars depict the percentage of toxic strains estimated by using the number of reads mapped to the V4 region of the *Microcystis* 16S rRNA gene. Blue bars depict the percentage of toxic strains estimated by using the number of reads that mapped to the single-copy housekeeping gene *rpoB* in *Microcystis.*

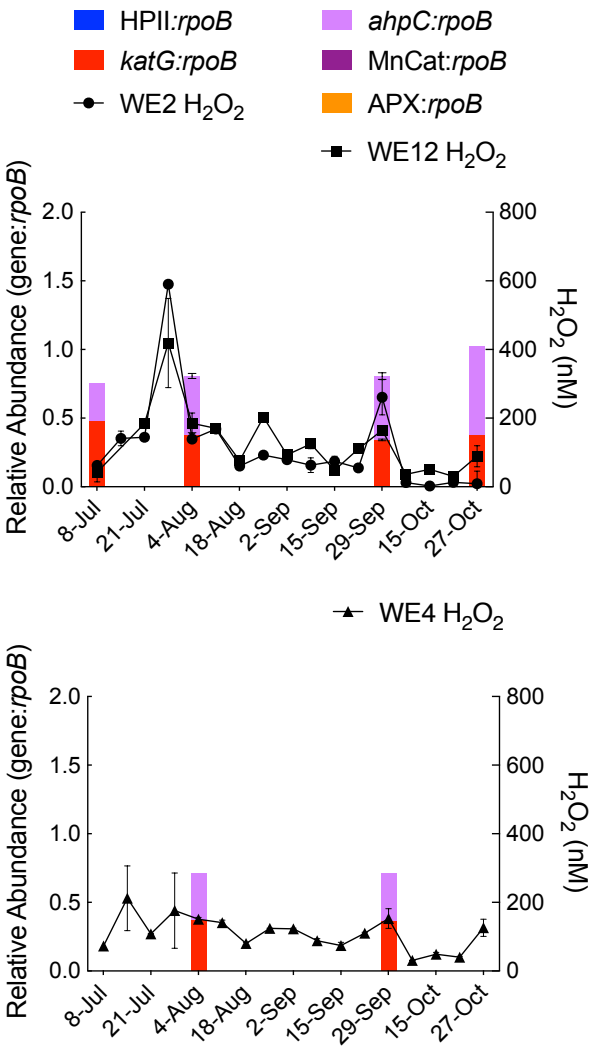

Figure S 2.3: Temporal and spatial variation in the relative abundance of catalase and peroxidase genes in Lake Erie metagenomes from the total community size fraction. Average abundance of genes at nearshore stations WE2 and WE12 are in top panel, average abundances of genes at the offshore station WE4 are in the bottom panel. Blue: *katE*, Red: *katG*, Purple: Manganese Catalase, Orange: APX, Green: *ahpC*, Top dotted line: WE2 H_2O_2, Top squared line: WE12 H_2O_2, Bottom dotted line: WE4 H_2O_2.

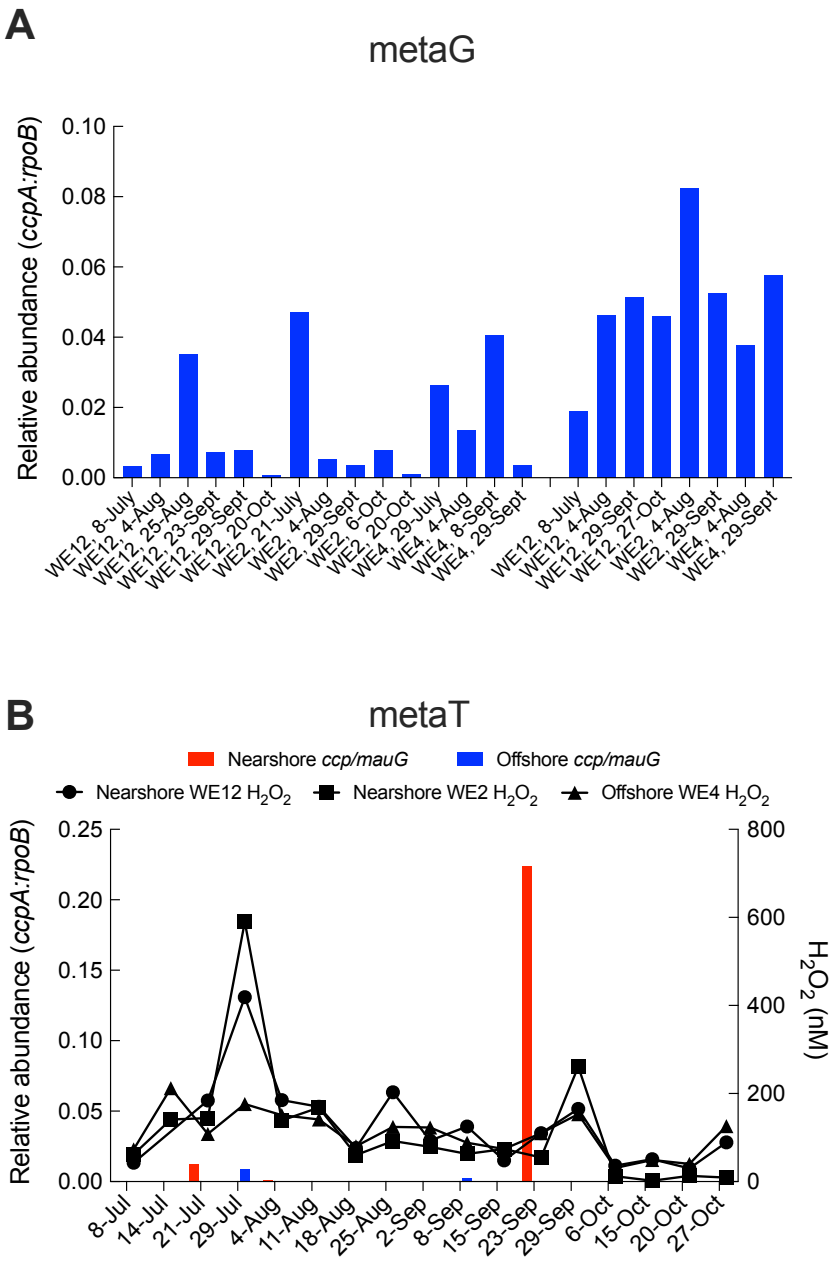

Figure S 2.4: Spatial and temporal variation in the relative abundance of *ccpA* and *mauG* homologs in metagenomes (A) and metatranscriptomes (B).

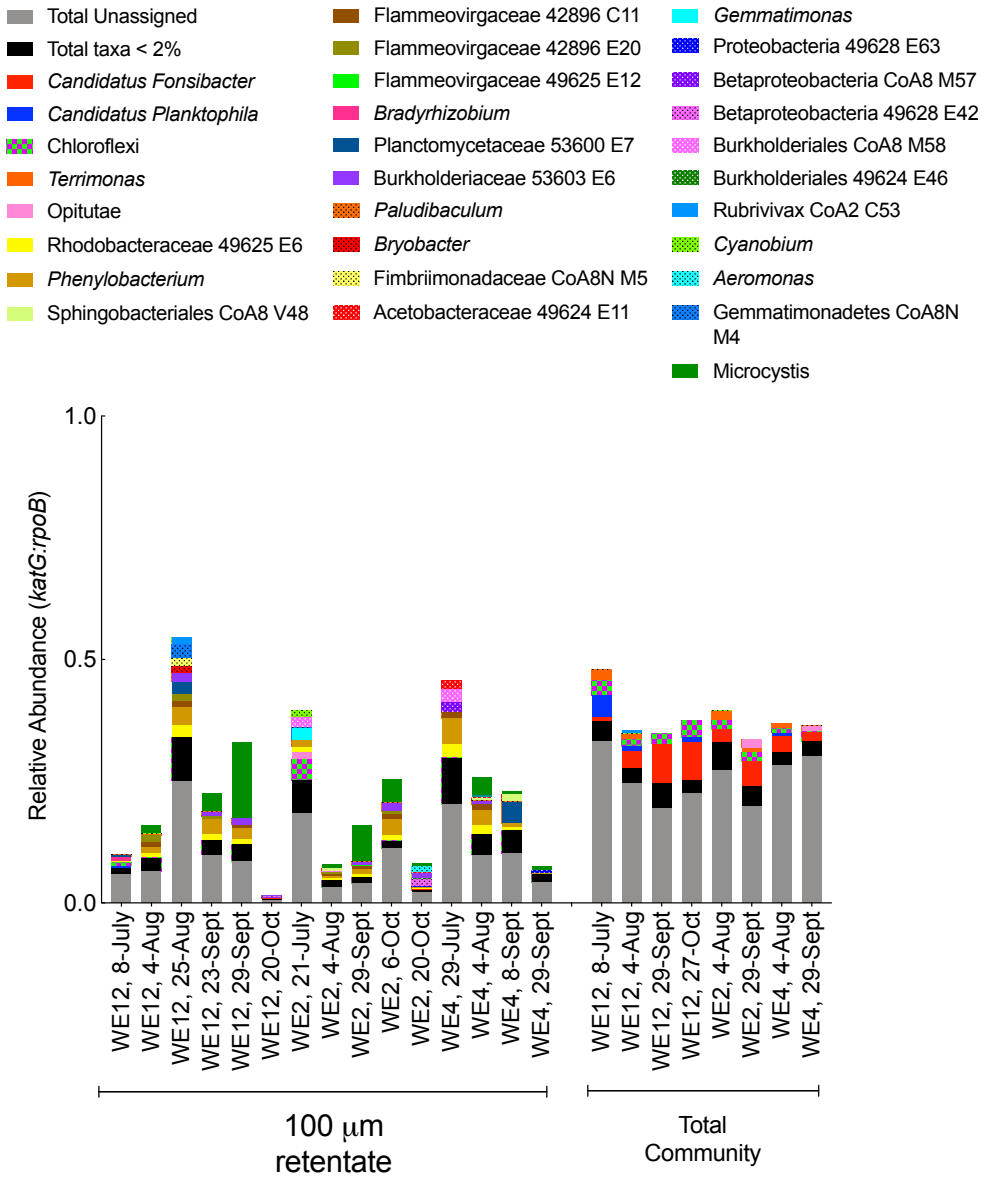

Figure S 2.5: Taxonomic composition of *katG* in >100 μm particle attached fraction and total community metagenomes from the 2014 western Lake Erie cyanobacterial bloom.

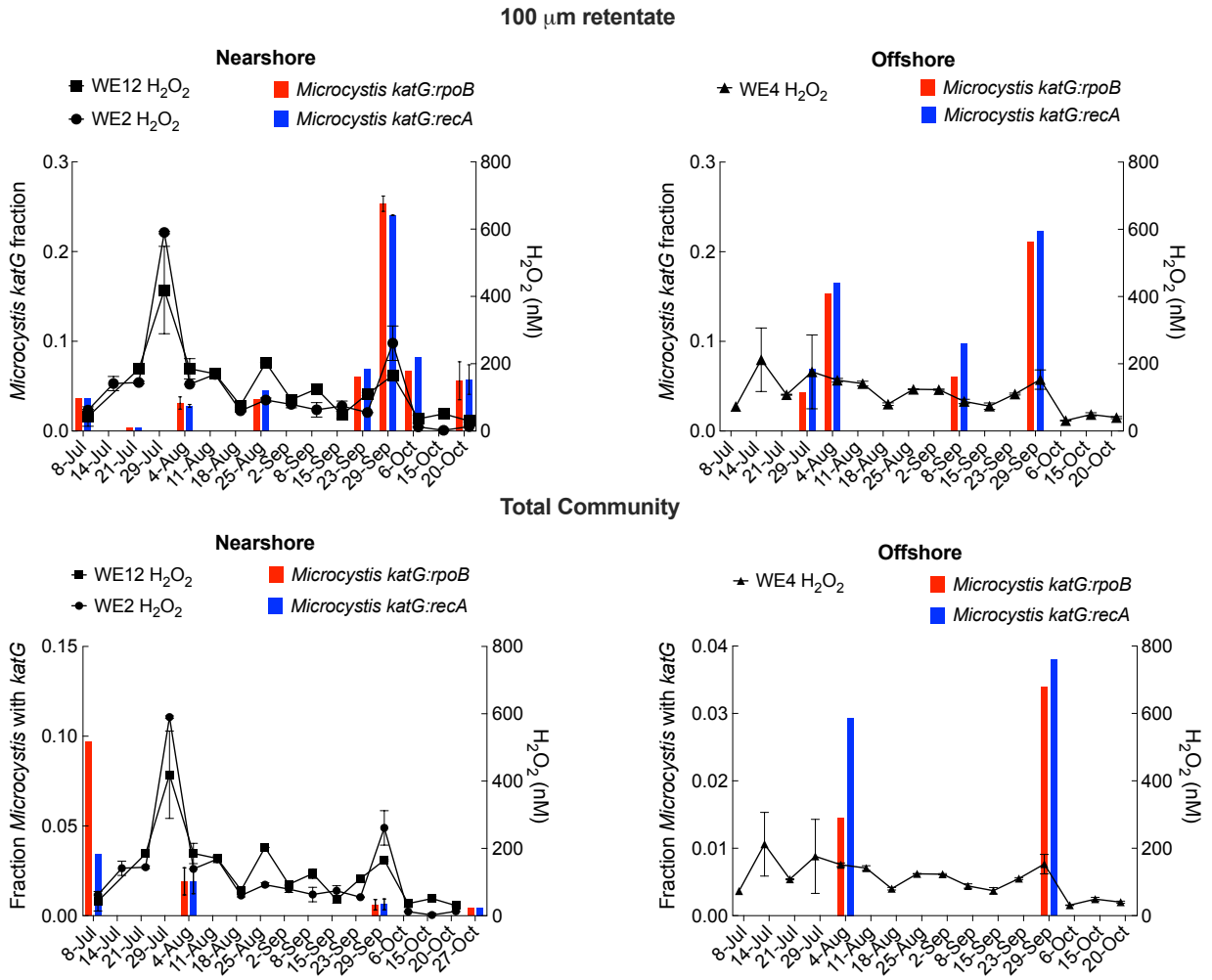

Figure S 2.6: Temporal and spatial variation in the fraction of *Microcystis* cells with *katG*, estimated by normalizing *Microcystis katG* read counts to counts of the single-copy housekeeping genes *rpoB* and *recA* from *Microcystis*.

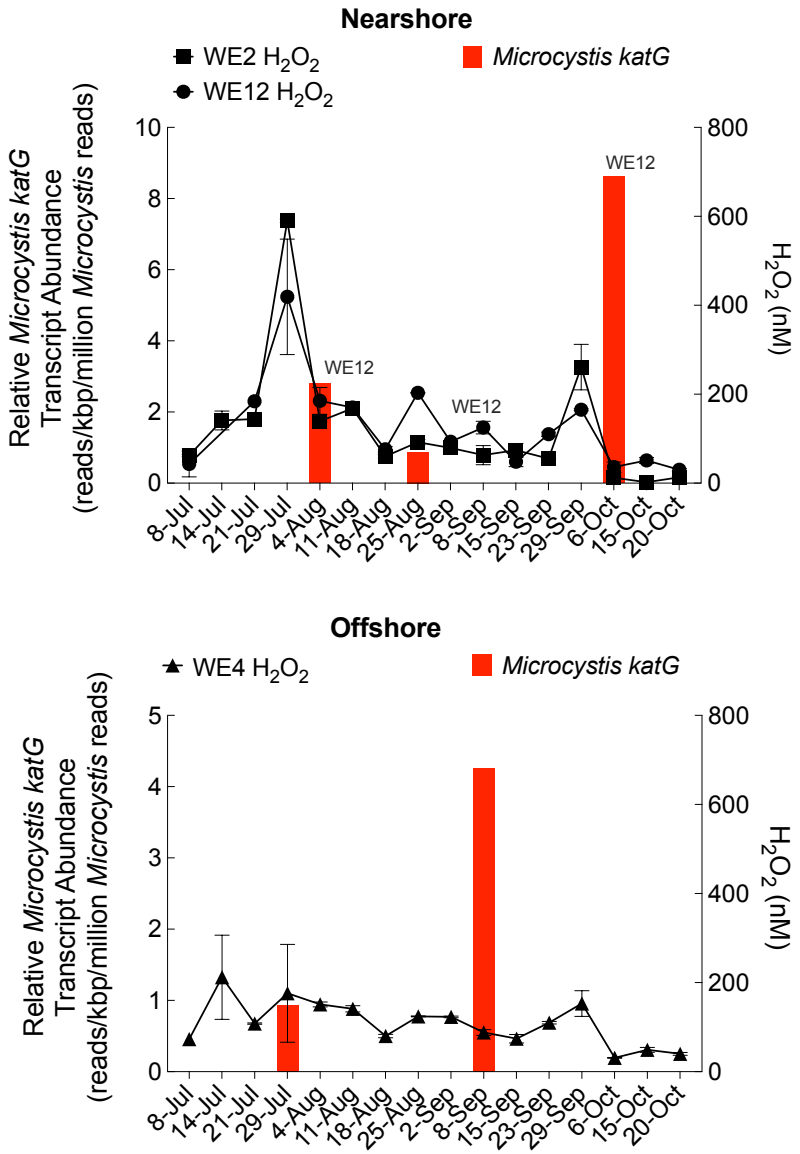

Figure S 2.7: Temporal and spatial variation in *Microcystis katG* relative transcript abundance. Transcript abundance is expressed as reads mapped to *Microcystis katG* per million reads that mapped to *Microcystis* genomes.

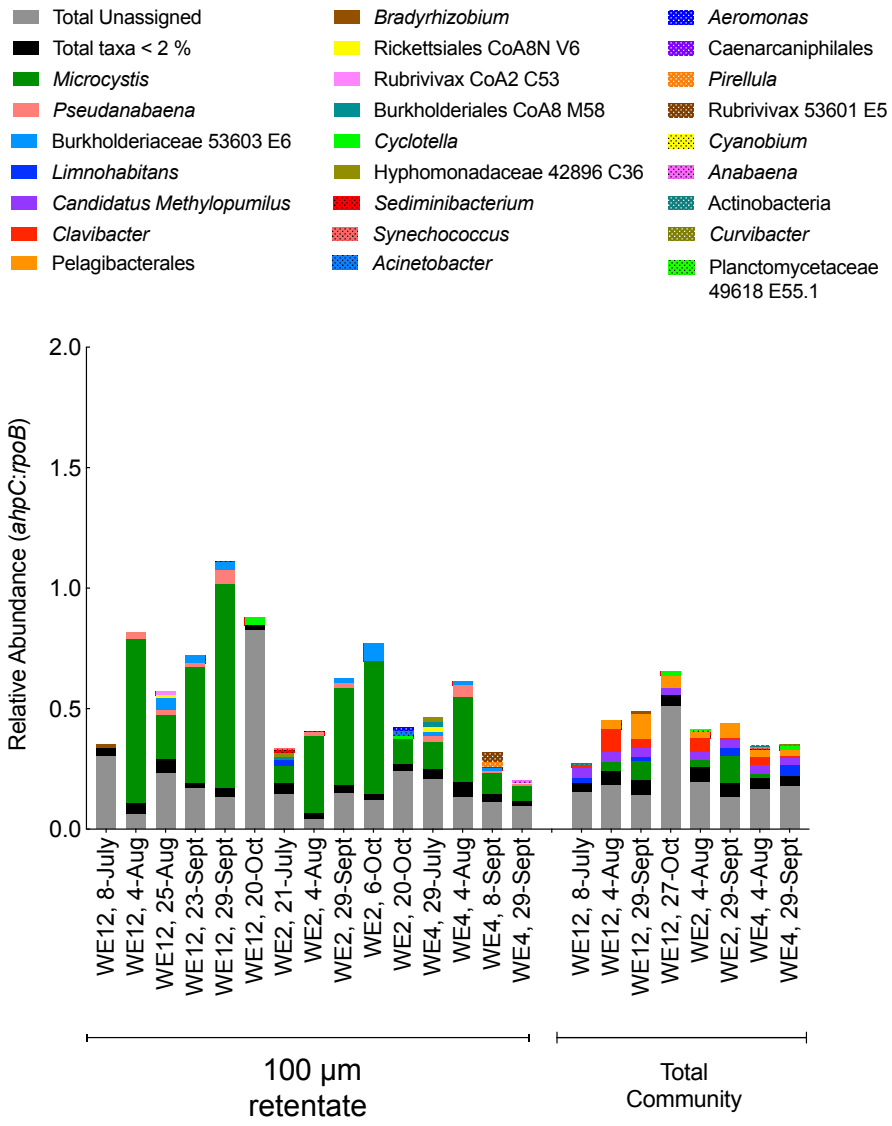

Figure S 2.8: Taxonomic composition of *ahpC* in >100 µm particle attached fraction and total community metagenomes from the 2014 western Lake Erie cyanobacterial bloom.

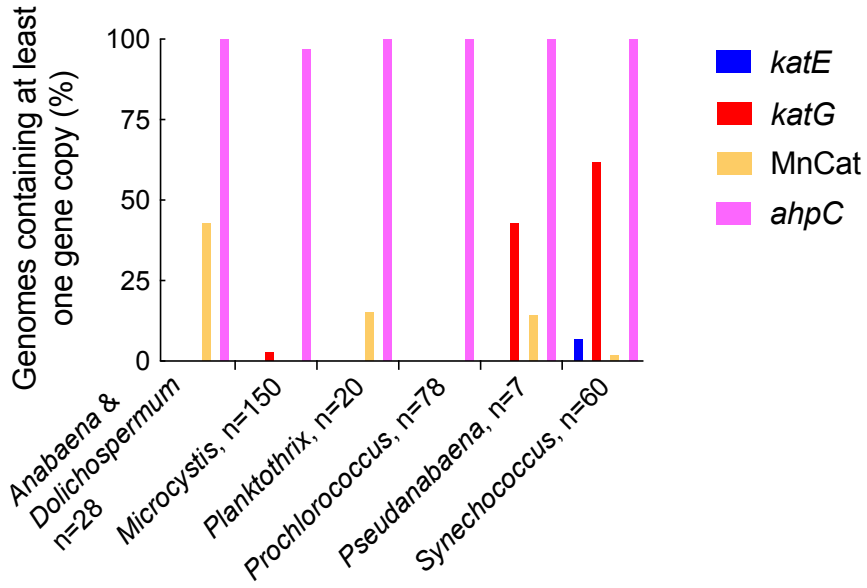

Figure S 2.9: Distribution of catalase and peroxidase genes of interest among publicly available genomes of targeted cyanobacteria. Blue: Monofunctional heme catalase *katE*. Red: catalase-peroxidase *katG*. Orange: Manganese catalase MnCat. Pink: peroxiredoxin *ahpC*. No APX homologs were detected in cyanobacteria genomes.

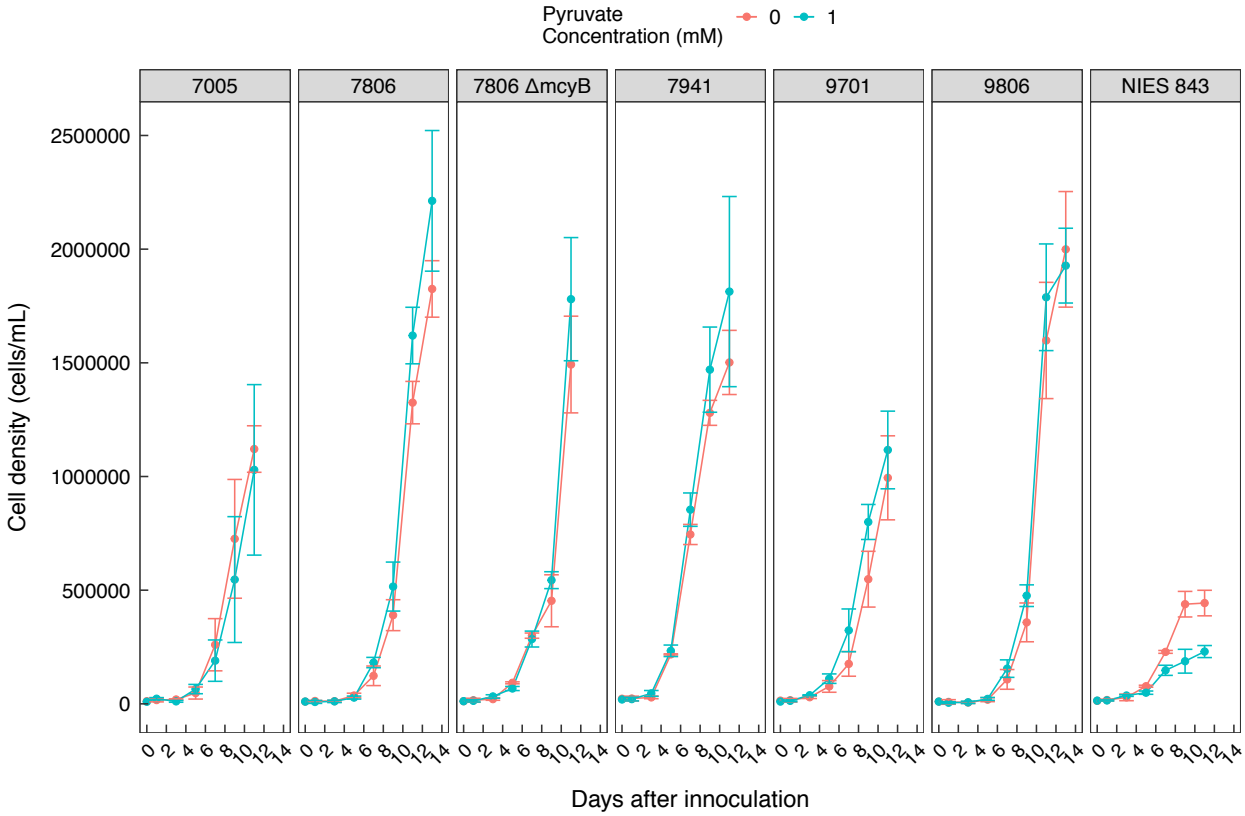

Figure S 2.10: Growth curves of seven axenic *Microcystis* strains cultured with and without 1 mM sodium pyruvate supplemented to the growth medium.

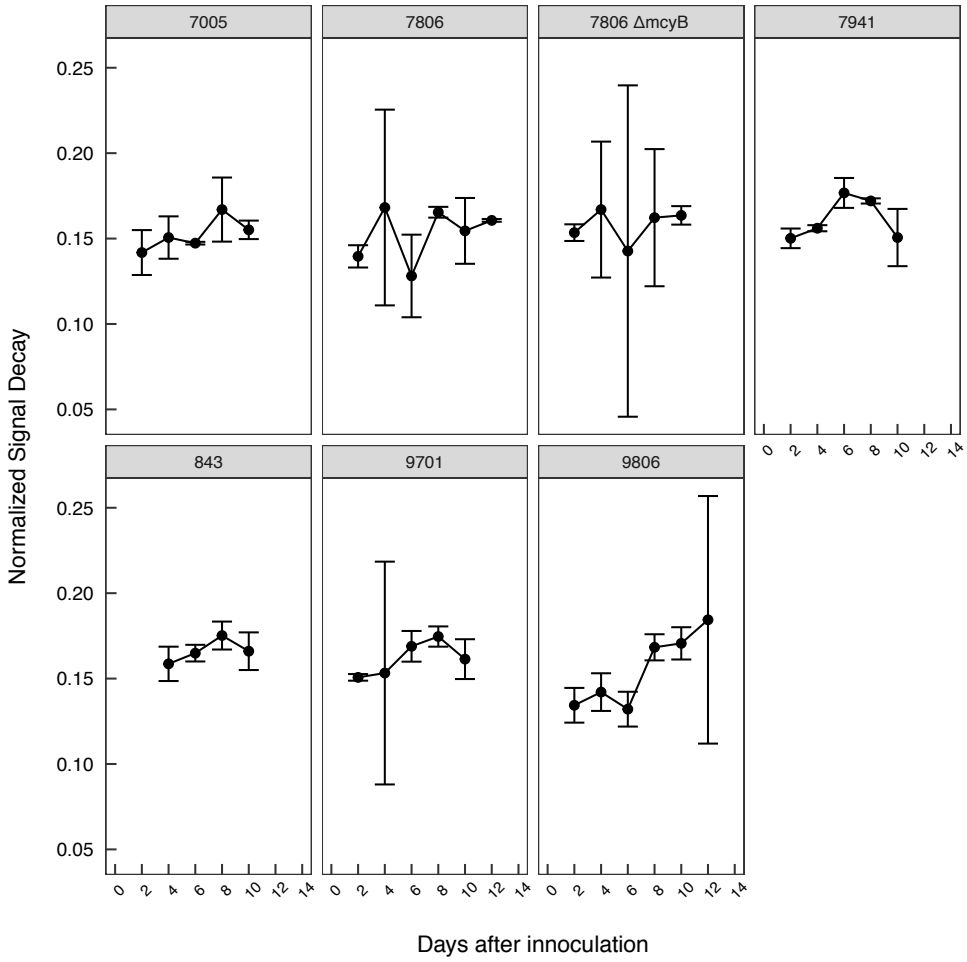

Figure S 2.11: Decay of 500 nM H_2O_2 standard in the filtrates of *Microcystis* cultures supplemented with1 mM sodium pyruvate. Decay is expressed as the difference in the chemiluminescent signal between two replication measurements collected 6 minutes apart, divided by the initial chemiluminescent signal at the beginning of replicate measurements. Shown is the mean normalized signal decay of three biological replicates. Error bars show 95% confidence intervals.

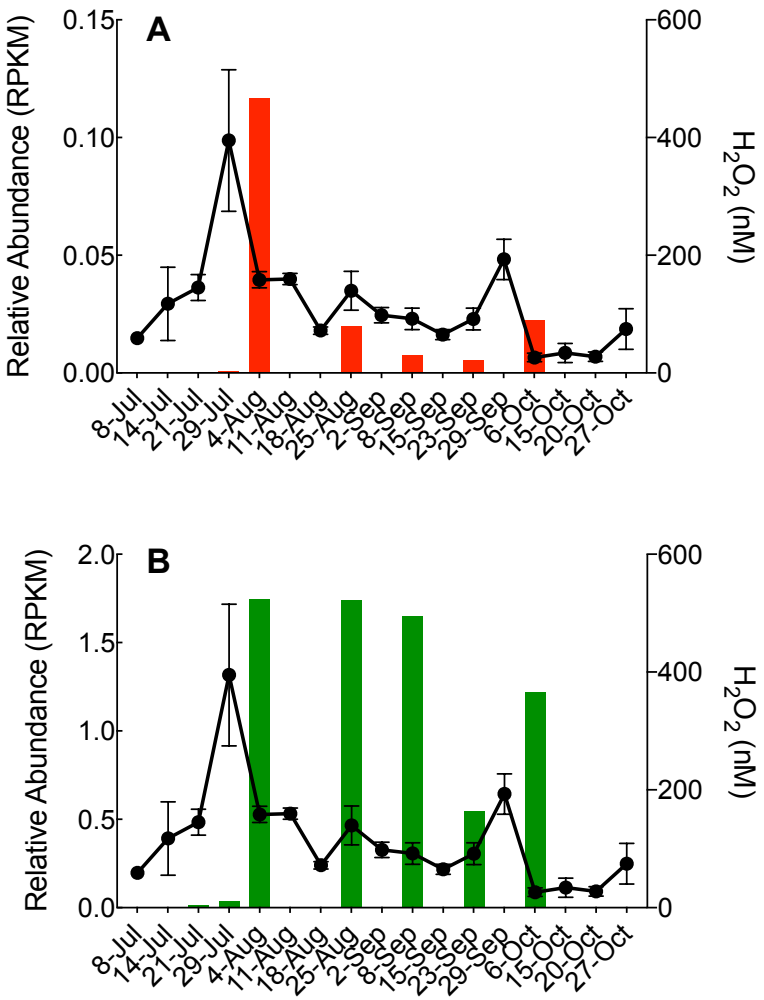

Figure S 2.12: Relative expression of *katG* (top) and *ahpC* (bottom) using read counts normalized by total library size. Included in the same plot are samples from all three stations and their average H_2O_2 concentrations (black dotted line). Error bars show standard error of average H_2O_2 concentration across the three stations.

Table 2.1: *Microcystis* 16S rRNA and *mcyD* gene copy numbers and percentage of *Microcystis* population with the potential to produce the toxin microcystin as determined by qPCR analysis.

Nearshore Station WE2								
Date	16S rRNA Copy Number	mcyD copy number	% Toxic *Micorcystis*	Average (%)	STDEV	Part. MC (µg/L)	Average	STD DEV
21-Jul	162,255	47,196	29.1	35.4	22.0	4.94	3.0	2.2
29-Jul	109,963	31,081	28.3			3.98		
18-Aug	6,318,419	4,396,621	69.6			4.71		
2-Sep	415,647	40,672	9.8			0.60		
8-Sep	110,701	44,739	40.4			0.60		
15-Sep	1,040,929	22,150	2.1	0.9	1.0	0.70	0.6	0.6
23-Sep	613,340	8,498	1.4			1.35		
6-Oct	571,508	BDL	0.0			0.00		
15-Oct	92,454	BDL	0.0			0.45		
Offshore Station WE4								
Date	16S rRNA Copy Number	mcyD copy number	% Toxic *Micorcystis*	Average (%)	STD DEV	Part. MC (µg/L)	Average	STD DEV
21-Jul	73,881	53,376	72.2	44.7	13.6	1.82	0.7	0.7
29-Jul	227,902	95,765	42.0			1.01		
18-Aug	280,301	113,234	40.4			0.21		
25-Aug	18,810	7,441	39.6			0.10		
2-Sep	47,629	17,683	37.1			0.20		
8-Sep	428,055	157,423	36.8			0.80		
15-Sep	128,190	1,514	1.2	10.5	20.3	0.10	0.3	0.2

23-Sep	53,261	21,818	41.0			0.30		
6-Oct	BDL	BDL	0.0			0.10		
15-Oct	67,891	BDL	0.0			0.54		
Nearshore Station WE12								
Date	16S rRNA Copy Number	mcyD copy number	% Toxic *Micorcystis*	Average (%)	STD DEV	Part. MC (µg/L)	Average	STD DEV
21-Jul	10,360	8,800	84.9	62.9	30.9	6.14	4.0	2.6
29-Jul	3,464,712	2,088,253	60.3			6.93		
18-Aug	410,386	189,368	46.1			3.39		
25-Aug	4,655,920	4,682,178	100.6			3.10		
2-Sep	589,887	133,209	22.6			0.30		
8-Sep	157,234	13,475	8.6	4.4	2.9	0.40	0.7	0.6
15-Sep	4,593,926	142,257	3.1			1.30		
23-Sep	1,748,321	31,412	1.8			0.90		
6-Oct	134,216	5,470	4.1			0.00		

Table 2.2: Coordinates of 16S rRNA genes in closed *Microcystis* genomes available in the NCBI genome database.

Microcystis strain	GenBank accession	16S rRNA gene coordinates
PCC 7806SL	CP020771.1	608249..609725 2236412..2237888
MC 19	CP020664.1	1023751..1025240 2178504..2180000
NIES 2481	CP012375.1	1..1460

		2452450..2453909
NIES 2549	CP011304.1	1..1460 2455677..2457136
NIES 298	CP046058.1	1267476..1268964 4095284..4096772
NIES 843	AP009552.1	1885807..1887295 3597272..3598760
FD4	CP046973.1	2373640..2375133 4731957..4733450
FACHB 1757	CP011339.1	4352152..4353641 4953781..4955270
NIES 102	AP019314.1	1512507..1513991 5700022..5701506

Table 2.3: Taxonomy of MAGs containing genes encoding the catalase and peroxidase genes of interest. An "X" indicates that the specified gene was found in at least one MAG of the listed taxonomy.

Bin Taxonomy	CAT	*katG*	Mn Cat	*ccpA/mauG*	*ahpC*
Algoriphagus				X	
Acetobacteraceae 49624 E11					X
Acidibacter		X			X
Alphaproteobacteria CoA8 M99					X
Alphaproteobacteria CoA8N C25					X
Alphaproteobacteria CoA8N M8					X

Alphaproteobacteria 49628 E19				X
Anabaena		X		X
Hyphomonadaceae 42896 C36	X			X
Bacteroidetes CoA8 C16			X	X
Bacteroidetes 49613 E12			X	
Bacteroidetes 49614 E21				X
Bacteroidetes 49618 E68	X		X	
Betaproteobacteria CoA8 M57	X		X	
Betaproteobacteria CoA8N M60	X		X	X
Betaproteobacteria CoA2 C61			X	
Betaproteobacteria 49628 E42	X		X	
Blastopirellula	X		X	
Burkholderiaceae 49618 E8				X
Burkholderiaceae 49638 E11			X	
Burkholderiales CoA8 M58	X			X
Burkholderiales CoA8N M101			X	
Burkholderiales 49624 E46	X			X
Burkholderiales 49632 E5	X		X	X
Burkholderiales 53603 E6			X	X
Bryobacter	X		X	X
Caenarcaniphilales CoA8 M2.1			X	X
Candidatus Jidaibacter				X
Chitinophagaceae 49614 E54			X	
Chitinophagaceae 49621 E24	X			
Chloroflexaceae 49614 E51	X			
Comamonadaceae 49613 E28				X
Comamonadaceae 49613 E45				X

Comamonadaceae 49618 E9	X	X	X
Cryomorphaceae 49613 E39		X	X
Cryomorphaceae 49618 E18	X	X	X
Cryomorphaceae 49628 E59	X	X	X
Cryomorphaceae 49632 E27		X	X
Cryomorphaceae 49632 E31		X	X
Cyanobium	X		X
Fimbriimonadaceae CoA8N M5	X		
Fimbriimonadaceae 49621 E14		X	
Flammeovirgaceae CoA8 M5	X		
Flammeovirgaceae CoA8N M18	X	X	
Flammeovirgaceae 42896 E20	X		
Flammeovirgaceae 42896 C11	X		
Flammeovirgaceae 49625 E12	X	X	
Fluviicola		X	X
Gemmataceae 49613 E7			X
Gemmataceae 49618 E45	X	X	
Gemmatimonadetes CoA8N M110	X	X	
Gemmatimonadetes CoA8N M4	X	X	X
Gemmatimonadetes CoA2 M2	X	X	X
Gemmatimonadetes 49618 E39	X		
Ignavibacteriae 49624 E23	X	X	
Ilumatobacteraceae 49618 E24	X		
Limnohabitans			X
Microcystis			X
Nitrosomonadaceae CoA8N V37			X
Novosphingobium	X		

Opitutus	X		
Oxalobacteraceae 49613 E41		X	X
Oxalobacteraceae 49613 E42		X	
Oxalobacteraceae 49613 E43		X	X
Oxalobacteraceae 49614 E52		X	X
Paludibaculum	X	X	X
Parachlamydia			X
Pedosphaeraceae 49614 E7		X	X
Phenylobacterium	X		
Pirellula	X	X	X
Planctomyces		X	X
Planctomycetaceae 49613 E24	X	X	
Planctomycetaceae 49613 E25	X		
Planctomycetaceae 49613 E27	X	X	
Planctomycetaceae 49618 E55.1		X	X
Planctomycetaceae 49618 E55.3		X	
Planctomycetaceae 49628 E33		X	X
Planctomycetaceae 53600 E7	X		
Proteobacteria CoA8 C15.2		X	X
Proetobacteria CoA8 M100	X		X
Proteobacteria 49628 E63	X		X
Pseudanabaena			X
Rhizobiales CoA2 C13	X		
Rhodobacteraceae 49625 E6	X		
Rickettsiaceae 49624 E59			X
Rickettsiales CoA8 M105.1	X		X
Rickettsiales 49632 E25	X		X

Rubrivivax CoA2 C44	X	X	X
Rubrivivax CoA2 C48	X	X	X
Rubrivivax CoA2 C53		X	X
Rubrivivax 49636 E6	X	X	X
Rubrivivax 53601 E5	X	X	X
Saprospiraceae 49614 E9	X	X	X
Saprospiraceae 49618 E65		X	
Saprospiraceae 49624 E15		X	
Sediminibacterium	X	X	X
Sphingobacteriales CoA8 V48	X	X	
Sphingobacteriales 49613 E9	X	X	
Sphingobacteriales 49618 E60		X	X
Sphingobacteriales 49624 E34	X	X	X
Sphingomonadaceae 49628 E11			X
Terrimonas	X	X	
Verrucomicrobiaceae 49632 E14	X	X	X
Xanthomonadaceae CoA8 M120	X		X
Xanthomonadaceae 49613 E30	X		
Xanthomonadales 49613 E26		X	

Table 2.4: Modified BG-11 recipe used in backwash solution for collecting biomass retentate on 100 μm filter mesh.

BG-11	
Chemical	Quantity per liter
$NaNO_3$	1 mg
$MgSO_4*7H_2O$	75 mg

K_2HPO_4	100 mg
$CaCl_2*2H_2O$	36 mg
Na_2CO_3	20 mg
Citric Acid	6 mg
Ferric Ammonium Citrate	6 mg
Disodium EDTA	1 mg
Trace metal mix A5	1 mL

Trace Metal Mix A5	
Chemical	Quantity per liter
H_3BO_3	2.86 g
$MnCl_2*4H_2O$	1.81 g
$Na_2MoO_4*2H_2O$	0.39 g
$ZnSO_4*7H_2O$	0.222 g
$CuSO_4*5H_2O$	0.079 g
$Co(NO_3)_2*6H_2O$	0.049 g

Table 2.5: A list of primers (Integrated DNA Technologies, IA, USA) and probes (Applied Biosystems, Foster City, CA, USA) used in the qPCR analysis.

DNA Target	Primer	Sequence (5'-3')	Reference
Microcystis 16s rDNA	184F	GCCGCRAGGTGAAAMCTAA	Ouellette et al. (2006)
	431R	AATCCAAARACCTTCCTCCC	Ouellette et al. (2006)
	Probe	(Taq) FAM-AAGAGCTTGCGTCTGATTAGCTAGT-BHQ-1[a]	Rinta-Kanto et al (2005)
Microcystis mcyD	F2	GGTTCGCCTGGTCAAAGTAA	Kaebernick et al. (2000)
	R2	CCTCGCTAAAGAAGGGTTGA	Kaebernick et al. (2000)
	Probe	(Taq) FAM-ATGCTCTAATGCAGCAACGGCAAA-BHQ-1[a]	Rinta-Kanto et al (2005)

F: forward primer R: reverse primer.

[a] Black Hole Quencher-1 (quenching range 480-580 nm)

2.8 References

Alexova, R., Haynes, P. A., Ferrari, B. C., & Neilan, B. A. (2011). Comparative protein expression in different strains of the bloom-forming cyanobacterium *Microcystis aeruginosa*. *Mol Cell Proteomics, 10*(9).

Allen, M. M., & Stanier, R. Y. (1968). Selective isolation of blue-green algae from water and soil. *Microbiology, 51*(2): 203-209.

Alneberg, J., Bjarnason, B. S., De Bruijn, I., Schirmer, M., Quick, J., Ijaz, U. Z. *et al.* (2014). Binning metagenomic contigs by coverage and composition. *Nature methods, 11*(11): 1144-1146.

Altschul, S. F., Gish, W., Miller, W., Myers, E. W., & Lipman, D. J. (1990). Basic local alignment search tool. *J Mol Biol, 215*(3): 403-410.

Barchewitz, T., Guljamow, A., Meissner, S., Timm, S., Henneberg, M., Baumann, O. *et al.* (2019). Non-canonical localization of RubisCO under high-light conditions in the toxic cyanobacterium Microcystis aeruginosa PCC7806. *Environ Microbiol, 21*(12): 4836-4851.

Bayer, B., Pelikan, C., Bittner, M. J., Reinthaler, T., Könneke, M., Herndl, G. J., & Offre, P. (2019). Proteomic Response of Three Marine Ammonia-Oxidizing Archaea to Hydrogen Peroxide and Their Metabolic Interactions with a Heterotrophic Alphaproteobacterium. *mSystems, 4*(4): e00181-00119.

Bernroitner, M., Zamocky, M., Furtmüller, P. G., Peschek, G. A., & Obinger, C. (2009). Occurrence, phylogeny, structure, and function of catalases and peroxidases in cyanobacteria. *J Exp Bot, 60*(2): 423-440.

Berry, M. A., Davis, T. W., Cory, R. M., Duhaime, M. B., Johengen, T. H., Kling, G. W. *et al.* (2017). Cyanobacterial harmful algal blooms are a biological disturbance to Western Lake Erie bacterial communities. *Environ Microbiol, 19*(3): 1149-1162.

Brunberg, A.-K. (1999). Contribution of bacteria in the mucilage of *Microcystis* spp.(Cyanobacteria) to benthic and pelagic bacterial production in a hypereutrophic lake. *FEMS Microbiol Ecol, 29*(1): 13-22.

Bui, T., Dao, T.-S., Vo, T.-G., & Lürling, M. (2018). Warming affects growth rates and microcystin production in tropical bloom-forming *Microcystis* strains. *Toxins, 10*(3): 123.

Bushnell, B. (2018). BBTools: a suite of fast, multithreaded bioinformatics tools designed for analysis of DNA and RNA sequence data: Joint Genome Institute.

Chaffin, J. D., Bridgeman, T. B., Heckathorn, S. A., & Mishra, S. (2011). Assessment of *Microcystis* growth rate potential and nutrient status across a trophic gradient in western Lake Erie. *J Great Lakes Res, 37*(1): 92-100.

Cooper, W. J., Lean, D., & Carey, J. (1989). Spatial and temporal patterns of hydrogen peroxide in lake waters. *Can J Fish Aquat Sci, 46*(7): 1227-1231.

Cory, R. M., Davis, T. W., Dick, G. J., Johengen, T., Denef, V. J., Berry, M. A. *et al.* (2016). Seasonal dynamics in dissolved organic matter, hydrogen peroxide, and cyanobacterial blooms in Lake Erie. *Front Mar Sci, 3*: 54.

Cory, R. M., Davis, T., Dick, G., Johengen, T., Denef, V. J., Berry, M. *et al.* (2017). Corrigendum: Seasonal dynamics in dissolved organic matter, hydrogen peroxide, and cyanobacterial blooms in Lake Erie. *Front Mar Sci, 4*: 377.

Cosgrove, K., Coutts, G., Jonsson, M., Tarkowski, A., Kokai-Kun, J. F., Mond, J. J., & Foster, S. J. (2007). Catalase (*KatA*) and alkyl hydroperoxide reductase (*AhpC*) have compensatory roles in peroxide stress resistance and are required for survival, persistence, and nasal colonization in *Staphylococcus aureus*. *J Bacteriol, 189*(3): 1025-1035.

Daniel, E., Weiss, G., Murik, O., Sukenik, A., Lieman-Hurwitz, J., & Kaplan, A. (2019). The response of *Microcystis aeruginosa* strain MGK to a single or two consecutive H2O2 applications. *Environ Microbiol Rep, 11*(5): 621-629.

Davis, T. W., Berry, D. L., Boyer, G. L., & Gobler, C. J. (2009). The effects of temperature and nutrients on the growth and dynamics of toxic and non-toxic strains of *Microcystis* during cyanobacteria blooms. *Harmful Algae, 8*(5): 715-725.

Davis, T. W., Watson, S. B., Rozmarynowycz, M. J., Ciborowski, J. J., McKay, R. M., & Bullerjahn, G. S. (2014). Phylogenies of microcystin-producing cyanobacteria in the lower Laurentian Great Lakes suggest extensive genetic connectivity. *PLoS One, 9*(9): e106093.

Davis, T. W., Bullerjahn, G. S., Tuttle, T., McKay, R. M., & Watson, S. B. (2015). Effects of increasing nitrogen and phosphorus concentrations on phytoplankton community growth and toxicity during *Planktothrix* blooms in Sandusky Bay, Lake Erie. *Environ Sci Technol, 49*(12): 7197-7207.

Dick, G. J., Andersson, A. F., Baker, B. J., Simmons, S. L., Thomas, B. C., Yelton, A. P., & Banfield, J. F. (2009). Community-wide analysis of microbial genome sequence signatures. *Genome Biol, 10*(8): R85.

Ding, Y., Gan, N., Li, J., Sedmak, B., & Song, L. (2012). Hydrogen peroxide induces apoptotic-like cell death in *Microcystis aeruginosa* (Chroococcales, Cyanobacteria) in a dose-dependent manner. *Phycologia, 51*(5): 567-575.

Dittmann, E., Neilan, B. A., Erhard, M., Von Döhren, H., & Börner, T. (1997). Insertional mutagenesis of a peptide synthetase gene that is responsible for hepatotoxin production in the cyanobacterium *Microcystis aeruginosa* PCC 7806. *Mol Microbiol, 26*(4): 779-787.

Dittmann, E., Erhard, M., Kaebernick, M., Scheler, C., Neilan, B. A., von Döhren, H., & Börner, T. (2001). Altered expression of two light-dependent genes in a microcystin-lacking mutant of *Microcystis aeruginosa* PCC 7806. *Microbiology, 147*(11): 3113-3119.

Dziallas, C., & Grossart, H.-P. (2011). Increasing oxygen radicals and water temperature select for toxic *Microcystis* sp. *PLoS One, 6*(9): e25569.

Eren, A. M., Esen, Ö. C., Quince, C., Vineis, J. H., Morrison, H. G., Sogin, M. L., & Delmont, T. O. (2015). Anvi'o: an advanced analysis and visualization platform for 'omics data. *PeerJ, 3*: e1319.

Forni, C., Telo', F. R., & Caiola, M. G. (1997). Comparative analysis of the polysaccharides produced by different species of *Microcystis* (Chroococcales, Cyanophyta). *Phycologia, 36*(3): 181-185.

Gao, L., Pan, X., Zhang, D., Mu, S., Lee, D.-J., & Halik, U. (2015). Extracellular polymeric substances buffer against the biocidal effect of H2O2 on the bloom-forming cyanobacterium *Microcystis aeruginosa*. *Water Res, 69*: 51-58.

Gobler, C. J., Burkholder, J. M., Davis, T. W., Harke, M. J., Johengen, T., Stow, C. A., & Van de Waal, D. B. (2016). The dual role of nitrogen supply in controlling the growth and toxicity of cyanobacterial blooms. *Harmful Algae, 54*: 87-97.

Häkkinen, P. J., Anesio, A. M., & Granéli, W. (2004). Hydrogen peroxide distribution, production, and decay in boreal lakes. *Can J Fish Aquat Sci, 61*(8): 1520-1527.

Harke, M. J., Steffen, M. M., Gobler, C. J., Otten, T. G., Wilhelm, S. W., Wood, S. A., & Paerl, H. W. (2016). A review of the global ecology, genomics, and biogeography of the toxic cyanobacterium, *Microcystis* spp. *Harmful Algae, 54*: 4-20.

Hosoya-Matsuda, N., Motohashi, K., Yoshimura, H., Nozaki, A., Inoue, K., Ohmori, M., & Hisabori, T. (2005). Anti-oxidative Stress System in Cyanobacteria: Significance Of Type II Peroxiredoxin and the Role of 1-Cys Peroxiredoxin in *Synechocystis* sp. strain PCC 6803. *J Biol Chem, 280*(1): 840-846.

Hug, L. A., Thomas, B. C., Sharon, I., Brown, C. T., Sharma, R., Hettich, R. L. *et al.* (2016). Critical biogeochemical functions in the subsurface are associated with bacteria from new phyla and little studied lineages. *Environ Microbiol, 18*(1): 159-173.

Huisman, J., Codd, G. A., Paerl, H. W., Ibelings, B. W., Verspagen, J. M., & Visser, P. M. (2018). Cyanobacterial blooms. *Nat Rev Microbiol, 16*: 471-483.

Huntemann, M., Ivanova, N. N., Mavromatis, K., Tripp, H. J., Paez-Espino, D., Palaniappan, K. *et al.* (2015). The standard operating procedure of the DOE-JGI microbial genome annotation pipeline (MGAP v. 4). *Stand Genomic Sci, 10*(1): 1-6.

Imlay, J. A. (2003). Pathways of oxidative damage. *Annu Rev Microbiol, 57*(1): 395-418.

Imlay, J. A. (2019). Where in the world do bacteria experience oxidative stress? *Environ Microbiol, 21*(2): 521-530.

Jensen, H. S., & Andersen, F. O. (1992). Importance of temperature, nitrate, and pH for phosphate release from aerobic sediments of four shallow, eutrophic lakes. *Limnol Oceanogr, 37*(3): 577-589.

Joshi, N., & Fass, J. (2011). Sickle: A sliding-window, adaptive, quality-based trimming tool for FastQ files (Version 1.33)[Software]. In.

Kaebernick, M., Neilan, B. A., Börner, T., & Dittmann, E. (2000). Light and the transcriptional response of the microcystin biosynthesis gene cluster. *Appl Environ Microbiol, 66*(8): 3387-3392.

Kanehisa, M., Sato, Y., & Morishima, K. (2016). BlastKOALA and GhostKOALA: KEGG tools for functional characterization of genome and metagenome sequences. *J Mol Biol, 428*(4): 726-731.

Kang, D. D., Li, F., Kirton, E., Thomas, A., Egan, R., An, H., & Wang, Z. (2019). MetaBAT 2: an adaptive binning algorithm for robust and efficient genome reconstruction from metagenome assemblies. *PeerJ, 7*: e7359.

Kawasaki, K., & Kamagata, Y. (2017). Phosphate-catalyzed hydrogen peroxide formation from agar, gellan, and κ-carrageenan and recovery of microbial cultivability via catalase and pyruvate. *Appl Environ Microbiol, 83*(21): e01366-01317.

Khademian, M., & Imlay, J. A. (2017). *Escherichia coli* cytochrome c peroxidase is a respiratory oxidase that enables the use of hydrogen peroxide as a terminal electron acceptor. *Proc Natl Acad Sci, 114*(33): E6922-E6931.

Kim, J.-G., Park, S.-J., Damsté, J. S. S., Schouten, S., Rijpstra, W. I. C., Jung, M.-Y. *et al.* (2016). Hydrogen peroxide detoxification is a key mechanism for growth of ammonia-oxidizing archaea. *Proc Natl Acad Sci, 113*(28): 7888-7893.

Kim, M., Shin, B., Lee, J., Park, H. Y., & Park, W. (2019a). Culture-independent and culture-dependent analyses of the bacterial community in the phycosphere of cyanobloom-forming *Microcystis aeruginosa*. *Sci Rep, 9*(1): 1-13.

Kim, S., Kang, I., Seo, J.-H., & Cho, J.-C. (2019b). Culturing the ubiquitous freshwater actinobacterial acI lineage by supplying a biochemical 'helper' catalase. *ISME J, 13*: 2252-2263.

King, D. W., Cooper, W. J., Rusak, S. A., Peake, B. M., Kiddle, J. J., O'Sullivan, D. W. *et al.* (2007). Flow injection analysis of H2O2 in natural waters using acridinium ester chemiluminescence: method development and optimization using a kinetic model. *Anal Chem, 79*(11): 4169-4176.

Kurmayer, R., Christiansen, G., & Chorus, I. (2003). The abundance of microcystin-producing genotypes correlates positively with colony size in *Microcystis* sp. and determines its microcystin net production in Lake Wannsee. *Appl Environ Microbiol, 69*(2): 787-795.

Laczny, C. C., Sternal, T., Plugaru, V., Gawron, P., Atashpendar, A., Margossian, H. H. *et al.* (2015). VizBin-an application for reference-independent visualization and human-augmented binning of metagenomic data. *Microbiome, 3*(1): 1.

Langmead, B., & Salzberg, S. L. (2012). Fast gapped-read alignment with Bowtie 2. *Nature methods, 9*(4): 357.

Latifi, A., Ruiz, M., & Zhang, C.-C. (2009). Oxidative stress in cyanobacteria. *FEMS Microbiol Rev, 33*(2): 258-278.

Li, D., Liu, C.-M., Luo, R., Sadakane, K., & Lam, T.-W. (2015). MEGAHIT: an ultra-fast single-node solution for large and complex metagenomics assembly via succinct de Bruijn graph. *Bioinformatics, 31*(10): 1674-1676.

Li, H., & Durbin, R. (2009). Fast and accurate short read alignment with Burrows–Wheeler transform. *Bioinformatics, 25*(14): 1754-1760.

Lopalco, A., Dalwadi, G., Niu, S., Schowen, R. L., Douglas, J., & Stella, V. J. (2016). Mechanism of decarboxylation of pyruvic acid in the presence of hydrogen peroxide. *J Pharm Sci, 105*(2): 705-713.

Lürling, M., Meng, D., & Faassen, E. J. (2014). Effects of hydrogen peroxide and ultrasound on biomass reduction and toxin release in the cyanobacterium, *Microcystis aeruginosa*. *Toxins, 6*(12): 3260-3280.

Ma, L., Calfee, B. C., Morris, J. J., Johnson, Z. I., & Zinser, E. R. (2018). Degradation of hydrogen peroxide at the ocean's surface: the influence of the microbial community on the realized thermal niche of *Prochlorococcus*. *ISME J, 12*(2): 473-484.

Markowitz, V. M., Chen, I.-M. A., Palaniappan, K., Chu, K., Szeto, E., Grechkin, Y. *et al.* (2011). IMG: the integrated microbial genomes database and comparative analysis system. *Nucleic Acids Res, 40*(D1): D115-D122.

Marsico, R. M., Schneider, R. J., Voelker, B. M., Zhang, T., Diaz, J. M., Hansel, C. M., & Ushijima, S. (2015). Spatial and temporal variability of widespread dark production and decay of hydrogen peroxide in freshwater. *Aquat Sci, 77*(4): 523-533.

Mas, A., Jamshidi, S., Lagadeuc, Y., Eveillard, D., & Vandenkoornhuyse, P. (2016). Beyond the black queen hypothesis. *ISME J, 10*(9): 2085.

Meissner, S., Steinhauser, D., & Dittmann, E. (2015). Metabolomic analysis indicates a pivotal role of the hepatotoxin microcystin in high light adaptation of *Microcystis*. *Environ Microbiol, 17*(5): 1497-1509.

Mikula, P., Zezulka, S., Jancula, D., & Marsalek, B. (2012). Metabolic activity and membrane integrity changes in *Microcystis aeruginosa* - new findings on hydrogen peroxide toxicity in cyanobacteria. *Eur J Phycol, 47*(3): 195-206.

Miller, C. S., Baker, B. J., Thomas, B. C., Singer, S. W., & Banfield, J. F. (2011). EMIRGE: reconstruction of full-length ribosomal genes from microbial community short read sequencing data. *Genome Biol, 12*(5): R44.

Mishra, S., & Imlay, J. (2012). Why do bacteria use so many enzymes to scavenge hydrogen peroxide? *Arch Biochem Biophys, 525*(2): 145-160.

Moffett, J. W., & Zafiriou, O. C. (1990). An investigation of hydrogen peroxide chemistry in surface waters of Vineyard Sound with $H_2{}^{18}O_2$ and $^{18}O_2$. *Limnol Oceanogr, 35*(6): 1221-1229.

Morris, J. J., Kirkegaard, R., Szul, M. J., Johnson, Z. I., & Zinser, E. R. (2008). Facilitation of robust growth of *Prochlorococcus* colonies and dilute liquid cultures by "helper" heterotrophic bacteria. *Appl Environ Microbiol, 74*(14): 4530-4534.

Morris, J. J., Johnson, Z. I., Szul, M. J., Keller, M., & Zinser, E. R. (2011). Dependence of the cyanobacterium *Prochlorococcus* on hydrogen peroxide scavenging microbes for growth at the ocean's surface. *PloS one, 6*(2): e16805.

Morris, J. J., Lenski, R. E., & Zinser, E. R. (2012). The Black Queen Hypothesis: evolution of dependencies through adaptive gene loss. *MBio, 3*(2): e00036-00012.

Morris, J. J., & Zinser, E. R. (2013). Continuous hydrogen peroxide production by organic buffers in phytoplankton culture media. *J Phycol, 49*(6): 1223-1228.

Morris, J. J. (2015). Black Queen evolution: the role of leakiness in structuring microbial communities. *Trends Genet, 31*(8): 475-482.

Morris, J. J., Johnson, Z. I., Wilhelm, S. W., & Zinser, E. R. (2016). Diel regulation of hydrogen peroxide defenses by open ocean microbial communities. *J Plankton Res, 38*(4): 1103-1114.

Nogoceke, E., Gommel, D. U., Kieß, M., Kalisz, H. M., & Flohé, L. (1997). A unique cascade of oxidoreductases catalyses trypanothione-mediated peroxide metabolism in *Crithidia fasciculata*. *Biol Chem, 378*(8): 827-836.

Olm, M. R., Brown, C. T., Brooks, B., & Banfield, J. F. (2017). dRep: a tool for fast and accurate genomic comparisons that enables improved genome recovery from metagenomes through de-replication. *ISME J, 11*(12): 2864.

Ouellette, A. J., Handy, S. M., & Wilhelm, S. W. (2006). Toxic *Microcystis* is widespread in Lake Erie: PCR detection of toxin genes and molecular characterization of associated cyanobacterial communities. *Microb Ecol, 51*(2): 154-165.

Paerl, H. W., Xu, H., McCarthy, M. J., Zhu, G., Qin, B., Li, Y., & Gardner, W. S. (2011). Controlling harmful cyanobacterial blooms in a hyper-eutrophic lake (Lake Taihu, China): the need for a dual nutrient (N & P) management strategy. *Water Res, 45*(5): 1973-1983.

Paerl, H. W., & Paul, V. J. (2012). Climate change: links to global expansion of harmful cyanobacteria. *Water Res, 46*(5): 1349-1363.

Paerl, H. W., & Otten, T. G. (2013). Blooms bite the hand that feeds them. *Science, 342*(6157): 433-434.

Parks, D. H., Imelfort, M., Skennerton, C. T., Hugenholtz, P., & Tyson, G. W. (2015). CheckM: assessing the quality of microbial genomes recovered from isolates, single cells, and metagenomes. *Genome Res, 25*(7): 1043-1055.

Parveen, B., Ravet, V., Djediat, C., Mary, I., Quiblier, C., Debroas, D., & Humbert, J. F. (2013). Bacterial communities associated with *Microcystis* colonies differ from free-living communities living in the same ecosystem. *Environ Microbiol Rep, 5*(5): 716-724.

Peng, Y., Leung, H. C., Yiu, S.-M., & Chin, F. Y. (2012). IDBA-UD: a de novo assembler for single-cell and metagenomic sequencing data with highly uneven depth. *Bioinformatics, 28*(11): 1420-1428.

Perelman, A., Uzan, A., Hacohen, D., & Schwarz, R. (2003). Oxidative stress in *Synechococcus* sp. strain PCC 7942: various mechanisms for H_2O_2 detoxification with different physiological roles. *J Bacteriol, 185*(12): 3654-3660.

Piel, T., Sandrini, G., White, E., Xu, T., Schuurmans, J. M., Huisman, J., & Visser, P. M. (2020). Suppressing Cyanobacteria with Hydrogen Peroxide Is More Effective at High Light Intensities. *Toxins, 12*(18): 2-20. doi:10.3390/toxins12010018

Plude, J. L., Parker, D. L., Schommer, O. J., Timmerman, R. J., Hagstrom, S. A., Joers, J. M., & Hnasko, R. (1991). Chemical Characterization of Polysaccharide from the Slime Layer of the Cyanobacterium *Microcystis flos-aquae* C3-40. *Appl Environ Microbiol, 57*(6): 1696-1700.

Price, M. N., & Arkin, A. P. (2017). PaperBLAST: text mining papers for information about homologs. *Msystems, 2*(4): e00039-00017.

Pruesse, E., Quast, C., Knittel, K., Fuchs, B. M., Ludwig, W., Peplies, J., & Glöckner, F. O. (2007). SILVA: a comprehensive online resource for quality checked and aligned ribosomal RNA sequence data compatible with ARB. *Nucleic Acids Res, 35*(21): 7188-7196.

Pruitt, K. D., Tatusova, T., & Maglott, D. R. (2007). NCBI reference sequences (RefSeq): a curated non-redundant sequence database of genomes, transcripts and proteins. *Nucleic Acids Res, 35*(suppl_1): D61-D65.

Rinta-Kanto, J., Ouellette, A., Boyer, G., Twiss, M., Bridgeman, T., & Wilhelm, S. (2005). Quantification of toxic *Microcystis* spp. during the 2003 and 2004 blooms in western Lake Erie using quantitative real-time PCR. *Environ Sci Technol, 39*(11): 4198-4205.

Robles-Rengel, R., Florencio, F. J., & Muro-Pastor, M. I. (2019). Redox interference in nitrogen status via oxidative stress is mediated by 2-oxoglutarate in cyanobacteria. *New Phytol*.

Roegner, A. F., Brena, B., González-Sapienza, G., & Puschner, B. (2014). Microcystins in potable surface waters: toxic effects and removal strategies. *J Appl Toxicol, 34*(5): 441-457.

Rognes, T., Flouri, T., Nichols, B., Quince, C., & Mahé, F. (2016). VSEARCH: a versatile open source tool for metagenomics. *PeerJ, 4*: e2584.

Roller, B. R., Stoddard, S. F., & Schmidt, T. M. (2016). Exploiting rRNA operon copy number to investigate bacterial reproductive strategies. *Nat Microbiol, 1*(11): 1-7.

Sandrini, G., Piel, T., Xu, T., White, E., Qin, H., Slot, P. C. *et al.* (2020). Sensitivity to hydrogen peroxide of the bloom-forming cyanobacterium *Microcystis* PCC 7806 depends on nutrient availability. *Harmful Algae, 99*: 101916.

Scanlan, D. J., Ostrowski, M., Mazard, S., Dufresne, A., Garczarek, L., Hess, W. R. *et al.* (2009). Ecological genomics of marine picocyanobacteria. *Microbiol Mol Biol Rev, 73*(2): 249-299.

Schloss, P. D., Westcott, S. L., Ryabin, T., Hall, J. R., Hartmann, M., Hollister, E. B. *et al.* (2009). Introducing mothur: open-source, platform-independent, community-supported software for describing and comparing microbial communities. *Appl Environ Microbiol, 75*(23): 7537-7541.

Schuurmans, J. M., Brinkmann, B. W., Makower, A. K., Dittmann, E., Huisman, J., & Matthijs, H. C. (2018). Microcystin interferes with defense against high oxidative stress in harmful cyanobacteria. *Harmful Algae, 78*: 47-55.

Seaver, L. C., & Imlay, J. A. (2001a). Hydrogen peroxide fluxes and compartmentalization inside growing *Escherichia coli*. *J Bacteriol, 183*(24): 7182-7189.

Seaver, L. C., & Imlay, J. A. (2001b). Alkyl hydroperoxide reductase is the primary scavenger of endogenous hydrogen peroxide in *Escherichia coli*. *J Bacteriol, 183*(24): 7173-7181.

Seymour, J. R., Amin, S. A., Raina, J.-B., & Stocker, R. (2017). Zooming in on the phycosphere: the ecological interface for phytoplankton-bacteria interactions. *Nat Microbiol, 2*(17065): 1-12. doi:10.1038/nmicrobiol.2017.65

Sieber, C. M., Probst, A. J., Sharrar, A., Thomas, B. C., Hess, M., Tringe, S. G., & Banfield, J. F. (2018). Recovery of genomes from metagenomes via a dereplication, aggregation and scoring strategy. *Nat Microbiol, 3*(7): 836-843.

Steffen, M. M., Dearth, S. P., Dill, B. D., Li, Z., Larsen, K. M., Campagna, S. R., & Wilhelm, S. W. (2014). Nutrients drive transcriptional changes that maintain metabolic homeostasis but alter genome architecture in *Microcystis*. *ISME J, 8*(10): 2080-2092.

Steffen, M. M., Davis, T. W., McKay, R. M. L., Bullerjahn, G. S., Krausfeldt, L. E., Stough, J. M. *et al.* (2017). Ecophysiological Examination of the Lake Erie *Microcystis* Bloom in 2014: Linkages between Biology and the Water Supply Shutdown of Toledo, OH. *Environ Sci Technol, 51*(12): 6745-6755.

Tanaka, T., Kawasaki, K., Daimon, S., Kitagawa, W., Yamamoto, K., Tamaki, H. *et al.* (2014). A hidden pitfall in the preparation of agar media undermines microorganism cultivability. *Appl Environ Microbiol, 80*(24): 7659-7666.

Tichy, M., & Vermaas, W. (1999). In Vivo Role of Catalase-Peroxidase in *Synechocystis* sp. Strain PCC 6803. *J Bacteriol, 181*(6): 1875-1882.

Tillett, D., Dittmann, E., Erhard, M., von Döhren, H., Börner, T., & Neilan, B. A. (2000). Structural organization of microcystin biosynthesis in *Microcystis aeruginosa* PCC7806: an integrated peptide–polyketide synthetase system. *Chem Biol, 7*(10): 753-764.

Wang, Q., Garrity, G. M., Tiedje, J. M., & Cole, J. R. (2007). Naive Bayesian classifier for rapid assignment of rRNA sequences into the new bacterial taxonomy. *Appl Environ Microbiol, 73*(16): 5261-5267.

Winter, J. G., Palmer, M. E., Howell, E. T., & Young, J. D. (2015). Long term changes in nutrients, chloride, and phytoplankton density in the nearshore waters of Lake Erie. *J Great Lakes Res, 41*(1): 145-155.

Worm, J., & Søndergaard, M. (1998). Dynamics of heterotrophic bacteria attached to *Microcystis* spp.(Cyanobacteria). *Aquat Microb Ecol, 14*(1): 19-28.

Xiao, M., Willis, A., & Burford, M. A. (2017). Differences in cyanobacterial strain responses to light and temperature reflect species plasticity. *Harmful Algae, 62*: 84-93.

Zilliges, Y., Kehr, J.-C., Meissner, S., Ishida, K., Mikkat, S., Hagemann, M. *et al.* (2011). The cyanobacterial hepatotoxin microcystin binds to proteins and increases the fitness of *Microcystis* under oxidative stress conditions. *PloS one, 6*(3): e17615.

Zinser, E. R. (2018a). The microbial contribution to reactive oxygen species dynamics in marine ecosystems. *Environ Microbiol Rep, 10*(4): 412-427.

Zinser, E. R. (2018b). Cross-protection from hydrogen peroxide by helper microbes: the impacts on the cyanobacterium *Prochlorococcus* and other beneficiaries in marine communities. *Environ Microbiol Rep, 10*(4): 399-411.

Chapter 3 Individual *Microcystis* Colonies Harbor Distinct Bacterial Communities That Differ by *Microcystis* Oligotype and With Time

3.1 Abstract

Interactions between bacteria and phytoplankton in the phycosphere have impacts at the scale of whole ecosystems, including the development of harmful algal blooms. The cyanobacterium *Microcystis* causes toxic blooms that threaten freshwater ecosystems and human health globally. *Microcystis* grows in colonies that harbor dense assemblages of other bacteria, yet the taxonomic composition of these phycosphere communities and the nature of their interactions with *Microcystis* are not well characterized. To identify the taxa and compositional variance within *Microcystis* phycosphere communities, we performed 16S rRNA V4 region amplicon sequencing on individual *Microcystis* colonies collected biweekly via high-throughput droplet encapsulation during a western Lake Erie cyanobacterial bloom. The *Microcystis* phycosphere communities were distinct from microbial communities in whole water and bulk phytoplankton seston in western Lake Erie but lacked "core" taxa found across all colonies. However, dissimilarity in phycosphere community composition correlated with sampling date and the *Microcystis* 16S rRNA oligotype. Several taxa in the phycosphere were specific to and conserved with *Microcystis* of a single oligotype or sampling date. Together, this suggests that physiological differences between *Microcystis* strains, temporal changes in strain phenotypes, and the composition of seeding communities may impact community composition of the *Microcystis* phycosphere.

3.2 Introduction

Microbial interactions play a central role in many biogeochemical processes and have ecosystem wide impacts. A familiar example is the interaction between phytoplankton and heterotrophic bacteria, which can often be mutualistic. Specifically, phytoplankton provide organic carbon and sulfur that support heterotrophic bacterial growth while their heterotrophic partners improve phytoplankton growth by producing essential vitamins and growth promotors (Croft *et al.*, 2005; Amin *et al.*, 2015; Durham *et al.*, 2015; Durham *et al.*, 2017), increasing the bioavailability of trace metals (Amin *et al.*, 2009; Basu *et al.*, 2019), regenerating nutrients from organic material (Van Mooy *et al.*, 2012; Amin *et al.*, 2015; Arandia-Gorostidi *et al.*, 2017; Christie-Oleza *et al.*, 2017), and detoxifying reactive oxygen species (Morris *et al.*, 2011; Ma *et al.*, 2018).

Many phytoplankton-bacteria interactions occur in close proximity or with physical attachment of the interacting cells (Paerl & Gallucci, 1985; Segev *et al.*, 2016; Arandia-Gorostidi *et al.*, 2017; Frischkorn *et al.*, 2017) within a zone of interaction called the phycosphere (Bell & Mitchell, 1972; Cole, 1982; Seymour *et al.*, 2017). The phycosphere is rich in dissolved organic carbon (DOC) exuded by phytoplankton or released upon cell lysis, which attracts chemotactic bacteria (Bell & Mitchell, 1972; Paerl & Gallucci, 1985; Barbara & Mitchell, 2003; Sonnenschein *et al.*, 2012; Smriga *et al.*, 2016). Interactions within the phycosphere can take place between conserved heterotrophic community members and phytoplankton taxa (Jasti *et al.*, 2005; Sison-Mangus *et al.*, 2014; Durham *et al.*, 2015; Frischkorn *et al.*, 2017; Lee *et al.*, 2017). The recruitment of specific heterotrophic taxa may be driven by the production of signaling-molecules (Durham *et al.*, 2015; Segev *et al.*, 2016; Durham *et al.*, 2017) or through the unique exometabolomes of each phytoplankton taxon (Bell & Mitchell, 1972; Seymour *et al.*, 2010; Landa *et al.*, 2017), which may elicit chemotactic responses in specific taxa (Bell & Mitchell,

1972; Bassler *et al.*, 1991; Miller *et al.*, 2004). Interactions within the phycosphere have impacts at the scale of whole ecosystems (Azam & Malfatti, 2007; Seymour *et al.*, 2017), such as driving carbon cycling (Smriga *et al.*, 2016) or algal bloom development and termination (Seyedsayamdost *et al.*, 2011) in marine systems.

While a growing body of literature has characterized phycosphere interactions between marine taxa (Ferrier *et al.*, 2002; Jasti *et al.*, 2005; Sison-Mangus *et al.*, 2014; Amin *et al.*, 2015; Segev *et al.*, 2016; Frischkorn *et al.*, 2017), comparatively little work has been conducted in freshwater systems despite their importance for recreation, fisheries, biodiversity, agriculture, and drinking water. Globally, freshwaters are increasingly threatened by cyanobacterial harmful algal blooms (CHABs) due to anthropogenic nutrient pollution and global climate change (Huisman *et al.*, 2018). *Microcystis* is a globally dominant cyanobacterium in many freshwater CHABs, and some strains produce microcystins, a class of potent hepatotoxins that can cause liver damage and death in mammals when ingested (Harke *et al.*, 2016). *Microcystis* spp. grow in large, buoyant colonies (50-1000 μm diameter) (Zhu *et al.*, 2014) that can be either clonal or nonclonal (Otten *et al.*, 2017; Jackrel *et al.*, 2019) and harbor other bacteria (Hindák, 1996; Worm & Søndergaard, 1998). Studies on bulk phytoplankton aggregates dominated by *Microcystis* suggest that the bacterial communities associated with *Microcystis* colonies are distinct from those associated with other cyanobacteria and free-living communities in the surrounding water column (Parveen *et al.*, 2013; Louati *et al.*, 2015; Zhu *et al.*, 2019; Jankowiak & Gobler, 2020). Interactions between other phytoplankton and bacteria influence the growth and toxin production of marine harmful algal blooms (Ferrier *et al.*, 2002; Adachi *et al.*, 2003; Sison-Mangus *et al.*, 2014), with some strain and species specific effects (Sison-Mangus *et al.*, 2014), and bacteria can influence the invasion capability of some *Microcystis* strains into

established green algae cultures (Schmidt *et al.*, 2020). Together, these observations suggest that bacteria associated with *Microcystis* could affect the relative fitness and proportion of *Microcystis* strains, which is an important determinant of *Microcystis* bloom microcystin concentrations (Kardinaal *et al.*, 2007; Davis *et al.*, 2009; Davis *et al.*, 2010; Otten *et al.*, 2012). While previous studies have characterized heterotrophic bacteria populations in enrichment culture with *Microcystis* (Jackrel *et al.*, 2019; Kim *et al.*, 2019) or in total communities during blooms (Parveen *et al.*, 2013; Louati *et al.*, 2015; Berry *et al.*, 2017a; Shi *et al.*, 2018; Chun *et al.*, 2019; Kim *et al.*, 2019; Zhu *et al.*, 2019; Chun *et al.*, 2020; Cook *et al.*, 2020; Jankowiak & Gobler, 2020), the microbes that comprise natural *Microcystis* colonies and the variation in community composition across individual colonies are comparatively understudied. To our knowledge, only two studies have identified the bacterial communities associated with single *Microcystis* colonies (Shia *et al.*, 2010; Tu *et al.*, 2019). Both were limited to single timepoints and low numbers of colonies, and one did not deeply characterize colony-associated communities with high-throughput sequencing (Shia *et al.*, 2010). Therefore, the extent to which *Microcystis* phycosphere communities on individual colonies vary across strains and species of *Microcystis* and with time and space is unknown.

In order to characterize the bacterial communities associated with the *Microcystis* phycosphere, we isolated single *Microcystis* colonies from a western Lake Erie CHAB in 2019 via droplet encapsulation, which provides higher throughput and precision than traditional methods of colony isolation. We then performed amplicon sequencing of the V4 region of the bacterial 16S rRNA genes. With the resulting dataset, we focus on answering the following questions: 1) Do *Microcystis* colonies harbor taxa that are regularly present, comprising a "core" phycosphere community? 2) How do *Microcystis* phycosphere communities vary between

individual colonies? 3) How do *Microcystis* phycosphere communities change throughout bloom development? We found that *Microcystis* colonies harbor phycosphere communities that are distinct from whole water bacterial communities and bulk phytoplankton seston (100 μm retentate, including *Microcystis* colonies) communities, and differ by sampling date and *Microcystis* oligotype. We hypothesize that these distinct phycosphere communities are shaped by strain-specific interactions as well as changes in either seeding communities or the physicochemical environment over time.

3.3 Methods

3.3.1 Field Sampling

Microcystis colonies were collected approximately biweekly at two locations in western Lake Erie (Figure S 3.1) during the 2019 CHAB. The majority of colonies were sampled from NOAA station WE8, with the exception of one date (9-Sep-19) on which station WE16 was sampled. Sample collection covered a range of bloom development stages and microcystin concentrations (Figure S 3.2). Microcystis biomass was collected with 2-4 casts of a 53 μm plankton net, which retains 99 % of *Microcystis* cells (Chaffin *et al.*, 2011). Biomass retained on the net was backwashed into 1-2 50 mL centrifuge tubes with 0.22 μm filtered and autoclaved Lake Erie water. The collected material was stored in a cooler filled with lake water until arrival back at the lab. Between each cruise, the plankton net was disinfected with 10% bleach and rinsed with DI water. Environmental and water chemistry data were obtained from NOAA's National Centers for Environmental Information (accession 0209116).

3.3.2 Individual Colony Isolation via Droplet Encapsulation

Immediately upon arrival to the lab, the biomass was filtered through a 300 μm pore size filter mesh and retained on filter mesh with 105 μm pore size. The 105 μm retentate from all

samples collected on a given date were transferred to a new 50 mL falcon tube using a squirt bottle containing molecular grade PBS. Then the falcon tube was filled to 30 mL with molecular grade PBS. The biomass was allowed to settle for 10 minutes, which caused non-cyanobacterial particles to sink and cyanobacteria colonies to buoyantly float to the top of the solution (Shi *et al.*, 2018; Zhu *et al.*, 2019). The buoyant colonies were then transferred to a new falcon tube using a sterile pipette, and resuspended in new molecular grade PBS solution. The colony wash and transfer was repeated 5 additional times to separate loosely attached or free-living bacteria from the colonies. On the final washing step, the colonies were collected and placed into a sterile 2 mL microcentrifuge tube. The concentration of colonies was estimated by dispensing 5 µL aliquots onto multiple glass slides and counting colonies under an inverted light microscope.

After washing, droplet encapsulation of the cyanobacterial colonies was performed using a syringe pump to encapsulate the colony suspension into droplets that could be individually processed (Figure 3.1). First, the cyanobacterial colonies were diluted to approximately 67 colonies/mL (1 colony in every 15 µL) with PBS solution and loaded into a 10 mL luer-lock syringe with a 23 gauge needle (337 µm inner diameter), along with 1 mL of air. The syringe was loaded into a syringe pump (Kent Scientific, GenieTouch™) set to a continuous flow rate of 600 µL/min and placed on top of an orbital shaker set to 100 - 150 rpm (Figure 3.1). Tubing (PTFE, 0.022x0.042'', Cole-Parmer EW-06417-21) attached to the syringe needle allowed a droplet (~15 µL volume) to form and fall onto a section of a sterile petri dish. Before droplets were formed with the colony suspension, several droplets were formed with sterile PBS solution to serve as blank controls for subsequent sequencing. All droplets were inspected and imaged with an inverted light microscope (Nikon Eclipse Ti-S). Droplets containing one *Microcystis* colony were transferred to a 96 well PCR plate using a P1000 micropipette tip. The larger

volume tip was required to prevent the colonies from clogging the tip. The PCR plate was covered with sterile aluminum foil (VWR 89049-034) and frozen at -20 °C until DNA extraction. In total, we screened 800 droplets and collected 210 droplets that contained a single *Microcystis* colony.

Colony dimensions were measured from microscopy images with ImageJ (2.0.0-rc-69/1.52i). Length and width were defined by drawing lines through the longest and shortest dimensions, respectively, on 2D colony images. Area was drawn by manual free-hand selection around the distinguishable boundary of the colony. The scale (μm/pixel) was calculated using scale bars from microscopy. Colony morphology was assigned using published morphospecies classifications (Otsuka *et al.*, 2000).

3.3.3 DNA Extraction and Sequencing

DNA extractions of colonies and PBS blanks were performed with ChargeSwitch® gDNA Mini Bacteria Kits (Invitrogen Life Technologies, California, USA) using a protocol modified for single *Microcystis* colonies (Pérez-Carrascal *et al.*, 2019). From the 210 droplets collected, DNA was extracted from 122 colonies (17-25 for each sampling date) in a laminar flow-hood to minimize contamination from the lab. Because single colony samples had very low biomass, the samples were subjected to a round of PCR using dual indexed primers targeting the V4 region of the bacterial 16S rRNA gene (Kozich *et al.*, 2013) to confirm the presence of amplifiable DNA in the samples and its absence in PBS blanks. The raw DNA extracts of blanks and all amplifiable samples (n=60) were submitted for sequencing using Illumina MiSeq V2 500 cycle chemistry (Illumina cat# MS102-2003) at the University of Michigan Microbial Community Analysis Core following their SOP (Schloss & Bishop, 2019).

DNA was collected from microbial communities in whole and 105 μm filtered water from western Lake Erie in the summer and fall of 2014 and 2017-2019 to compare with phycosphere communities. Amplicon data from the 2014 bloom was obtained from a previously published study (Berry *et al.*, 2017a). Whole water microbial communities from 2017-2019 were collected by filtering 100-200 mL of lake water through a 0.22 μm PES filter. The filter was preserved in RNAlater and frozen at -80 °C until DNA extraction. Microbial communities from the < 100 μm size fraction (smaller than the *Microcystis* colonies sequenced) were collected by filtering whole lake water through a 100 μm plankton mesh and collecting the filtrate into an acid-washed 2L polycarbonate bottle. Then, 200 mL of the 100 μm filtrate was filtered through a 0.22 μm PES filter, preserved in RNAlater and frozen at -80 °C until DNA extraction. In 2017, filters were collected weekly at NOAA monitoring station WE2 and periodically near the drinking water intake for Toledo, OH, and at various Environment Canada monitoring sites during two research cruises (Figure S 3.1). In 2018 and 2019, filters were collected during pre-bloom, early bloom, mid bloom, and late bloom phases from NOAA station WE2 and the drinking water intake for Toledo, OH in 2018, and at locations of highest bloom density as predicted by the NOAA HAB tracker in 2019 (Wynne *et al.*, 2013). The water used for total microbial communities in 2017-2019 was stored for 12-15 hours in an outdoor water bath set to lake water temperature before sample collection. DNA was extracted from the filters using QIAgen DNeasy Blood & Tissue Kits with QIAshredder columns (QIAGEN, Maryland, USA). Genomic DNA from *Thermus thermophilus* strain DSM 7039 was added to the samples after the cell lysis step of the extraction as an internal standard. *Thermus thermophilus* DNA was obtained from the American Type Culture Collection (ATCC; product number BAA-163D-5). The internal standard was added as ~ 1 % of DNA yield, which was estimated based on an

empirically determined relationship between total mass of chlorophyll *a* on the filter and DNA yield. DNA yields were measured with Quant-iT Picogreen dsDNA Assay Kit (Invitrogen, Carlsbad, CA). The true percentage of the internal standard was 0.72 ± 0.37 % of total DNA yield on average. The extraction protocol is included as a supplemental data file.

3.3.4 Bioinformatic and Statistical Analyses

Forward and reverse reads were quality screened to remove sequences below 250 bases and trimmed to Q20 using BBDuk (Bushnell, 2018). Any read pairs in which a read had 50 % or more of the bases trimmed were removed from downstream analysis. Any samples that had fewer than 1000 reads after QC were not included in downstream analysis (final n=44). Following trimming, overlapping forward and reverse reads were assembled into contigs, aligned, screened for chimeras, and clustered into operational taxonomic units (OTUs) using MOTHUR v. 1.43.0, following the SOP as of February 2020 (Kozich *et al.*, 2013). OTU clustering was performed using a 97 % similarity cutoff with the OptiClust algorithm (Westcott & Schloss, 2017). Contigs were aligned with the align.seqs function in MOTHUR, and taxonomy was assigned using the Wang method (Wang *et al.*, 2007). v. 138 SSU database (Pruesse *et al.*, 2007) was used as the reference to align and classify the contigs. The data were also clustered into oligotype OTUs (referred to as nodes in the original paper) using minimum entropy decomposition (MED) without outlier replacement (Eren *et al.*, 2015). The minimum substantial abundance at which an MED node was reported was set to 854, following the previously published suggestion of using N/10 000, where N is the total number of sequences in the dataset (Eren *et al.*, 2015). The relative abundance of the 97 % OTUs and MED nodes in each sample was calculated as the proportion of the total reads from a sample that were assigned to a given OTU or MED node. MED nodes were used to resolve finer-scale variation in

Microcystis sequences, and 97% OTUs were used for overall comparisons of non-*Microcystis* community composition to avoid confounding effects of sequence variation in MED nodes that may reflect nonidentical gene copies originating from a single genome rather than genes from different species. All OTUs classified as *Thermus* in bulk samples were removed from the dataset prior to NMDS analysis.

To determine the nucleotide similarity of multiple 16S rRNA gene copies in *Microcystis* genomes, we downloaded 16S rRNA gene sequences from each closed *Microcystis* genome available in NCBI (as of June 24, 2020; n = 9). Then the gene copies from each genome were aligned using Blastn in the NCBI web tool. *Microcystis* colonies were assigned to oligotype groups based on the identity of their pairs of MED sequence variants (Oligoype 1 = Nodes 8432-8432, Oligoype 2 = Nodes 1993-8432, Oligoype 3 = Nodes 8437-8437, Oligoype 4 = Nodes 8432-8437).

Because interpretations of community structure in low biomass samples are significantly altered by contamination from the lab and DNA extraction kits (Salter *et al.*, 2014), we screened the final OTUs for contaminating taxa, following previously published suggestions (Salter *et al.*, 2014; Sheik *et al.*, 2018). First, all OTUs comprised of 1-2 sequences or present in only one colony at ≤ 0.1 % abundance were removed from the data set. Second, we checked the legitimacy of any OTUs in the *Microcystis* colonies classified with a taxonomy that matched to known contaminants from DNA extraction kits (Salter *et al.*, 2014; Sheik *et al.*, 2018) by screening for their presence in the field samples. Potential contaminant OTUs with a relative abundance that was not significantly different from zero in all field samples were removed from the colony dataset. The taxonomic assignments of contaminant OTUs flagged for removal were confirmed by blasting the representative sequence against the NCBI nr database.

Alpha diversity metrics, Bray-Curtis dissimilarities between colonies, non-metric multidimensional scaling (NMDS) ordinations, mantel tests, and ANOSIM tests were computed using the R package Vegan v. 2.5-6 (Oksanen *et al.*, 2013). Bray-Curtis dissimilarity was used as the distance metric for all beta-diversity calculations. Euclidean distance was used to measure dissimilarity in environmental parameters. Hierarchical clustering (HC) of samples by Bray-Curtis dissimilarity was performed using an average linkage algorithm. All calculations of beta-diversity were performed without including *Microcystis* OTUs. Diagnostic species (species that are statistical predictors for classes of sites or samples) of sample date and oligotype were identified by calculating a complete Indval.g metric for each OTU using the R package indicspecies v. 1.7.9 (Cáceres & Legendre, 2009). Correlation analyses and other standard calculations were calculated using base R. Three-dimensional NMDS plots were made with plotly v. 4.9.2 (https://github.com/ropensci/plotly). All other plots were made with ggplot2 v. 3.2.1 (https://cran.r-project.org/web/packages/ggplot2/index.html). The code for the entire bioinformatic and statistical analysis pipeline is publicly available at (https://github.com/Geo-omics/Characterizing-individual-Microcystis-colony-phycosphere-communities). The raw sequence data is deposited in NCBI SRA under BioProjects PRJNA645738 and PRJNA646259.

3.4 Results and Discussion

3.4.1 Microcystis Colony Oligotype Assignment

MED analysis showed that the *Microcystis* sequences in each colony were primarily composed of either a single oligotype or two oligotypes at approximately equal proportions (Figure S 3.3). We interpret that the colonies with primarily two oligotypes represent clonal colonies comprised of *Microcystis* strains with two distinct 16S rRNA gene copies, while the colonies with primarily one oligotype represent clonal *Microcystis* colonies comprised of strains

with two identical V4 regions of the 16S rRNA gene. Although some atypical colonies can form from aggregation of multiple strains (Otten *et al.*, 2017), *Microcystis* colonies from eutrophic environments are primarily clonal (Jackrel *et al.*, 2019). Furthermore, if colonies were comprised of multiple *Microcystis* strains, the proportions of the oligotypes should be more variable across the sequenced colonies. Inspection of all publicly available and closed *Microcystis* genomes (n=9) confirmed that all have two 16S rRNA gene copies. Pairwise alignment of the two gene copies from each genome showed that the shared nucleotide composition of the gene copies varies between *Microcystis* strains, and the nucleotide sequence variation occurred at different nucleotide positions in each strain (Table 3.1). From these MED results, we classified the colonies into oligotype groups based on their pair of sequence variants (see methods). While oligotypes do not perfectly represent all genotypic differences between closely related bacterial strains (Berry *et al.*, 2017b), oligotyping has been shown to identify closely related sequence variants that covary along environmental and biological gradients while ignoring artifactual sequence variation (Eren *et al.*, 2013; Eren *et al.*, 2014; Berry *et al.*, 2017b). Here, we use *Microcystis* oligotypes as an approximation of closely related *Microcystis* strains/species.

3.4.2 Microcystis Phycosphere Community Diversity

Microscopy showed that *Microcystis* colonies from western Lake Erie are densely packed with small, non-*Microcystis* bacterial cells (Figure 3.2). Amplicon sequencing of individual colonies revealed the presence of many different non-*Microcystis* taxa, some of which occurred frequently at high relative abundance across different colonies (Figure 3.3). In total, we identified 197 different non-*Microcystis* OTUs in the phycosphere. Of all the non-*Microcystis* OTUs identified in the phycosphere, the most frequently occurring and abundant were from the Bacteroidetes, Alphaproteobacteria, Betaproteobacteria, and Cyanobacteria as previously

observed in bulk colony samples (Parveen *et al.*, 2013; Louati *et al.*, 2015; Shi *et al.*, 2018; Zhu *et al.*, 2019). There were also abundant but less frequent OTUs from the Acidobacteria, Oligoflexia, and Gammaproteobacteria (Figure 3.3).

Estimated species richness of individual colonies ranged from 2-74 non-*Microcystis* OTUs (Figure S 3.4). However, the majority of colonies had 10-40 non-*Microcystis* OTUs and a Shannon Index of 1.2-2.6 (a higher Shannon Index indicates a more diverse community in terms of species richness and evenness) and were less diverse than the communities in whole and 105 μm filtered water (Figure S 3.4). Mean colony species richness and diversity was highest in July and August (Figure S 3.5) and differed by *Microcystis* oligotype (Figure S 3.6). Phycosphere communities from oligotype 3 colonies had significantly greater estimated species richness and Shannon index than those of other *Microcystis* oligotypes, and oligotype 1 had higher richness and Shannon index than oligotype 2 on average. There were no significant correlations between species richness or Shannon index and colony size (Figure S 3.7).

3.4.3 Microcystis Phycosphere Communities are Dissimilar From Bulk Community Samples

To compare *Microcystis* phycosphere communities with surrounding communities, we performed hierarchical clustering (HC) and ordination of the colony-associated sequences together with those from whole water, 105 μm filtered samples, and bulk 100 μm retentate from western Lake Erie CHAB communities in 2014 and 2017-2019. HC and NMDS yielded four clearly separated main clusters (Figure 3.4): one containing all whole and 105 μm filtered water samples (Cluster 1), another containing *Microcystis* colonies dominated by *Cyanobium* (Cluster 2), another containing the remaining *Microcystis* colonies (Cluster 3), and another containing all the bulk 100 μm retentate samples from 2014 (Cluster 4). This clustering is supported by the results of an ANOSIM test, which showed statistically significant differences in mean

community dissimilarity between the HC groups ($R = 0.9787$, $p = 1x10^{-5}$). Whole water samples across the four sampling seasons clustered together by month collected (Figure S 3.8) and chlorophyll *a* concentration (Figure S 3.9), suggesting that the whole water microbial communities in western Lake Erie are similar between years and change in a consistent manner both seasonally and as *Microcystis* blooms develop. Despite these shifts in bulk community composition, the dissimilarity within sample types (whole water, filter fraction, or individual colony) across all years was significantly lower than the dissimilarity across sample types (ANOSIM, $R = 0.7534$, $p = 1x10^{-5}$) and indicates that the *Microcystis* phycosphere harbors a community of bacteria distinct from the total and free-living communities, as suggested previously in bulk cyanobacterial colony samples dominated by *Microcystis* (Parveen *et al.*, 2013; Louati *et al.*, 2015; Jankowiak & Gobler, 2020). In addition, high dissimilarity between single colony communities and bulk 100 μm retentate communities demonstrates that bacterial communities in bulk seston samples include communities associated with multiple phytoplankton and other particles that are not representative of *Microcystis* phycosphere communities. While the retentate samples were collected in a different year from the single *Microcystis* colonies, the low dissimilarity within groups of the same sample type across multiple years supports that this comparison is robust, albeit imperfect. These results support the idea that the *Microcystis* phycosphere provides an ecologically distinct microenvironment, similar to the phycospheres of other algae (Hasegawa *et al.*, 2007; Burke *et al.*, 2011b) and cyanobacteria (Hmelo *et al.*, 2012; Zhu *et al.*, 2019). The distinct communities directly associated with *Microcystis* colonies versus those in the filter fraction dominated by *Microcystis* coloines (i.e., bulk 100 μm retentate) also shows that bacteria in the latter should not necessarily be considered

physically associated with *Microcystis* and may be attached to other phytoplankton or particles > 100 μm in size.

3.4.4 The Microcystis Phycosphere Lacks a Core Community

While the *Microcystis* phycosphere communities are more similar to each other than whole water communities, there was high variation in phycosphere community composition. Dissimilarity was higher between *Microcystis* phycosphere communities than between bulk samples (Figure S 3.10). Consistent with this finding, only 9 OTUs were conserved across all colonies of a specific date or oligotype (Table 3.2). The majority of non-*Microcystis* OTUs occurred infrequently, yet some could comprise a large proportion of the phycosphere community when present (Figure 3.3). A few OTUs occurred more frequently, and the top 4 most frequently observed non-*Microcystis* OTUs were present in 61 - 84 % of all *Microcystis* colonies sequenced (n = 44, Figure 3.3, Table 3.4), suggesting that while these taxa are not universally present, they are more conserved taxa across the phycospheres of multiple *Microcystis* strains. Supporting this interpretation, OTUs 7 and 11 (*Pseudanabaena*) and OTU 32 (uncultured Microscillaceae) were found at high relative abundance on multiple *Microcystis* oligotypes (Figure 3.5). The observation of more conserved taxa across multiple strains is consistent with previously published results with bulk communities that identified a few bacterial taxa as regular members of the *Microcystis* phycosphere (Parveen *et al.*, 2013; Cook *et al.*, 2020; Jankowiak & Gobler, 2020).

Although some OTUs were frequently associated with *Microcystis* colonies, the relative abundance of all OTUs that were detected showed high variance across all colonies, as reflected in the difference between their maximum and mean relative abundances (Figure 3.3). Furthermore, no non-*Microcystis* OTUs were found in every colony (Figure 3.3). The high

variability in *Microcystis* phycosphere community composition contrasts with the phycosphere communities of other phytoplankton taxa, which have more stable core phycosphere communities (Frischkorn *et al.*, 2017; Lee *et al.*, 2017; Behringer *et al.*, 2018). However, high variation in the phycosphere communities of *Microcystis* has been previously observed (Shia *et al.*, 2010; Parveen *et al.*, 2013; Kim *et al.*, 2019; Jankowiak & Gobler, 2020), and the phycospheres of other phytoplankton can vary based on morphology (Hmelo *et al.*, 2012; Rouco *et al.*, 2016), strain (Jasti *et al.*, 2005; Sapp *et al.*, 2007; Ajani *et al.*, 2018; Jackrel *et al.*, 2019; Kim *et al.*, 2019), stage of growth (Sapp *et al.*, 2007), location (Rouco *et al.*, 2016; Ajani *et al.*, 2018; Kim *et al.*, 2019; Jankowiak & Gobler, 2020), and time of year (Jankowiak & Gobler, 2020). Our results from individual colonies suggest that few bacterial taxa are commonly associated with all *Microcystis* strains or inhabit the phycosphere throughout the growing season. Thus, *Microcystis* lacks a "core" microbiome from a taxonomic perspective.

3.4.5 Microcystis Phycosphere Communities Vary With Time and Microcystis Oligotype

To investigate drivers of the differences in *Microcystis* phycosphere community composition, we performed HC and NMDS ordination of *Microcystis* phycosphere communities alone. This analysis revealed that the *Microcystis* phycosphere communities could be assigned to five groups based on Bray-Curtis dissimilarity. Group membership is correlated with sampling date and oligotype as supported by an ANOSIM test, which revealed significant differences in mean colony dissimilarity by sampling date ($R = 0.4111$, $p = 1x10^{-4}$) and *Microcystis* oligotype ($R = 0.4933$, $p = 1x10^{-4}$, Figures 3.6 & 3.7) . There was also a significant difference based on colony morphology, but the correlation coefficient was low ($R = 0.1974$, $p = 0.004$). Results using MED nodes were similar, showing significant correlations with sampling date ($R = 0.476$, $p = 1x10^{-4}$) and oligotype ($R = 0.3747$, $p = 1x10^{-4}$) that were similar in value to the results with

OTUs, although the effect was stronger with date when using MED nodes. One HC cluster was comprised of a community from a single oligotype 1 colony (cluster 2), while the remaining four HC groups included communities from multiple colonies (Figure 3.7). In the following, we consider the evidence for oligotype and sampling date as drivers of phycosphere community composition, then discuss these results in the context of two competing hypotheses: (1) recruitment of *Microcystis* microbiome is selective based on allelopathic or metabolic interactions, or (2) recruitment of the *Microcystis* microbiome is neutral or influenced by different "seeding communities" in the surrounding water that change through time.

Microcystis oligotype appears to be a strong driver of community dissimilarity. Three of the four major groups identified with HC were comprised of communities from a single *Microcystis* oligotype (clusters 1, 3, 4), with the exception of one colony in cluster 3 (Figure 3.7). suggesting that *Microcystis* oligotype is a major driver of community dissimilarity. In addition, some abundant OTUs were primarily associated with a single *Microcystis* oligotype (Figure 3.5). For example, while present on colonies throughout the bloom season, OTU 43 (uncultured Sutterellaceae) and OTU 46 (*Tabrizicola*) were predominantly found on oligotype 1 and oligotype 3 colonies, respectively (Figure 3.5). This finding is consistent with previous studies that have shown that the abundance of certain bacterial OTUs during blooms are correlated with the abundance of specific *Microcystis* genotypes (Chun *et al.*, 2020). The clustering by colony oligotype suggests that different *Microcystis* strains harbor characteristic microbiomes.

There were also significant differences in phycosphere communities by sampling date. Two of the HC clusters (clusters 1 and 3), were comprised of primarily one sampling date. Three clusters were comprised primarily of colonies collected within a single month; clusters 1 and 3

were comprised entirely of colonies collected in September, while cluster 5 was comprised of colonies from July and August, with the exception of one colony that was collected in September (Figure 3.7). The abundances of *Microcystis* MED nodes in the colonies had comparable abundances in whole water samples, and both were most abundant in July-August and decreased in September (Figure S 3.11), which supports that the effect of time cannot be attributed to an autocorrelation with shifts in *Microcystis* oligotype abundance. Further supporting this, colonies in cluster 5 where all collected in July and August, yet spanned multiple oligotypes, and oligotype 1 colonies collected in September were separated into two HC clusters (clusters 3 and 4, Figure 3.6). These clustering patterns suggest that temporal effects play a role in driving phycosphere community dissimilarity. However, with our data, we cannot rule out the possibility that the significant clustering by time is not due to shifts in the abundance of *Microcystis* strains that are not differentiated with 16S V4 oligotypes. Overall, the currently available data are not sufficient to determine the relative influence of colony oligotype and sampling date.

Of the HC clusters that separated by *Microcystis* oligotype, cluster 1 included all the samples from station WE16 (Figure 3.7, station WE16 was sampled on 9-Sep-19). While this cluster was not exclusive to colonies from station WE16, the predominance of colonies from station WE16 could indicate that differences in this cluster are driven by spatial differences in bacterial communities rather than by differences in date or *Microcystis* oligotype. However, the dissimilarity in whole water communities from multiple nearshore sites in the lake were low (Figure 3.4), and a previous study showed that microbial communities in western Lake Erie vary more seasonally than spatially (Berry *et al.*, 2017a). Therefore, it unlikely that cluster 1 is an effect of station rather than *Microcystis* oligotype or time.

3.4.6 Potential Mechanisms to Explain Clustering by Microcystis Oligotype

Several mechanisms could feasibly explain a strain-dependence in *Microcystis* phycosphere community composition. Different *Microcystis* strains may release distinct antibiotics that differently inhibit the growth of various bacterial taxa in the phycosphere. Production of antibiotic compounds has been observed in *Microcystis* (Casamatta & Wickstrom, 2000) and other phytoplankton (Ribalet *et al.*, 2008). Likewise, given that many bacteria are able to colonize the phycosphere via chemotaxis (Bell & Mitchell, 1972; Paerl & Gallucci, 1985; Sonnenschein *et al.*, 2012; Raina *et al.*, 2019) to specific types of organic compounds (Bell & Mitchell, 1972; Bassler *et al.*, 1991; Casamatta & Wickstrom, 2000; Miller *et al.*, 2004; Seymour *et al.*, 2010), different *Microcystis* strains may excrete a unique pool of organic molecules that attract different heterotroph populations. Differences in the production of secondary metabolites (Le Manach *et al.*, 2019) and the sugar composition of exopolysacchrides (Forni *et al.*, 1997) have been observed between *Microcystis* strains and species, suggesting that metabolites in the phycospheres of different strains vary. Similarly, the production and consumption of metabolites by the bacteria that colonize the phycosphere may also impact the chemotaxis of other bacterial populations. For example, *Cyanobium, Pseudanabeana,* uncultured Sutterellaceae, and uncultured Microscillaceae likely play a major role in uptake and production of metabolites in the *Microcystis* phycosphere due to their high relative abundance in the colonies on which they were present (Figure 3.3). To our knowledge, the composition and structure of DOC in the *Microcystis* phycosphere has not been fully characterized. Future studies that identify the organic compounds that are in the phycosphere and transferred among community members, characterize their ability to attract chemotactic bacteria, and determine how they vary between different *Microcystis* strains are required to describe the mechanism of how different strains of *Microcystis* harbor distinct phycosphere communities.

Despite significant clustering by *Microcystis* oligotype, there was also substantial dissimilarity between phycosphere communities that shared a colony oligotype. For example, oligotype 1 colony communities were separated into two main HC clusters (clusters 3 and 4, Figure 3.7). The Bray-Curtis dissimilarity between these groups was > 0.8 and could be > 0.6 within the groups (Figure 3.7). The effect of sampling date alone is unlikely to explain the differences between clusters 3 and 4 because cluster 4 included colonies from a range of different sampling dates, which included colonies from September. The high dissimilarity within and between HC groups that share an oligotype and sampling dates suggests that *Microcystis* oligotype and date alone are insufficient to describe all of the dissimilarity in phycosphere community composition.

Dissimilarity in phycosphere communities between colonies that share an oligotype and sampling date could be explained by unresolved *Microcystis* strain differences, or by neutral effects. Because *Microcystis* 16S oligotypes are paraphyletic (Berry *et al.*, 2017b), colonies of the same oligotype may not necessarily be similar strains. Therefore, distinct HC clusters of primarily the same *Micorcystis* oligotype may reflect microbiomes of *Microcystis* strains that share a 16S oligotype but vary in other traits that determine phycosphere community composition. Alternatively, neutral processes such as the random colonization of the phycosphere could explain the differences in phycosphere communities from colonies of the same oligotype. Neutral processes were hypothesized as the primary determinant of the community composition in epiphytic communities of macroalgae (Burke *et al.*, 2011b). Indeed, the lack of a core microbiome and the low number of consistently present taxa in *Microcystis* phycosphere communities is similar to the epiphytic communities of macroalgae (Burke *et al.*, 2011b). Random colonization of distinct niches within the phycosphere by specific bacterial

groups with similar ecologies, referred to as the "lottery hypothesis" (Burke *et al.*, 2011a; Burke *et al.*, 2011b), may reconcile the significant clustering by both time and oligotype and the high phycosphere community dissimilarity between colonies of the same oligotype. The lottery hypothesis requires functional redundancy across the potential colonizing species (Burke *et al.*, 2011a), which has been observed in taxonomically different bacterial communities in *Microcystis* dominated bulk seston (Cook *et al.*, 2020) and *Microcystis* enrichment cultures (Jackrel *et al.*, 2019). However, the significant clustering by date and oligotype (Figures 3.6, 3.7), and the consistent patterns in the abundance of certain OTUs with time and *Microcystis* oligotype (Figure 3.5) conflict with the hypothesis that random colonization is a major determinant of *Microcystis* phycosphere community composition and rather suggest that selective mechanisms have a role in determining the differences in *Microcystis* phycosphere community composition, at least in part. The idea that selective mechanisms determine *Microcystis* phycosphere community composition is congruent with previous observations in that phytoplankton cultures of the same genus or species have more similar associated bacteria communities than those from other phytoplankton taxa (Grossart *et al.*, 2005; Jasti *et al.*, 2005; Sapp *et al.*, 2007; Bagatini *et al.*, 2014; Behringer *et al.*, 2018), and bacteria colonize diatom cultures in a predictable manner (Mönnich *et al.*, 2020). Ultimately, future datasets with better resolution of *Microcystis* strains, along with colonization experiments using different *Microcystis* strains and bacterial inocula, are required to determine the relative importance of selective and neutral processes in shaping *Microcystis* phycosphere community composition.

3.4.7 Potential Mechanisms to Explain Clustering by Sampling Date

Our results provide evidence that shifts in seeding communities from the surrounding water may have a significant role in shaping phycosphere community structure. Supporting this

hypothesis, several OTUs (OTU 7 *Pseudanabaena*, OTU 10 *Roseomonas*, OTU 11 *Pseudanabaena*) that were present on multiple *Microcystis* oligotypes showed decreases in the average relative abundances of these OTUs on the colonies that corresponded with decreases in their average relative abundance in 105 µm filtered water (Figure 3.5). This observation is consistent with previous work showing that inoculum source had a significant impact on bacterial community composition in a *Microcystis* culture colonization experiment (Dziallas & Grossart, 2011), and that the composition of bacterial communities in western Lake Erie show strong seasonal shifts (Berry *et al.*, 2017a). Therefore, shifts in the dominant members of chemotactic populations that seed the phycosphere may change phycosphere community composition over time. However, the abundance patterns of other OTUs (OTU 43 Sutterellaceae and OTU 46 *Tabrizicola*) on *Microcysits* colonies are not similar to trends in abundance in 105 µm filtered water (Figure 3.5), which suggests that shifts in seeding communities may impact the abundances of only some phycosphere taxa.

Phenotypic differences based on changes in physiological state may impact the *Microcystis* phycosphere, as previously observed in other phytoplankton (Bell & Mitchell, 1972; Sapp *et al.*, 2007). Indeed, *Microcystis* produces different classes and amounts of DOC at different growth phases, growth rates, and temperature and nutrient regimes (Dziallas & Grossart, 2012; Li *et al.*, 2013; Xu *et al.*, 2013), which may serve as chemoattractants for different bacterial populations. The decline in both bulk phycocyanin and bulk chlorophyll *a* concentration in September (Figure S 3.2) indicates that a change in physiological state due to bloom termination could explain differences in the phycosphere communities collected at this time (Figure 3.5). Larger data sets across multiple years with better resolution of *Microcystis* genotypes along with studies of how *Microcystis* metabolite excretion changes with

physiological state are required to determine the relative importance of phenotypic changes across bloom development or growth stages on *Microcystis* phycosphere community composition.

Finally, we evaluated the potential influence of physicochemical environment on phycosphere community composition. Mantel tests revealed that most environmental parameters (and combinations thereof) did not have a strong, significant correlation to phycosphere community dissimilarity. The exceptions were chromophoric dissolved organic matter (CDOM) absorbance (a proxy for CDOM concentration), depth-integrated PAR (surface - 0.5 m), nitrate concentration, and temperature (Table 3.5). However, linear regression models of community dissimilarity versus Euclidean distances of each environmental parameter had poor fits to the data ($R^2 < 0.1$ for all parameters, Figure S 3.12). Furthermore, there is high dissimilarity between colonies collected on the same date and location (Figure 3.7), which would experience the same bulk water chemistry. Therefore, differences in the measured environmental parameters of the surrounding water cannot explain *Microcystis* phycosphere dissimilarity. However, changes in bulk DOC and nutrient concentrations relative to concentrations in the phycosphere may alter phycosphere community composition because the chemotactic response of heterotrophic bacteria is reduced under lower concentration gradients of chemoattractants (Paerl & Gallucci, 1985; Bassler *et al.*, 1991).

3.4.8 Interactions Between Cyanobacteria in the Phycosphere

In addition to non-cyanobacteria, the phycosphere communities included two *Pseudanabaena* OTUs and one *Cyanobium* OTU (highly similar to an OTU classified as *Synechococcus* in a previous western Lake Erie study (Berry *et al.*, 2017a)), that occurred at high relative abundance whenever present (Figure 3.2). While *Cyanobium* dominated the colonies in

which it occurred, micrograph images showed that *Microcystis* cells still made up the inner structure of those colonies and comprised a high percentage of the total colony communities (19.9 - 38.6 %). While both cyanobacterial genera have been observed in *Microcystis* blooms (Ouellette *et al.*, 2006; Berry *et al.*, 2017a; Chun *et al.*, 2019; Chun *et al.*, 2020), only interactions between *Pseudanabaena* and *Microcystis* have been studied to our knowledge (Agha *et al.*, 2016; Zhang *et al.*, 2020). We note that *Cyanobium* was only observed in colonies collected on two dates, and single *Microcystis* cells were present in the droplets containing these colonies on one date (Figure S 3.13). We interpreted the stray *Microcystis* cells as breaking off colonies, and because *Cyanobium* is known to form aggregates by itself (Jezberová & Komárková, 2007), we cannot rule out that the *Cyanobium* in these samples are contaminants from broken *Cyanobium* colonies. However, other picocyanobacteria like *Cyanobium* were previously observed growing attached to *Microcystis* colonies (Hindák, 1996), so their association with *Microcystis* here likely reflects a true interaction within the phycosphere. The association of cyanobacteria within the *Microcystis* phycosphere is intriguing because it indicates that colonization of the phycosphere is not driven solely by a need for organic carbon to fuel respiration. It may indicate that *Pseudanabaena* and *Cyanobium* adhere to *Microcystis* colonies in order to obtain organic compounds (either from *Microcystis* or other attached bacteria) for which they are auxotrophic, or to actively inhibit growth of *Microcystis* via allelopathic interactions. Indeed, allelopathic interactions between *Pseudanabaena* and *Microcystis* have been observed previously, although the harmful effects on growth were limited to certain *Microcystis* strains (Agha *et al.*, 2016). Further characterization of the nature of the interactions between cyanobacteria genera in *Microcystis* colonies is required to fully understand their significance to *Microcystis* physiology.

3.5 Conclusions

This study found that bacterial communities in the *Microcystis* phycosphere of individual *Microcystis* colonies vary both with time and *Microcystis* oligotype and are distinct from communities in surrounding lake water as well as 100 μm community assemblages. Although *Microcystis* harbors a distinct microbiome in which certain bacterial taxa are commonly present and abundant, the absence of universal members of these communities indicates that there is no core *Microcystis* microbiome from a taxonomic perspective. The mechanism behind associations of *Microcystis* phycosphere community composition with time and oligotype are uncertain, but our data suggest that both selective and neutral processes are likely involved. The link of *Microcystis* phycosphere community composition to time and *Microcystis* oligotype suggest that interactions in the phycosphere may differentially impact specific *Microcystis* strains at different times. The impacts bacteria have on the growth of *Microcystis* (Agha *et al.*, 2016; Schmidt *et al.*, 2020) and other phytoplankton taxa (Sison-Mangus *et al.*, 2014; Amin *et al.*, 2015) vary depending on the phytoplankton strain. Therefore, the taxa occupying the phycosphere could influence competition between *Microcystis* strains through their different impacts on *Microcystis* growth, which may in turn change *Microcystis* strain composition in blooms and influence bloom development and production of microcystins. However, recent studies found that phycosphere communities of *Microcystis* enrichment cultures (Jackrel *et al.*, 2019) and bulk cyanobacteria colonies (Cook *et al.*, 2020) that were taxonomically distinct between strains had similar functional potential. Therefore, the extent to which phycosphere communities yield different outcomes on *Microcystis* growth and physiology remains unclear. Additionally, further investigation is needed to better understand how changes in phycosphere community composition of individual colonies interact with surrounding physicochemical conditions and free-living heterotrophic bacteria communities to influence *Microcystis* bloom development and

production of microcystins. These results highlight the crucial need to characterize the interactions that take place between *Microcystis* spp. and their phycosphere communities and determine how they influence *Microcystis* biology and bloom development.

3.6 Figures and Tables

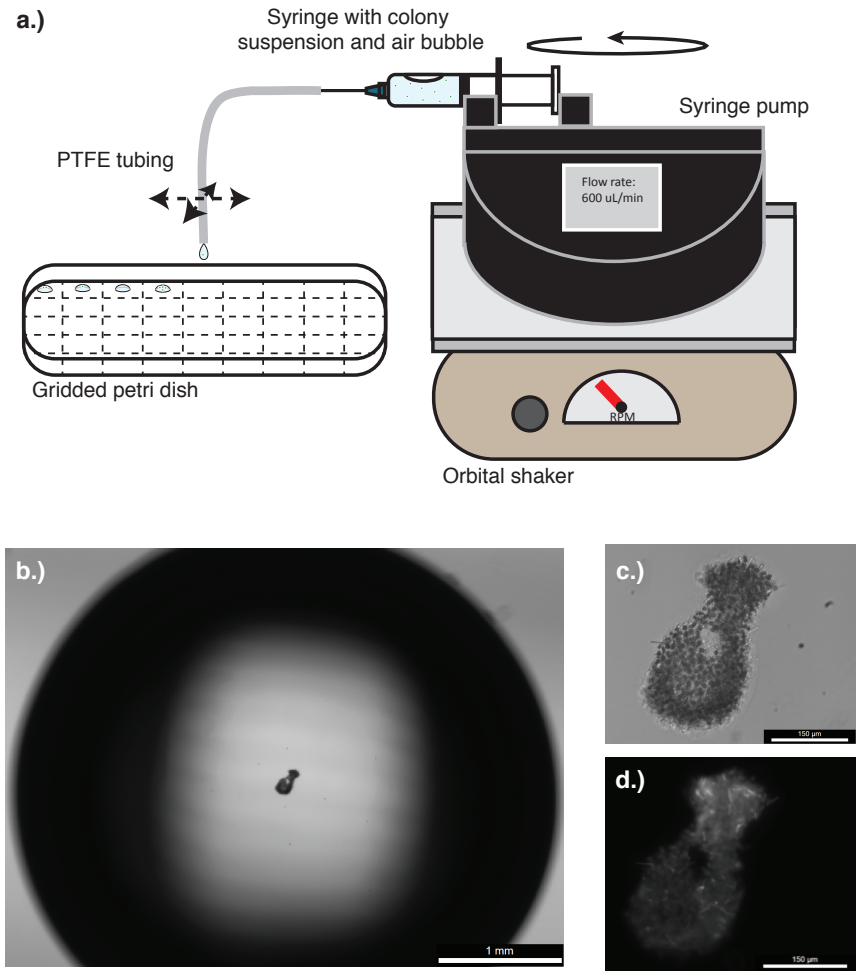

Figure 3.1: Description of individual *Microcystis* colony sampling via droplet encapsulation. a) Encapsulation of *Microcystis* colonies into droplets with a syringe-pump on an orbital shaker. The colony suspension flowed out of the syringe into the tubing at a constant rate of 600 µL/min. A homogenous suspension of buoyant colonies was maintained through the jostling of the air bubble in the syringe using the orbital shaker (100-150 RPM). Tubing was manually moved so that droplets were dispensed onto number sections of a sterile petri dish. Each droplet was then examined with an inverted light microscope. b) Example micrograph image of a droplet

containing one *Microcystis* colony. c) Higher-resolution image of the colony in b. d) Image of the colony in c shown with phycocyanin autofluorescence.

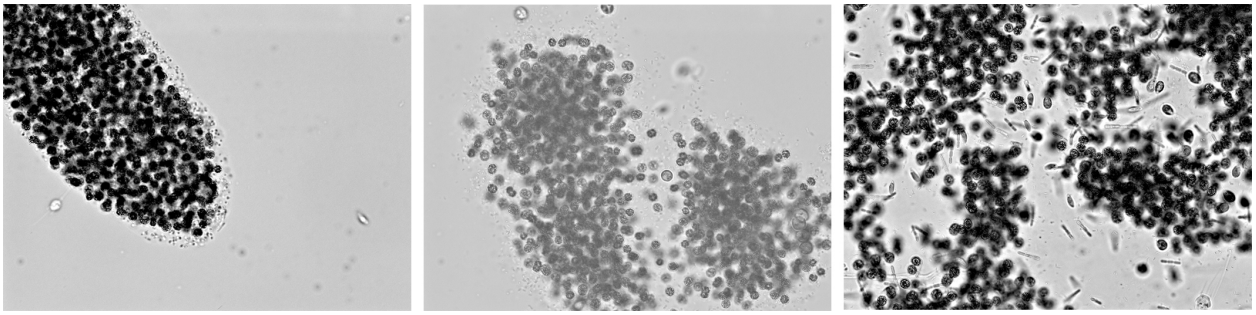

Figure 3.2: Example black and white micrographs of *Microcystis* colonies in bulk phytoplankton seston collected from western Lake Erie blooms. The larger, dark cells are *Microcystis* cells, and the surrounding rod and cocci cells are the non-*Microcystis* cells that colonize the phycosphere.

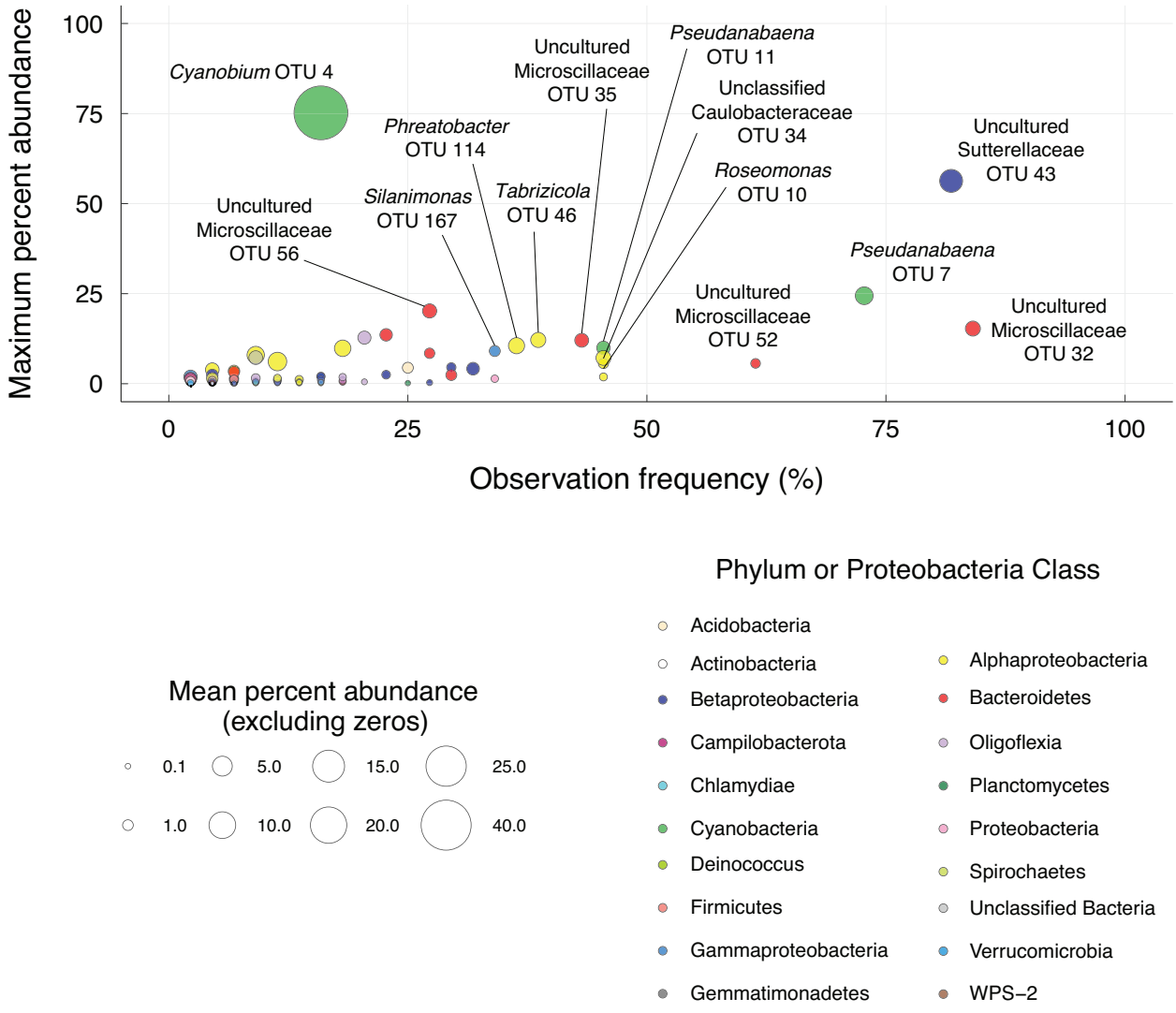

Figure 3.3: Maximum and mean relative abundance of all non-*Microcystis* OTUs identified in the *Microcystis* phycosphere plotted against their observation frequency. Observation frequency was calculated as the percent of total colonies on which a given OTU was observed. Bubble size is scaled to mean relative abundance of the OTU in colonies where it was present. Bubble color represents the OTU phylum (or class in the case of Proteobacteria).

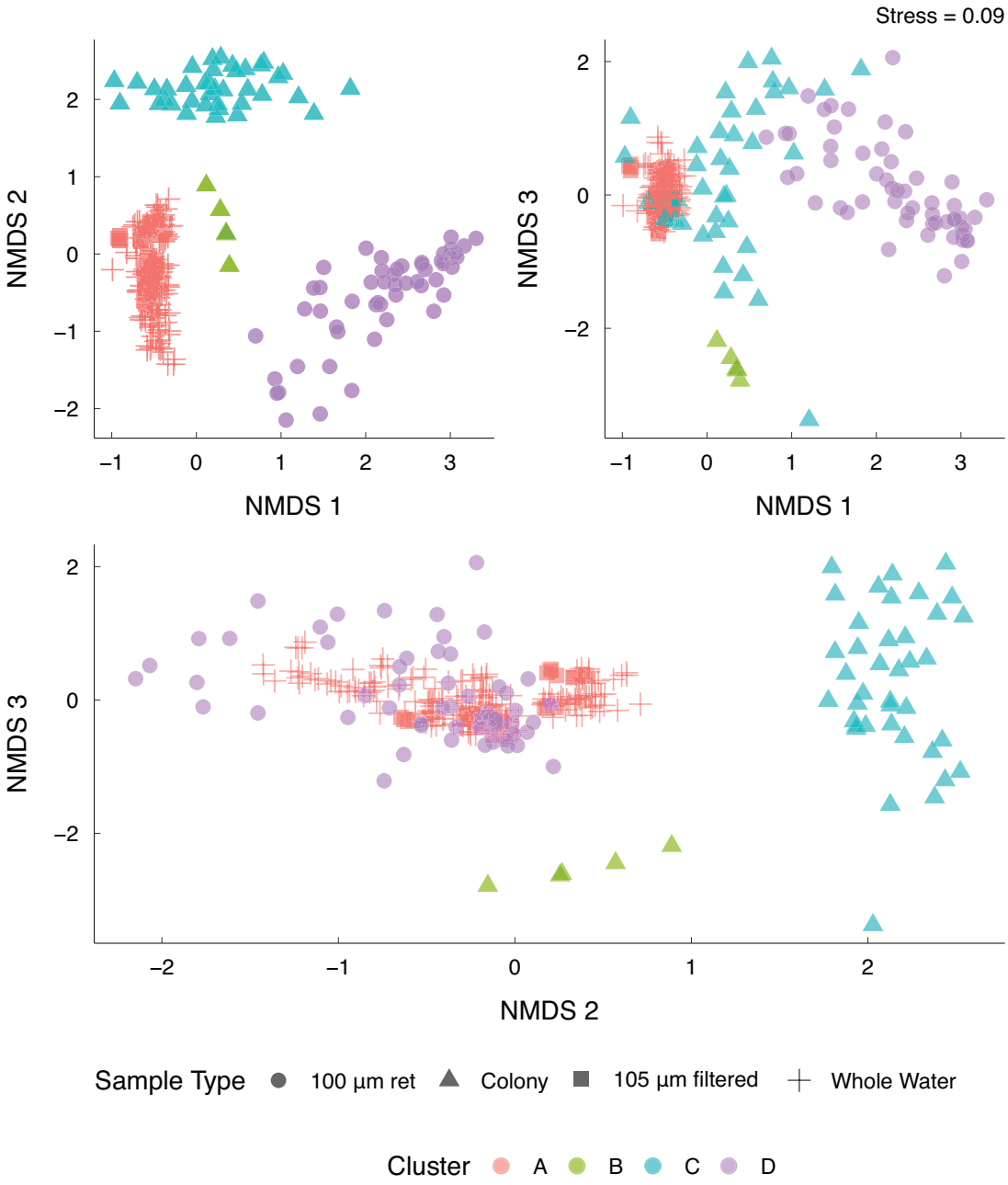

Figure 3.4: NMDS ordination and hierarchical clustering of bacterial communities in the *Microcystis* phycosphere, 100 µm retentate, whole water communities from western Lake Erie. The plot axes show NMDS scores. Points in the ordination are colored by hierarchical clustering assignment. The point shapes in the ordination reflect sample type.

Figure 3.5: Changes in the relative abundance of OTUs that are frequently present or indicators of date and *Microcystis* oligotype in *Microcystis* phycosphere communities. Mean relative

abundances in both 105 µm filtered water samples from 2019 (top) and single *Microcystis* colonies (bottom) are shown. Error bars depict 95 % confidence intervals. No error bars indicate that only one colony of the given oligotype was sampled on that particular date.

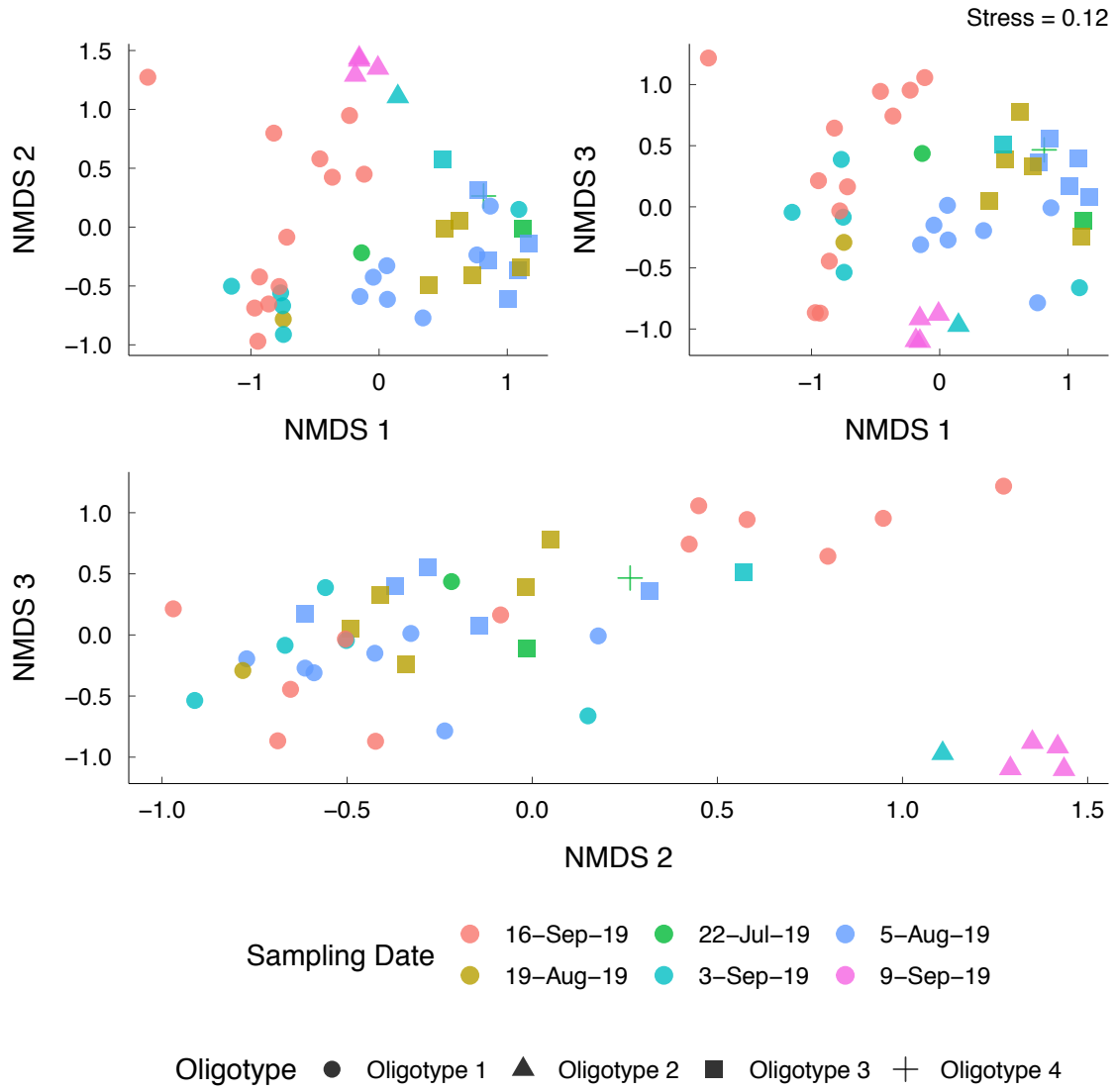

Figure 3.6: NMDS ordination of bacterial communities in the *Microcystis* phycosphere. Points in the ordination are colored by sampling date, while their shape reflects the oligotype of *Microcystis* from that colony.

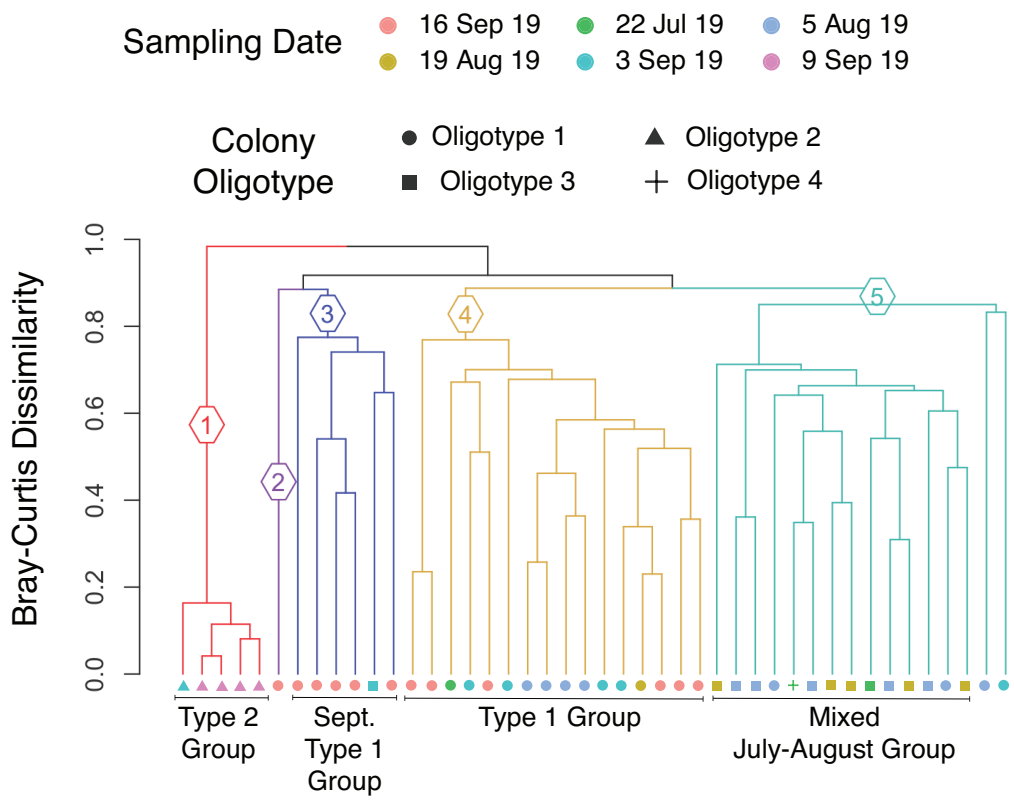

Figure 3.7: Hierarchical clustering of bacterial communities in the *Microcystis* phycosphere. Clades in the dendrogram are colored by hierarchical clustering assignments (shown as numbers in hexagons) based on Bray-Curtis dissimilarity. The shape and color of the points at the leaves of the dendrogram indicates oligotype and sampling date, respectively, and match the corresponding point in the NMDS ordination (Figure 6).

Figure S 3.1: Sampling sites in western Lake Erie. Colony samples from 9-September-2019 were collected at station WE16; colony samples from all other dates were collected at WE8. The other stations shown were used only for collection of bulk communities.

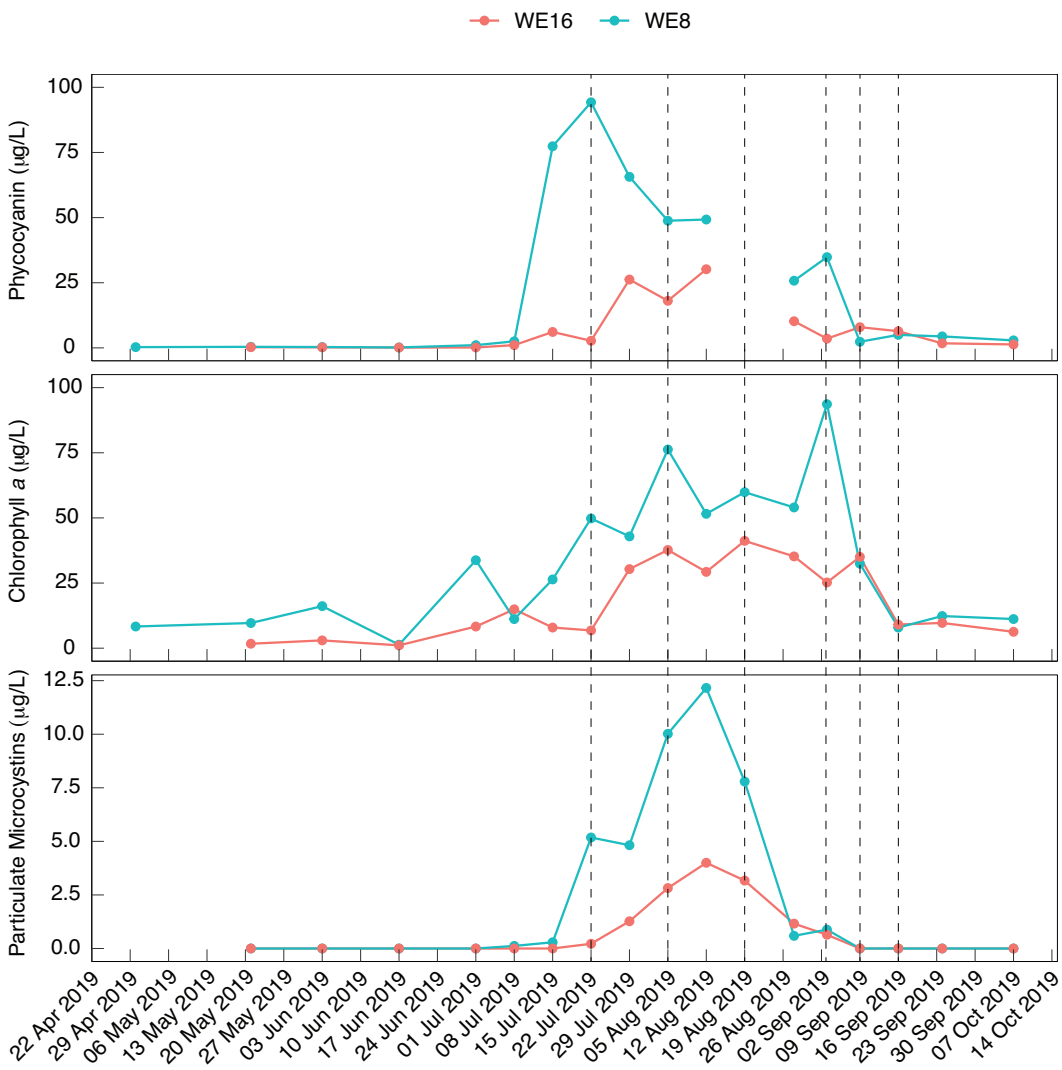

Figure S 3.2: Weekly changes in bloom pigments and microcystin concentrations over time at the sites sampled. Vertical dashed lines indicate times when *Microcystis* colonies were collected for phycosphere characterization. All samples were collected at WE8, with the exception of the 9-Sep-19 sample, which was collected at WE16.

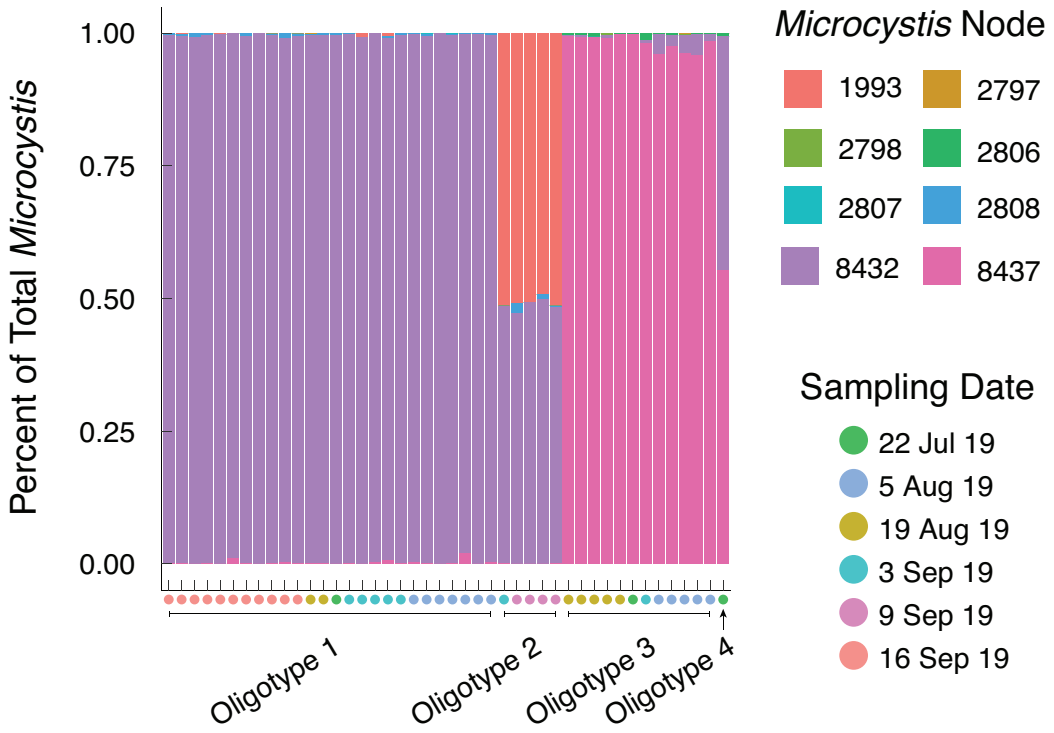

Figure S 3.3: The relative proportions of each *Microcystis* MED node identified in *Microcystis* colonies. Each x-axis entry represents a single *Microcystis* colony, ordered by the final colony oligotype assignment based on the major two MED nodes in the colony. Colored circles at the x-axis depict sampling date.

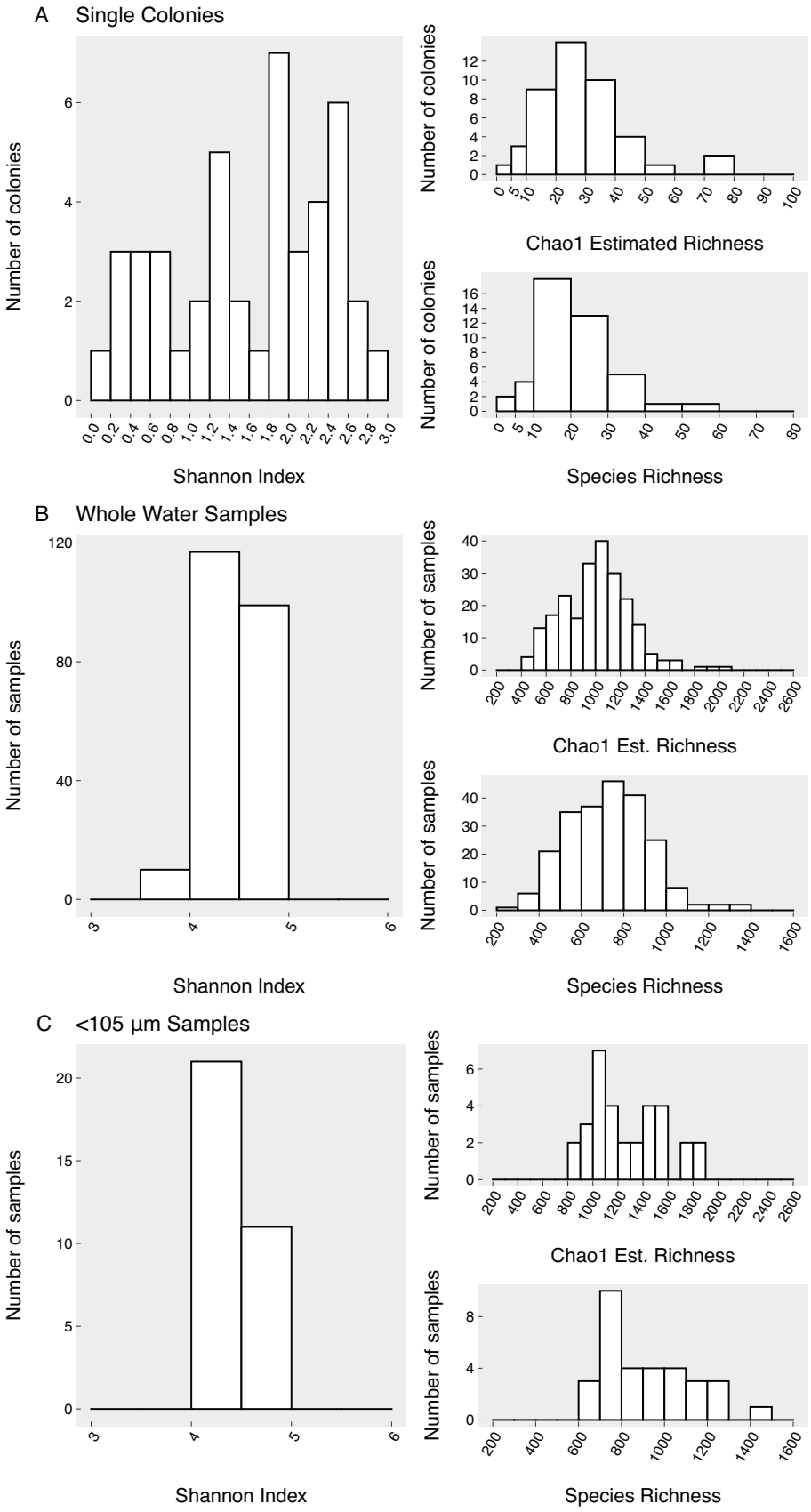
A Single Colonies
Number of colonies
Shannon Index
Chao1 Estimated Richness
Species Richness
B Whole Water Samples
Number of samples
Chao1 Est. Richness
C <105 µm Samples

Figure S 3.4: Distribution of observed richness, estimated richness, and Shannon diversity index of *Microcystis* colony phycosphere communities (A), whole water field samples (B), and 105 µm filtered field samples (C). *Microcystis* OTUs were excluded in calculations.

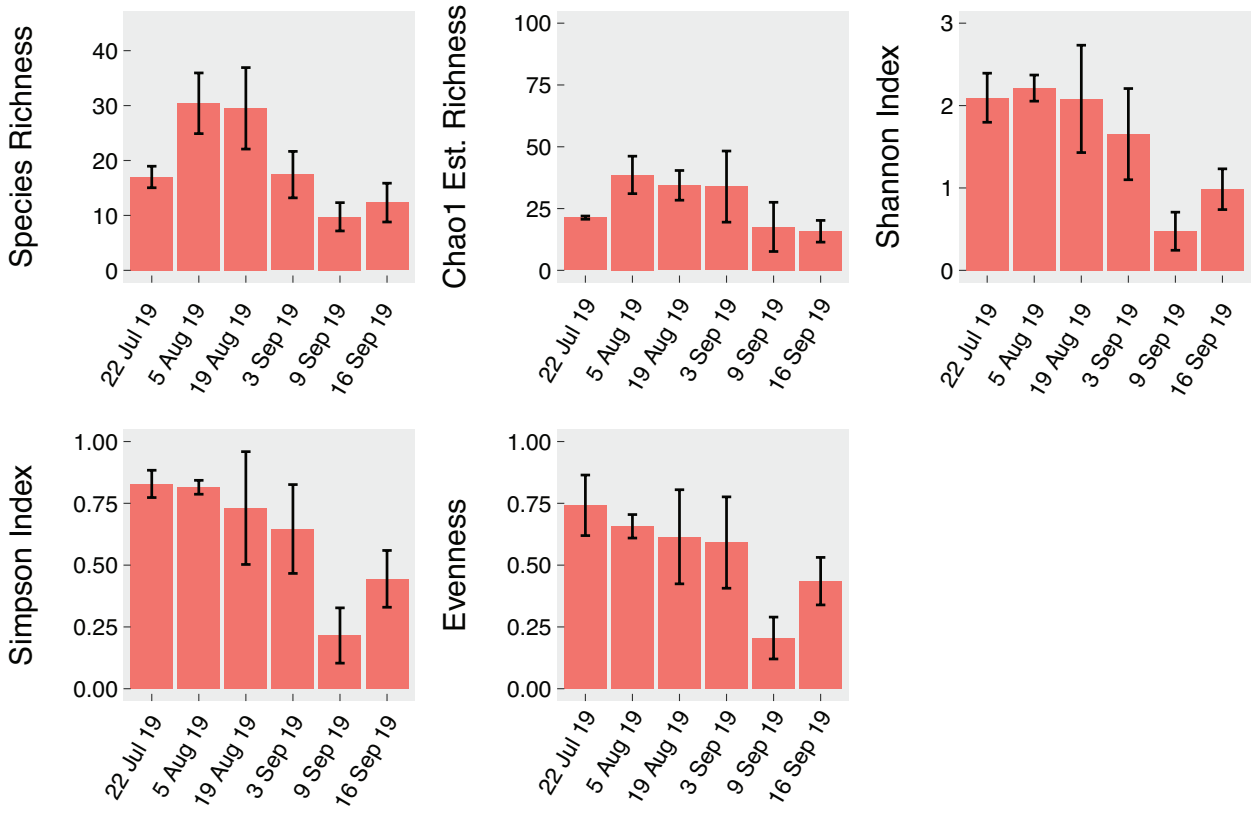

Figure S 3.5: Temporal change of alpha diversity metrics. Bar height shows the mean values at each date and error bars show the 95% confidence intervals.

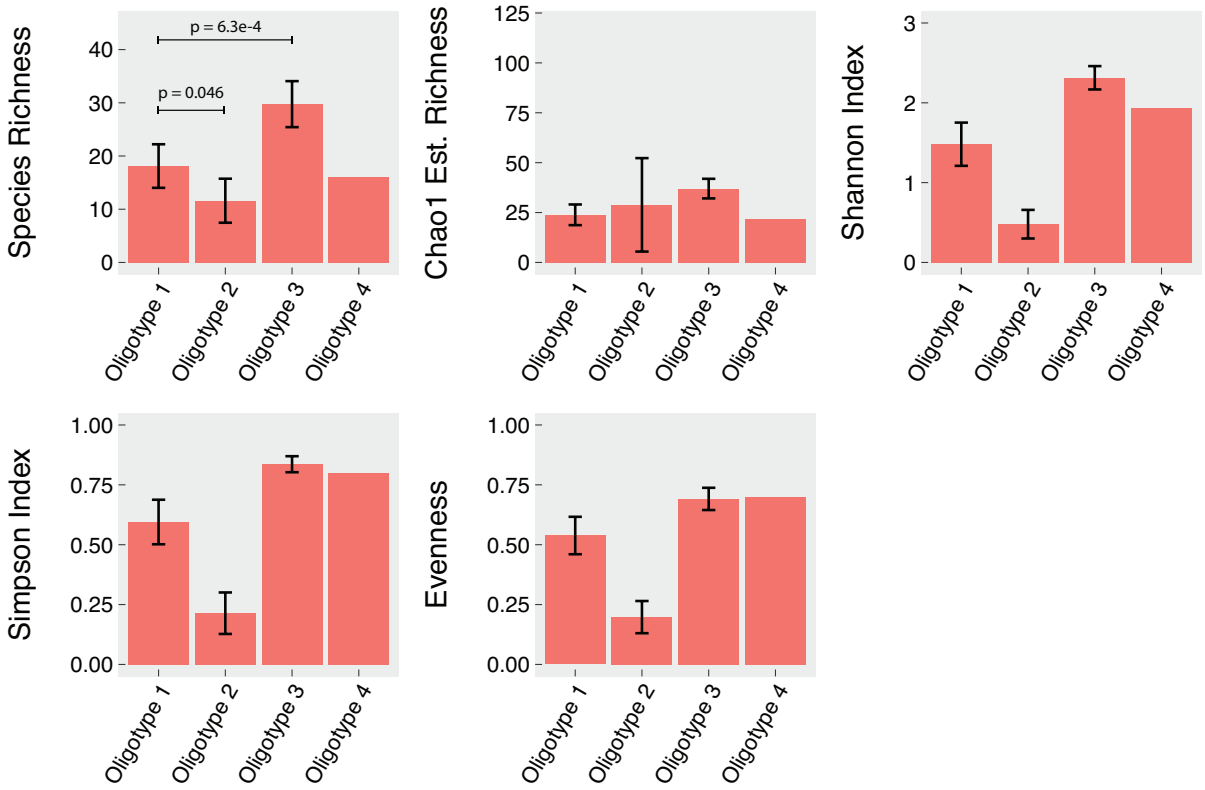

Figure S 3.6: Mean alpha diversity metrics of phycosphere communities associated with different *Microcystis* oligotypes. Bar height shows the mean value for each *Microcystis* oligotype and error bars show the 95% confidence intervals. Significance values computed from Welch's two-sided T tests.

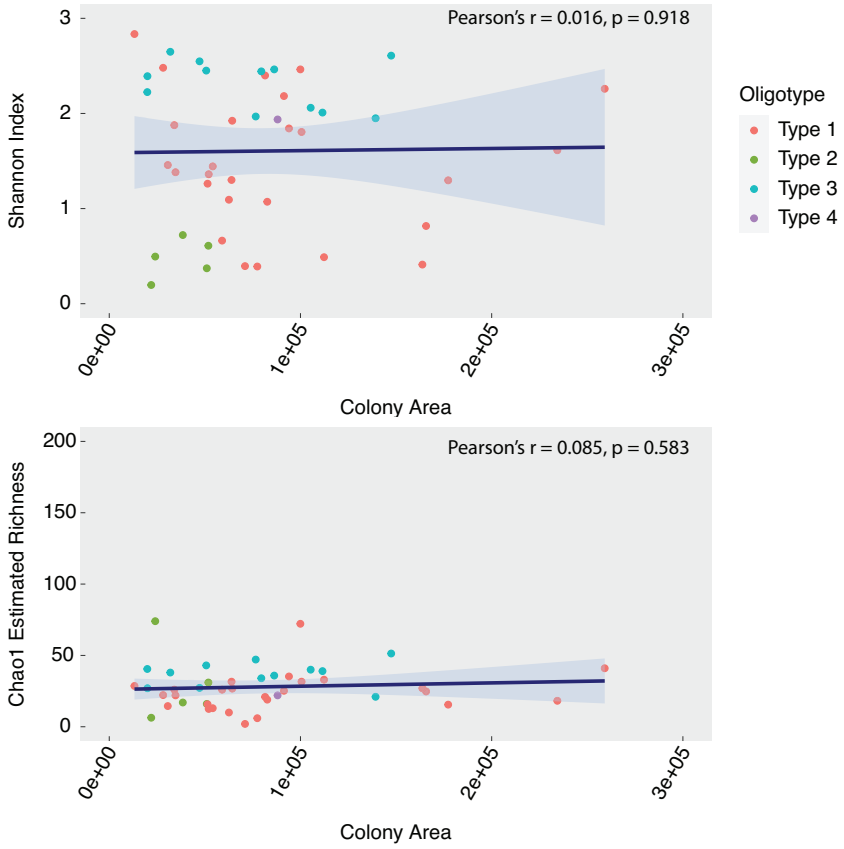

Figure S 3.7: Linear regression between Shannon Index (A) and Chao1 estimated species richness (B) and colony area. The solid line shows the regression line, while the shaded region shows the standard error of the slope. Significance values on slopes were computed via an F-test.

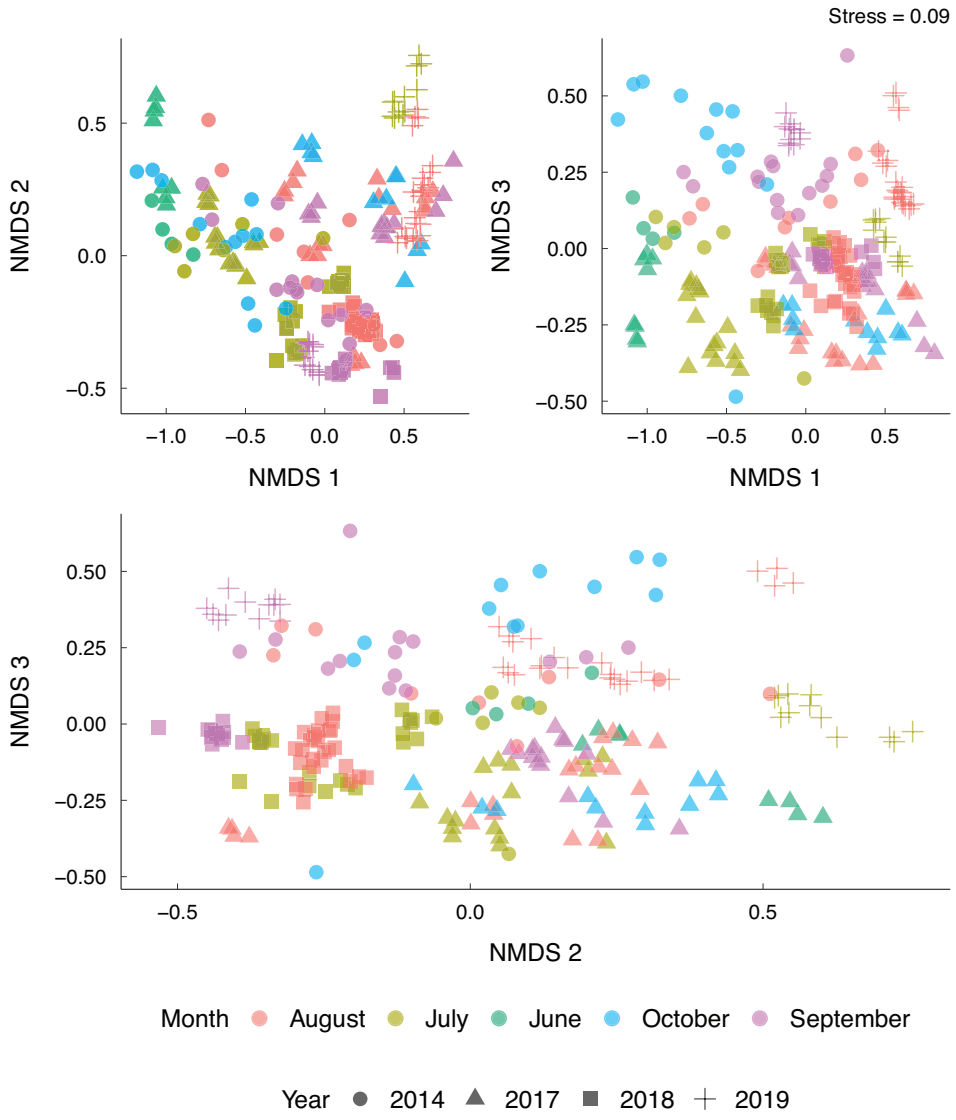

Figure S 3.8: NMDS ordination of whole water bacterial communities in western Lake Erie over four years colored by month. Data point shapes indicate the year of sample collection. *Microcystis* OTUs were not included in the analysis.

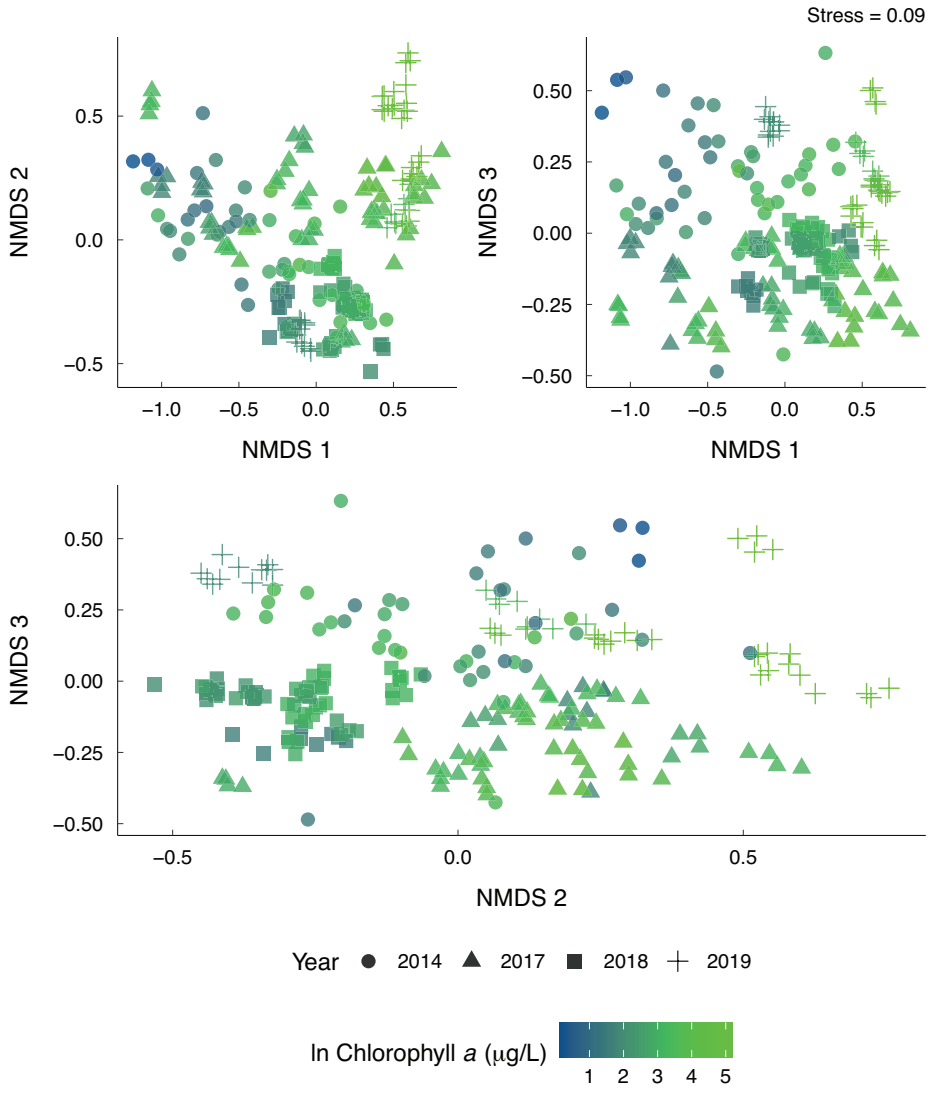

Figure S 3.9: NMDS ordination of whole water bacterial communities in western Lake Erie over four years colored by the natural log of chlorophyll *a* concentration. Data point shapes indicate the year of sample collection. *Microcystis* OTUs were not included in the analysis.

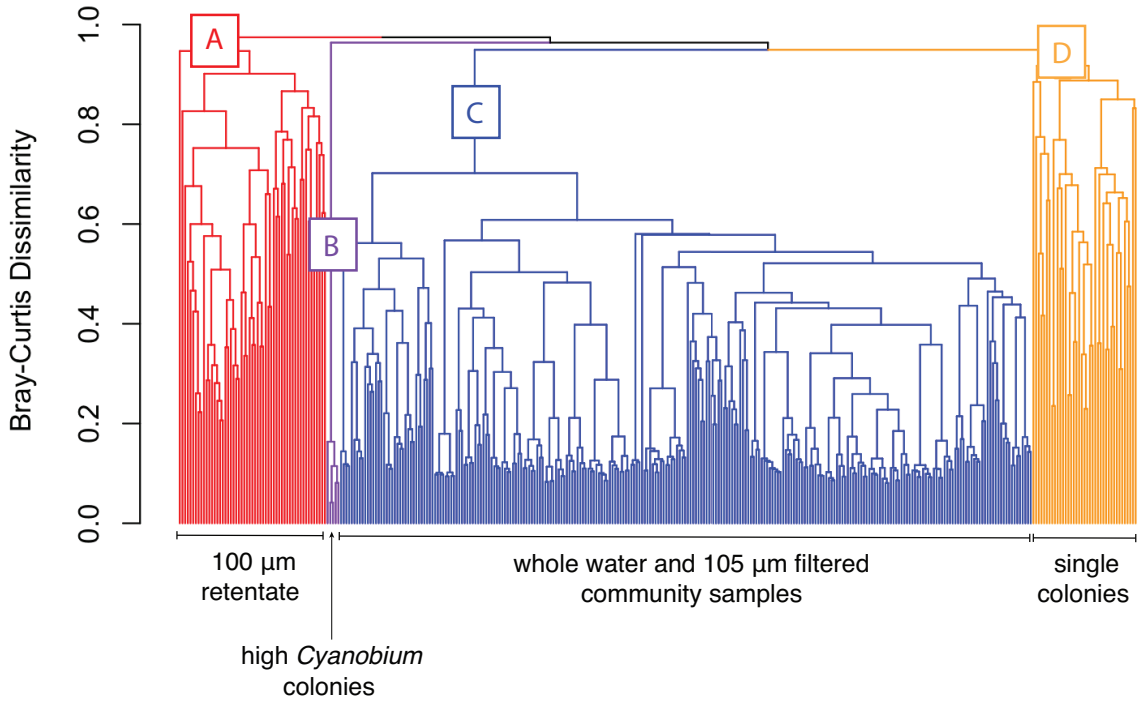

Figure S 3.10: Dendogram of Bray-Curtis dissimilarity in bacterial communities in the *Microcystis* phycosphere, 100 µm retentate, whole water communities from Lake Erie. Groups are colored by hierarchical clustering assignment.

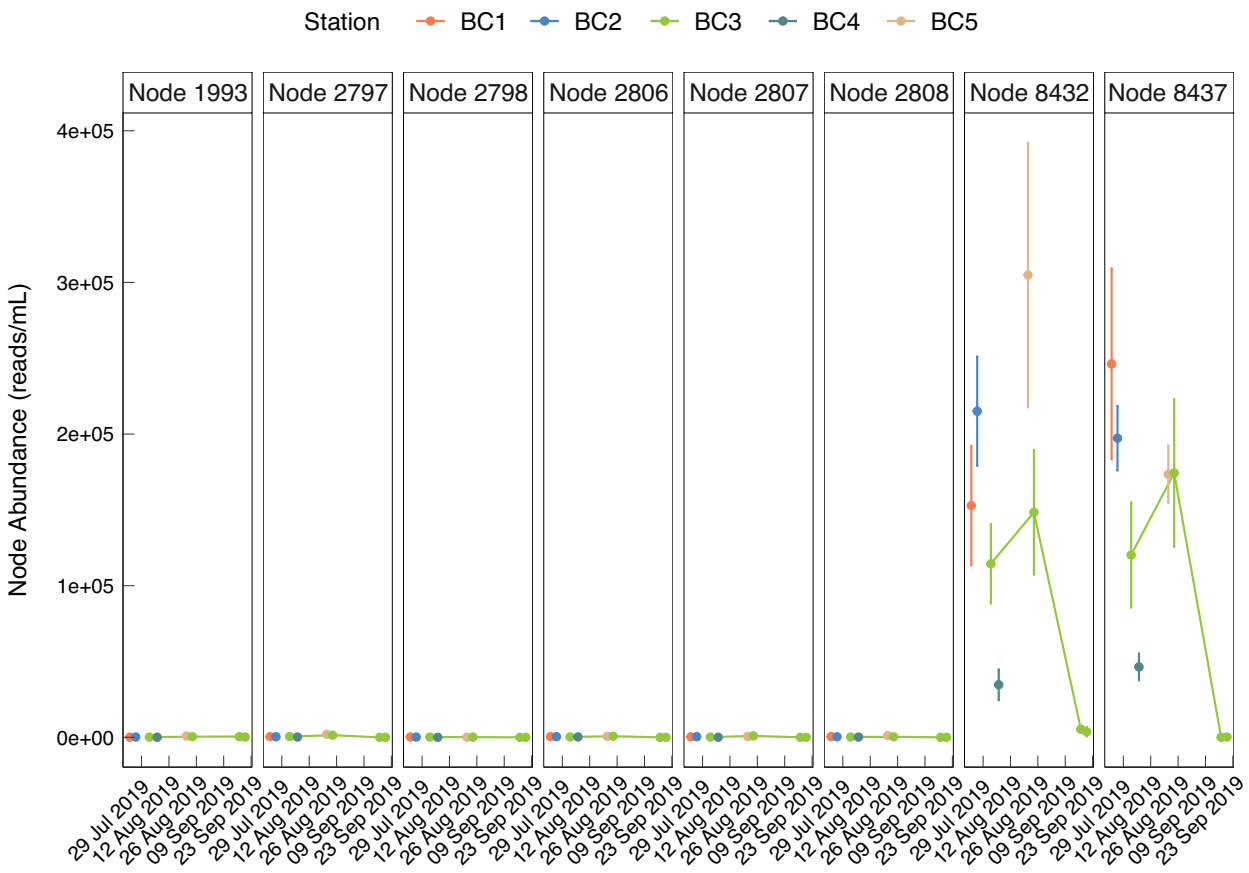

Figure S 3.11: Absolute abundances of *Microcystis* MED nodes in whole water communities collected in 2019. Error bars show the 95% confidence intervals of replicate filters (n = 4).

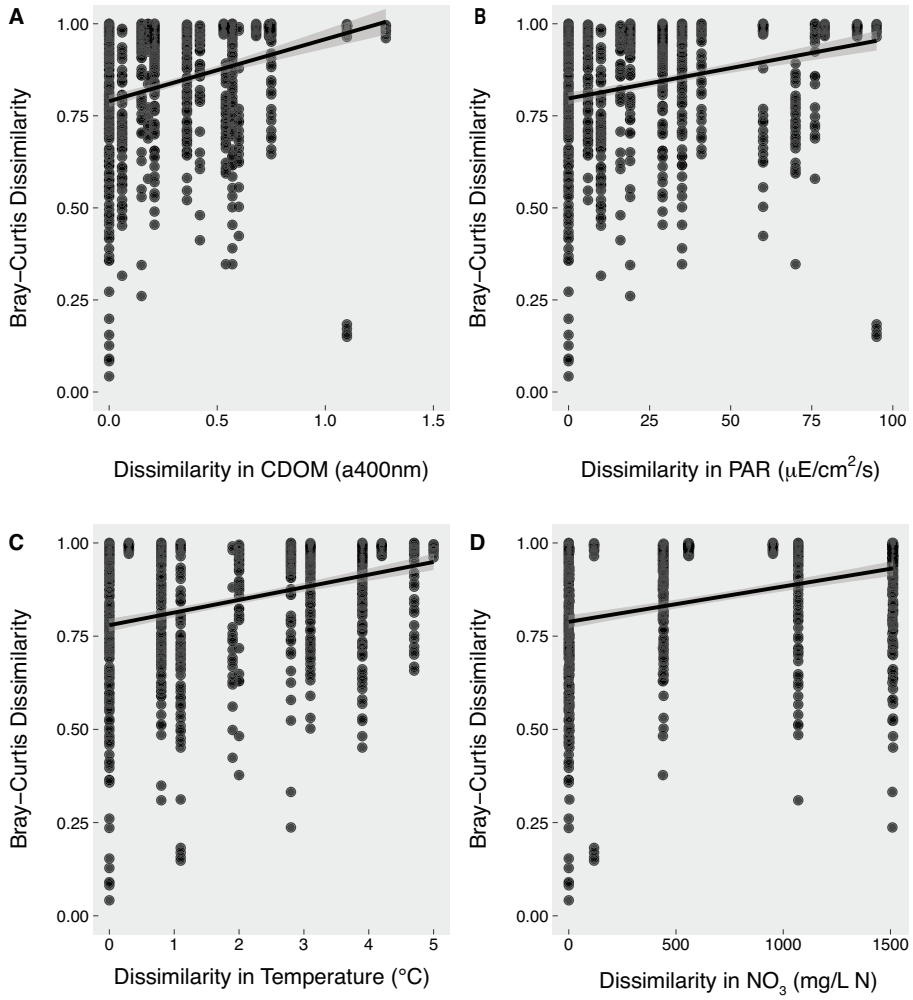

Figure S 3.12: Correlation in Bray-Curtis dissimilarity between *Microcystis* phycosphere communities and Euclidean distance in CDOM absorbance (A), total PAR in top 0.5 m (B), temperature (C), and nitrate concentration (D) at the time of colony collection. For each panel, the solid line shows the regression line, while the shaded region shows the standard error of the slope.

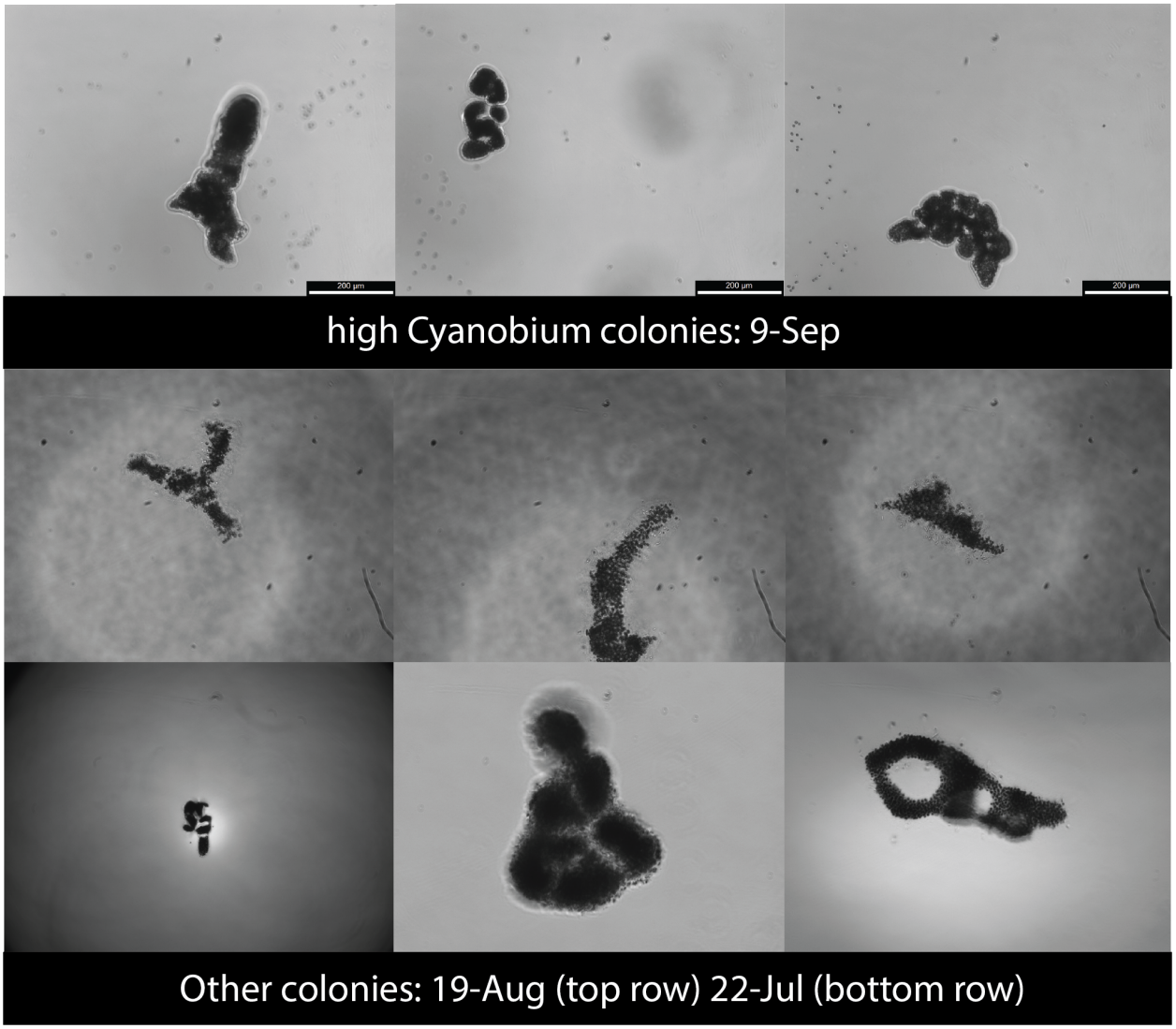

Figure S 3.13: Representative colony droplet micrographs. The colonies collected on 9 Sep 19 had a large amount of loose *Microcystis* that presumably were broken off colonies.

Table 3.1: The number and position of nucleotide variations between 16S rRNA gene copies found within each closed *Microcystis* genome.

Strain	Number of copies	Nucleotide Mismatches	Gaps	Positions of sites with differences
PCC 7806	2	2	0	165, 227
MC19	2	19	3	233, 338, 842, 843, 850, 851, 1064, 1065, 1091, 1117, 1147, 1148, 1153, 1164, 1165, 1170, 1179, 1198, 1260
NIES 2481	2	0	0	n/a
NIES 2549	2	0	0	n/a
NIES 298	2	0	0	n/a
NIES 843	2	4	0	84, 165, 233, 234
FD4	2	0	0	n/a
FACHB 1757	2	0	0	n/a
NIES 102	2	0	0	n/a

Table 3.2: OTUs identified as significant diagnostic OTUs for either sampling date or oligotype along with their Indval g statistics.

OTU #	Lowest Taxonomic Assignment	Obs. Freq. (%)	Indicator Group	Group size	Specificity	Sens-itivity	Indval. g	p
603	Rickettsiaceae	4.55	22-Jul-19	3	1.00	0.67	0.82	0.0034
59	Comamonadaceae	18.18	5-Aug-19	12	0.96	0.50	0.69	0.0342
246	*Bdellovibrio*	18.18	5-Aug-19	12	1.00	0.67	0.82	0.0080
108	Alphaproteobacteria	13.64	19-Aug-19	6	0.99	0.67	0.81	0.0014
200	*Candidatus Paracaedibacter*	11.36	19-Aug-19	6	0.99	0.67	0.81	0.0018
210	Neisseriaceae	11.36	19-Aug-19	6	0.95	0.67	0.80	0.0028
396	Gemmatimonadaceae	13.64	19-Aug-19	6	0.79	0.67	0.72	0.0066
402	Vampirovibrio	4.55	19-Aug-19	6	1.00	0.33	0.58	0.0239
415	Parachlamydiaceae	4.55	19-Aug-19	6	1.00	0.33	0.58	0.0261
442	Silvanigrellaceae	4.55	19-Aug-19	6	1.00	0.33	0.58	0.0261
571	Rickettsiales; SM2D12	6.82	19-Aug-19	6	1.00	0.50	0.71	0.0091
694	*Peredibacter*	4.55	19-Aug-19	6	1.00	0.33	0.58	0.0266
55	Alphaproteobacteria	45.45	3-Sep-19	7	0.68	0.86	0.76	0.0424
130	Silvanigrellaceae	18.18	3-Sep-19	7	0.82	0.71	0.76	0.0052
164	Comamonadaceae	15.91	3-Sep-19	7	0.91	0.71	0.81	0.0030
4	*Cyanobium*	15.91	9-Sep-19	4	0.90	1.00	0.95	0.0002
171	Rhizobiales	9.09	9-Sep-19	4	1.00	0.50	0.71	0.0154
312	*Reyranella*	11.36	9-Sep-19	4	0.90	1.00	0.95	0.0001

4787	*Cyanobium*	4.55	9-Sep-19	4	1.00	0.50	0.71	0.0107
342	*Roseomonas*	18.18	16-Sep-19	12	1.00	0.67	0.82	0.0023
357	Hydrogenophaga	11.36	16-Sep-19	12	1.00	0.42	0.65	0.0301
80	Nitrosomonadaceae; DSSD61	31.82	August	18	1.00	0.78	0.88	0.0001
87	Proteobacteria	34.09	August	18	0.98	0.78	0.87	0.0012
140	Bacteroidia	29.55	August	18	0.98	0.67	0.81	0.0017
220	*Labrys*	15.91	August	18	1.00	0.39	0.62	0.0490
226	Nitrosomonadaceae; 966-1	27.27	August	18	0.96	0.61	0.77	0.0066
256	*Pirellula*	25.00	August	18	0.97	0.56	0.74	0.0094
10	*Roseomonas*	45.45	July-August	21	0.99	0.76	0.87	0.0021
34	Caulobacteraceae	45.45	July-August	21	0.94	0.81	0.87	0.0002
11	*Pseudanabaena*	45.45	July-August	21	1.00	0.86	0.93	0.0030
35	Microscillaceae	43.18	July-August	21	1.00	0.90	0.95	0.0001
46	*Tabrizicola*	38.64	July-August	21	1.00	0.76	0.87	0.0007
7	*Pseudanabaena*	72.73	July-August	21	0.91	1.00	0.95	0.0001
4	*Cyanobium*	15.91	Type_2	5	1.00	1.00	1.00	0.0001
312	*Reyranella*	11.36	Type_2	5	1.00	1.00	1.00	0.0001
35	Microscillaceae	43.18	Type_3	12	0.89	0.92	0.91	0.0423
19	Kapabacteriales	2.27	Type_4	1	1.00	1.00	1.00	0.0216
2	Sporichthyaceae; hgcI_clade	18.18	Type_4	1	0.86	1.00	0.93	0.0265
304	Caedibacteraceae	11.36	Type_4	1	0.98	1.00	0.99	0.0151
445	*Bdellovibrio*	4.55	Type_4	1	0.93	1.00	0.97	0.0322
603	Rickettsiaceae	4.55	Type_4	1	0.99	1.00	1.00	0.0190
8161	Microscillaceae	2.27	Type_4	1	1.00	1.00	1.00	0.0216

Table 3.3: Maximum and mean percent abundance for each OTU with observation frequency between 50 and 18% or lower than 18% with maximum abundance higher than 5%.

OTU #	Lowest Taxonomic Assignment	Observation Frequency (%)	Maximum Percent Abundance	Mean Percent Abundance (excluding zeros)
11	*Pseudanabaena*	45.45	9.96	1.89
34	Caulobacteraceae	45.45	7.20	2.49
10	*Roseomonas*	45.45	5.70	0.88
55	Alphaproteobacteria	45.45	1.92	0.41
35	Microscillaceae	43.18	12.12	2.07
46	*Tabrizicola*	38.64	12.32	2.55
114	*Phreatobacter*	36.36	10.65	3.02
167	*Silanimonas*	34.09	9.10	1.08
87	Proteobacteria	34.09	1.39	0.32
80	Nitrosomonadaceae; DSSD61	31.82	4.17	1.63
82	Oxalobacteraceae	29.55	4.59	0.66
140	Bacteroidia	29.55	2.42	1.07
56	Microscillaceae	27.27	20.14	2.17

53	Sphingobacteriales; OPS 17	27.27	8.43	0.93
226	Nitrosomonadaceae; 966-1	27.27	0.31	0.14
96	*Bryobacter*	25.00	4.42	1.07
256	*Pirellula*	25.00	0.17	0.087
4	*Cyanobium*	15.91	75.19	46.66
312	*Reyranella*	11.36	6.15	4.23
171	Rhizobiales	9.09	7.96	3.61
342	*Roseomonas*	18.18	9.90	3.20
182	Bacteria	9.09	7.26	1.98
64	*Oligoflexus*	20.45	12.93	1.79
63	Microscillaceae	22.73	13.56	1.54
169	Comamonadaceae	22.73	2.51	0.54
246	*Bdellovibrio*	18.18	1.85	0.31
72	Microscillaceae	18.18	0.67	0.31
130	Silvanigrellaceae	18.18	0.96	0.27
59	Comamonadaceae	18.18	0.53	0.14
215	*Peredibacter*	20.45	0.54	0.13
2	Sporichthyaceae	18.18	0.32	0.090

Table 3.4: Maximum and mean percent abundance of each frequent OTU (observation frequency greater than 50%).

OTU #	Lowest Taxonomic Rank	Observation Frequency (%)	Maximum Percent Abundance	Mean Percent Abundance (excluding zeros)
32	Microscillaceae	84.09	15.36	2.51
43	Sutterellaceae	81.82	56.1	7.07
7	*Pseudanabaena*	72.73	24.45	3.85
52	Microscillaceae	61.36	5.69	0.75

Table 3.5: Mantel test results.

Environmental Parameter(s)	Mantel spearman's rank ρ	p-value
temperature	0.3009	1.00E-04
specific conductivity	0.1697	4.00E-04
particulate microcystin	0.2062	2.00E-04
dissolved oxygen	0.1248	7.30E-03
surface to 0.5m integrated PAR	0.3915	1.00E-04
total phosphorus	0.02254	3.56E-01
total dissolved phosphorus	0.2719	1.00E-04

soluble reactive phosphorus	0.2676	2.00E-04
ammonium	0.299	1.00E-04
nitrate	0.3335	1.00E-04
CDOM absorbance (400 nm)	0.381	1.00E-04
CDOM + PAR	0.3895	1.00E-04
all nutrients	0.3564	1.00E-04
all phosphorus	0.278	1.00E-04
all nitrogen	0.3335	1.00E-04
colony area	-0.01037	5.28E-01

3.7 References

Adachi, M., Kanno, T., Okamoto, R., Itakura, S., Yamaguchi, M., & Nishijima, T. (2003). Population structure of *Alexandrium* (Dinophyceae) cyst formation-promoting bacteria in Hiroshima Bay, Japan. *Appl Environ Microbiol, 69*(11): 6560-6568.

Agha, R., del Mar Labrador, M., de los Ríos, A., & Quesada, A. (2016). Selectivity and detrimental effects of epiphytic *Pseudanabaena* on *Microcystis* colonies. *Hydrobiologia, 777*(1): 139-148.

Ajani, P. A., Kahlke, T., Siboni, N., Carney, R., Murray, S. A., & Seymour, J. R. (2018). The microbiome of the cosmopolitan diatom *Leptocylindrus* reveals significant spatial and temporal variability. *Front Microbiol, 9*: 2758.

Amin, S. A., Green, D. H., Hart, M. C., Krüpper, F. C., Sunda, W. G., & Carrano, C. J. (2009). Photolysis of iron-siderophore chelates promotes bacterial-algal mutualism. *Proc Natl Acad Sci, 106*(40): 17071-17076. doi:10.1073 pnas.0905512106

Amin, S. A., Hmelo, L. R., van Tol, H. M., Durham, B. P., Carlson, L. T., Heal, K. R. *et al.* (2015). Interaction and signalling between a cosmopolitan phytoplankton and associated bacteria. *Nature, 522*(7554): 98-101. doi:10.1038/nature14488

Arandia-Gorostidi, N., Weber, P. K., Alonso-Sáez, L., Morán, X. A. G., & Mayali, X. (2017). Elevated temperature increases carbon and nitrogen fluxes between phytoplankton and heterotrophic bacteria through physical attachment. *ISME J, 11*(3): 641-650.

Azam, F., & Malfatti, F. (2007). Microbial structuring of marine ecosystems. *Nat Rev Microbiol, 5*(10): 782-791.

Bagatini, I. L., Eiler, A., Bertilsson, S., Klaveness, D., Tessarolli, L. P., & Vieira, A. A. H. (2014). Host-specificity and dynamics in bacterial communities associated with bloom-forming freshwater phytoplankton. *PLoS One, 9*(1): e85950.

Barbara, G. M., & Mitchell, J. G. (2003). Bacterial tracking of motile algae. *FEMS Microbiol Ecol, 44*(1): 79-87.

Bassler, B. L., Gibbons, P., Yu, C., & Roseman, S. (1991). Chitin utilization by marine bacteria. Chemotaxis to chitin oligosaccharides by *Vibrio furnissii*. *J Biol Chem, 266*(36): 24268-24275.

Basu, S., Gledhill, M., de Beer, D., Matondkar, S. P., & Shaked, Y. (2019). Colonies of marine cyanobacteria *Trichodesmium* interact with associated bacteria to acquire iron from dust. *Commun Biol, 2*(284): 1-8.

Behringer, G., Ochsenkühn, M. A., Fei, C., Fanning, J., Koester, J. A., & Amin, S. A. (2018). Bacterial communities of diatoms display strong conservation across strains and time. *Front Microbiol, 9*: 659.

Bell, W., & Mitchell, R. (1972). Chemotactic and growth responses of marine bacteria to algal extracellular products. *Biol. Bull, 143*(2): 265-277.

Berry, M. A., Davis, T. W., Cory, R. M., Duhaime, M. B., Johengen, T. H., Kling, G. W. *et al.* (2017a). Cyanobacterial harmful algal blooms are a biological disturbance to Western Lake Erie bacterial communities. *Environ Microbiol, 19*(3): 1149-1162.

Berry, M. A., White, J. D., Davis, T. W., Jain, S., Johengen, T. H., Dick, G. J. *et al.* (2017b). Are oligotypes meaningful ecological and phylogenetic units? A case study of *Microcystis* in freshwater lakes. *Front Microbiol, 8*: 365.

Burke, C., Steinberg, P., Rusch, D., Kjelleberg, S., & Thomas, T. (2011a). Bacterial community assembly based on functional genes rather than species. *Proc Natl Acad Sci, 108*(34): 14288-14293.

Burke, C., Thomas, T., Lewis, M., Steinberg, P., & Kjelleberg, S. (2011b). Composition, uniqueness and variability of the epiphytic bacterial community of the green alga *Ulva australis*. *ISME J, 5*(4): 590-600.

Bushnell, B. (2018). BBTools: a suite of fast, multithreaded bioinformatics tools designed for analysis of DNA and RNA sequence data: Joint Genome Institute.

Cáceres, M. D., & Legendre, P. (2009). Associations between species and groups of sites: indices and statistical inference. *Ecology, 90*(12): 3566-3574.

Casamatta, D., & Wickstrom, C. (2000). Sensitivity of two disjunct bacterioplankton communities to exudates from the cyanobacterium *Microcystis aeruginosa* Kützing. *Microb Ecol, 40*(1): 64-73.

Chaffin, J. D., Bridgeman, T. B., Heckathorn, S. A., & Mishra, S. (2011). Assessment of *Microcystis* growth rate potential and nutrient status across a trophic gradient in western Lake Erie. *J Great Lakes Res, 37*(1): 92-100.

Christie-Oleza, J. A., Sousoni, D., Lloyd, M., Armengaud, J., & Scanlan, D. J. (2017). Nutrient recycling facilitates long-term stability of marine microbial phototroph-heterotroph interactions. *Nat Microbiol, 2*(17100): 1-10.

Chun, S.-J., Cui, Y., Lee, C. S., Cho, A. R., Baek, K., Choi, A. *et al.* (2019). Characterization of distinct cyanoHABs-related modules in microbial recurrent association network. *Front Microbiol, 10*: 1637.

Chun, S.-J., Cui, Y., Lee, J. J., Choi, I.-C., Oh, H.-M., & Ahn, C.-Y. (2020). Network analysis reveals succession of Microcystis genotypes accompanying distinctive microbial modules with recurrent patterns. *Water Res, 170*: 115326.

Cole, J. J. (1982). Interactions between bacteria and algae in aquatic ecosystems. *Annu Rev Ecol Syst, 13*(1): 291-314.

Cook, K. V., Li, C., Cai, H., Krumholz, L. R., Hambright, K. D., Paerl, H. W. *et al.* (2020). The global *Microcystis* interactome. *Limnol Oceanogr, 65*(S1): S194-S207. doi:10.1002/lno.11361

Croft, M. T., Lawrence, A. D., Raux-Deery, E., Warren, M. J., & Smith, A. G. (2005). Algae acquire vitamin B_{12} through a symbiotic relationship with bacteria. *Nature, 438*(7064): 90-93. doi:doi:10.1038/nature04056

Davis, T. W., Berry, D. L., Boyer, G. L., & Gobler, C. J. (2009). The effects of temperature and nutrients on the growth and dynamics of toxic and non-toxic strains of *Microcystis* during cyanobacteria blooms. *Harmful Algae, 8*(5): 715-725.

Davis, T. W., Harke, M. J., Marcoval, M. A., Goleski, J., Orano-Dawson, C., Berry, D. L., & Gobler, C. J. (2010). Effects of nitrogenous compounds and phosphorus on the growth of toxic and non-toxic strains of *Microcystis* during cyanobacterial blooms. *Aquat Microb Ecol, 61*(2): 149-162.

Durham, B. P., Sharma, S., Luo, H., Smith, C. B., Amin, S. A., Bender, S. J. *et al.* (2015). Cryptic carbon and sulfur cycling between surface ocean plankton. *Proc Natl Acad Sci, 112*(2): 453-457.

Durham, B. P., Dearth, S. P., Sharma, S., Amin, S. A., Smith, C. B., Campagna, S. R. *et al.* (2017). Recognition cascade and metabolite transfer in a marine bacteria-phytoplankton model system. *Environ Microbiol, 19*(9): 3500-3513. doi:10.1111/1462-2920.13834

Dziallas, C., & Grossart, H.-P. (2011). Temperature and biotic factors influence bacterial communities associated with the cyanobacterium *Microcystis* sp. *Environ Microbiol, 13*(6): 1632-1641.

Dziallas, C., & Grossart, H.-P. (2012). Microbial interactions with the cyanobacterium *Microcystis aeruginosa* and their dependence on temperature. *Mar Biol, 159*(11): 2389-2398.

Eren, A. M., Maignien, L., Sul, W. J., Murphy, L. G., Grim, S. L., Morrison, H. G., & Sogin, M. L. (2013). Oligotyping: differentiating between closely related microbial taxa using 16S rRNA gene data. *Methods Ecol Evol, 4*(12): 1111-1119.

Eren, A. M., Borisy, G. G., Huse, S. M., & Welch, J. L. M. (2014). Oligotyping analysis of the human oral microbiome. *Proc Natl Acad Sci, 111*(28): E2875-E2884.

Eren, A. M., Morrison, H. G., Lescault, P. J., Reveillaud, J., Vineis, J. H., & Sogin, M. L. (2015). Minimum entropy decomposition: unsupervised oligotyping for sensitive partitioning of high-throughput marker gene sequences. *ISME J, 9*(4): 968-979.

Ferrier, M., Martin, J., & Rooney-Varga, J. (2002). Stimulation of *Alexandrium fundyense* growth by bacterial assemblages from the Bay of Fundy. *J Appl Microbiol, 92*(4): 706-716.

Forni, C., Telo', F. R., & Caiola, M. G. (1997). Comparative analysis of the polysaccharides produced by different species of *Microcystis* (Chroococcales, Cyanophyta). *Phycologia, 36*(3): 181-185.

Frischkorn, K. R., Rouco, M., Van Mooy, B. A., & Dyhrman, S. T. (2017). Epibionts dominate metabolic functional potential of *Trichodesmium* colonies from the oligotrophic ocean. *ISME J, 11*(9): 2090-2101.

Grossart, H. P., Levold, F., Allgaier, M., Simon, M., & Brinkhoff, T. (2005). Marine diatom species harbour distinct bacterial communities. *Environ Microbiol, 7*(6): 860-873.

Harke, M. J., Steffen, M. M., Gobler, C. J., Otten, T. G., Wilhelm, S. W., Wood, S. A., & Paerl, H. W. (2016). A review of the global ecology, genomics, and biogeography of the toxic cyanobacterium, *Microcystis* spp. *Harmful Algae, 54*: 4-20.

Hasegawa, Y., Martin, J. L., Giewat, M. W., & Rooney-Varga, J. N. (2007). Microbial community diversity in the phycosphere of natural populations of the toxic alga, *Alexandrium fundyense*. *Environ Microbiol, 9*(12): 3108-3121.

Hindák, F. (1996). Cyanophytes colonizing mucilage of chroococcal water blooms. *Beih Nova Hedwigia, 112*: 69-82.

Hmelo, L., Van Mooy, B., & Mincer, T. (2012). Characterization of bacterial epibionts on the cyanobacterium *Trichodesmium*. *Aquat Microb Ecol, 67*(1): 1-14.

Huisman, J., Codd, G. A., Paerl, H. W., Ibelings, B. W., Verspagen, J. M., & Visser, P. M. (2018). Cyanobacterial blooms. *Nat Rev Microbiol, 16*: 471-483.

Jackrel, S. L., White, J. D., Evans, J. T., Buffin, K., Hayden, K., Sarnelle, O., & Denef, V. J. (2019). Genome Evolution and Host Microbiome Shifts Correspond with Intraspecific Niche Divergence within Harmful Algal Bloom-Forming *Microcystis aeruginosa*. *Mol Ecol, 28*(17): 3994-4011.

Jankowiak, J. G., & Gobler, C. J. (2020). The composition and function of microbiomes within *Microcystis* colonies are significantly different than native bacterial assemblages in two North American lakes. *Front Microbiol, 11*: 1016.

Jasti, S., Sieracki, M. E., Poulton, N. J., Giewat, M. W., & Rooney-Varga, J. N. (2005). Phylogenetic diversity and specificity of bacteria closely associated with *Alexandrium* spp. and other phytoplankton. *Appl Environ Microbiol, 71*(7): 3483-3494. Retrieved from https://www.ncbi.nlm.nih.gov/pmc/articles/PMC1169014/pdf/2054-04.pdf

Jezberová, J., & Komárková, J. (2007). Morphological transformation in a freshwater *Cyanobium* sp. induced by grazers. *Environ Microbiol, 9*(7): 1858-1862.

Kardinaal, W. E. A., Janse, I., Kamst-van Agterveld, M., Meima, M., Snoek, J., Mur, L. R. *et al.* (2007). *Microcystis* genotype succession in relation to microcystin concentrations in freshwater lakes. *Aquat Microb Ecol, 48*(1): 1-12.

Kim, M., Shin, B., Lee, J., Park, H. Y., & Park, W. (2019). Culture-independent and culture-dependent analyses of the bacterial community in the phycosphere of cyanobloom-forming *Microcystis aeruginosa*. *Sci Rep, 9*(1): 1-13.

Kozich, J. J., Westcott, S. L., Baxter, N. T., Highlander, S. K., & Schloss, P. D. (2013). Development of a Dual-Index Sequencing Startegy and Curation Pipeline for Analyzing Amplicon Sequence Data on the MiSeq Illumina Sequencing Platform. *Appl Environ Microbiol, 79*(17): 5112-5120.

Landa, M., Burns, A. S., Roth, S. J., & Moran, M. A. (2017). Bacterial transcriptome remodeling during sequential co-culture with a marine dinoflagellate and diatom. *ISME J, 11*(12): 2677-2690.

Le Manach, S., Duval, C., Marie, A., Djediat, C., Catherine, A., Edery, M. *et al.* (2019). Global metabolomic characterizations of *Microcystis* spp. highlights clonal diversity in natural bloom-forming populations and expands metabolite structural diversity. *Front Microbiol, 10*: 791.

Lee, M. D., Walworth, N. G., McParland, E. L., Fu, F.-X., Mincer, T. J., Levine, N. M. *et al.* (2017). The *Trichodesmium* consortium: conserved heterotrophic co-occurrence and genomic signatures of potential interactions. *ISME J, 11*(8): 1813-1824. doi:10.1038/ismej.2017.49

Li, M., Zhu, W., Gao, L., & Lu, L. (2013). Changes in extracellular polysaccharide content and morphology of *Microcystis aeruginosa* at different specific growth rates. *J Appl Phycol, 25*(4): 1023-1030.

Louati, I., Pascault, N., Debroas, D., Bernard, C., Humbert, J.-F., & Leloup, J. (2015). Structural diversity of bacterial communities associated with bloom-forming freshwater cyanobacteria differs according to the cyanobacterial genus. *PloS one, 10*(11): e0140614.

Ma, L., Calfee, B. C., Morris, J. J., Johnson, Z. I., & Zinser, E. R. (2018). Degradation of hydrogen peroxide at the ocean's surface: the influence of the microbial community on the realized thermal niche of *Prochlorococcus*. *ISME J, 12*(2): 473-484.

Miller, T. R., Hnilicka, K., Dziedzic, A., Desplats, P., & Belas, R. (2004). Chemotaxis of *Silicibacter* sp. strain TM1040 toward dinoflagellate products. *Appl Environ Microbiol, 70*(8): 4692-4701.

Mönnich, J., Tebben, J., Bergemann, J., Case, R., Wohlrab, S., & Harder, T. (2020). Niche-based assembly of bacterial consortia on the diatom *Thalassiosira rotula* is stable and reproducible. *ISME J*: 1-12. doi:https://doi.org/10.1038/s41396-020-0631-5

Morris, J. J., Johnson, Z. I., Szul, M. J., Keller, M., & Zinser, E. R. (2011). Dependence of the cyanobacterium *Prochlorococcus* on hydrogen peroxide scavenging microbes for growth at the ocean's surface. *PloS one, 6*(2): e16805.

Oksanen, J., Blanchet, F. G., Kindt, R., Legendre, P., Minchin, P. R., O'hara, R. *et al.* (2013). Package 'vegan'.

Otsuka, S., Suda, S., Li, R., Matsumoto, S., & Watanabe, M. M. (2000). Morphological variability of colonies of *Microcystis* morphospecies in culture. *J Gen Appl Microbiol, 46*(1): 39-50.

Otten, T., Xu, H., Qin, B., Zhu, G., & Paerl, H. (2012). Spatiotemporal patterns and ecophysiology of toxigenic *Microcystis* blooms in Lake Taihu, China: implications for water quality management. *Environ Sci Technol, 46*(6): 3480-3488.

Otten, T. G., Paerl, H. W., Dreher, T. W., Kimmerer, W. J., & Parker, A. E. (2017). The molecular ecology of *Microcystis* sp. blooms in the San Francisco Estuary. *Environ Microbiol, 19*(9): 3619-3637.

Ouellette, A. J., Handy, S. M., & Wilhelm, S. W. (2006). Toxic *Microcystis* is widespread in Lake Erie: PCR detection of toxin genes and molecular characterization of associated cyanobacterial communities. *Microb Ecol, 51*(2): 154-165.

Paerl, H. W., & Gallucci, K. K. (1985). Role of chemotaxis in establishing a specific nitrogen-fixing cyanobacterial-bacterial association. *Science, 227*(4687): 647-649.

Parveen, B., Ravet, V., Djediat, C., Mary, I., Quiblier, C., Debroas, D., & Humbert, J. F. (2013). Bacterial communities associated with *Microcystis* colonies differ from free-living communities living in the same ecosystem. *Environ Microbiol Rep, 5*(5): 716-724.

Pérez-Carrascal, O. M., Terrat, Y., Giani, A., Fortin, N., Greer, C. W., Tromas, N., & Shapiro, B. J. (2019). Coherence of *Microcystis* species revealed through population genomics. *ISME J, 13*(12): 2887-2900.

Pruesse, E., Quast, C., Knittel, K., Fuchs, B. M., Ludwig, W., Peplies, J., & Glöckner, F. O. (2007). SILVA: a comprehensive online resource for quality checked and aligned ribosomal RNA sequence data compatible with ARB. *Nucleic Acids Res, 35*(21): 7188-7196.

Raina, J.-B., Fernandez, V., Lambert, B., Stocker, R., & Seymour, J. R. (2019). The role of microbial motility and chemotaxis in symbiosis. *Nat Rev Microbiol, 17*: 284-294.

Ribalet, F., Intertaglia, L., Lebaron, P., & Casotti, R. (2008). Differential effect of three polyunsaturated aldehydes on marine bacterial isolates. *Aquatic Toxicology, 86*(2): 249-255.

Rouco, M., Haley, S. T., & Dyhrman, S. T. (2016). Microbial diversity within the *Trichodesmium* holobiont. *Environ Microbiol, 18*(12): 5151-5160.

Salter, S. J., Cox, M. J., Turek, E. M., Calus, S. T., Cookson, W. O., Moffatt, M. F. *et al.* (2014). Reagent and laboratory contamination can critically impact sequence-based microbiome analyses. *BMC biology, 12*(87): 1-12.

Sapp, M., Schwaderer, A. S., Wiltshire, K. H., Hoppe, H.-G., Gerdts, G., & Wichels, A. (2007). Species-specific bacterial communities in the phycosphere of microalgae? *Microb Ecol, 53*(4): 683-699.

Schloss, P. D., & Bishop, L. (2019). MiSeq Wet Lab SOP. Retrieved from https://github.com/SchlossLab/MiSeq_WetLab_SOP/blob/master/MiSeq_WetLab_SOP.md

Schmidt, K. C., Jackrel, S. L., Smith, D. J., Dick, G. J., & Denef, V. J. (2020). Genotype and host microbiome alter competitive interactions between *Microcystis aeruginosa* and *Chlorella sorokiniana*. *Harmful Algae, 99*(101939).

Segev, E., Wyche, T. P., Kim, K. H., Petersen, J., Ellebrandt, C., Vlamakis, H. *et al.* (2016). Dynamic metabolic exchange governs a marine algal-bacterial interaction. *eLife, 5*(1): e17473.

Seyedsayamdost, M. R., Case, R. J., Kolter, R., & Clardy, J. (2011). The Jekyll-and-Hyde chemistry of *Phaeobacter gallaeciensis*. *Nat Chem, 3*(4): 331-335. Retrieved from https://www.nature.com/articles/nchem.1002.pdf

Seymour, J., Ahmed, T., Durham, W., & Stocker, R. (2010). Chemotactic response of marine bacteria to the extracellular products of *Synechococcus* and *Prochlorococcus*. *Aquat Microb Ecol, 59*(2): 161-168.

Seymour, J. R., Amin, S. A., Raina, J.-B., & Stocker, R. (2017). Zooming in on the phycosphere: the ecological interface for phytoplankton-bacteria interactions. *Nat Microbiol, 2*(17065): 1-12. doi:10.1038/nmicrobiol.2017.65

Sheik, C. S., Reese, B. K., Twing, K. I., Sylvan, J. B., Grim, S. L., Schrenk, M. O. *et al.* (2018). Identification and removal of contaminant sequences from ribosomal gene databases: lessons from the census of deep life. *Front Microbiol, 9*: 840.

Shi, L., Huang, Y., Zhang, M., Shi, X., Cai, Y., Gao, S. *et al.* (2018). Large buoyant particles dominated by cyanobacterial colonies harbor distinct bacterial communities from small

suspended particles and free-living bacteria in the water column. *MicrobiologyOpen, 7*(6): e00608.

Shia, L., Cai, Y., Wang, X., Li, P., Yu, Y., & Kong, F. (2010). Community structure of bacteria associated with *Microcystis* colonies from cyanobacterial blooms. *J Freshw Ecol, 25*(2): 193-203.

Sison-Mangus, M. P., Jiang, S., Tran, K. N., & Kudela, R. M. (2014). Host-specific adaptation governs the interaction of the marine diatom, *Pseudo-nitzschia* and their microbiota. *ISME J, 8*(1): 63-76.

Smriga, S., Fernandez, V. I., Mitchell, J. G., & Stocker, R. (2016). Chemotaxis toward phytoplankton drives organic matter partitioning among marine bacteria. *Proc Natl Acad Sci, 113*(6): 1576-1581.

Sonnenschein, E. C., Syit, D. A., Grossart, H.-P., & Ullrich, M. S. (2012). Chemotaxis of *Marinobacter adhaerens* and its impact on attachment to the diatom *Thalassiosira weissflogii*. *Appl Environ Microbiol, 78*(19): 6900-6907.

Tu, J., Chen, L., Gao, S., Zhang, J., Bi, C., Tao, Y. *et al.* (2019). Obtaining Genome Sequences of Mutualistic Bacteria in Single *Microcystis* Colonies. *Int J Mol Sci, 20*(20): 5047.

Van Mooy, B. A., Hmelo, L. R., Sofen, L. E., Campagna, S. R., May, A. L., Dyhrman, S. T. *et al.* (2012). Quorum sensing control of phosphorus acquisition in *Trichodesmium* consortia. *ISME J, 6*(2): 422-429.

Wang, Q., Garrity, G. M., Tiedje, J. M., & Cole, J. R. (2007). Naive Bayesian classifier for rapid assignment of rRNA sequences into the new bacterial taxonomy. *Appl Environ Microbiol, 73*(16): 5261-5267.

Westcott, S. L., & Schloss, P. D. (2017). OptiClust, an improved method for assigning amplicon-based sequence data to operational taxonomic units. *MSphere, 2*(2): e00073-00017.

Worm, J., & Søndergaard, M. (1998). Dynamics of heterotrophic bacteria attached to *Microcystis* spp.(Cyanobacteria). *Aquat Microb Ecol, 14*(1): 19-28.

Wynne, T. T., Stumpf, R. P., Tomlinson, M. C., Fahnenstiel, G. L., Dyble, J., Schwab, D. J., & Joshi, S. J. (2013). Evolution of a cyanobacterial bloom forecast system in western Lake Erie: development and initial evaluation. *J Great Lakes Res, 39*: 90-99.

Xu, H., Cai, H., Yu, G., & Jiang, H. (2013). Insights into extracellular polymeric substances of cyanobacterium *Microcystis aeruginosa* using fractionation procedure and parallel factor analysis. *Water Res, 47*(6): 2005-2014.

Zhang, K., Pan, R., Zhang, L., Zhang, T., & Fan, J. (2020). Interspecific competition between *Microcystis aeruginosa* and *Pseudanabaena* and their production of T&O compounds. *Chemosphere, 252*: 126509.

Zhu, C.-M., Zhang, J.-Y., Guan, R., Hale, L., Chen, N., Li, M. *et al.* (2019). Alternate succession of aggregate-forming cyanobacterial genera correlated with their attached bacteria by co-pathways. *Sci Total Environ, 688*: 867-879.

Zhu, W., Li, M., Luo, Y., Dai, X., Guo, L., Xiao, M. *et al.* (2014). Vertical distribution of *Microcystis* colony size in Lake Taihu: Its role in algal blooms. *J Great Lakes Res, 40*(4): 949-955.

Chapter 4 Metagenomic and Metatranscriptomic Evidence for Uptake of Phytoplankton-Derived Carbon by Novel Acidobacteria Genera in *Microcystis* Blooms

4.1 Abstract

Bacteria and phytoplankton often interact in close physical association in a zone termed the phycosphere. Interactions between heterotrophic bacteria and their phytoplankton hosts have important outcomes on primary production, community composition, and algal bloom development. However, these interactions are poorly described for many phycosphere consortia, particularly for freshwater bloom-forming cyanobacteria. In this study, gene expression was assessed in two uncultivated Acidobacteria genomes from Lake Erie *Microcystis* bloom metagenomes. These organisms were targeted because they were previously identified as important catalase producers, suggesting that they may protect *Microcystis* from H_2O_2. Metatranscriptomics revealed that both Acidobacteria transcribed genes for uptake of organic compounds that are known cyanobacterial products and exudates, including lactate, glycolate, amino acids, peptides, and vitamin B_{12}. Expressed pathways for amino acid metabolism in the Acidobacteria suggest that they may provide regenerated nitrogen for *Microcystis* growth in return. Although correlations between Acidobacteria and *Microcystis* abundance were weak, both organisms were detected in *Microcystis* blooms worldwide. Together, the data support that uncultured and previously unidentified Acidobacteria exchange metabolites with phytoplankton during harmful cyanobacteria blooms and influence the form and availability of nitrogen available to phytoplankton. Thus, Acidobacteria may play a role in cyanobacterial physiology and bloom development in western Lake Erie.

4.2 Introduction

Interactions between microorganisms have profound impacts on global biogeochemistry by influencing microbial fitness, metabolism, and community composition. For example, many microbes may use the waste products of others in the community for growth or produce compounds required by other community members (Embree *et al.*, 2015; Anantharaman *et al.*, 2016; Hug & Co, 2018). A widely recognized example of such metabolic handoffs is in the interactions between phytoplankton and heterotrophic bacteria. Phytoplankton support heterotrophic bacterial growth by providing organic carbon and sulfur, and their heterotrophic partners can improve phytoplankton growth by producing essential vitamins and growth factors, such as B_{12} vitamins (cobalamins) (Croft *et al.*, 2005; Durham *et al.*, 2017), increasing the bioavailability of trace metal cofactors (Amin *et al.*, 2009), regenerating nutrients from organic material (Amin *et al.*, 2015; Arandia-Gorostidi *et al.*, 2017; Christie-Oleza *et al.*, 2017), and detoxifying reactive oxygen species (Morris *et al.*, 2011). Heterotrophic bacteria are known to impact the fitness of phytoplankton through the transfer of metabolites (Amin *et al.*, 2009; Seyedsayamdost *et al.*, 2011; Amin *et al.*, 2015; Segev *et al.*, 2016) in a zone of close physical association termed the phycosphere (Bell & Mitchell, 1972; Seymour *et al.*, 2017).

Interactions between heterotrophic bacteria and phytoplankton also influence competition between phytoplankton taxa (Schmidt *et al.*, 2020). Therefore, phycosphere interactions likely play a role in shaping successions of phytoplankton taxa (Cole, 1982) and may have implications at the level of whole ecosystems by modulating primary productivity and phytoplankton bloom formation (Seyedsayamdost *et al.*, 2011; Smriga *et al.*, 2016; Seymour *et al.*, 2017). Interactions in the phycosphere can have both strain and species and specific outcomes (Sison-Mangus *et al.*, 2014; Amin *et al.*, 2015), and the fitness impacts on phytoplankton have been linked to the exchange of specific metabolites (Croft *et al.*, 2005; Seyedsayamdost *et al.*, 2011; Segev *et al.*,

2016). Therefore, identifying the bacterial taxa associated with a given phytoplankton taxon and the metabolites exchanged between them can improve our understanding of phytoplankton physiology and competition between phytoplankton in natural assemblages with co-occurring bacteria.

An improved understanding of the impact of phycosphere interactions on phytoplankton fitness and successions will likely improve our predictions and modelling of ecosystem wide processes such as primary productivity and harmful algal bloom formation (Seyedsayamdost *et al.*, 2011; Smriga *et al.*, 2016; Seymour *et al.*, 2017). For example, successions in toxin-producing and non-producing strains of the cyanobacterial harmful algal blooms (CHAB)-forming genus *Microcystis* are an important driver of toxin concentrations in many freshwater CHABs (Kardinaal *et al.*, 2007; Davis *et al.*, 2010). *Microcystis* grow in colonies that harbor heterotrophic bacterial communities (Shia *et al.*, 2010; Parveen *et al.*, 2013). In Chapter 3 of this dissertation, the *Microcystis* phycosphere communities were found to be distinct from the surrounding microbial communities and differ both seasonally and by colony genotype. However, the nature of the interactions between *Microcystis* and its associated phycosphere communities and their impact on *Microcystis* growth and physiology remain uncharacterized, in part because many of the microbes associated with *Microcystis* colonies are yet uncultured (Shia *et al.*, 2010; Parveen *et al.*, 2013). Direct recovery of bacterial genomes from the environment can provide insights into the biochemical and ecological characteristics of these uncultivated organisms of interest.

In Chapter 2, metagenome-assembled genomes (MAGs) of two uncultivated Acidobacteria from a western Lake Erie cyanobacterial bloom in the summer-fall of 2014 were identified to have high abundance of catalase genes relative to catalases from other taxa in

metatranscriptomes despite having low catalase relative abundance in metagenomes. Both genomes were reconstructed from phytoplankton and particle attached size-fractions, and one of the Acidobacteria was represented in amplicon sequences from *Microcystis* phycosphere communities characterized in Chapter 3. Together, these results suggest that the Acidobacteria may interact with *Microcystis* and other phytoplankton and decompose H_2O_2. Here, the gene content and expression of the Acidobacteria MAGs during the 2014 western Lake Erie cyanobacterial bloom was examined in order to explore potential interactions with freshwater cyanobacteria and other phytoplankton. In addition, the abundance of both Acidobacteria in amplicon datasets from a range of eutrophic environments and size fractionated samples was examined to determine their specificity to cyanobacterial blooms and *Microcystis* colonies.

4.3 Methods

4.3.1 Genome Assembly and Gene Annotation

Acidobacteria metagenome-assembled genomes (MAGs) were obtained from a MAG collection assembled with metagenomic Illumina reads from Lake Erie *Microcystis* blooms in the summer-fall of 2014, which is described in more detail in Chapter 2 methods. Both genomes were assembled from metagenomes collected in 100 μm retentate samples, which indicates that they are attached to phytoplankton seston or other particles retained on the filter. One MAG (CoA2 C42) was not binned with a ribosomal RNA operon, but an unbinned contig with the full rRNA operon was assigned to the bin by examining the assembly De Bruijn graph using Bandage v. 0.8.1 (Wick *et al.*, 2015) and the paired-end mapping information. Gene calls and functional annotations were generated using the Integrated Microbial Genomes annotation pipeline (Huntemann *et al.*, 2015). Genes annotated as iron complex transporters were compared to biochemically confirmed cobalamin transporters from E coli str. K-12 (UniProtKB accessions:

P06129, P06609, P06611) via protein BLAST v. 2.2.31+ (Altschul *et al.*, 1990). We excluded any significant hits in the results with alignment coverage less than 70% of the gene in the Acidobacterium genomes. All predicted open reading frames were compared to proteins in NCBI non-redundant protein database (as of October 17th, 2018) via protein BLAST v. 2.2.31+ (Altschul *et al.*, 1990). Gene expression was determined by mapping metatranscriptomic short reads to predicted gene sequences using nucleotide BLAST v. 2.2.31+ (Altschul *et al.*, 1990). Only alignments with percent identity ≥ 95% and e-value ≥ $1x10^{-5}$, and alignment coverage ≥ 80 % of read length were counted. Some reads below the alignment coverage cutoff were counted if they mapped to either the start or stop end of the gene. Relative abundance of transcripts for each gene was calculated as reads mapped per gene kilobase per million reads mapped (RPKM), using total number of reads mapped to the appropriate genome.

From the predicted gene calls, functional annotations, and metatranscriptomic gene mapping, we predicted the *in situ* metabolism of *Bryobacter* and Acidobacterium CoA2 C42. Due to the novelty of the Acidobacteria genomes reported here, most of the predicted protein coding genes have low shared amino acid identities with published protein sequences with the same function (< 70 % shared identity to the best matches in many cases, Figure S 4.1), so we present these results as putative functions and interactions of interest that require validation with future work. Because Acidobacterium CoA2 C42 only had a sufficient amount of reads in the August 4th sample (Figure S 4.2), which coincides with an early peak in pigments at this station (Berry *et al.*, 2017), this sample is the focus when reporting RPKM values in the main text and figures. Both Acidobacterial MAGs are deposited in the IMG database (IMG Genome IDs: 2806310633 and 2806310632).

4.3.2 16S rRNA Phylogenetic Analysis

The 16S rRNA genes from each MAG were compared to the SILVA SSU database v. 138.1 (Pruesse *et al.*, 2007) using the online SINA Aligner v. 1.2.11 (Pruesse *et al.*, 2012). Maximum likelihood phylogenetic trees with published 16S rRNA genes from Acidobacteria available in NCBI (as of 8 Nov 2020) was computed with RAxML v. 8.2.4 using the GTRGAMMA nucleotide substitution model (Stamatakis, 2006). The 16S rRNA genes were aligned using Clustal Omega v. 1.2.1 (Sievers *et al.*, 2011). Shared average nucleotide identity (gANI) was performed with whole genome alignments of Acidobacteria genomes available in IMG (as of November 5th 2018), which were computed using the compare function in dRep v. 2.0.5 (Olm *et al.*, 2017) without the MASH pre-clustering step. Genomes were only included in the gANI analysis if the completeness was above 90% and the contamination was below 5% calculated with the CheckM lineage workflow (Parks *et al.*, 2015).

4.3.3 Amplicon Dataset Mining

To assess if these Acidobacteria regularly occur in or are specific to *Microcystis* blooms, we searched for their presence in previously published rRNA amplicon datasets (Kara *et al.*, 2013; Berry *et al.*, 2017; Tromas *et al.*, 2017; Shi *et al.*, 2018; Chun *et al.*, 2019; Rozmarynowycz *et al.*, 2019; Cook *et al.*, 2020; Paver *et al.*, 2020), which are described in Table 4.1. To assess the MAGs abundance in western Lake Erie, the relative abundance of OTUs generated in Chapter 3 were reported. For the *Bryobacter* CoA8 C33 MAG, the relative abundance of OTUs classified as *Bryobacter* were reported. For the Acidobacterium CoA2 C42 MAG, the relative abundance of OTUs classified as *Paludibaculum* were reported if the 16S rRNA gene in the MAG aligned to the amplicon sequence with 97 % or more shared nucleotide identity as determined via nucleotide BLAST v. 2.2.31+ (Altschul *et al.*, 1990). Because the public datasets used a range of

different primer sets, we determined the abundance of each organism in these datasets by mapping amplicon reads to the 16S rRNA gene sequence in each MAG with BLAST v. 2.2.31+ (Altschul *et al.*, 1990). The relative abundance of *Microcystis*, *Synechococcous*, and *Dolichosperumum* were similarly determined in these datasets by mapping amplicon reads to reference sequences. We mapped to full-length 16S rRNA sequences from *Anabaena cylindrica* PCC 7122, *Microcystis aeruginosa* PCC 7806SL, *Microcystis aeruginosa* PCC 9806, *Synechococcus elongatus* PCC 6301, *Synechococcus elongatus* PCC 7942, as well as sequences assembled from Lake Erie metagenomes using EMIRGE (Miller *et al.*, 2011) and classified as *Microcystis*, *Anabaena*, *Dolichospermum*, and *Synechococcus* using the Wang classifier (Wang *et al.*, 2007) in MOTHUR v 1.43.0 (Schloss *et al.*, 2009). The relative abundance of each organism in a given sample was calculated as the number of reads mapped for that given organism divided by the total number of reads in the dataset.

4.3.4 Identification of Pseudocobalamin in Microcystis Cultures

Two strains of *Microcystis aeruginosa* (PCC 7806 and PCC 9806) were grown on a variant of BG-11 growth media (Allen & Stanier, 1968) with the sodium nitrate concentration reduced to 2 mM in preparation for screening for pseudocobalamin production via liquid chromatography-mass spectrometry (LC-MS) analysis. The *Microcystis* strains were grown as batch cultures at room temperature under cool white fluorescent bulbs. The light intensity was kept between 30-60 µmol photons/m^2/sec by covering the lights with a single layer of neutral density 0.3 filter screen (product 209R, LEE Filters, Burbank, CA). For each strain, 300 mL of late log phase culture was split into six 50 mL aliquots and harvested by centrifugation at 10,000 x*g* for 15 minutes, decanting liquid media, and freezing at -80 °C until extraction. Analysis of cell pellets was carried out using a previously published method (Heal *et al.*, 2017), with some

modifications. Briefly, cell pellets were resuspended in 6 mL of cold acetonitrile:methanol:water (40:40:20 ratio by volume) with 0.1% formic acid and transferred to 15 mL centrifuge tubes. The cells where lysed via bead beating with 250 mg each of 100 and 500 µm glass beads on a vortex mixer set to max speed for 40 sec. Bead beating was performed three times, with samples resting on ice for five minutes between each treatment. The suspension was pelleted via centrifugation at 10,000 x*g* and the supernatant was transferred to a round bottom flask. The pooled supernatants from each strain were dried in a rotary evaporator under 300 mbar pressure at 30 °C, then resuspended in a small volume of solvent A (described below) before LC-MS analysis. Extraction from ~ 6 g *Spirulina* powder was also performed as a positive control (Heal *et al.*, 2017) following the same procedure described above for the *Microcystis* cells, with the exception that the powder was suspended in 10 mL of cold acetonitrile:methanol:water solution. All extraction and processing steps were conducted under low light conditions to minimize photodegradation of pseudocobalamin.

LC-MS analysis was carried out on a Thermo Scientific UHPLC coupled to a Q-Exactive Orbitrap High Resolution Mass Spectrometer equipped with an ESI source and running in positive mode. Sample (1 µL) was injected onto a 2.6 µm Kinetex RP C18 column (150 x 4.6 mm inside diameter) held at 25 °C. The HPLC gradient used was 5% to 95% solvent B over 22 minutes, where solvent A consisted of 20 mM ammonium formate and 0.1% formic acid in water, and solvent B consisted of 0.1% formic acid in acetonitrile. MS data was collected over a mass range of 600-1400 m/z, using data-dependent MS/MS analysis with 0.5 s dynamic exclusion enabled. Pseudocobalamin variants were identified by comparing the obtained compound masses and MS/MS spectra to previously reported literature values (Heal *et al.*, 2014; Heal *et al.*, 2017) and the *Spirulina* extract.

4.4 Results and Discussion

4.4.1 The MAGs From Western Lake Erie are Novel Species of Subdivision 3 Acidobacteria

Metagenome assembled genomes (MAGs) of two Acidobacteria were obtained from published metagenomic assemblies of microbial communities from a western Lake Erie *Microcystis* bloom during the summer-fall of 2014. We focused on these genomes because they contained catalase-peroxidase genes (*katG*) that were among the most highly expressed during peak *katG* expression during a cyanobacteria bloom in western Lake Erie and were in particle or phytoplankton attached samples (described in Chapter 2 of this dissertation). Therefore, they may be important H_2O_2 degraders in phytoplankton-associated communities.

Both genomes are near-complete with low contamination (Table 4.2) and have assembly metrics that meet the standards for high-quality draft genomes (Bowers *et al.*, 2017). The 16S rRNA gene sequences of MAGs CoA2 C42 and CoA8 C33 were classified as *Paludibaculum* and *Bryobacter* (see methods), and were closest matches to 16S sequences from *Paludibaculum fermentans* and *Bryobacter aggregatus* strains (92.29 and 96.5 %), respectively, which were both isolated from peat bogs (Kulichevskaya *et al.*, 2010; Kulichevskaya *et al.*, 2014). The 16S rRNA percent similarity score for the CoA8 C33 MAG with *Bryobacter aggregatus* is above genus level thresholds, and the similarity score for the CoA2 C42 MAG with *Paludibaculum fermentans* is below genus level but above family level thresholds (Yarza *et al.*, 2014). A maximum likelihood tree including published acidobacterial 16S rRNA sequences placed both genomes within subdivision 3 Acidobacteria, *Bryobacteraceae*, with high bootstrap support (Figure 4.1A). While the CoA8 C33 MAG was placed as a sister lineage to *Bryobacter aggregatus* with high confidence, the specific placement of the CoA2 C42 MAG within subdivision 3 Acidobacteria had lower bootstrap support. The percent identity scores of the 16S matches and the bootstrap support of the 16S tree supports a taxonomic placement of genome

CoA8 C33 as a novel species of *Bryobacter*, while genome CoA2 C42 likely represents a novel genus within the subdivision 3 Acidobacteria sister to *Paludibaculum*. Here, both species will be referred to as *Bryobacter* CoA8 C33 and Acidobacteria CoA2 C42.

The 16S rRNA based taxonomic classification is further supported by whole genome alignments. Both genomes were most similar to Acidobacteria genomes from subdivision 3 (Figures 4.1B, 4.1C). The CoA8 C33 genome was most similar to *Bryobacter aggregatus* strains. The gANI and coverage values were within the range of other intragenus comparisons but below species level cutoffs (Konstantinidis & Tiedje, 2005; Varghese *et al.*, 2015), further supporting that this genome sequence represents a novel species of *Bryobacter*. The CoA2 C42 genome was most similar to another uncultivated MAG from a drinking water metagenome (IMG Gold Study ID: Gs0114768), with the next most similar genomes being the CoA8 C33 genome from Lake Erie, both *Bryobacter aggregatus* strains, and *Candidatus Solibacter usitatus*. While subdivision 3 Acidobacteria have been recognized as numerically important in soils (Jones *et al.*, 2009; Serkebaeva *et al.*, 2013) and present in freshwaters (Chun *et al.*, 2020), to our knowledge, this study represents the first detailed description of *Bryobacteraceae* genomes from an aquatic environment.

4.4.2 Evidence for Expression of Genes Involved in Biofilm Adhesion and Respiration of Exopolysaccharides and Phytoplankton Exudates

In both the *Bryobacter* CoA8 C33 and Acidobacterium CoA2 C42 genomes, the most highly expressed genes were involved in translation, ribosomal proteins, secretion proteins, peptidases of unknown function, chaperonins, H_2O_2 detoxification, and ATP synthesis, along with hypothetical or uncharacterized proteins (Figures S 4.3 & S 4.4). Highly expressed genes encoding hypothetical proteins did not align to RNA gene sequences in NCBI, and either had best hits to other hypothetical proteins or no significant hits to any proteins in the database

(Appendix 1). Both genomes have a complete TCA cycle, near complete glycolysis and Entner-Doudoroff pathways (Figure S 4.5), and lack known pathways for carbon fixation and synthesis of bacteriochlorophyll and rhodopsin pigments, which indicates that these organisms are chemoheterotrophs and fits the description of known subdivision 3 Acidobacteria isolates (Dedysh & Damsté, 2018). Included among the more highly expressed membrane associated genes were genes involved in biofilm adhesion, chemotaxis, flagellum biosynthesis, and motility, which indicates that these organisms are chemotactic, seeking out and adhering to phytoplankton or other particles (Figures S6, S7).

The functional annotations and expression of predicted protein coding genes suggests that both Acidobacteria appear to obtain carbon from the breakdown of complex exopolysaccharides produced by phytoplankton. Both genomes possess putative pectate-lyase, alpha-mannosidase, and xylan esterase exoenzymes to completely degrade homogalacturonan, mannose, and xylose polymers completely to the constituent monosaccharides (Figure S5). Additionally, the *Bryobacter* MAG contains genes for degradation of galactose and arabinofuranose polymers, while the Acidobacteria CoA2 C42 MAG contains genes for the degradation of alginate (Figure S5). Cyanobacteria, including *Microcystis*, have an exopolysaccharide (EPS) mucilage encasing their cells that is comprised mainly of galacturonan polymers in certain strains and species (Wolk, 1973; Plude *et al.*, 1991; Forni *et al.*, 1997), suggesting that the EPS in *Microcystis* colonies could be a substrate of these exoenzymes. Furthermore, both genomes possess and expressed genes involved in the degradation of galacturonate monomers along with other constituents of cyanobacterial EPS such as xylose, glucose, galactose, and mannose (Wolk, 1973; Plude *et al.*, 1991; Forni *et al.*, 1997; Li *et al.*, 2009), suggesting that they can derive carbon from the degradation of cyanobacterial EPS. Supporting this, bacterial degradation of

Microcystis EPS has been observed in co-cultures with heterotrophic bacteria (Li *et al.*, 2009). Eukaryotic phytoplankton also produce extracellular polysaccharides composed of these same constituents (Meon & Kirchman, 2001; Grossart & Simon, 2007; Mühlenbruch *et al.*, 2018), which could potentially provide carbon to these organisms (Meon & Kirchman, 2001; Grossart & Simon, 2007; Mühlenbruch *et al.*, 2018; Ferrer-González *et al.*, 2020).

4.4.3 Evidence for Uptake of Low Molecular Weight Organics in Phytoplankton Exudates

In addition to sugar uptake, the metatranscriptomic data suggest that low molecular weight phytoplankton exudates are a source of carbon and nitrogen for both Acidobacteria in Lake Erie cyanobacteria blooms and further support the hypothesis that both Acidobacteria participate in metabolic exchanges within phycosphere communities (Figure 4.2). Among the most highly expressed transporters in both Acidobacteria during the *Microcystis* bloom were concentrative nucleoside transporters (CNT, Figures S 4.7 & S 4.8), suggesting that they uptake nucleosides released into the environment as a carbon source. Although their relative abundance in the metatranscriptomes was lower, there was also detectable expression of many proteins putatively involved in amino acid, peptide, and polyamine uptake (Figure 4.2). This suggests that a substantial portion of the nitrogen demand for both Acidobacteria is likely met by the uptake of organic nitrogen in dissolved amino acids, peptides, and nucleosides. Indeed, nucleosides and amino acids are a common component of phytoplankton exudates that can serve as carbon and nitrogen sources for bacteria in marine phytoplankton co-cultures (Beliaev *et al.*, 2014; Christie-Oleza *et al.*, 2017; Durham *et al.*, 2017; Ferrer-González *et al.*, 2020), and amino acids are an important source of nitrogen for natural bacterial assemblages (Kirchman *et al.*, 1989; Tupas & Koike, 1990; Tupas *et al.*, 1994). Expression of amino acid oxidases was also detected,

suggesting that both Acidobacteria may need to deaminate some amino acids in order to access the nitrogen (Palenik & Morel, 1990b; Palenik & Morel, 1990a; Tupas & Koike, 1990).

Both Acidobacteria also expressed genes to oxidize lactate and glycolate and dephosphorylate phosphoglycolate (Figure 4.2), which are common exudates of cyanobacteria (Bateson & Ward, 1988; Beliaev *et al.*, 2014; Barchewitz *et al.*, 2019) and eukaryotic phytoplankton (Hellebust, 1965; Tolbert, 1979). Expression of lactate permease, which is involved in uptake of both lactate and glycolate (Núñez *et al.*, 2001), was detected, along with transporters putatively involved in the uptake of other organic acids (Figure 4.2). Both genomes lack genes in the glyoxylate cycle, methylaspartate cycle, and the majority of genes in the ethylmalonyl-CoA and 3-hydroxypropanoate cycles, but possess and express genes in the serine pathway (Figure 4.2). The presence of genes in the serine pathway suggest that the glyoxylate formed from the oxidation of glycolate is incorporated into amino acids (Sinha & Cossins, 1965; Renström-Kellner & Bergman, 1989; But *et al.*, 2019) and the metabolism of C1 compounds (But *et al.*, 2019). The final two genes of the serine pathway, which regenerate glyoxylate from malate, were missing from both genomes. While a putative malate synthase enzyme in the *Bryobacter* genome could potentially fill this role, it is unclear from our data if the absence of the glyoxylate regeneration steps in Acidobacterium CoA2 C42 is indicative of glyoxylate auxotrophy, an artifact of incomplete genome reconstruction, or the use of an as of yet uncharacterized pathway for use of glyoxylate formed from glycolate oxidation. The potential for glyoxylate auxotrophy is intriguing, as this may implicate glycolate excreted by phytoplankton as an essential growth factor for these Acidobacteria. More recently described pathways for glyoxylate assimilation (von Borzyskowski *et al.*, 2019) may also be present; however, genes involved in these pathway could not be confidently identified in this study due to

the limited annotations for these pathways and low shared amino acid identities of the Acidobacteria genomes with published sequences (Figure S 4.1).

4.4.4 Evidence for Regeneration of Nitrogen From Peptides and Amino Acids

The detectable expression of dipeptide and oligopeptide transporters, peptidases, and cyanophycinase-like proteins along with amino acid efflux proteins suggests that amino acid efflux by the Acidobacteria may be linked to peptide degradation (Figure 4.2) and, along with the detectable expression of amino acid oxidases, may regenerate reduced nitrogen from dissolved peptides and amino acids that is subsequently used for phytoplankton growth. Because intracellular accumulation of some amino acids can inhibit the biosynthesis of other amino acids (Zakataeva *et al.*, 1999; Livshits *et al.*, 2003), amino acid secretion via efflux proteins allow bacteria to excrete excess amino acids and their derivatives, thus allowing the biosynthesis of other amino acids to proceed and meet cellular amino acid demands (Zakataeva *et al.*, 1999; Bellmann *et al.*, 2001; Livshits *et al.*, 2003). This amino acid efflux activity is essential for maintaining balanced growth from the degradation of oligopeptides (Payne & Bell, 1979; Nisbet & Payne, 1982; Bellmann *et al.*, 2001) by allowing bacteria access to specific amino acid moieties while remaining unimpacted by moieties within the peptide that would lead to an amino acid imbalance (Payne & Bell, 1979). Assuming that amino acid quotas between phytoplankton and phycosphere bacteria differ such that excess amino acids in heterotrophic bacteria are limiting growth in their phytoplankton hosts, peptide degradation followed by amino acid efflux by bacteria could regenerate amino acids from peptides released from phytoplankton cells by cell lysis or excretion.

Additionally, expression of amino acid oxidases on the cell membranes of bacteria (Duerre & Chakrabarty, 1975; Bouvrette & Luong, 1994) and phytoplankton (Palenik & Morel,

1990b; Palenik & Morel, 1990a) may convert excess amino acids excreted by bacteria into inorganic nitrogen that could subsequently be taken up by phytoplankton and phycosphere bacteria for growth (Palenik & Morel, 1990b; Palenik & Morel, 1990a). Supporting this hypothesis, exchange of nitrogen between phytoplankton and bacteria was detected in co-cultures (Arandia-Gorostidi *et al.*, 2017; Christie-Oleza *et al.*, 2017), and linked to regeneration of nitrogen from DOM (Christie-Oleza *et al.*, 2017). Furthermore, amino acid use by natural bacterial assemblages coincides with ammonia excretion under conditions when amino acids are the major sources of nitrogen for growth (Kirchman *et al.*, 1989) or under carbon limiting conditions (Goldman *et al.*, 1987; Goldman & Dennett, 1991), although simultaneous ammonia uptake by bacteria was measured in some systems (Tupas & Koike, 1990; Tupas *et al.*, 1994). The C:N ratio of dissolved organic matter in cyanobacterial blooms can be within the range that favors ammonia regeneration from amino acids in marine systems (Ye *et al.*, 2011; Lehman *et al.*, 2015), and ammonium uptake can outpace regeneration in eutrophic systems, including *Microcystis* blooms (Gardner *et al.*, 2017). Thus, conditions during *Microcystis* blooms can favor bacterial amino acid uptake or deamination and subsequent ammonium regeneration. Cultivation of freshwater Acidobacteria along with measurements of amino acid fluxes and demand in natural microbial communities is required to fully constrain the importance of peptide degradation and amino acid efflux by Acidobacteria on phytoplankton growth *in situ*.

4.4.5 Evidence for Vitamin B_{12} Auxotrophy and Uptake

The gene annotation and expression data of both Acidobacteria genomes suggest that both organisms are auxotrophs of vitamin B_{12}. There are many variants of vitamin B_{12} that differ in the chemical groups that make up the upper and lower axial ligands (Banerjee & Ragsdale, 2003; Helliwell *et al.*, 2016). Some B_{12}-dependent enzymes are involved in critical cellular

functions such as methionine and nucleotide synthesis (Banerjee & Ragsdale, 2003), thus B_{12} availability is important for growth of organisms with these enzymes. Organisms that lack genes for cobalamin biosynthesis must obtain B_{12} released into the environment by B_{12}-producing organisms (Croft *et al.*, 2005; Helliwell *et al.*, 2016). Both Acidobacteria lack the entire pathway for biosynthesis of the corrin ring structure of vitamin B_{12}s, and the *Bryobacter* genome expressed genes annotated as cobalamin transporters (Figure 4.3A); however, the Acidobacteria CoA2 C42 MAG lacked genes annotated as cobalamin transporters. Expression of genes encoding TonB-family proteins, required to energize the membrane for cobalamin transport (Bassford *et al.*, 1976; Reynolds *et al.*, 1980), were also detected in both genomes and were among the most highly expressed membrane associated proteins in Acidobacteria CoA2 C42 (Figure S 4.6). In addition, the expression of the B_{12}-dependent enzymes *nrdJ*, encoding a class II ribonucleotide reductase, and *metH*, encoding methionine synthase, was detected in *Bryobacter* (Figure 4.3B). *Bryobacter* lacks B_{12}-independent alternatives to *nrdJ*, which suggests that B_{12} is a requirement for this organism. Acidobacteria CoA2 C42 uses B_{12}-independent alternatives to *nrdJ*, *nrdA* and *nrdB* (Supplemental Datafile 1). However, Acidobacteria CoA2 C42 expressed *metH* despite having the B_{12}-independent version *metE*, for which no expression was detected (Table 4.3). Together, this suggests that both Acidobacteria cannot synthesize vitamin B_{12}s *de novo*, were actively transporting B_{12} from the water column into the cell, and were producing B_{12}-dependent enzymes during the cyanobacteria bloom.

We detected expression of genes involved in remodeling cobalamin axial ligands in both Acidobacteria genomes. Mechanisms to remodel B_{12} are necessary for microbes to convert the various exogenous B_{12} forms into the correct chemical forms needed for growth (Anderson *et al.*, 2008; Helliwell *et al.*, 2016; Ma *et al.*, 2019) because most microbial taxa exclusively use

specific lower axial ligand variants of vitamin B_{12} (Stupperich & Kräutler, 1988; Helliwell *et al.*, 2016; Heal *et al.*, 2017). Genes for attaching an adenosyl group to the upper ligand were present in both genomes (Figure 4.3C, Table 4.3), but we only found genes for remodeling the lower axial ligand in the *Bryobacter* genome (Figure 4.3C). The absence of remodeling genes together with the presence of B_{12}-independent nucleotide synthesis enzymes and lack of annotated cobalamin transporters may indicate that Acidobacterium CoA2 C42 is not reliant on vitamin B_{12} for growth to the same extent as *Bryobacter.*

Several lines of evidence suggest that *Bryobacter* CoA8 C33 obtains pseudocobalamin from cyanobacteria, including *Microcystis*. *Bryobacter* CoA8 C33 expresses genes that are involved in cobalamin remodeling (Figure 4.3B), expresses genes that require vitamin B_{12} for nucleotide and methionine synthesis (Figure 4.3C), and amplicon sequences classified as *Bryobacter* were identified in *Microcystis* phycosphere communities (Table 3.3). Furthermore, we identified pseudocobalamin in axenic cultures of *Microcystis aeruginosa* PCC 7806 and PCC 9806 (Figure 4.4). This confirms that *Microcystis* produces pseudocobalamin for growth, as do other cyanobacteria (Bonnet *et al.*, 2010; Helliwell *et al.*, 2016), which contrasts previous studies that suggested *Microcystis* could not synthesize pseudocobalamin based on the absence of a few genes in B_{12} biosynthesis pathway annotations from MAG sequences (Xie *et al.*, 2016; Cook *et al.*, 2020). Therefore, *Microcystis* could be a potential source of B_{12} for *Bryobacter* CoA8 C33. However, it is unclear from our data which chemical forms are required by *Bryobacter* CoA8 C33, and by extension which organisms *Bryobacter* CoA8 C33 rely on for vitamin B_{12}. Pseudocobalamin (lower axial ligand is adenosine) is produced by cyanobacteria (Helliwell *et al.*, 2016; Heal *et al.*, 2017) and some *Lactobacillus* (Santos *et al.*, 2007) and methanogenic bacteria (Stupperich & Kräutler, 1988) while cobalamin (the lower axial ligand is 5,6-

dimethylbenzimidazol [DMB]) is produced by Thaumarchaeota and some proteobacteria (Heal *et al.*, 2017), and used by most eukaryotic phytoplankton (Helliwell *et al.*, 2016; Heal *et al.*, 2017). *Bryobacter* CoA8 C33 lacks the ability to synthesize the nucleotide DMB required for the axial ligand of cobalamin, which may indicate that *Bryobacter* CoA8 C33 uses pseudocobalamin and derives pseudocobalamin from cyanobacterial cell lysis or excretion (Bonnet *et al.*, 2010). However, other organisms that lack DMB synthesis pathways in fact use cobalamin, and can remodel other B_{12} vitamins in the presence of an exogenous source of DMB (Anderson *et al.*, 2008). Therefore, we cannot rule out that the Acidobacteria either directly uptake cobalamin from other sources, or convert pseudocobalamin into cobalamin using DMB derived from other phycosphere bacteria. Regardless, our data support the idea that freshwater *Bryobacter* spp. rely on other microorganisms to meet vitamin B_{12} demands.

4.4.6 Presence and Relative Abundance in Amplicon Datasets

To determine if these Acidobacteria regularly occur in, or are specific to, *Microcystis*-dominated blooms, we measured their abundance in published 16S rRNA amplicon datasets spanning a range of freshwater systems where *Microcystis*-dominated blooms occur (Table 4.1, see methods). Amplicon sequences with high percent similarity (97 %) to variable regions of the 16S rRNA sequences in both Acidobacteria MAGs were present at low relative abundance in western Lake Erie (*Bryobacter* mean 0.072 %, range 0-1.41 %; Acidobacterium CoA2 C42 mean 0.13 %, range 0-0.69 %) and other systems (*Bryobacter* mean 0.006 %, range 0-0.40 %; Acidobacterium CoA2 C42 mean 0.048 %, range 0-0.72 %). There was a weak but significant, positive relationship between the relative abundance of both Acidobacteria taxa and *Microcystis* relative abundance in western Lake Erie cyanobacterial blooms (Figures 4.5A & 4.5B). In other freshwater systems, there was also a significant, positive correlation between *Bryobacter* relative

abundance and *Microcystis* relative abundance (Figure 4.5C). In contrast, Acidobacterium CoA2 C42 had a significant negative correlation in the other datasets, however the correlation was weak (Figure 4.5D), indicating that while it can co-occur with *Microcystis* blooms, it is a generalist that also occurs in freshwater systems when and where *Microcystis* is absent. *Bryobacter* amplicon sequences were also present in some freshwater datasets when *Microcystis* relative abundance was low, indicating that a few species or strains may also occur outside *Microcystis* blooms. However, *Bryobacter* relative abundance in these samples was typically low, averaging at 0.001 % in samples where *Microcystis* relative abundance was below 1 %. The weak positive correlation between *Microcystis* and *Bryobacter* in Lake Erie and other lakes suggests that *Bryobacter* often associates with *Microcystis* during cyanobacterial blooms, although the interaction is not conserved across all bloom periods and locations. Both Acidobacteria could also be absent while *Microcystis* was present at high abundance, suggesting that while both may occur in *Microcystis* blooms, they are not consistently present in *Microcystis* bloom communities. *Bryobacter* spp. were previously found to be correlated with specific *Microcystis* genotypes (Chun *et al.*, 2020), which could suggest that *Bryobacter* associates with only some *Microcystis* strains.

We assessed the abundance of both Acidobacteria groups in particle-attached microbial communities of various sizes, which may indicate a physical association with phytoplankton, including *Microcystis,* which grow in large, buoyant colonies (Zhu *et al.*, 2014). The relative abundance of both *Bryobacter* and Acidobacteria CoA2 C42 amplicons were enriched in particle-attached communities (> 100 µm retentate samples) during the 2014 western Lake Erie *Microcystis* bloom (Figure 4.6). Similarly, although it was only present in August and September, *Bryobacter* was associated with the size fraction that contained the majority of

Microcystis in Lake Taihu, but absent from smaller particles and free-living communities (Figure 4.7). In contrast, Acidobacterium CoA2 C42 was absent from large aggregates and present in smaller particles and free-living communities in Lake Taihu (Figure 4.7), which is in contrast with the results from Lake Erie (Figure 4.6). *Bryobacter* was also absent from free-living communities throughout the Great Lakes, while Acidobacterium CoA2 C42 was present (Figure S 4.8). A previous study identified *Bryobacter* in ~25 % of *Microcystis* colonies sampled, while other Acidobacteria largely were absent (Table 3.3), and another study found that *Bryobacter* relative abundance was significantly correlated with the relative abundance of certain *Microcystis* genotypes (Chun *et al.*, 2020). Together with the relationships between Acidobacteria percent abundance and *Microcystis* percent abundance (Figure 4.5), this suggests that *Bryobacter* is present in some *Microcystis* blooms when conditions are favorable and physically attaches to *Microcystis* colonies, while Acidobacterium CoA2 C42 facultatively colonizes other particles and is not specifically associated with *Microcystis* blooms.

4.5 Conclusions

The abundance patterns and putative metabolic exchanges identified here suggest that *Bryobacter* and Acidobacterium CoA2 C42 interact with phytoplankton as members of phycosphere communities and may influence phytoplankton physiology. Metatranscriptomic evidence suggests that both bacteria play a role in the regeneration of reduced N which can fuel phytoplankton growth, including certain *Microcystis* strains (Davis *et al.*, 2010; Chaffin *et al.*, 2018; Newell *et al.*, 2019). While both organisms were detected in *Microcystis* blooms, only *Bryobacter* was found directly associated with *Microcystis* colonies. Conversely, while it occurs in *Microcystis* blooms, Acidobacterium CoA2 C42 is not physically associated with *Microcystis* but may be associated with other phytoplankton groups. However, we cannot rule out that

Acidobacterium CoA2 C42 instead attaches to abiotic or detrital particles, a common trait of Acidobacteria (Dedysh & Damsté, 2018), so its involvement in phycosphere interactions is uncertain. Future studies are needed to determine which particle types Acidobacterium CoA2 C42 physically associates with. In addition, the cultivation of novel, uncultivated freshwater Acidobacteria and co-culture experiments with phytoplankton, including *Microcystis*, are required to confirm if the inferred metabolite exchanges between Acidobacteria and phytoplankton occur, are a result of mutualistic growth or decomposition of lysed phytoplankton cells, and to characterize their impacts on *Microcystis* growth.

4.6 Figures and Tables

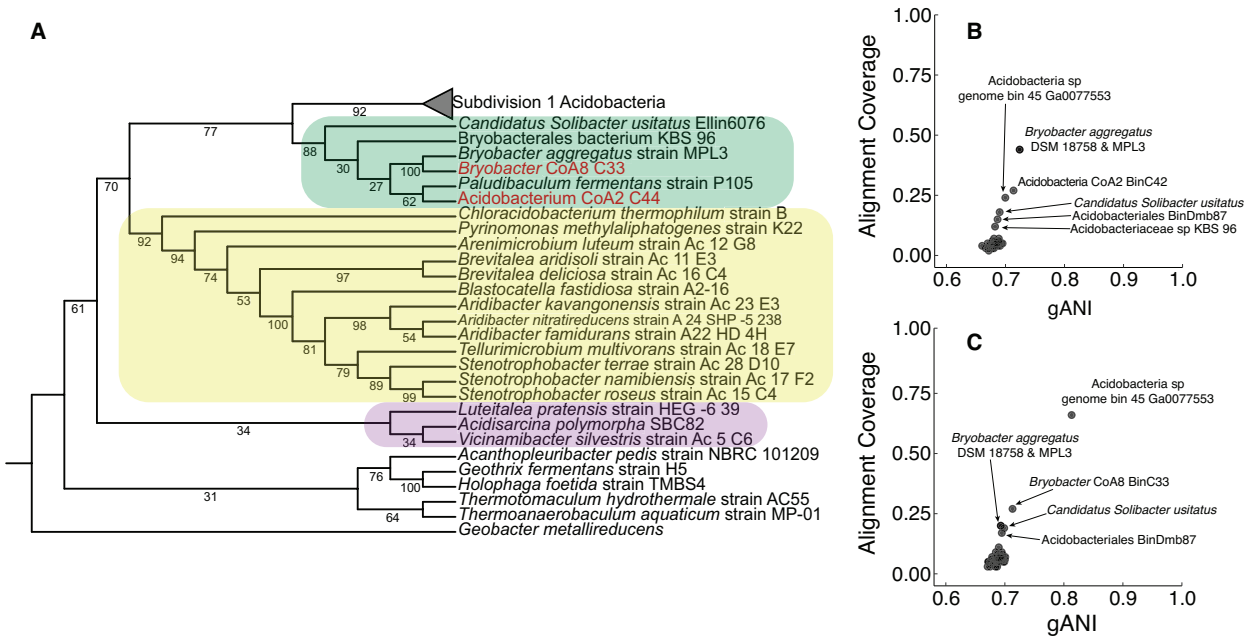

Figure 4.1: Taxonomic assignment of novel Acidobacteria MAGs based on 16S rRNA phylogeny and whole genome alignments (gANI). **A**: Maximum likelihood tree of published, full-length Acidobacteria 16S rRNA gene sequences. The tree is rooted with the sequence from the Deltaproteobacterium *Geobacter metallireducens*. Branch labels show bootstrap support (n = 2000). Branch lengths have no information. Subdivision 3 Acidobacteria are highlighted in green, subdivision 4 Acidobacteria are highlighted in gold, and subdivision 6 Acidobacteria are highlighted in. The leaf labels for the 16S rRNA sequences from the Lake Erie MAGs are

colored red. **B and C**: gANI comparisons of *Bryobacter* CoA8 C33 (B) and Acidobacteria CoA2 C42 (C) with published, high-quality Acidobacteria genomes in IMG (n = 63).

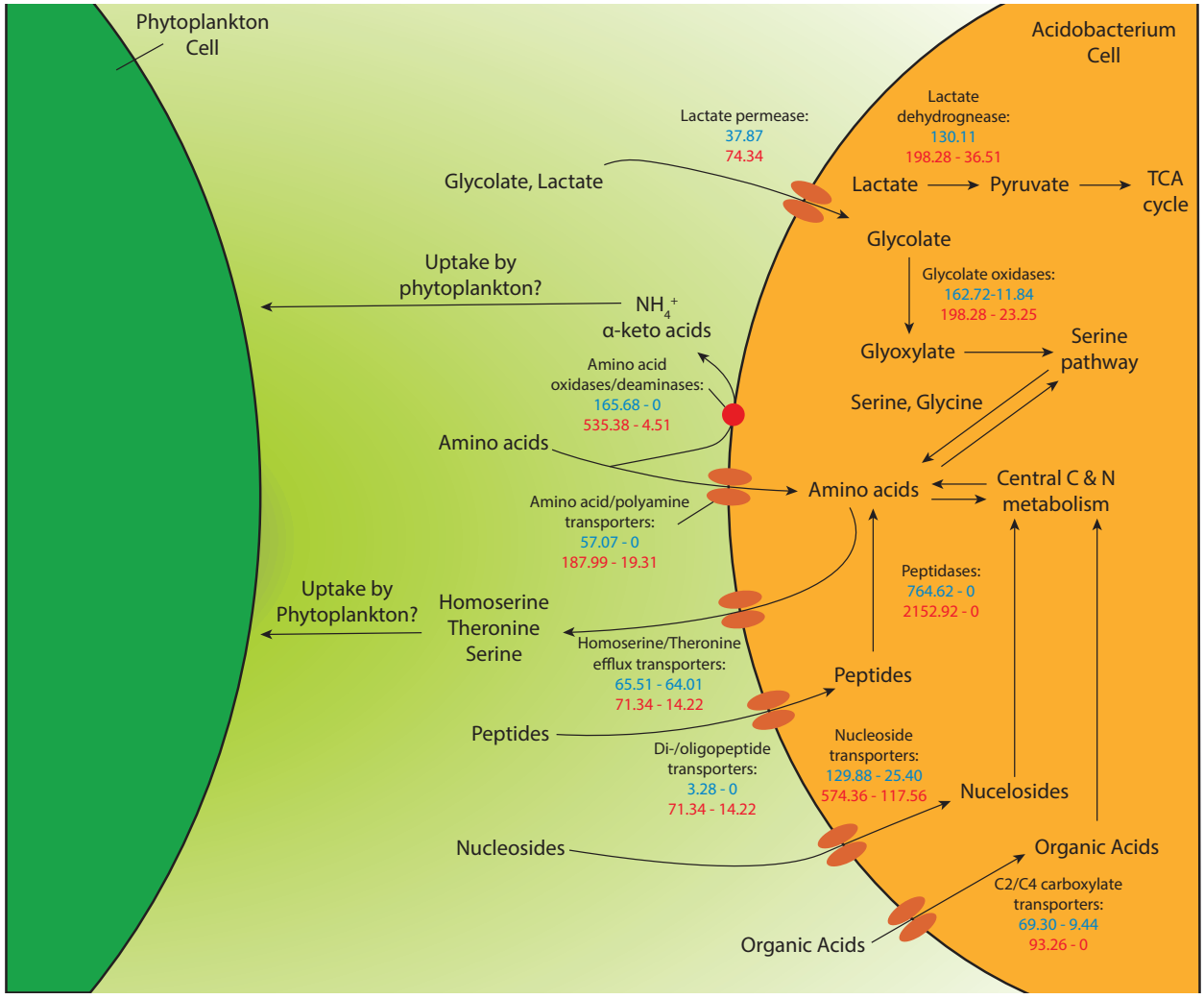

Figure 4.2: Relative abundance of low molecular weight organic carbon transporters and enzymes related to their metabolism by *Bryobacter* CoA8 C33 (blue) and Acidobacterium CoA2 C42 (red) associated with phytoplankton seston in the August 4th metatranscriptome from nearshore western Lake Erie station WE12. Relative abundance is expressed as reads mapped per kb of gene per million reads mapped to the respective genome (RPKM). A range of RPKM values indicates that multiple genes were predicted to drive the indicated reactions, and only maximum and minimum RPKM values are shown.

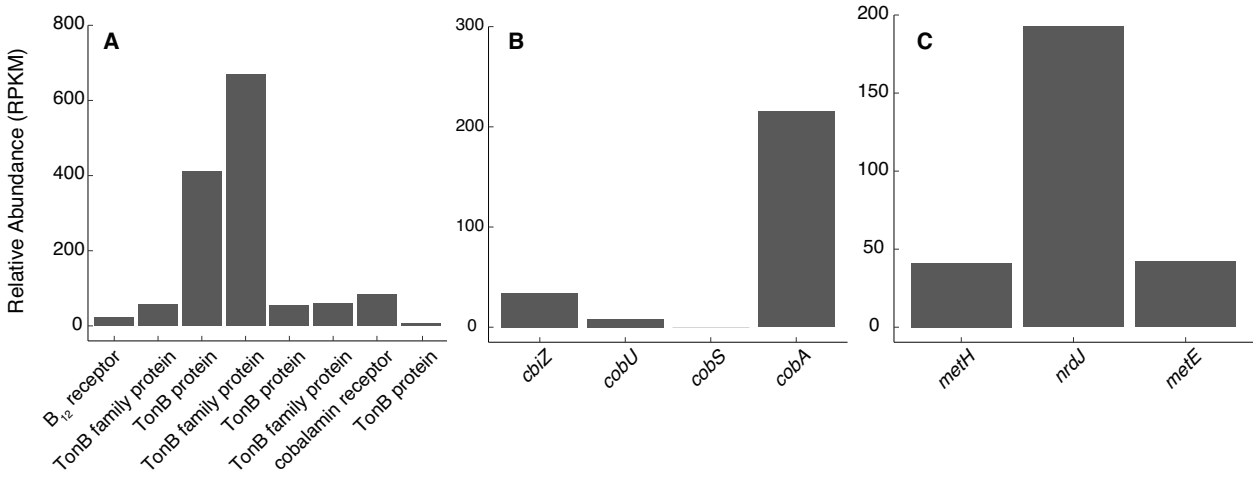

Figure 4.3: Relative abundance of transcripts from *Bryobacter* CoA8 C33 genes involved in cobalamin transport (A), cobalamin remodeling (B), and cobalamin-dependent genes and their independent counterparts (C) in the August 4th metatranscriptome from western Lake Erie nearshore station WE12. Relative abundance is expressed as reads mapped per kbp of gene per million reads mapped to the genome (RPKM).

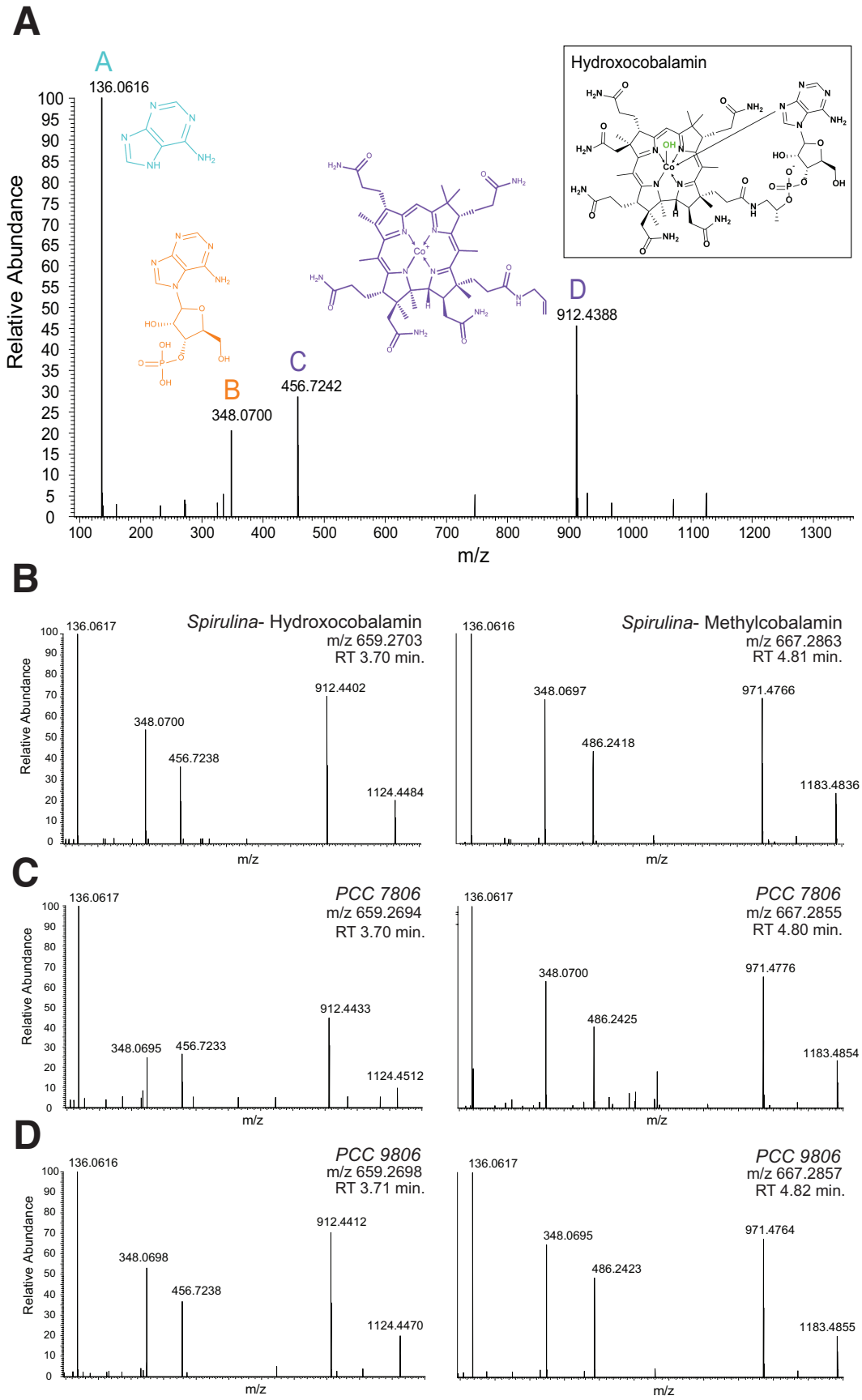
A
A
136.0616
B
348.0700
C
456.7242
D
912.4388
Hydroxocobalamin
Relative Abundance
m/z
B
Spirulina- Hydroxocobalamin
m/z 659.2703
RT 3.70 min.
136.0617
348.0700
456.7238
912.4402
1124.4484
Spirulina- Methylcobalamin
m/z 667.2863
RT 4.81 min.
136.0616
348.0697
486.2418
971.4766
1183.4836
C
PCC 7806
m/z 659.2694
RT 3.70 min.
136.0617
348.0695
456.7233
912.4433
1124.4512
PCC 7806
m/z 667.2855
RT 4.80 min.
136.0617
348.0700
486.2425
971.4776
1183.4854
D
PCC 9806
m/z 659.2698
RT 3.71 min.
136.0616
348.0698
456.7238
912.4412
1124.4470
PCC 9806
m/z 667.2857
RT 4.82 min.
136.0617
348.0695
486.2423
971.4764
1183.4855

Figure 4.4: MS2 spectra of pseudocobalamin forms in *Microcystis* cultures and *Spirulina* powder, which served as a positive control. **6A:** Detailed mass spectrum of hydroxopseudocobalamin from *Microcystis aeruginosa* PCC 7806 with the chemical structures for each fragment associated with the mass peaks (colored) and for the entire molecule (black box). **6B:** Mass spectra of hydroxopseudocobalamin and methylpseudocobalamin detected in *Spirulina* powder. **6C:** Mass spectra of hydroxopseudocobalamin and methylpseudocobalamin detected in *Microcystis aeruginosa* PCC 7806. **6D:** Mass spectra of hydroxopseudocobalamin and methylpseudocobalamin detected in *Microcystis aeruginosa* PCC 9806.

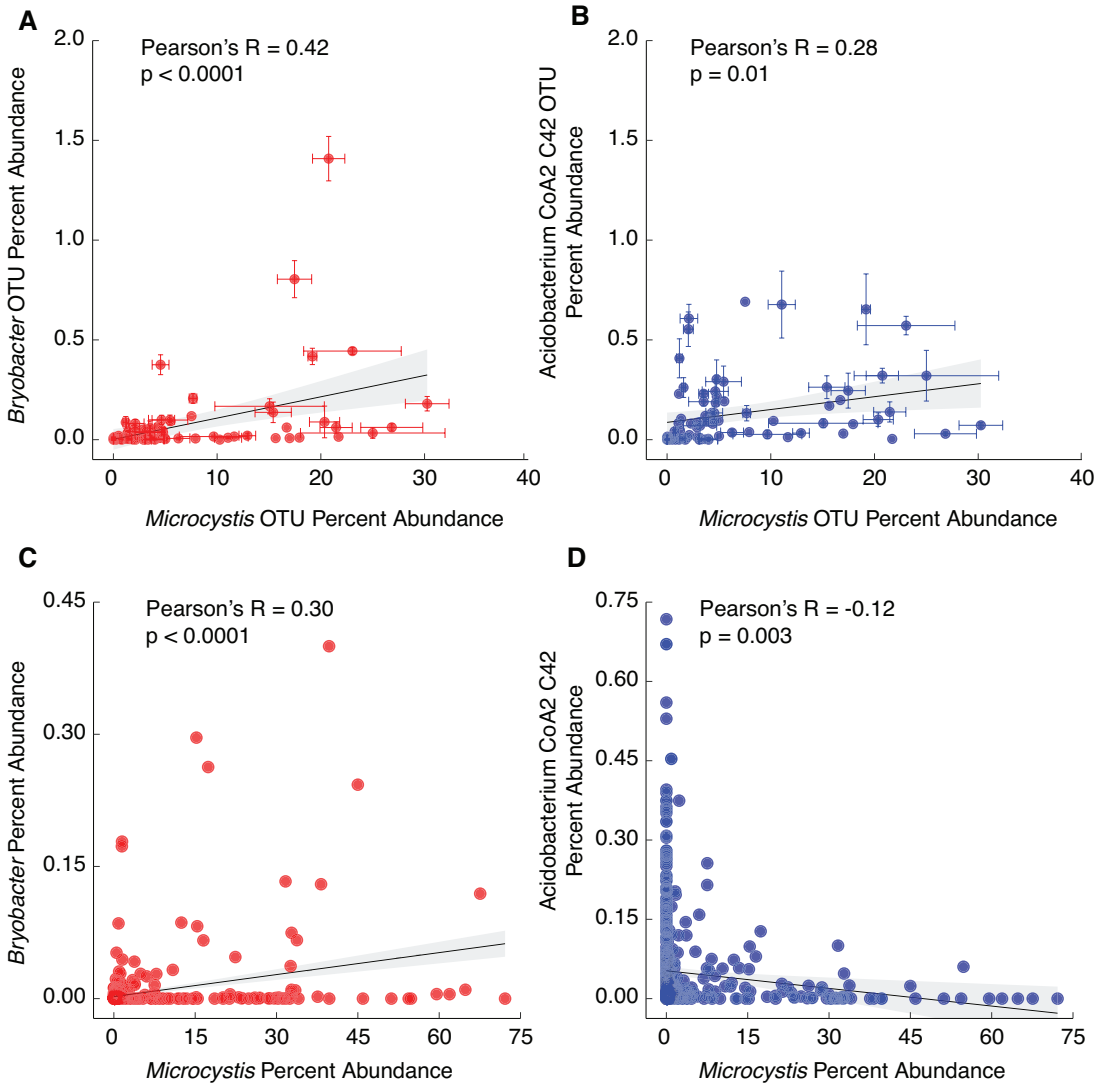

Figure 4.5: Percent abundance of *Bryobacter* and Acidobacterium CoA2 C42 as a function of Microcystis percent abundance in whole water microbial community rRNA amplicon datasets from freshwaters. **A:** *Bryobacter* OTU percent abundance vs. *Microcystis* OTU percent abundance in V4 16S rRNA amplicon datasets collected during western Lake Erie cyanobacterial blooms. **B:** Acidobacterium CoA2 C42 OTU percent abundance vs. *Microcystis* OTU percent abundance in V4 16S rRNA amplicon datasets collected during western Lake Erie cyanobacterial

blooms. **C:** The percent abundance of reads in published amplicon datasets that mapped to the 16S rRNA gene from the *Bryobacter* CoA8 C33 MAG vs. the percent abundance of amplicon reads that mapped to 16S rRNA from *Microcystis*. **D:** The percent abundance of reads in published amplicon datasets that mapped to the 16S rRNA gene from the Acidobacterium CoA2 C42 MAG vs. the percent abundance of amplicon reads that mapped to 16S rRNA from *Microcystis*. In all panels, the shaded area around the regression line indicates the regression standard error, error bars show the 95% confidence intervals determined from replicate filters (n = 4 or 8), and p-values show the significance of the regression slope calculated with an F-test.

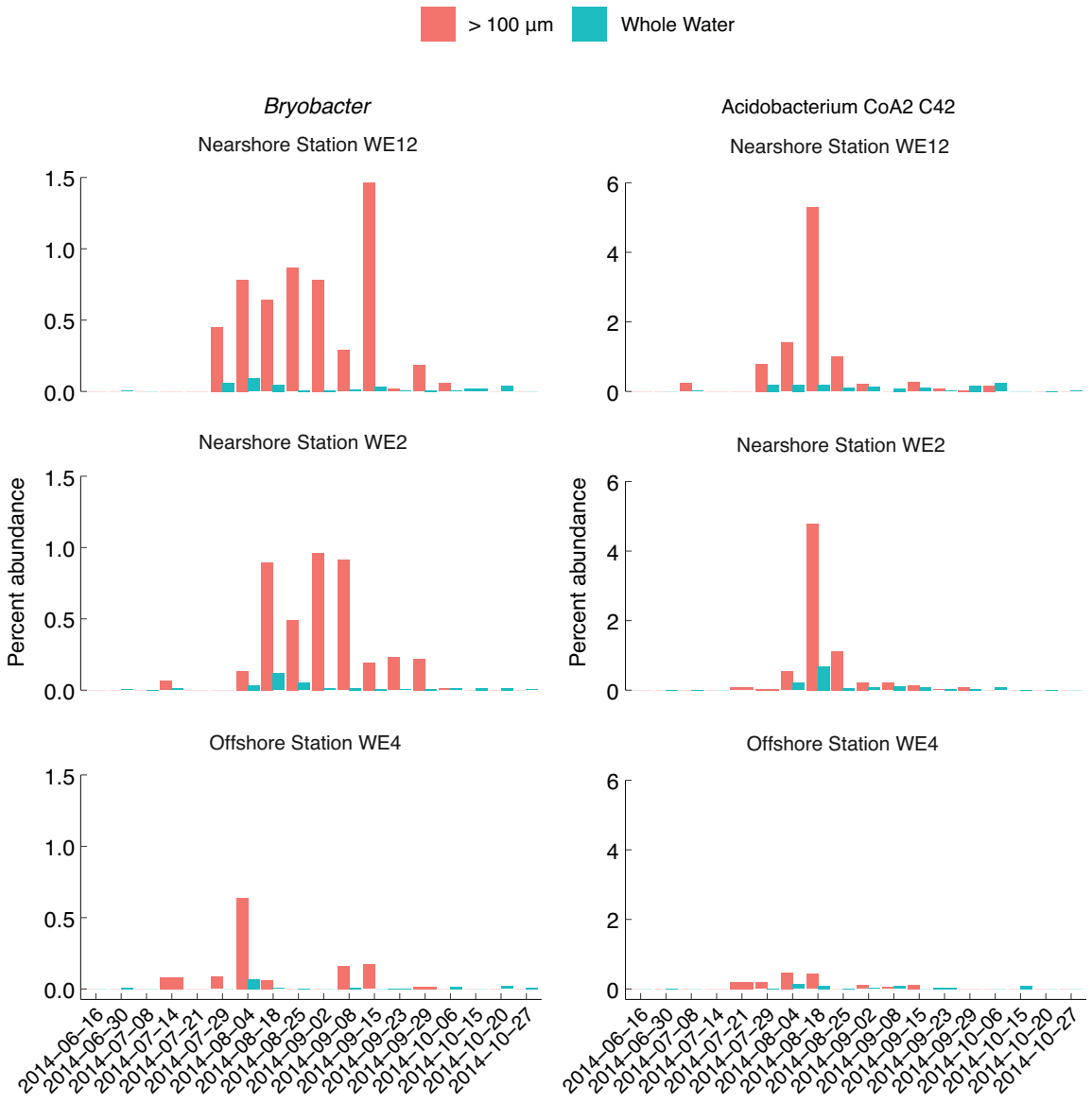

Figure 4.6: Percent abundance of *Bryobacter* and Acidobacterium CoA2 C42 OTUs in size fractionated samples from a western Lake Erie time series collected in the summer-fall of 2014. Bar colors depict size fraction.

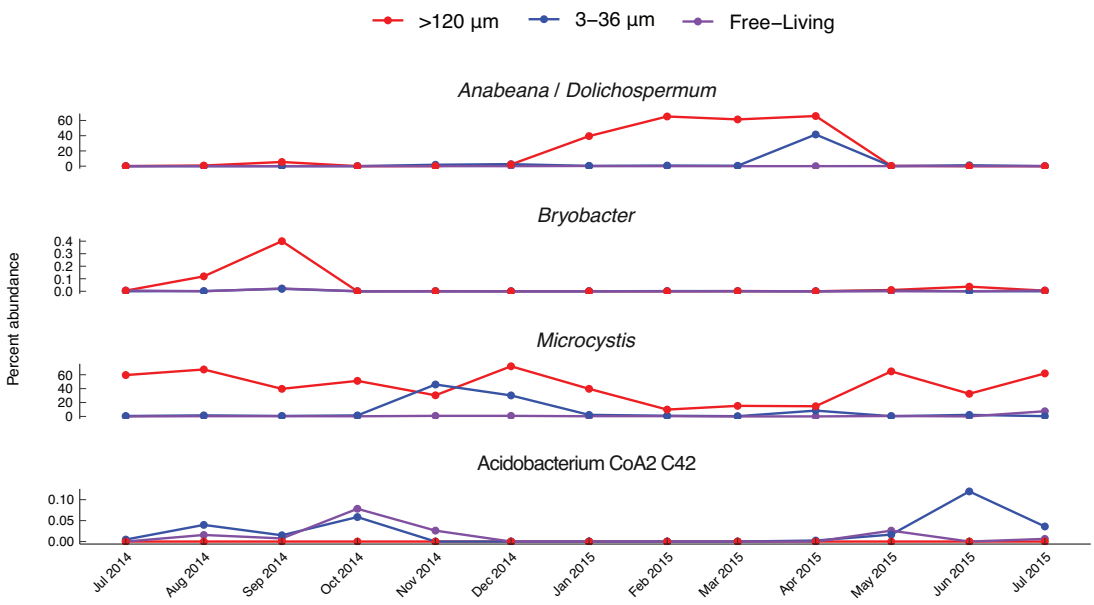

Figure 4.7: Percent abundance of Acidobacteria of interest and major Cyanobacteria taxa, *Anabaena* / *Dolichospermum* and *Microcystis* in size fractionated samples from a time series of Lake Taihu cyanobacterial blooms.

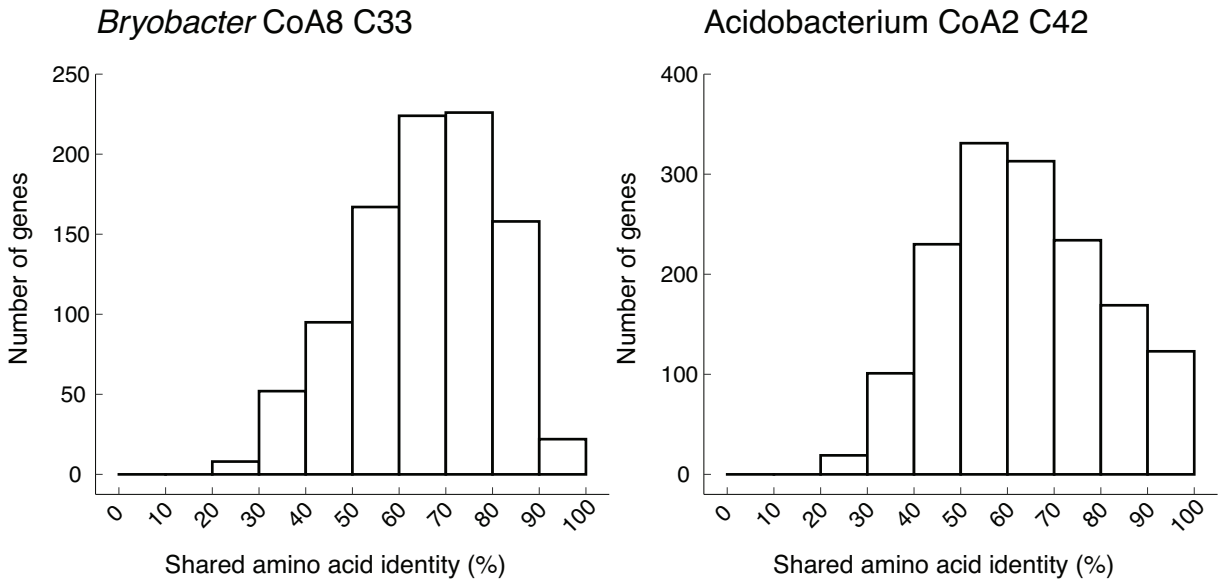

Figure S 4.1: Histogram of shared amino acid identity between protein coding genes in Acidobacteria MAGs and NCBI non-redundant database.

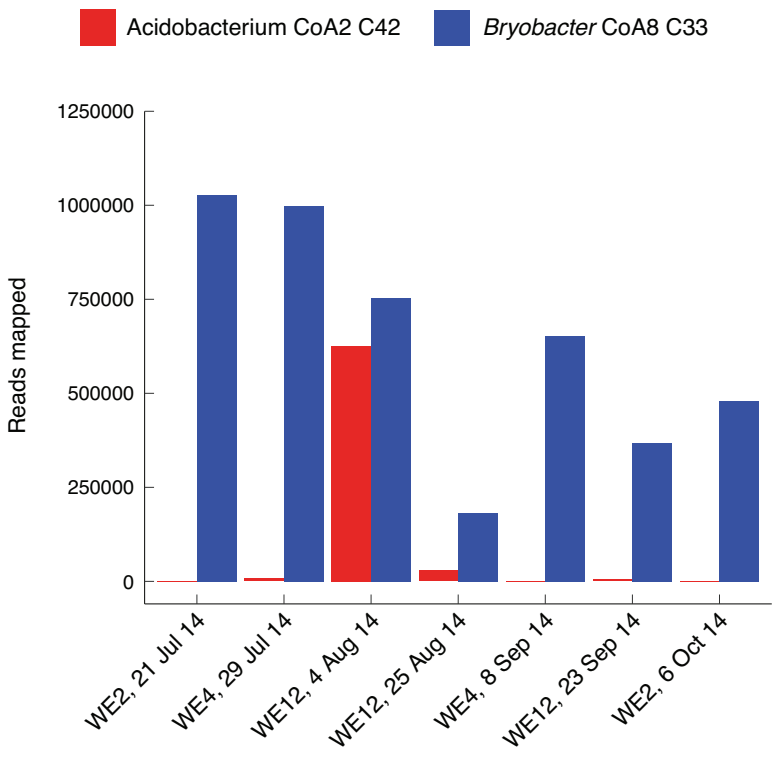

Figure S 4.2: Total number of metatranscriptomic reads mapped to each Acidobacterium MAG.

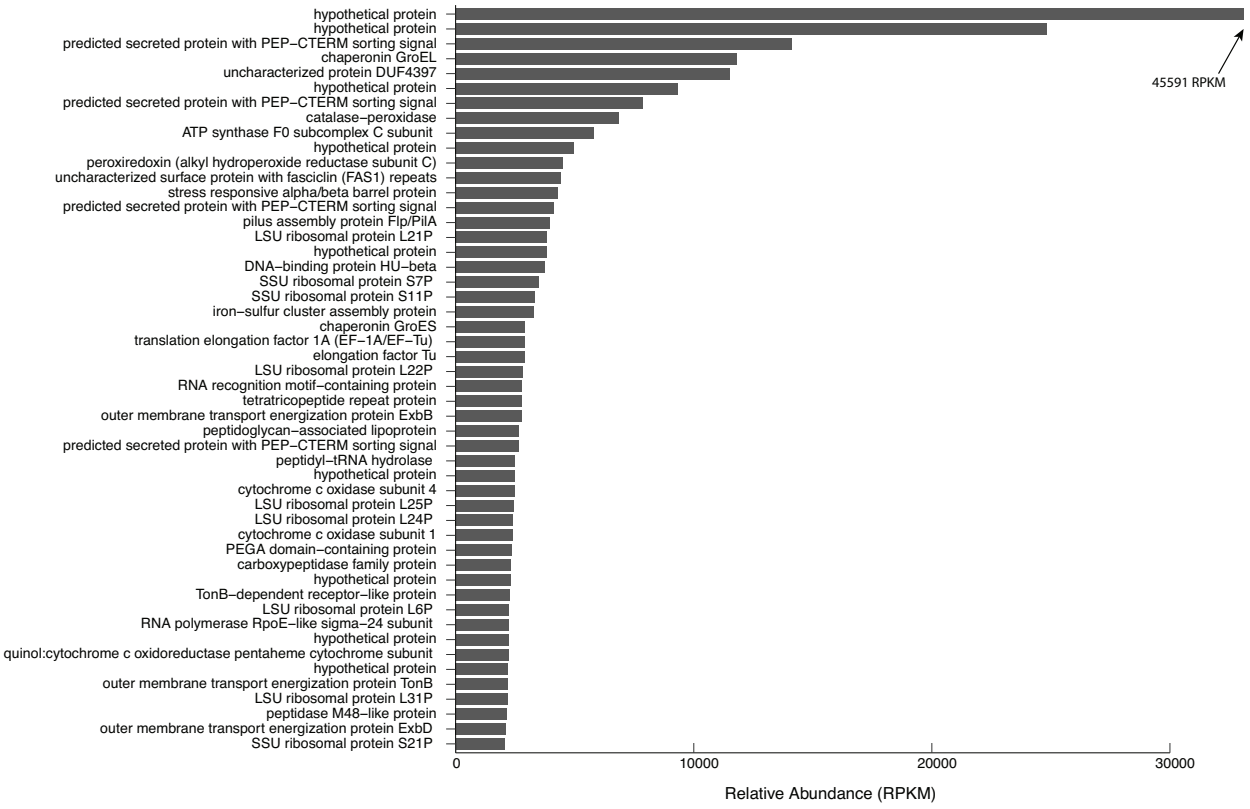

Figure S 4.3: Ranked relative abundance plot of top 50 most abundant genes from the Acidobacterium CoA2 C42 MAG in the 2014 western Lake Erie metatranscriptome collected from > 100 µm size fraction during August phycocyanin peaks (nearshore station WE12, August 4th). Relative abundance was calculated by normalizing to gene length (kbp) and total reads mapped to all genes in the Acidobacterium CoA2 C42 MAG.

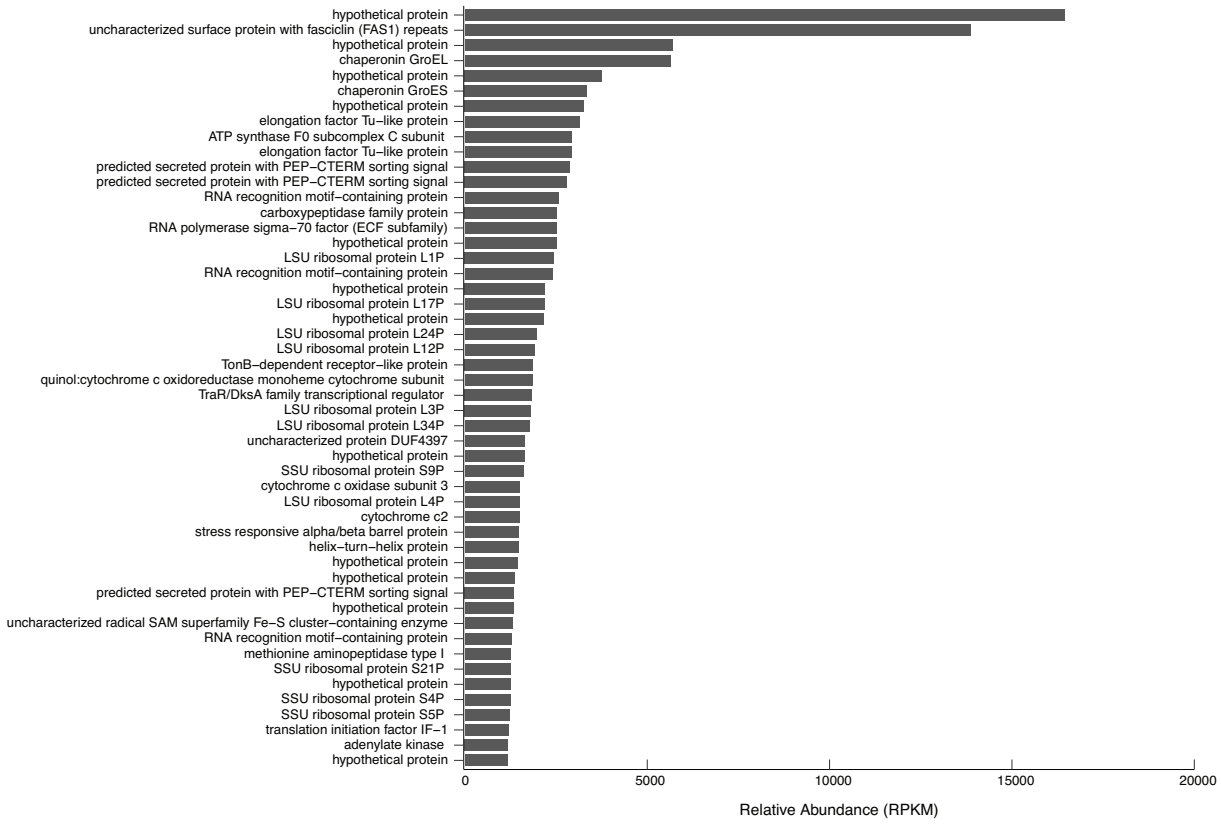

Figure S 4.4: Ranked relative abundance plot of top 50 most abundant genes from the *Bryobacter* CoA8 C33 MAG in the 2014 western Lake Erie metatranscriptome collected from > 100 µm size fraction during August phycocyanin peaks (nearshore station WE12, August 4th). Relative abundance was calculated by normalizing to gene length (kbp) and total reads mapped to all genes in the *Bryobacter* MAG.

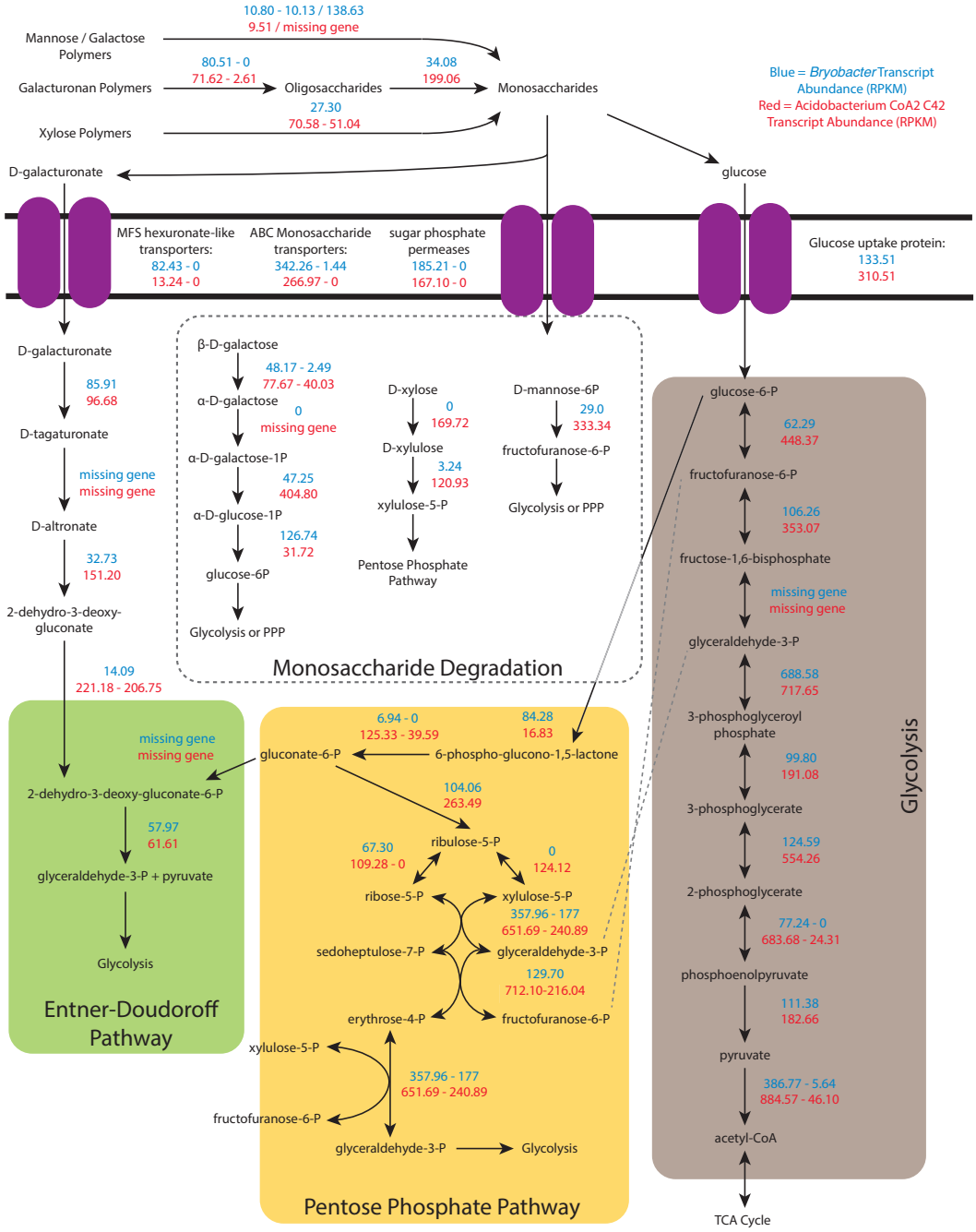

Figure S 4.5: Putative central carbon metabolism and sugar degradation pathways in *Bryobacter* CoA8 C33 and Acidobacterium CoA2 C42. Blue values indicate the relative transcript abundance of the gene from *Bryobacter* CoA8 C33. Red values indicate the relative transcript abundance of the gene from Acidobacterium CoA2 C42. A range of values show the highest and lowest relative abundance values when multiple gene copies are present. Relative abundance was calculated by normalizing to gene length (kbp) and total reads mapped to all genes in each respective genome (RPKM).

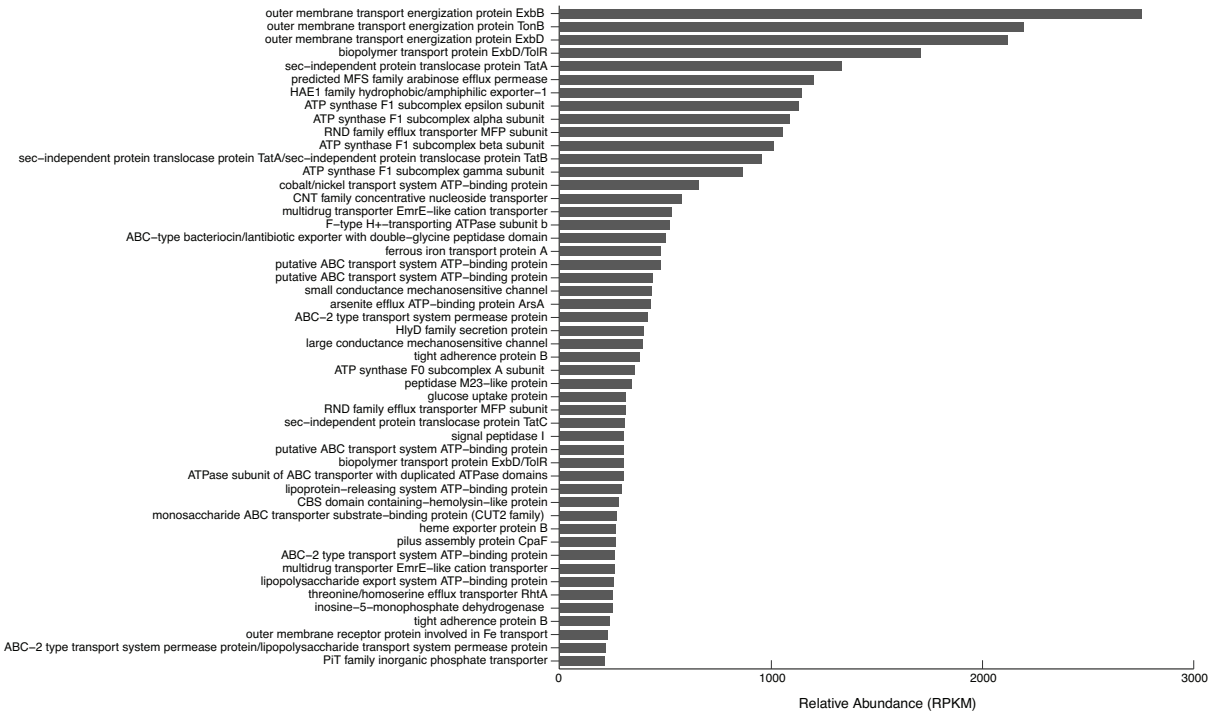

Figure S 4.6: Ranked relative abundance plot of top 50 most abundant genes encoding transporters from the Acidobacterium CoA2 C42 MAG in the 2014 western Lake Erie metatranscriptome collected from > 100 µm size fraction during August phycocyanin peaks (nearshore station WE12, August 4th). Relative abundance was calculated by normalizing to gene length (kbp) and total reads mapped to all genes in the Acidobacterium CoA2 C42 MAG.

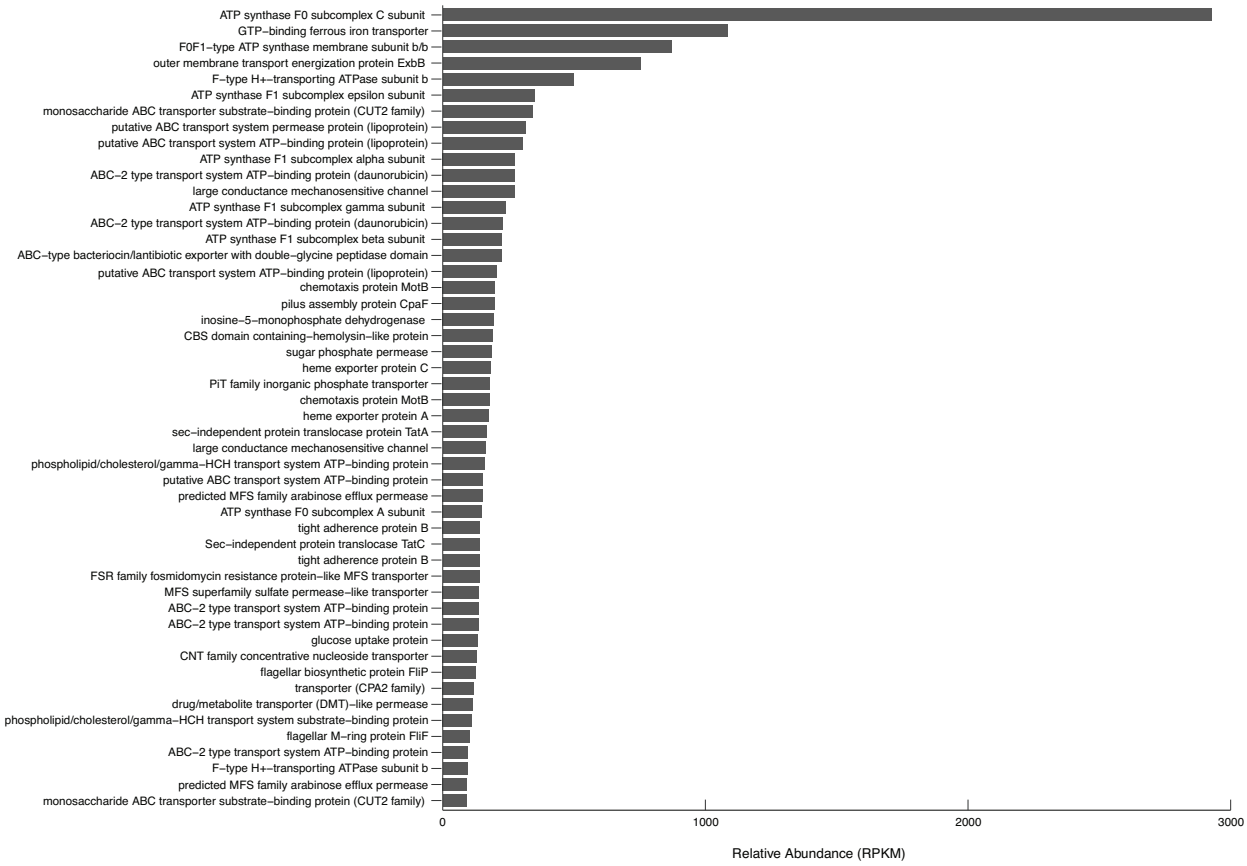

Figure S 4.7: Ranked relative abundance plot of top 50 most abundant genes encoding transporters from the *Bryobacter* CoA8 C33 MAG in the 2014 western Lake Erie metatranscriptome collected from > 100 µm size fraction during August phycocyanin peaks (nearshore station WE12, August 4th). Relative abundance was calculated by normalizing to gene length (kbp) and total reads mapped to all genes in the *Bryobacter* MAG.

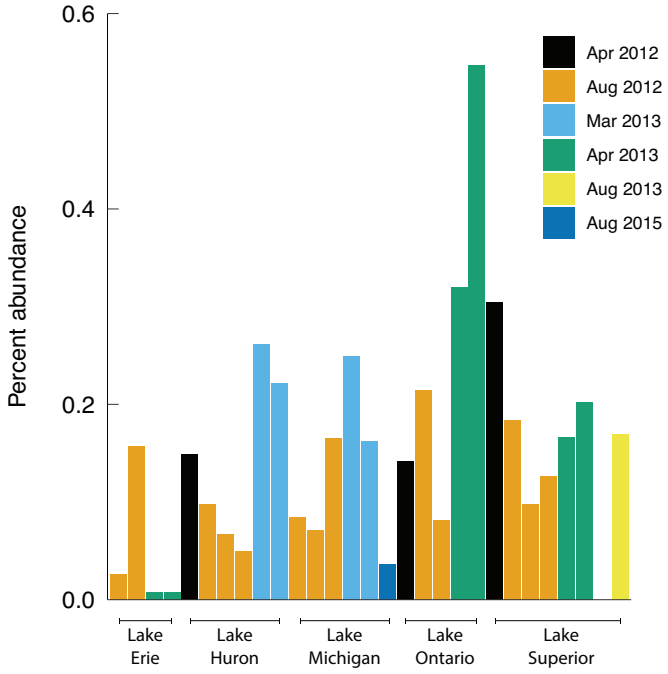

Figure S 4.8: Percent abundance of Acidobacterium CoA2 C42 in free-living microbial communities in the Great Lakes. Bar color depicts sampling date. *Bryobacter* was not detected in these samples.

Table 4.1: Description of public datasets mined for Acidobacteria 16S rRNA sequences in this study.

NCBI Accession	Location and Sampling Scheme	Material Type	Size Fraction(s)	Reference
PRJNA575023	discrete sampling of eutrophic lakes around the globe	bulk phytoplankton seston dominated by *Microcystis*	> 100 µm	Cook et al. 2020
PRJNA386411	Lake Taihu, China time series	size fractionated communities	>120 µm, 3-36 µm, 0.2-3 µm	Shi et al. 2018
PRJNA591360	transects across the Laurentian Great Lakes in spring and summer	free-living communities	0.22-1.6 µm	Paver et al. 2020

PRJNA479553	monthly sampling of Nakdong River, South Korea	whole water communities	>0.22 µm	Chun et al. 2019
SRA211417	transect across the Laurentian Great Lakes	whole water communities	>0.22 µm	Rozmarynowycz et al. 2019
PRJNA353865	Lake Champlain, Canada time series	whole water communities	>0.22 µm	Tromas et al. 2017
PRJEB14911	Lake Mendota, USA time series	whole water communities	>0.22 µm	Kara et al. 2012

Table 4.2: Quality information for Acidobacteria MAGs from western Lake Erie cyanobacterial blooms.

BinID	Genus	Complete-ness (%)	Contam-ination (%)	GC %	Size (Mbp)	N50	Gene #	16S #	23S #	tRNA #
CoA8_C33	*Bryobacter*	98.21	0.87	60.89	5.053647	7548	4488	1	1	47
CoA2_C42	unclassified	98.70	2.17	64.93	6.067278	38916	5163	1	1	47

Table 4.3: Expression of B_{12} dependent genes in Acidobacteria CoA2 C42 MAG.

Gene	Kegg number	KO	IMG annotation	gene symbol	4-Aug transcript abundance nearshore (RPKM)	Gene
2806999884	2.1.1.13	K00548	methionine synthase (B12-dependent)	*metH*	216.8002	2806999884
2807002171	2.1.1.14	K00549	5-methyltetrahydropteroyltriglutamate--homocysteine methyltransferase	*metE*	0	2807002171
2807000579	2.5.1.17	K00798	cob(I)alamin adenosyltransferase	*cobA, pduO*	93.77295	2807000579

4.7 References

Allen, M. M., & Stanier, R. Y. (1968). Selective isolation of blue-green algae from water and soil. *Microbiology, 51*(2): 203-209.

Altschul, S. F., Gish, W., Miller, W., Myers, E. W., & Lipman, D. J. (1990). Basic local alignment search tool. *J Mol Biol, 215*(3): 403-410.

Amin, S. A., Green, D. H., Hart, M. C., Krüpper, F. C., Sunda, W. G., & Carrano, C. J. (2009). Photolysis of iron-siderophore chelates promotes bacterial-algal mutualism. *Proc Natl Acad Sci, 106*(40): 17071-17076. doi:10.1073 pnas.0905512106

Amin, S. A., Hmelo, L. R., van Tol, H. M., Durham, B. P., Carlson, L. T., Heal, K. R. *et al.* (2015). Interaction and signalling between a cosmopolitan phytoplankton and associated bacteria. *Nature, 522*(7554): 98-101. doi:10.1038/nature14488

Anantharaman, K., Brown, C. T., Hug, L. A., Sharon, I., Castelle, C. J., Probst, A. J. *et al.* (2016). Thousands of microbial genomes shed light on interconnected biogeochemical processes in an aquifer system. *Nat Comm, 7*(13219): 1-11.

Anderson, P. J., Lango, J., Carkeet, C., Britten, A., Kräutler, B., Hammock, B. D., & Roth, J. R. (2008). One pathway can incorporate either adenine or dimethylbenzimidazole as an α-axial ligand of B12 cofactors in Salmonella enterica. *J Bacteriol, 190*(4): 1160-1171.

Arandia-Gorostidi, N., Weber, P. K., Alonso-Sáez, L., Morán, X. A. G., & Mayali, X. (2017). Elevated temperature increases carbon and nitrogen fluxes between phytoplankton and heterotrophic bacteria through physical attachment. *ISME J, 11*(3): 641-650.

Banerjee, R., & Ragsdale, S. W. (2003). The many faces of vitamin B12: catalysis by cobalamin-dependent enzymes. *Annu Rev Biochem, 72*: 209-247.

Barchewitz, T., Guljamow, A., Meissner, S., Timm, S., Henneberg, M., Baumann, O. *et al.* (2019). Non-canonical localization of RubisCO under high-light conditions in the toxic

cyanobacterium Microcystis aeruginosa PCC7806. *Environ Microbiol, 21*(12): 4836-4851.

Bassford, P., Bradbeer, C., Kadner, R. J., & Schnaitman, C. A. (1976). Transport of vitamin B12 in tonB mutants of *Escherichia coli*. *J Bacteriol, 128*(1): 242-247.

Bateson, M. M., & Ward, D. M. (1988). Photoexcretion and fate of glycolate in a hot spring cyanobacterial mat. *Appl Environ Microbiol, 54*(7): 1738-1743.

Beliaev, A. S., Romine, M. F., Serres, M., Bernstein, H. C., Linggi, B. E., Markillie, L. M. *et al.* (2014). Inference of interactions in cyanobacterial-heterotrophic co-cultures via transcriptome sequencing. *ISME J, 8*(11): 2243-2255.

Bell, W., & Mitchell, R. (1972). Chemotactic and growth responses of marine bacteria to algal extracellular products. *Biol. Bull, 143*(2): 265-277.

Bellmann, A., Vrljić, M., Patek, M., Sahm, H., Krämer, R., & Eggeling, L. (2001). Expression control and specificity of the basic amino acid exporter LysE of *Corynebacterium glutamicum*. *Microbiology, 147*(7): 1765-1774.

Berry, M. A., Davis, T. W., Cory, R. M., Duhaime, M. B., Johengen, T. H., Kling, G. W. *et al.* (2017). Cyanobacterial harmful algal blooms are a biological disturbance to Western Lake Erie bacterial communities. *Environ Microbiol, 19*(3): 1149-1162.

Bonnet, S., Webb, E. A., Panzeca, C., Karl, D. M., Capone, D. G., & Wilhelmy, S. A. S. (2010). Vitamin B12 excretion by cultures of the marine cyanobacteria *Crocosphaera* and *Synechococcus*. *Limnol Oceanogr, 55*(5): 1959-1964.

Bouvrette, P., & Luong, J. H. (1994). Isolation, purification, and further characterization of an L-phenylalanine oxidase from *Morganella morganii*. *Appl Biochem Biotechnol, 48*(2): 61-74.

Bowers, R. M., Kyrpides, N. C., Stepanauskas, R., Harmon-Smith, M., Doud, D., Reddy, T. *et al.* (2017). Minimum information about a single amplified genome (MISAG) and a metagenome-assembled genome (MIMAG) of bacteria and archaea. *Nat Biotechnol, 35*(8): 725-731.

But, S., Egorova, S., Khmelenina, V., & Trotsenko, Y. (2019). Serine-glyoxylate aminotranferases from methanotrophs using different C1-assimilation pathways. *ANTON LEEUW INT J G, 112*(5): 741-751.

Chaffin, J. D., Davis, T. W., Smith, D. J., Baer, M. M., & Dick, G. J. (2018). Interactions between nitrogen form, loading rate, and light intensity on *Microcystis* and *Planktothrix* growth and microcystin production. *Harmful Algae, 73*: 84-97.

Christie-Oleza, J. A., Sousoni, D., Lloyd, M., Armengaud, J., & Scanlan, D. J. (2017). Nutrient recycling facilitates long-term stability of marine microbial phototroph-heterotroph interactions. *Nat Microbiol, 2*(17100): 1-10.

Chun, S.-J., Cui, Y., Lee, C. S., Cho, A. R., Baek, K., Choi, A. *et al.* (2019). Characterization of distinct cyanoHABs-related modules in microbial recurrent association network. *Front Microbiol, 10*: 1637.

Chun, S.-J., Cui, Y., Lee, J. J., Choi, I.-C., Oh, H.-M., & Ahn, C.-Y. (2020). Network analysis reveals succession of Microcystis genotypes accompanying distinctive microbial modules with recurrent patterns. *Water Res, 170*: 115326.

Cole, J. J. (1982). Interactions between bacteria and algae in aquatic ecosystems. *Annu Rev Ecol Syst, 13*(1): 291-314.

Cook, K. V., Li, C., Cai, H., Krumholz, L. R., Hambright, K. D., Paerl, H. W. *et al.* (2020). The global *Microcystis* interactome. *Limnol Oceanogr, 65*(S1): S194-S207. doi:10.1002/lno.11361

Croft, M. T., Lawrence, A. D., Raux-Deery, E., Warren, M. J., & Smith, A. G. (2005). Algae acquire vitamin B_{12} through a symbiotic relationship with bacteria. *Nature, 438*(7064): 90-93. doi:doi:10.1038/nature04056

Davis, T. W., Harke, M. J., Marcoval, M. A., Goleski, J., Orano-Dawson, C., Berry, D. L., & Gobler, C. J. (2010). Effects of nitrogenous compounds and phosphorus on the growth of toxic and non-toxic strains of *Microcystis* during cyanobacterial blooms. *Aquat Microb Ecol, 61*(2): 149-162.

Dedysh, S. N., & Damsté, J. S. S. (2018). *AcidobacteriaeLS* (pp. 1-10). doi:10.1002/9780470015902.a0027685

Duerre, J. A., & Chakrabarty, S. (1975). L-amino acid oxidases of *Proteus rettgeri*. *J Bacteriol, 121*(2): 656-663.

Durham, B. P., Dearth, S. P., Sharma, S., Amin, S. A., Smith, C. B., Campagna, S. R. *et al.* (2017). Recognition cascade and metabolite transfer in a marine bacteria-phytoplankton model system. *Environ Microbiol, 19*(9): 3500-3513. doi:10.1111/1462-2920.13834

Embree, M., Liu, J. K., Al-Bassam, M. M., & Zengler, K. (2015). Networks of energetic and metabolic interactions define dynamics in microbial communities. *Proc Natl Acad Sci, 112*(50): 15450-15455.

Ferrer-González, F. X., Widner, B., Holderman, N. R., Glushka, J., Edison, A. S., Kujawinski, E. B., & Moran, M. A. (2020). Resource partitioning of phytoplankton metabolites that support bacterial heterotrophy. *ISME J*: 1-12.

Forni, C., Telo', F. R., & Caiola, M. G. (1997). Comparative analysis of the polysaccharides produced by different species of *Microcystis* (Chroococcales, Cyanophyta). *Phycologia, 36*(3): 181-185.

Gardner, W. S., Newell, S. E., McCarthy, M. J., Hoffman, D. K., Lu, K., Lavrentyev, P. J. *et al.* (2017). Community biological ammonium demand: a conceptual model for Cyanobacteria blooms in eutrophic lakes. *Environ Sci Technol, 51*(14): 7785-7793.

Goldman, J., & Dennett, M. (1991). Ammonium regeneration and carbon utilization by marine bacteria grown on mixed substrates. *Mar Biol, 109*(3): 369-378.

Goldman, J. C., Caron, D. A., & Dennett, M. R. (1987). Regulation of gross growth efficiency and ammonium regeneration in bacteria by substrate C:N ratio. *Limnol Oceanogr, 32*(6): 1239-1252.

Grossart, H.-P., & Simon, M. (2007). Interactions of planktonic algae and bacteria: effects on algal growth and organic matter dynamics. *Aquat Microb Ecol, 47*(2): 163-176.

Heal, K. R., Carlson, L. T., Devol, A. H., Armbrust, E. V., Moffett, J. W., Stahl, D. A., & Ingalls, A. E. (2014). Determination of four forms of vitamin B12 and other B vitamins in seawater by liquid chromatography/tandem mass spectrometry. *Rapid Comm Mass Spec, 28*(22): 2398-2404.

Heal, K. R., Qin, W., Ribalet, F., Bertagnolli, A. D., Coyote-Maestas, W., Hmelo, L. R. *et al.* (2017). Two distinct pools of B12 analogs reveal community interdependencies in the ocean. *Proc Natl Acad Sci, 114*(2): 364-369.

Hellebust, J. A. (1965). Excretion Of Some Organic Compounds By Marine Phytoplankton. *Limnol Oceanogr, 10*(2): 192-206.

Helliwell, K. E., Lawrence, A. D., Holzer, A., Kudahl, U. J., Sasso, S., Kräutler, B. *et al.* (2016). Cyanobacteria and eukaryotic algae use different chemical variants of vitamin B12. *Curr Biol, 26*(8): 999-1008.

Hug, L. A., & Co, R. (2018). It Takes a Village: Microbial Communities Thrive through Interactions and Metabolic Handoffs. *mSystems, 3*(2): 1-5.

Huntemann, M., Ivanova, N. N., Mavromatis, K., Tripp, H. J., Paez-Espino, D., Palaniappan, K. *et al.* (2015). The standard operating procedure of the DOE-JGI microbial genome annotation pipeline (MGAP v. 4). *Stand Genomic Sci, 10*(1): 1-6.

Jones, R. T., Robeson, M. S., Lauber, C. L., Hamady, M., Knight, R., & Fierer, N. (2009). A comprehensive survey of soil acidobacterial diversity using pyrosequencing and clone library analyses. *ISME J, 3*(4): 442-453.

Kara, E. L., Hanson, P. C., Hu, Y. H., Winslow, L., & McMahon, K. D. (2013). A decade of seasonal dynamics and co-occurrences within freshwater bacterioplankton communities from eutrophic Lake Mendota, WI, USA. *ISME J, 7*(3): 680-684.

Kardinaal, W. E. A., Janse, I., Kamst-van Agterveld, M., Meima, M., Snoek, J., Mur, L. R. *et al.* (2007). *Microcystis* genotype succession in relation to microcystin concentrations in freshwater lakes. *Aquat Microb Ecol, 48*(1): 1-12.

Kirchman, D. L., Keil, R. G., & Wheeler, P. A. (1989). The effect of amino acids on ammonium utilization and regeneration by heterotrophic bacteria in the subarctic Pacific. *Deep Sea Res Part I Oceanogr Res Pap, 36*(11): 1763-1776.

Konstantinidis, K. T., & Tiedje, J. M. (2005). Genomic insights that advance the species definition for prokaryotes. *Proc Natl Acad Sci, 102*(7): 2567-2572.

Kulichevskaya, I. S., Suzina, N. E., Liesack, W., & Dedysh, S. N. (2010). *Bryobacter aggregatus* gen. nov., sp. nov., a peat-inhabiting, aerobic chemoorganotroph from subdivision 3 of the *Acidobacteria*. *Int J Syst Evol Microbiol, 60*(2): 301-306.

Kulichevskaya, I. S., Suzina, N. E., Rijpstra, W. I. C., Damste, J. S. S., & Dedysh, S. N. (2014). *Paludibaculum fermentans* gen. nov., sp. nov., a facultative anaerobe capable of dissimilatory iron reduction from subdivision 3 of the Acidobacteria. *Int J Syst Evol Microbiol, 64*(8): 2857-2864.

Lehman, P., Kendall, C., Guerin, M., Young, M., Silva, S., Boyer, G., & Teh, S. J. (2015). Characterization of the *Microcystis* bloom and its nitrogen supply in San Francisco Estuary using stable isotopes. *Estuaries and Coasts, 38*(1): 165-178.

Li, P., Cai, Y., Shi, L., Geng, L., Xing, P., Yu, Y. *et al.* (2009). Microbial Degradation and Preliminary Chemical Characterization of *Microcystis* Exopolysaccharides from a Cyanobacterial Water Bloom of Lake Taihu. *Int Rev Hydrobiol, 94*(6): 645-655.

Livshits, V. A., Zakataeva, N. P., Aleshin, V. V., & Vitushkina, M. V. (2003). Identification and characterization of the new gene rhtA involved in threonine and homoserine efflux in *Escherichia coli*. *Res Microbiol, 154*(2): 123-135.

Ma, A. T., Tyrell, B., & Beld, J. (2019). Specificity of cobamide remodeling, uptake, and utilization in *Vibrio cholerae*. *Mol Microbiol*.

Meon, B., & Kirchman, D. L. (2001). Dynamics and molecular composition of dissolved organic material during experimental phytoplankton blooms. *Mar Chem, 75*(3): 185-199.

Miller, C. S., Baker, B. J., Thomas, B. C., Singer, S. W., & Banfield, J. F. (2011). EMIRGE: reconstruction of full-length ribosomal genes from microbial community short read sequencing data. *Genome Biol, 12*(5): R44.

Morris, J. J., Johnson, Z. I., Szul, M. J., Keller, M., & Zinser, E. R. (2011). Dependence of the cyanobacterium *Prochlorococcus* on hydrogen peroxide scavenging microbes for growth at the ocean's surface. *PloS one, 6*(2): e16805.

Mühlenbruch, M., Grossart, H. P., Eigemann, F., & Voss, M. (2018). Mini-review: Phytoplankton-derived polysaccharides in the marine environment and their interactions with heterotrophic bacteria. *Environ Microbiol, 20*(8): 2671-2685.

Newell, S. E., Davis, T. W., Johengen, T. H., Gossiaux, D., Burtner, A., Palladino, D., & McCarthy, M. J. (2019). Reduced forms of nitrogen are a driver of non-nitrogen-fixing harmful cyanobacterial blooms and toxicity in Lake Erie. *Harmful Algae, 81*: 86-93.

Nisbet, T. M., & Payne, J. W. (1982). The characteristics of peptide uptake in *Streptococcus faecalis*: studies on the transport of natural peptides and antibacterial phosphonopeptides. *Microbiology, 128*(6): 1357-1364.

Núñez, M. F., Pellicer, M. T., Badía, J., Aguilar, J., & Baldomà, L. (2001). The gene yghK linked to the glc operon of *Escherichia coli* encodes a permease for glycolate that is structurally and functionally similar to L-lactate permease. *Microbiology, 147*(4): 1069-1077.

Olm, M. R., Brown, C. T., Brooks, B., & Banfield, J. F. (2017). dRep: a tool for fast and accurate genomic comparisons that enables improved genome recovery from metagenomes through de-replication. *ISME J, 11*(12): 2864.

Palenik, B., & Morel, F. M. (1990a). Amino acid utilization by marine phytoplankton: a novel mechanism. *Limnol Oceanogr, 35*(2): 260-269.

Palenik, B., & Morel, F. M. (1990b). Comparison of cell-surface L-amino acid oxidases from several marine phytoplankton. *Mar Ecol Prog Ser, 59*: 195-201.

Parks, D. H., Imelfort, M., Skennerton, C. T., Hugenholtz, P., & Tyson, G. W. (2015). CheckM: assessing the quality of microbial genomes recovered from isolates, single cells, and metagenomes. *Genome Res, 25*(7): 1043-1055.

Parveen, B., Ravet, V., Djediat, C., Mary, I., Quiblier, C., Debroas, D., & Humbert, J. F. (2013). Bacterial communities associated with *Microcystis* colonies differ from free-living communities living in the same ecosystem. *Environ Microbiol Rep, 5*(5): 716-724.

Paver, S. F., Newton, R. J., & Coleman, M. L. (2020). Microbial communities of the Laurentian Great Lakes reflect connectivity and local biogeochemistry. *Environ Microbiol, 22*(1): 433-446.

Payne, J., & Bell, G. (1979). Direct determination of the properties of peptide transport systems in *Escherichia coli*, using a fluorescent-labeling procedure. *J Bacteriol, 137*(1): 447-455.

Plude, J. L., Parker, D. L., Schommer, O. J., Timmerman, R. J., Hagstrom, S. A., Joers, J. M., & Hnasko, R. (1991). Chemical Characterization of Polysaccharide from the Slime Layer of the Cyanobacterium *Microcystis flos-aquae* C3-40. *Appl Environ Microbiol, 57*(6): 1696-1700.

Pruesse, E., Quast, C., Knittel, K., Fuchs, B. M., Ludwig, W., Peplies, J., & Glöckner, F. O. (2007). SILVA: a comprehensive online resource for quality checked and aligned ribosomal RNA sequence data compatible with ARB. *Nucleic Acids Res, 35*(21): 7188-7196.

Pruesse, E., Peplies, J., & Glöckner, F. O. (2012). SINA: accurate high-throughput multiple sequence alignment of ribosomal RNA genes. *Bioinformatics, 28*(14): 1823-1829.

Renström-Kellner, E., & Bergman, B. (1989). Glycolate metabolism in cyanobacteria. III. Nitrogen controls excretion and metabolism of glycolate in Anabaena cylindrica. *Physiol Plant, 77*(1): 46-51.

Reynolds, P. R., Mottur, G. P., & Bradbeer, C. (1980). Transport of vitamin B12 in *Escherichia coli*. Some observations on the roles of the gene products of *BtuC* and *TonB*. *J Biol Chem, 255*(9): 4313-4319.

Rozmarynowycz, M. J., Beall, B. F., Bullerjahn, G. S., Small, G. E., Sterner, R. W., Brovold, S. S. *et al.* (2019). Transitions in microbial communities along a 1600 km freshwater trophic gradient. *J Great Lakes Res, 45*(2): 263-276.

Santos, F., Vera, J. L., Lamosa, P., de Valdez, G. F., de Vos, W. M., Santos, H. *et al.* (2007). Pseudovitamin is the corrinoid produced by *Lactobacillus reuteri* CRL1098 under anaerobic conditions. *FEBS Lett, 581*(25): 4865-4870.

Schloss, P. D., Westcott, S. L., Ryabin, T., Hall, J. R., Hartmann, M., Hollister, E. B. *et al.* (2009). Introducing mothur: open-source, platform-independent, community-supported software for describing and comparing microbial communities. *Appl Environ Microbiol, 75*(23): 7537-7541.

Schmidt, K. C., Jackrel, S. L., Smith, D. J., Dick, G. J., & Denef, V. J. (2020). Genotype and host microbiome alter competitive interactions between *Microcystis aeruginosa* and *Chlorella sorokiniana*. *Harmful Algae, 99*(101939).

Segev, E., Wyche, T. P., Kim, K. H., Petersen, J., Ellebrandt, C., Vlamakis, H. *et al.* (2016). Dynamic metabolic exchange governs a marine algal-bacterial interaction. *eLife, 5*(1): e17473.

Serkebaeva, Y. M., Kim, Y., Liesack, W., & Dedysh, S. N. (2013). Pyrosequencing-based assessment of the bacteria diversity in surface and subsurface peat layers of a northern wetland, with focus on poorly studied phyla and candidate divisions. *PloS one, 8*(5): e63994.

Seyedsayamdost, M. R., Case, R. J., Kolter, R., & Clardy, J. (2011). The Jekyll-and-Hyde chemistry of *Phaeobacter gallaeciensis*. *Nat Chem, 3*(4): 331-335. Retrieved from https://www.nature.com/articles/nchem.1002.pdf

Seymour, J. R., Amin, S. A., Raina, J.-B., & Stocker, R. (2017). Zooming in on the phycosphere: the ecological interface for phytoplankton-bacteria interactions. *Nat Microbiol, 2*(17065): 1-12. doi:10.1038/nmicrobiol.2017.65

Shi, L., Huang, Y., Zhang, M., Shi, X., Cai, Y., Gao, S. *et al.* (2018). Large buoyant particles dominated by cyanobacterial colonies harbor distinct bacterial communities from small

suspended particles and free-living bacteria in the water column. *MicrobiologyOpen, 7*(6): e00608.

Shia, L., Cai, Y., Wang, X., Li, P., Yu, Y., & Kong, F. (2010). Community structure of bacteria associated with *Microcystis* colonies from cyanobacterial blooms. *J Freshw Ecol, 25*(2): 193-203.

Sievers, F., Wilm, A., Dineen, D., Gibson, T. J., Karplus, K., Li, W. *et al.* (2011). Fast, scalable generation of high-quality protein multiple sequence alignments using Clustal Omega. *Molecular systems biology, 7*(1): 539.

Sinha, S., & Cossins, E. (1965). The importance of glyoxylate in amino acid biosynthesis in plants. *Biochem J, 96*(1): 254-261.

Sison-Mangus, M. P., Jiang, S., Tran, K. N., & Kudela, R. M. (2014). Host-specific adaptation governs the interaction of the marine diatom, *Pseudo-nitzschia* and their microbiota. *ISME J, 8*(1): 63-76.

Smriga, S., Fernandez, V. I., Mitchell, J. G., & Stocker, R. (2016). Chemotaxis toward phytoplankton drives organic matter partitioning among marine bacteria. *Proc Natl Acad Sci, 113*(6): 1576-1581.

Stamatakis, A. (2006). RAxML-VI-HPC: maximum likelihood-based phylogenetic analyses with thousands of taxa and mixed models. *Bioinformatics, 22*(21): 2688-2690.

Stupperich, E., & Kräutler, B. (1988). Pseudo vitamin B 12 or 5-hydroxybenzimidazolyl-cobamide are the corrinoids found in methanogenic bacteria. *Arch Micobiol, 149*(3): 268-271.

Tolbert, N. (1979). Glycolate metabolism by higher plants and algae. In *Photosynthesis II* (pp. 338-352): Springer.

Tromas, N., Fortin, N., Bedrani, L., Terrat, Y., Cardoso, P., Bird, D. *et al.* (2017). Characterising and predicting cyanobacterial blooms in an 8-year amplicon sequencing time course. *ISME J, 11*(8): 1746-1763.

Tupas, L., & Koike, I. (1990). Amino acid and ammonium utilization by heterotrophic marine bacteria grown in enriched seawater. *Limnol Oceanogr, 35*(5): 1145-1155.

Tupas, L. M., Koike, I., Karl, D. M., & Holm-Hansen, O. (1994). Nitrogen metabolism by heterotrophic bacterial assemblages in Antarctic coastal waters. *Polar Biol, 14*(3): 195-204.

Varghese, N. J., Mukherjee, S., Ivanova, N., Konstantinidis, K. T., Mavrommatis, K., Kyrpides, N. C., & Pati, A. (2015). Microbial species delineation using whole genome sequences. *Nucleic Acids Res, 43*(14): 6761-6771.

von Borzyskowski, L. S., Severi, F., Krüger, K., Hermann, L., Gilardet, A., Sippel, F. *et al.* (2019). Marine Proteobacteria metabolize glycolate via the β-hydroxyaspartate cycle. *Nature*: 1-5.

Wang, Q., Garrity, G. M., Tiedje, J. M., & Cole, J. R. (2007). Naive Bayesian classifier for rapid assignment of rRNA sequences into the new bacterial taxonomy. *Appl Environ Microbiol, 73*(16): 5261-5267.

Wick, R. R., Schultz, M. B., Zobel, J., & Holt, K. E. (2015). Bandage: interactive visualization of de novo genome assemblies. *Bioinformatics, 31*(20): 3350-3352. Retrieved from https://www.ncbi.nlm.nih.gov/pmc/articles/PMC4595904/pdf/btv383.pdf

Wolk, C. P. (1973). Physiology and cytological chemistry blue-green algae. *Bacteriol Rev, 37*(1): 32.

Xie, M., Ren, M., Yang, C., Yi, H., Li, Z., Li, T., & Zhao, J. (2016). Metagenomic analysis reveals symbiotic relationship among bacteria in *Microcystis*-dominated community. *Front Microbiol, 7*: 56.

Yarza, P., Yilmaz, P., Pruesse, E., Glöckner, F. O., Ludwig, W., Schleifer, K.-H. *et al.* (2014). Uniting the classification of cultured and uncultured bacteria and archaea using 16S rRNA gene sequences. *Nat Rev Microbiol, 12*(9): 635.

Ye, L., Shi, X., Wu, X., Zhang, M., Yu, Y., Li, D., & Kong, F. (2011). Dynamics of dissolved organic carbon after a cyanobacterial bloom in hypereutrophic Lake Taihu (China). *Limnologica, 41*(4): 382-388.

Zakataeva, N. P., Aleshin, V. V., Tokmakova, I. L., Troshin, P. V., & Livshits, V. A. (1999). The novel transmembrane *Escherichia coli* proteins involved in the amino acid efflux. *FEBS Lett, 452*(3): 228-232.

Zhu, W., Li, M., Luo, Y., Dai, X., Guo, L., Xiao, M. *et al.* (2014). Vertical distribution of *Microcystis* colony size in Lake Taihu: Its role in algal blooms. *J Great Lakes Res, 40*(4): 949-955.

Chapter 5 Characterization of Biological H_2O_2 Production and Decay During Lake Erie Cyanobacterial Blooms

5.1 Abstract

Hydrogen peroxide (H_2O_2) is ubiquitous in freshwaters, where it stresses microbes. Microbes are likely a substantial source of H_2O_2 during cyanobacterial harmful algal blooms (CHABs), where H_2O_2 may impact the strain composition of *Microcystis* within blooms. However, biological H_2O_2 production and the H_2O_2-producing organisms in freshwater CHABs are poorly characterized. Therefore, net and gross H_2O_2 production and decay were measured in both whole water and 0.22 μm filtered water approximately weekly in 2017 and at various stages of bloom development in 2018 and 2019. To determine if H_2O_2 fluxes were linked to photosynthesis by *Microcystis* colonies, H_2O_2 production and decay was measured in light and dark incubations and in water with large phytoplankton assemblages removed in 2018 and 2019. Microbes were the dominant source and sink of H_2O_2 on average. While some biotic H_2O_2 production was independent of light, biotic H_2O_2 production was higher in light-exposed water, and H_2O_2 production was significantly correlated with chlorophyll *a* concentration and primary production rates. Filtration of phytoplankton assemblages did not affect biotic H_2O_2 production and decay. The results indicate that most biotic H_2O_2 production in western Lake Erie is light-dependent and related to photosynthesis, but that neither production nor decay are directly from large *Microcystis* colonies. This suggests that free-living microbial populations are the main sources and sinks of H_2O_2 in Lake Erie CHABs rather than *Microcystis* colonies. The biological H_2O_2 production may be linked to respiration of phytoplankton exudates or produced directly by small phytoplankton.

5.2 Introduction

The reactive oxygen species (ROS) superoxide radical anion (O_2^-), hydrogen peroxide (H_2O_2), and hydroxyl radical (·OH) are unstable intermediates in sequential one electron reductions of oxygen to water. They are ubiquitous in oxygenated aquatic ecosystems, where they influence biogeochemical cycles by controlling the redox state of dissolved transition metals such as iron (Rose & Waite, 2006; Fujii *et al.*, 2011; Trusiak *et al.*, 2018), manganese (Wuttig *et al.*, 2013; Andeer *et al.*, 2015), and copper (Voelker *et al.*, 2000) and by oxidizing organic matter (Andrews *et al.*, 2000; Goldstone & Voelker, 2000; Xie *et al.*, 2004; Heller & Croot, 2010; Trusiak *et al.*, 2018). ROS also impact biogeochemistry by affecting microbial growth. ROS can stimulate respiration by increasing the lability of dissolved organic matter (DOM) via oxidation (Anesio *et al.*, 2005) but also inhibit microbial growth by damaging cellular structures (Imlay, 2003). For example, ROS can inhibit microbial respiration and secondary production in natural assemblages (Xenopoulos & Bird, 1997; Weinbauer & Suttle, 1999; Anesio *et al.*, 2005) and constrain the growth (Morris *et al.*, 2011; Kim *et al.*, 2016; Tolar *et al.*, 2016; Ma *et al.*, 2018; Bayer *et al.*, 2019) and thermal niche (Ma *et al.*, 2018) of globally dominant marine autotrophs, thus impacting carbon and nitrogen cycling.

In addition to their impacts on biogeochemistry, ROS also impact microbial community composition and ecology. While some microbes are highly sensitive to ROS (Morris *et al.*, 2011; Kim *et al.*, 2016; Ma *et al.*, 2018; Bayer *et al.*, 2019), others readily degrade and tolerate ROS concentrations that exceed those measured in natural waters by orders of magnitude (Seaver & Imlay, 2001; Cosgrove *et al.*, 2007; Morris *et al.*, 2008; Morris *et al.*, 2011). Differing sensitivities to ROS between microbial taxa can create inter-dependencies, where sensitive organisms depend on more resistant microbes to degrade environmental H_2O_2 (Morris *et al.*, 2011; Morris, 2015; Kim *et al.*, 2016; Zinser, 2018b). Some microbes exploit differences in ROS

sensitivities. For example, microbes from marine (Lucas-Elío *et al.*, 2006) and human-host systems (Eschenbach *et al.*, 1989; Lucas-Elío *et al.*, 2006; Tong *et al.*, 2007; Tong *et al.*, 2008) secrete H_2O_2 to inhibit the growth of other organisms, resulting in a growth advantage for the H_2O_2-producing taxa. These differences in ROS sensitivity can drive community dynamics. For example, in human microbiomes, an absence of H_2O_2-producing species can lead to the proliferation of H_2O_2-sensitive pathogens (Eschenbach *et al.*, 1989). In aquatic systems, the relative abundances of cyanobacteria and certain heterotrophic taxa were reduced in lake water amended with H_2O_2 while some bacterial and phytoplankton taxa remained unaffected (Matthijs *et al.*, 2012; Lin *et al.*, 2018; Lusty & Gobler, 2020). Although the H_2O_2 concentrations added were 2-3 orders of magnitude above some of the highest concentrations observed in natural waters, these experiments suggest that H_2O_2 production may also impact microbial community composition in aquatic systems. However, the outcome of natural H_2O_2 production dynamics on microbial community composition is unknown.

Because of the impact ROS have in aquatic ecosystems, characterization of their sources and sinks is critical for a complete understanding of microbial community composition, stressors of microbial growth, and biogeochemistry in aquatic ecosystems. ROS are produced photochemically from the reduction of O_2 by photo-excited chromophoric dissolved organic matter (CDOM) (Cooper & Zika, 1983; Garg *et al.*, 2011). The initial product of the reaction is O_2^-, which can then dismutate, forming H_2O_2 and O_2 (Petasne & Zika, 1987; Zafiriou, 1990). This photochemical source was originally thought to be the dominant source of O_2^- and H_2O_2 in surface waters (Cooper & Zika, 1983; Petasne & Zika, 1987; Cooper *et al.*, 1988). However, microorganisms also produce extracellular O_2^- (Diaz *et al.*, 2013; Hansel *et al.*, 2016; Schneider *et al.*, 2016; Diaz & Plummer, 2018; Diaz *et al.*, 2018; Hansel *et al.*, 2019; Bond *et al.*, 2020)

and H_2O_2 (Lucas-Elío *et al.*, 2006; Tong *et al.*, 2007; Kim *et al.*, 2016; Schneider *et al.*, 2016; Diaz *et al.*, 2018; Bayer *et al.*, 2019; Bond *et al.*, 2020). Microbial production can be a significant source of both H_2O_2 and O_2^- in natural waters (Rose *et al.*, 2008; Vermilyea *et al.*, 2010a; Vermilyea *et al.*, 2010b; Dixon *et al.*, 2013; Marsico *et al.*, 2015; Sutherland *et al.*, 2020), and may exceed photochemical H_2O_2 production in some systems (Dixon *et al.*, 2013; Cory *et al.*, 2016). Because H_2O_2 and O_2^- production rates vary widely between microbial taxa (Diaz *et al.*, 2013; Schneider *et al.*, 2016; Diaz & Plummer, 2018; Diaz *et al.*, 2018; Bond *et al.*, 2020) and in the same organism at different growth phases (Hansel *et al.*, 2019), microbial community composition and physiology likely determine the magnitude of biotic H_2O_2 production in the environment, which can vary by 1-2 orders of magnitude between systems (Vermilyea *et al.*, 2010b; Dixon *et al.*, 2013; Marsico *et al.*, 2015). Therefore, the magnitude of biological H_2O_2 production is likely shaped by dynamics in H_2O_2-producing microbes. While many enzymes and organisms are known to produce extracellular ROS, it is unknown which organisms and pathways are the largest contributors to environmental ROS production (Zinser, 2018a; Hansel & Diaz, 2020), and the relationships between natural H_2O_2 production dynamics and microbial community composition have not been explored.

ROS are also thought to have important impacts on cyanobacterial harmful algal blooms (CHABs). For example, strains of *Microcystis*, a potentially toxic cyanobacterium that forms blooms globally (Harke *et al.*, 2016), have different sensitivities to H_2O_2 additions in culture (Dziallas & Grossart, 2011; Schuurmans *et al.*, 2018). Therefore, changing H_2O_2 concentrations during blooms have been hypothesized to effect the relative proportions of *Microcystis* strains (Paerl & Otten, 2013), which is one determinant of microcystin concentrations during blooms (Kardinaal *et al.*, 2007; Briand *et al.*, 2009; Davis *et al.*, 2009). H_2O_2 concentrations during

blooms can vary by two orders of magnitude, and accumulate to levels that can impact the growth of some cyanobacteria species (Morris *et al.*, 2011; Ma *et al.*, 2018). In some cases, peak H_2O_2 concentrations cannot be explained by photochemical production rates, which suggests that biological production is a substantial and important source of H_2O_2 during blooms (Cory *et al.*, 2016; Cory *et al.*, 2017). Therefore, changes in H_2O_2 production and decay by CHAB microbial communities may influence the relative proportions of *Microcystis* strains, interactions between microorganisms, and cyanobacteria physiology during CHABs. While microbial catalases are known as a major sink for H_2O_2 in aquatic environments (Moffett & Zafiriou, 1990; Cooper *et al.*, 1994), the organisms and pathways responsible for H_2O_2 production in aquatic microbial communities are largely unknown. Thus, it is unclear whether increasing H_2O_2 production during blooms impacts or results from *Microcystis* growth.

To determine how H_2O_2 production in western Lake Erie is related to the development of *Microcystis* blooms, we measured H_2O_2 production and decay rates over different periods of a *Microcystis* bloom in summer-fall 2017, 2018, and 2019. Significant correlations between modeled gross and net H_2O_2 production rates and chlorophyll *a* concentration, respiration rate, primary production rate, and microbial community composition were detected, supporting that H_2O_2 production and decay rates are related to differences in microbial growth rates and microbial community composition. While net H_2O_2 production rates were correlated with *Microcystis* abundance and light-dependent, filtration of large *Microcystis* colonies did not reduce H_2O_2 production and decay rates, and *Microcystis* OTUs were not an important predictor of H_2O_2 production in random forest models. Therefore, increasing H_2O_2 production rates in *Microcystis* blooms is not directly attributed to *Microcystis* and is rather from other microbial

populations, suggesting that *Microcystis* physiology and fitness may be impacted by changes in biological H_2O_2 production during CHABs.

5.3 Methods

5.3.1 Field Sampling

Whole water was collected from various sites across western Lake Erie during the summer and fall of 2017, 2018, and 2019 (Figure S 5.1). In 2017, water was collected approximately biweekly from NOAA station WE2 in conjunction with the NOAA Great Lakes Environmental Research Lab harmful algal bloom monitoring program. Various sites in Environment and Climate Change Canada's monitoring program were also sampled during two research cruises in August and October 2017. In 2018 and 2019, water was collected at several stages of bloom development (pre-bloom, early bloom, late bloom, and post bloom). In 2018, water was collected at NOAA monitoring stations WE2 and WE12 and at the drinking water intake for the City of Toledo (TWI). In order to ensure capture of microbial communities from dense cyanobacteria blooms, in which biotic H_2O_2 production rates are hypothesized to be highest (Cory *et al.*, 2016), areas predicted to have high bloom biomass in the NOAA HAB forecast model and HAB tracker bulletins (Wynne *et al.*, 2013) were targeted in 2019. Exact sampling locations were chosen based on the presence of surface scums and cyanobacterial colonies. Non-bloom samples in this year, water was collected near Turtle Island.

For all sites, 20 L (2017) or 60 L (2018 & 2019) depth integrated water samples (surface to 1 meter from lake bottom) were collected in 20 or 60 L acid-washed carboys. Water was collected from the NOAA stations using a peristaltic pump by slowly moving the pump hose up and down through the water column. From the Toledo water intake, and targeted high biomass samples, water was collected at discrete depths of 1 meter intervals from surface to 1 meter from

lake bottom using a Van Dorn bottle and pooled to create a depth integrated sample. During Environment Canada cruises, water was collected using a depth-integrating sampler. Back at the lab, pH was measured using a benchtop meter, water was filtered through a 0.22 μm PES filter to measure dissolved nutrients, and a subsample of whole water was taken for total phosphorus analysis. For 2017, pH data was obtained from monitoring buoys. The water samples were stored in carboys placed in an outdoor aquaculture tank and held at water temperature measured at the time of collection using copper piping attached to a NESLAB RTE refrigerated water bath (Thermo Scientific, Newington, NH) until the start of the bottle experiments the following morning.

5.3.2 H_2O_2 Bottle Experiments and H_2O_2 Measurements

The day following field sampling, carboys containing whole water were retrieved from the outdoor tank at approximately 6:00 EDT and whole water was distributed into 2L acid-washed, transparent, polycarbonate bottles to measure H_2O_2 production and decay rates. The water was allowed to acclimate to the bottles for 1 hour before the start of the experiments at approximately 8:00 EDT. All experiments were performed at the same time of day, with the exception of two experiments from the Environment Canada cruises, which started 0.5-1 hour later due to the timing of ship arrival on site.

Observed H_2O_2 production rates in aquatic systems are the net result of co-occurring and rapid production and decay processes, which makes measurements of H_2O_2 challenging as decay processes can potentially mask production and vise-versa (Moffett & Zafiriou, 1990; Vermilyea *et al.*, 2010b; Dixon *et al.*, 2013). Therefore, gross H_2O_2 production rates (PH_2O_2) were estimated measured using a spike-batch incubation approach as described previously (Vermilyea *et al.*, 2010b; Marsico *et al.*, 2015). Briefly, this method estimates gross H_2O_2 production rates

from measured net H_2O_2 in unspiked and measured net H_2O_2 decay from spiked incubations of lake water. Paired bottles of unamended water and water spiked with a nominal 10 mM H_2O_2 solution to a final target concentration of 1 µM were placed in the outdoor tank and the H_2O_2 concentrations were measured every 3 hours over a 9 hour period. Observed H_2O_2 concentrations in both the spiked and unamended bottles are related to PH_2O_2 and k_{loss} via the following differential equation:

$$1. \quad \frac{d[H_2O_2]}{dt} = PH_2O_2 - k_{loss}[H_2O_2]$$

Assuming that PH_2O_2 and k_{loss} are both constant with time and independent of $[H_2O_2]$, the following integrated form of the equation gives $[H_2O_2]$ as a function of time (t):

$$2. \quad [H_2O_2]_t = \frac{PH_2O_2}{K_{loss}} - (1 - Ae^{-k_{loss}*t})$$

$$3. \quad \text{Where } A = 1 - (\frac{k_{loss}}{PH_2O_2})[H_2O_2]_0$$

Measured H_2O_2 concentrations from both the spike and unamended bottles were fit to equation 2 by choosing values for PH_2O_2 and K_{loss} that minimized the error sum of squares in the modelled $[H_2O_2]$ at each timepoint using Microsoft Excel's Solver function. In five of the 34 experiments, Solver could not converge on a solution in one or both replicate experiments, so PH_2O_2 and K_{loss} were not calculated on these dates. Gross biotic H_2O_2 production rates were calculated by subtracting net H_2O_2 production in 0.22 µm filtered controls from total gross production rates calculated with the above model.

Net H_2O_2 production rates were calculated from unamended bottles in all experiments as the difference in $[H_2O_2]$ from the start of the experiment to maximum $[H_2O_2]$ over the experimental time period. Net H_2O_2 decay rates were calculated from the spiked bottles as the difference in $[H_2O_2]$ at the start and end of the experiment. In the five experiments where the measured data did not fit the model, rates of H_2O_2 decay were exceptionally fast; within 3-6

hours H_2O_2 reached concentrations similar to those reached within 6-9 hours in the majority of experiments. In these experiments, net decay was calculated as the difference in $[H_2O_2]$ divided by the difference in time between the start and the time when $[H_2O_2]_{spike}$ approached $[H_2O_2]_{unamended}$ prior to subsequent increases in $[H_2O_2]$ concentrations (t=3 hours). These time windows for net H_2O_2 production and decay were chosen as a best representation of H_2O_2 production and decay that were not confounded by any subsequent net production and decay throughout the day.

Experiments were conducted in 2018 and 2019 to measure the impact of light exposure, large particles (i.e., large phytoplankton and *Microcystis* colonies), and biology on H_2O_2 production. The effect of light exposure was measured by including a set of spike and unamended bottles with whole water in dark 2L chocolate HDPE bottles. The impact of large particles was measured by including a set of spiked and unamended bottles with water filtered via a 105 µm nylon mesh (item # U-CMN-105-C, Component Supply Company, Inc., Sparta, TN) attached to PVC pipe via epoxy resin. For all experiments, 2L polycarbonate bottles were also filled with 0.22 µm filtered water to serve as abiotic controls. In 2017, duplicate unamended and spiked 0.22 µm filtered water controls were run in transparent, polycarbonate bottles (allowing light exposure and photochemical H_2O_2 production). In 2018 and 2019, dark 0.22 µm filtered water controls were also included. Because the average decay in replicate abiotic controls was not significantly different from zero for all but one date (19-Sep-17) in 2017, and were only 10 ± 0.06 % of whole water net decay rates on average, 0.22 µm filtered water decay controls were not performed in 2018 and 2019 due to sampling and measurement throughput.

Samples for DNA and H_2O_2 were collected by filtering 100-200 mL of water from each bottle through a 0.22 µm pore size PES filter, and collecting the last 50 mL of filtrate into a

centrifuge tube. The filter was saved for DNA extraction by freezing in a cryovial containing 1 mL RNAlater at -80 °C. The filtered H_2O_2 samples were stored in the dark at 4 °C until later analysis (within 4 hours of collection). H_2O_2 concentrations were measured using the chemiluminescent reaction of the conjugate base of H_2O_2 with 10-methyl-9-(p-formylphenyl)acridinium carboxylate trifluoromethanesulfonate (AE) in an FeLume flow injection analysis (King *et al.*, 2007). Matrix effects were corrected using standard additions of dilute H_2O_2 solution. The standard solution was made fresh to a nominal concentration of 200 µM the day prior to the experiments, stored at 4 °C, and wrapped in aluminum foil to protect it from light. The exact concentration of the H_2O_2 standard was determined with its absorbance at 240 nm in a 5 cm pathlength quartz cuvette and the H_2O_2 molar absorptivity of 38.1 $M^{-1}cm^{-1}$ (King *et al.*, 2007). While in transit for Environment Canada cruises, the standard was prepared ahead of time and kept frozen at -20 °C until the day of experiments.

5.3.3 Calculations of Experimental Light Conditions and In Situ Profiling

The opening of the outdoor tank used for experimental incubations was covered with neutral density 0.3 filter screen (product 209R, LEE Filters, Burbank, CA) to shade the bottles and mimic light conditions in the PAR range at approximately 1 meter depth (Figure S 5.2). To compare light conditions in the experimental bottles with *in situ* conditions, spectral irradiance profiles in the PAR range were measured approximately biweekly using a Sea-Bird HyperPro II profiler equipped with up- and down-facing HyperOCR radiometers measuring wavelengths 348 – 801 nm (bin size = 3.3 nm), plus an identical fixed surface radiometer to record sky conditions (Sea-Bird Scientific, WA, USA). Duplicate casts were performed on each date. Profiles in the UV wavelengths were collected using a compact optical profiling system for UV light in natural waters (UV C-OPS Biospherical Instruments Inc., CA, USA), which measures downwelling

irradiance at seven wavebands (305, 313, 320, 340, 380, 395, 412 nm). Replicate C-OPS casts were collected at 5 nearshore stations on 25 Sept. 2017. Both profilers were deployed on the sunny side of the vessel and allowed to free-fall through the water column to avoid the vessel shadow. In order to minimize disturbance of the water column, profiles were collected after the vessel had been drifting without power for several minutes. Data were processed using ProSoft (Sea-Bird Scientific) proprietary software. Attenuation coefficients ($K_{d,\lambda}$) for 305-801 nm were calculated from the profiles using the following relationship between irradiance and depth:

$$4. \quad I_{\lambda,z} = I_{\lambda,0} * e^{-(K_{d,\lambda} * z)}$$

Where $I_{\lambda,z}$ is the down-welling irradiance at depth (z) for a given wavelength (λ), and $I_{\lambda,0}$ is surface irradiance for a given wavelength. The above equation was rearranged into the linear form:

$$5. \quad \ln(I_{\lambda,z}) = \ln(I_{\lambda,0}) - K_{d,\lambda} * z$$

so that the slope of the regression of log transformed irradiance vs depth yields $K_{d,\lambda}$. To compare light conditions *in situ* with those in the experiments, the depth at which the fraction of light transmitted at each wavelength ($\frac{I_{\lambda,z}}{I_{\lambda,0}}$) equals the fraction of light transmitted through the neutral density screening and polycarbonate bottles was calculated using average $K_{d,\lambda}$ values and equation 4. PAR conditions during the experiments were representative of light levels within the top meter of western Lake Erie based on replicate Sea-Bird casts; however, UV conditions in the experiment were lower than surface water conditions. Light transmission of the polycarbonate and neutral density filter was measured using a diffuse reflectance accessory (Cary 5000, Varian Inc., CA, USA).

5.3.4 Chlorophyll a, CDOM, DIC, Nutrient, Respiration, and Primary Production Measurements

Samples for chlorophyll *a* concentration were collected at the start and end of each experiment by filtering 50 mL of water from each bottle with 0.22 µm PES filters. The filters were stored frozen at -20 °C with the biomass folded inwards until extraction in the lab. Chlorophyll *a* was extracted from the collected biomass by suspending the filters in 8 mL of dimethylformamide in plastic 15 mL centrifuge tubes followed by a 45 minute incubation in a 65 °C water bath. After the incubation, the samples were agitated via vortexing at speed setting 7 and centrifuged for 10 minutes at 10,000 x*g* at 25 °C. Chlorophyll *a* fluorescence was measured by decanting dimethylformamide into clean borosilicate glass cuvettes, and measuring the fluorescence in a 10-AU field fluorometer (Turner Designs, CA, USA) using excitation/emission wavelengths 436/680 nm. Clean filters were included during each round of extractions as blanks, and extractions were performed in the dark to prevent degradation of extracted chlorophyll. There were no significant differences for chlorophyll concentration in the start and end of all but one experiment on 31 May 2017, so chlorophyll concentrations were averaged from both time points.

Samples for CDOM absorbance were taken from each 0.22 µm filtered water bottle (n=4) at the start of each experiment and measured following procedures described in (Cory *et al.*, 2016). Samples for dissolved inorganic carbon (DIC) concentration were taken from each whole water bottle at the start of each experiment and killed with 1% $HgCl_2$ in air-tight, pre-combusted 12 mL borosilicate exetainer vials. The samples were stored at 4 °C until analysis using a DIC analyzer (Apollo SciTech, DE, USA).

Concentrations of soluble reactive phosphorus (SRP), total dissolved nitrite+nitrate (NO_2^- +NO_3^-), and ammonium (NH_4^+) in 0.22 µm filtrate samples were measured via segment flow

analysis on a Seal AA3 AutoAnalyzer with AutoSampler (SEAL Analytical, WI, USA) using method-specific reagents. SRP was measured using the molybdenum blue technique (Murphy & Riley, 1962). Briefly, ammonium molybdate and antimony potassium tartrate react with orthophosphate in an acid medium to form an antimony-phosphomolybdate complex. The complex is then exposed to ascorbic acid, which produces a blue complex and the absorbance is measured at 880 nm. NO_2^-+NO_3^- was measured by passing the water sample through a cadmium reduction column to reduce nitrate to nitrite, mixing with sulfanilamide followed by N-(1-napthyl)ethylenediamine to form a red azo dye, the absorbance of which is read at 520 nm (Wood *et al.*, 1967). Ammonium was measured via a variant of the Berthelot reaction (Ivančič & Degobbis, 1984), where dichloro isocyanuric acid, phenol, and sodium nitroprusside are mixed with NH_4^+ in the sample under basic conditions to form a blue iodophenol complex and the absorbance is measured at 630 nm.

Total phosphorus (TP) and total dissolved phosphorus (TDP) were measured in whole water and 0.22 μm filtered water samples, respectively, using a QuAAtro Auto Analyzer and AutoSampler (SEAL Analytical, WI, USA). Samples were treated with an acidic potassium persulfate digestion, which converts organic phosphate groups to free phosphate ions that are subsequently measured using the molybdenum blue method described above.

In 2018 and 2019, respiration in whole water and 105 μm filtered water was measured by incubating the water for approximately 24 hours in the outdoor tank alongside controls killed with 1% $HgCl_2$ in air-tight, pre-combusted 12 mL borosilicate exetainer vials. The exetainer vials were protected from light by wrapping in 2 layers of aluminum foil. Respiration was measured as the dissolved oxygen consumption relative to the killed controls using a membrane

inlet mass spectrometer (Cory *et al.*, 2014). From total DIC concentration and pH data, $H_2CO_3^*$, HCO_3^-, and CO_3^{2-} concentrations were calculated.

Primary production in whole and 105 µm filtered water was measured as the uptake of ^{14}C in light relative to a dark control by incubating 20 mL of water in triplicate glass scintillation vials in a Precision 818 Plant Growth Chamber (Thermo Scientific, MA, USA) for 1 hour. The vials were rested on their side to prevent shading from the vial caps. The temperature was held at water temperature at the time of sample collection. Light levels were kept at ~ 45 % of those measured at noon on the day of measurements using a LiCor QUANTUM PAR sensor attached to a LI-250A light meter (Li-Cor Biosciences, Lincoln, NE, USA). Light levels in the incubator were adjusted by covering the lamp with neutral density screen and adjusting the distance between the vials and the lamp. The light source was a King Plus 1000W full spectrum LED lamp (Shenzheng King Lighting Co., Ltd, Shenzhen, China). The ^{14}C was added as sodium bicarbonate to a final concentration of 0.1 µCi/mL. After the incubation, 250 µL aliquots were sampled from each bottle and filtered onto a 25 mm Whatman GF/F via vacuum filtration. Any remaining inorganic ^{14}C was removed by placing the filters in a new 20 mL glass scintillation vial with 250 µL of 0.5 N HCl. The vials were uncapped and loosely covered with foil while the HCl was allowed to completely dry for 2-3 days. Once dry, the filters were resuspended in 10 mL of Scinti-Safe scintillation cocktail and allowed to sit overnight before measuring activity in counts per minute (CPM) using a liquid scintillation counter. CPM was converted to mol C/L/hr as described previously (Knap *et al.*, 1996).

5.3.5 DNA Extraction, Sequencing, and Bioinformatics Analysis

To measure microbial community composition, DNA was extracted from the filters collected from each bottle at the beginning (T=0) of each experiment using a Qiagen DNeasy

Blood & Tissue Kit with QIAshredder columns (QIAGEN, MD, USA). The extraction protocol is included as a supplemental file. For absolute quantification of sequence data, genomic DNA from *Thermus thermophilus* strain DSM 7039 was added to the samples after the cell lysis step of the extraction as an internal standard. *Thermus thermophilus* DNA was obtained from the American Type Culture Collection (ATCC; product number BAA-163D-5). The internal standard was added as ~ 1 % of DNA yield, which was estimated based on an empirically determined relationship between total mass of chlorophyll *a* on the filter and DNA yield. DNA yields were measured with Quant-iT Picogreen dsDNA Assay Kit (Invitrogen, Carlsbad, CA). The true percentage of the internal standard was 0.72 ± 0.37 % of total DNA yield on average.

The V4 region of the bacterial 16S rRNA gene was amplified using a dual indexed primer set (Kozich *et al.*, 2013), and amplicon sequencing was performed using Illumina MiSeq V2 500 cycle chemistry (Illumina cat# MS102-2003) at the University of Michigan Microbial Community Analysis Core following their SOP (Schloss & Bishop, 2019). Forward and reverse reads were quality screened to remove sequences below 250 bases and trimmed to Q20 using the BBDuk tool in BBTools (Bushnell, 2018). Following trimming, overlapping forward and reverse reads were assembled into contigs, aligned, screened for chimeras, and clustered into operational taxonomic units (OTUs) using MOTHUR v. 1.43.0, following the SOP as of February 2020 (Kozich *et al.*, 2013). OTU clustering was performed using a 97 % similarity cutoff with the OptiClust algorithm (Westcott & Schloss, 2017). Contigs were aligned with the align.seqs function in MOTHUR, and taxonomy was assigned using the Wang method (Wang *et al.*, 2007). The Silva v. 138 SSU database (Pruesse *et al.*, 2007) was used as the reference to align and classify contigs. The absolute abundance of each OTU per volume of lake water was estimated from the recovery of the internal standard as described in (Lin *et al.*, 2019). All OTUs classified

as *Thermus* were removed from downstream analysis. The raw sequence data is available in NCBI under BioProject PRJNA646259.

5.3.6 Statistical Analyses

Bray-Curtis dissimilarities between microbial communities and Principle Coordinates Analysis (PCoA) were computed using the R package Vegan v. 2.5-6 (Oksanen *et al.*, 2013). Stepwise linear regression analyses between environmental and biological parameters and the score of microbial communities on PCoA axes were computed using the stepAIC function in the R package boot.stepAIC v. 1.2-0 (Rizopoulos, 2009). Models were chosen for each PCoA axis by initially including all environmental parameters and removing variables that did not significantly increase the Bayesian Information Criterion (BIC). A bootstrap analysis was performed to assess the stability of each variable in the final regression models. Regressions were performed both with and without samples in which gross H_2O_2 production and decay could be calculated. Linear regression and other standard calculations were made using base R v. 4.0.2.

Random forest regression models were generated to predict gross and net H_2O_2 production rates with bacterial OTU abundances using Scikit-learn v. 0.23.1 (Pedregosa *et al.*, 2011). In the model for gross production, samples missing values for gross production and decay were excluded. Hyperparameters for each model were tuned with a grid search using k-fold cross validation (k = 4 for both models). Hyperparameters that yielded the highest R^2 score across each training set generated during cross validation were used for the final model. OTUs with maximum abundances below 500 reads/mL were left out of the analysis, because important OTUs below this abundance threshold were often found to be near the limit of detection based on 95 % confidence intervals on the average abundance. The final model for net H_2O_2 production had the following hyperparameters: number of decision trees (n_estimators) = 4000, number of

randomly chosen features to consider when splitting tree branches (max_features) = 40 % of total features, minimum number of samples required to split an internal node in a decision tree (min_samples_split) = 4. The final model for gross biotic H_2O_2 production had the following hyperparameters: n_estimators = 500, max_features = 70 % of total features, min_samples_split = 3. The importance of each OTU in the random forest models was calculated as the permutation importance, or the average decline in model R^2 when the abundance of each OTU is randomly shuffled over a series of permutations (n = 10).

5.4 Results

5.4.1 H_2O_2 Concentrations, Net H_2O_2 Production, and Modeled Gross H_2O_2 Production

H_2O_2 concentrations during the experiments were within the range of concentrations observed in coastal marine (Zika *et al.*, 1985) and freshwaters (Häkkinen *et al.*, 2004; Dixon *et al.*, 2013; Ueki *et al.*, 2020), including Lake Erie (Cory *et al.*, 2016). In the majority of the bottle experiments, hydrogen peroxide concentrations increased during the day, peaking between 11:00 and 17:00 EST (Figure S 5.3). H_2O_2 concentrations ranged from 16-1540 nM during the day in all unamended incubations (Appendix 2), with peak H_2O_2 concentrations ranging from 50-1540 (mean 420 ± 63 nM).

Net whole water H_2O_2 production rates ranged from -14 – 165 nM/hr (mean 30 ± 16 nM/hr) in the light (Figure 5.1) and -5 - 0.7 nM/hr in the dark (Figure 5.2). Net 0.22 μm filtered water H_2O_2 production rates were similar to those in whole water, ranging from 4 – 188 nM/hr (Figure 5.1, mean 30 ± 16 nM/hr). On average, net H_2O_2 production rates in whole water and 0.22 μm filtered water were not significantly different ($p = 0.36$, Welch's two-sided T-test), and were not significantly different in 26 experiments (76 % of total, n = 34). Net H_2O_2 production was significantly lower in whole water than in 0.22 μm filtered water in 6 experiments (18 % of

total, $p < 0.05$, Welch's two-sided T-test), and only significantly higher in whole water in one experiment (Sept 14, 2018).

Rates of gross H_2O_2 production estimated using paired unamended and H_2O_2 spiked bottles (see methods) ranged from 14-432 (mean 109 ± 36 nM/hr, Appendix 2) in the light and 3-31 nM/hr in the dark (mean 11 ± 3 nM/hr, Appendix 2). The gross production rates in both the light and dark are within the range of gross H_2O_2 production rates previously reported in freshwater systems (Vermilyea *et al.*, 2010a; Dixon *et al.*, 2013; Marsico *et al.*, 2015). Gross H_2O_2 production rates were 2-21 times higher than corresponding net production rates on days when net production was observed (Table 5.1). Gross biotic H_2O_2 production was calculated as the difference in total gross H_2O_2 production and observed H_2O_2 production in 0.22 μm filtered water and ranged from 9-244 nM/hr in the light (mean 70 ± 23 nM/hr) and 3-28 nM/hr in the dark (mean 10 ± 3 nM/hr, Figure 5.2). Biotic production accounted for 44 - 94 % of total gross production in the light (mean 66 ± 5 %) and 90 - 100% of total gross production in the dark (mean 99 ± 1 %). On average, gross biotic production in the dark was 35 ± 3 % of that in the light. There were no significant differences in gross biotic and net H_2O_2 production rates in whole and 105 μm filtered water (Figure 5.3).

Net whole water H_2O_2 decay rates ranged from 51 – 397 nM/hr (Figure 5.1, mean 110 ± 25 nM/hr). On average, net H_2O_2 decay rates in 0.22 μm filtered water were significantly lower than those in whole water ($p = 6.3 \times 10^{-9}$, Welch's two-sided T-test), ranging from 0-54 nM/hr (mean 13 ± 6 nM/hr). In 0.22 μm filtered water, net H_2O_2 decay was only observed in spiked bottles, and not significantly different from zero on any date ($p > 0.05$, Welch's one sample T-test). Whole water net H_2O_2 decay rates in spiked bottles had a weak positive correlation with net

H_2O_2 production rates in the paired unamended bottles, and absolute decay constants ($k_{loss,H2O2}$) had a weak positive correlation with total gross H_2O_2 production rates (Figure 5.4).

5.4.2 Failed Model Assumptions and Uncertainty in Gross H_2O_2 Production Rates

Gross biotic H_2O_2 production in the light could not be calculated during experiments conducted on five dates because the change in H_2O_2 concentrations over time did not conform to the underlying assumptions in the spike-decay model, suggesting that the model assumptions were invalid in these waters. The spike-batch incubation model assumes that PH_2O_2 and k_{loss} are both constant over time (see methods); however, experiments with poor model fit had midday increases and decreases H_2O_2 concentration at different time periods during the incubation which suggest that one or both model parameters changed with time (Figures S 5.4-S 5.10). The model error was related to chemical and biological parameters. Error sum of squares in model fit was significantly correlated with chlorophyll *a* concentrations, primary production rates, and CDOM absorbance (Figure S 5.11), and experiments that had poor model fit had significantly higher chlorophyll *a* concentration, CDOM absorbance, and pH and significantly lower $H_2CO_3^*$ concentration and areal UVA over the experimental period (Figure 5.5). Exclusion of bottles with poor model fit resulted in stronger correlation between the error sum of squares in model fit and CDOM absorbance was stronger (Figure S 5.11).

In experiments with poor model fit, H_2O_2 concentrations in the spike bottles were rapidly decayed, approaching the concentrations in the control bottles within 3-6 hours (Figures S 5.4-S 5.10). In three of these experiments, the majority of the decay took place within the first 3 hours. The rapid decay within 3 hours is in contrast to most other experiments, where H_2O_2 concentrations in the spiked bottles either reached concentrations in the control between 6-9 hours after the addition of the spike, or not at all (Appendix 3). This result suggests that gross

H_2O_2 decay rates were faster in these experiments and that the three-hour sampling window was inadequate for capturing the H_2O_2 decay curve in these experiments, which may have contributed to poor model fit. Despite the initial decline in the spike concentrations, midday H_2O_2 concentrations increased to levels equal to or higher than the spike in two of these experiments (Figures S 5.4 & S 5.6), suggesting high gross H_2O_2 production rates midday. Higher variation in H_2O_2 concentrations between replicates was also observed in these experiments, which may be explained by higher H_2O_2 decay during sample processing.

5.4.3 Correlations Between H_2O_2 Production and Chemical and Biological Parameters

CDOM absorbance was significantly correlated with both gross biotic H_2O_2 (Figure 5.6) and net H_2O_2 production rates (Figure 5.7). The correlation between CDOM absorbance and gross biotic H_2O_2 production was weaker than the correlations with chlorophyll *a* concentration, respiration rate, and primary production rates, although the correlation with respiration and primary production was driven by one data point (Figure 5.6). However, net H_2O_2 production rates were also correlated with these parameters and were supported by multiple data points (Figure 5.7). There were also significant correlations between net H_2O_2 production and phosphorus and nitrate concentrations, although the R^2 values were lower than the regressions with CDOM, chlorophyll *a*, respiration, and primary production (Figure S 5.12).

Dark biotic production rates in Lake Erie were not significantly correlated with chlorophyll *a* concentration, respiration rate, primary production rates, nor any water chemistry measurements (Appendix 4). The difference between gross biotic production in the light and dark bottles was significantly correlated with respiration rates, primary production rates, and CDOM absorbance; however, the correlation between the difference in light and dark biotic

H_2O_2 production and primary production rates and CDOM absorbance were driven by one data point (Figure S 5.13).

5.4.4 Correlations Between H_2O_2 Production and Microbial Community Dissimilarity and OTU Abundances

Net H_2O_2 production rates, $k_{loss,H2O2}$, and maximum H_2O_2 concentrations were significantly correlated with microbial community composition (Tables 5.2 and 5.3). In some cases, H_2O_2 production and decay were among the best predictors of PCoA score. In the analysis with gross production rates, absolute K_{loss} was the most significant predictor of ordination along PCoA1, and maximum H_2O_2 concentration was a highly significant predictor for PCoA3 with high bootstrap support (Table 5.2). Gross biotic H_2O_2 production rate was also significantly correlated with PCoA1 score and had higher bootstrap support than k_{loss}. However, nitrate and chlorophyll *a* concentration had high bootstrap support and p-values comparable to gross biotic H_2O_2 production, which makes interpretation of the correlations with this axis difficult. In the analysis with net H_2O_2 production and decay, PCoA3 was significantly correlated with net H_2O_2 decay rate and maximum H_2O_2 concentrations, which also had the strongest bootstrap support along this axis (Table 5.3). Net H_2O_2 production rates were also significantly correlated with PCoA3 score, although bootstrap support was lower, suggesting that H_2O_2 dynamics are related to differences in microbial community composition along this axis.

The random forest models using OTU abundances had better fits to the data than linear regressions with both chlorophyll *a* concentration and CDOM absorbance when predicting both gross biotic and net H_2O_2 production rates (Table 5.4). Random forest models increased the R^2 values by 197 and 95 % for net H_2O_2 production and by 147 and 345 % for gross biotic H_2O_2 production when compared to regression models for both chlorophyll *a* and CDOM, respectively. Average R^2 values from cross validation were also higher than chlorophyll *a*

regression models for both gross and net rates, but only higher than the CDOM regression models for the gross biotic H_2O_2 production rates. In both models, the majority of the OTUs only resulted in minor reductions in R^2 values during the permutation tests (Tables 5.5 and 5.6); only three OTUs across both models reduced R^2 values by ~ 0.1 or more (OTU 123 Unclassified Comamonadaceae, OTU 311 *Flavobacterium*, and OTU 822 *Lacihabitans*). Of the three OTUs with relatively higher impacts on random forest R^2, only one (Unclassified Comamonadaceae OTU 123) was ever present at high abundance (Figure 5.9).

5.5 Discussion

5.5.1 Biological Production was a Major Source of H_2O_2 During the Experiments

While not always the predominant source, modeled gross biological production was a substantial source of H_2O_2 (> 40 % of total gross production) in all experiments. While complications with estimating gross biological H_2O_2 production (discussed in further detail below) create hidden uncertainty in the relative proportion of biological versus photochemical in these experiments, several additional lines of evidence support that substantial biological H_2O_2 production occurred in the bottle experiments. Total net H_2O_2 production rates in whole water were not significantly different from production rates measured in 0.22 µm filtered water despite zero or low rates of H_2O_2 decay in 0.22 µm filtered water (Figure 5.1), which indicates that total H_2O_2 production is masked by decay in whole water. Therefore, gross whole water H_2O_2 production rates in western Lake Erie are higher than production measured in 0.22 µm filtered water and suggests a particle dependent source of H_2O_2. Such particle-dependent H_2O_2 production has been previously attributed to microorganisms (Dixon *et al.*, 2013; Marsico *et al.*, 2015; Palenik & Morel, 1988; Vermilyea, Paul Hansard*, et al.*, 2010). Further supporting that H_2O_2 production was attributed to biological processes in the experiments, both gross biotic and

total net H_2O_2 production rates were correlated with chlorophyll *a* concentration, respiration rate, and primary production rate (Figures 5.6 & 5.7), which suggests that H_2O_2 production in western Lake Erie increases with phytoplankton biomass and microbial growth rates. This observation is consistent with previous observations that the highest H_2O_2 concentrations in western Lake Erie precede peaks in chlorophyll *a* and respiration rate (Cory *et al.*, 2016).

The observation that, on average, H_2O_2 production during the experiments is predominantly biological adds more support to the previous hypothesis that elevated H_2O_2 concentrations during cyanobacterial blooms are primarily from biological sources (Cory *et al.*, 2016). However, some aspects of the experimental design prevent a quantitative assessment of the relative contribution of biological and photochemical sources of H_2O_2 *in situ*. First, exclusion of UV wavelengths in the experiment biased biological production over photochemical production as UV wavelengths have the highest H_2O_2 yield per photon (Powers & Miller, 2014). Second, model assumptions failed in some waters. While poor model fit may be attributed to inadequate sampling of rapid decay curves in some experiments (Figures S 5.4-S 5.10), midday peaks in H_2O_2 concentrations (Figure S 5.6-S 5.10) and lags in H_2O_2 accumulation (Figure S 5.4 & S 5.5) indicate that H_2O_2 production rates changed over time in some experiments with poor model fit. Supporting this interpretation, higher amplitude diel peaks in H_2O_2 concentration were previously attributed to high gross H_2O_2 decay coinciding with decreasing photochemical production rates as solar irradiation decreased with solar zenith angle (Ueki *et al.*, 2020). Furthermore, photochemical production of H_2O_2 should show complex dynamics throughout the day as solar irradiation increases with sunrise, decreases with sunset, and changes with variation in cloud cover throughout the day. Indeed, the experiments with poor model fit had significantly higher CDOM absorbance and significantly lower UVA irradiance than the other experiments

where the error in model fit was lower (Figure 5.5), all dark experiments fit the model (Appendix 2), and CDOM absorbance became a significant predictor of model error when the poorly fit experiments were excluded from the regression (Figure S 5.11). Thus, experiments with higher photochemical production rates or larger changes in light exposure throughout the incubation period may have larger error in estimates of biological H_2O_2 production.

While photochemical production likely prevented accurate measurement of gross H_2O_2 production in some experiments, the conclusion that biological production was substantial is still supported. Biological mechanisms may have also contributed to changing PH_2O_2 over the diel cycle. This is supported in that the experiments with poor fit to the model had significantly higher chlorophyll *a* concentration (Figure 5.5), and production of extracellular O_2^- (a precursor to H_2O_2) by eukaryotic phytoplankton (Diaz & Plummer, 2018; Diaz *et al.*, 2018; Schneider *et al.*, 2016) and cyanobacteria (Diaz & Plummer, 2018; Hansel *et al.*, 2016) increases with light exposure. While CDOM absorbance was also correlated with gross biotic H_2O_2 production, the correlation strength was weaker than correlations with chlorophyll *a* concentration, respiration, and primary production (Figure 5.6), and OTU abundances could describe more of the variation in gross biotic H_2O_2 production than CDOM absorbance (Table 5.4). Furthermore, patterns in net H_2O_2 production and H_2O_2 decay are independent of the model, yet still support the presence of a particle-dependent source that is related to chlorophyll *a* concentration, respiration rates, and primary production rates. Thus, while the relative contribution of biological and photochemical sources to total H_2O_2 production remains uncertain, the experiments support that biological controls on H_2O_2 production are substantial during western Lake Erie cyanobacterial blooms.

5.5.2 Biological H_2O_2 Production is Light-Dependent but not Directly Attributed to Large Phytoplankton and Microcystis Colonies

Despite the correlation between H_2O_2 production rates, chlorophyll *a* concentration, and primary production rates (Figures 5.6 & 5.7), and that much of the biotic H_2O_2 production was light-dependent (Figure 5.2), the production cannot be directly attributed to *Microcystis* or large phytoplankton. While *Microcystis* 16S rRNA read abundance was significantly correlated with net H_2O_2 production rates, it was not correlated with gross biotic H_2O_2 production rates (Figure S 5.14). Furthermore, both gross biotic and net H_2O_2 production rates did not significantly decrease with filtration of particles 105 µm and greater (Figure 5.3), which reduced *Microcystis* 16S rRNA read abundance by 60 ± 10 % and chlorophyll *a* concentrations by 50 ± 7 % on average (Figure 5.8). The interpretation that H_2O_2 production is not directly attributed to *Microcystis* is further supported by the random forest regression models, as *Microcystis* OTU abundance was not a significantly important model feature when predicting either gross biotic H_2O_2 or net H_2O_2 production rates (Tables 5.5 & 5.6). Therefore, biological H_2O_2 production is primarily from free-living bacteria or smaller nano- and microplankton. Indeed, the abundances of the most important OTUs in the random forest models were not significantly different in whole and 105 µm filtered water (Appendix 5), which mirrors H_2O_2 production rates in whole vs. 105 µm filtered water.

Although it is unlikely that large *Microcystis* colonies are directly responsible for the H_2O_2 production, the evidence for light-dependent biotic production and the significant correlations between H_2O_2 concentration and chlorophyll *a* concentration suggest that the variation in biotic H_2O_2 production during Lake Erie cyanobacterial blooms is connected to photosynthesis. One mechanism that may reconcile the apparent relationship with photosynthesis with the lack of difference between H_2O_2 production in whole water and 105 µm filtered water is

the respiration of algal exudates. Cyanobacteria and other phytoplankton are known to excrete a variety of organic carbon compounds as a product of photosynthesis or photorespiration (Hellebust, 1965; Beliaev *et al.*, 2014). Of these, glycolate is a major exudate in many species of cyanobacteria and algae, including *Microcystis* (Cheng *et al.*, 1972; Renström & Bergman, 1989; Barchewitz *et al.*, 2019) and can be up to 58 % of the excreted photosynthate in cyanobacterial mats (Bateson & Ward, 1988). Excretion of glycolate and other photosynthates is light-dependent (Hellebust, 1965; Han & Eley, 1973; Bateson & Ward, 1988; Renström & Bergman, 1989). Plants process glycolate in the photorespiratory cycle by oxidizing it to glyoxylate with the enzyme glycolate oxidase, and a by-product of this reaction is H_2O_2 (de Duve, 1969; Rojas *et al.*, 2012). While some microbes use an alternative enzyme to oxidize glycolate that does not produce H_2O_2 (Codd *et al.*, 1969; Nelson & Tolbert, 1970; Lord, 1972; Eisenhut *et al.*, 2006; Lau & Armbrust, 2006; Lau *et al.*, 2007; Hackenberg *et al.*, 2011; Kern *et al.*, 2011; Aboelmy & Peterhansel, 2014; Schmitz *et al.*, 2017), some cyanobacteria, green algae, and heterotrophic bacteria possess homologs of H_2O_2-producing lactate oxidases that have promiscuous glycolate oxidase activity (Xu *et al.*, 1996; Seki *et al.*, 2004; Tong *et al.*, 2007; Hackenberg *et al.*, 2011; Kern *et al.*, 2011). In addition to glycolate, the oxidation of other photosynthates such as lactate (Beliaev *et al.*, 2014) and amino acids (Hellebust, 1965; Tolbert, 1979; Beliaev *et al.*, 2014) could also produce H_2O_2 through L-amino acid oxidase (Palenik & Morel, 1990; Geueke & Hummel, 2002; Lucas-Elío *et al.*, 2006; Tong *et al.*, 2008) and lactate oxidase activity (Xu *et al.*, 1996). Therefore, photosynthate excretion by cyanobacteria may induce H_2O_2 production in some heterotrophic bacterial taxa, and link H_2O_2 production in free-living heterotrophic communities to photosynthesis. Further supporting this interpretation, respiration rates had the

most robust correlation with the difference between gross biotic production rates in the light and dark (Figure S 5.13).

We cannot rule out an alternative hypothesis that smaller eukaryotic phytoplankton or single-celled cyanobacteria are sources of H_2O_2 in western Lake Erie. O_2^- production has been documented across a diverse array of heterotrophic bacteria and phytoplankton (Rose *et al.*, 2008; Diaz *et al.*, 2013; Hansel *et al.*, 2016; Schneider *et al.*, 2016). O_2^- is a precursor to H_2O_2, and the conversion of O_2^- to H_2O_2 can occur by reactions with microbial enzymes (Zinser, 2018a), dissolved transition metal complexes (Voelker *et al.*, 2000; Rose & Waite, 2006; Wuttig *et al.*, 2013), dissolved organic matter (Heller & Croot, 2010) and uncatalyzed dismutation (Zafiriou, 1990). While this process occurs in the dark (Diaz *et al.*, 2013), light exposure increases O_2^- production by eukaryotic phytoplankton (Schneider *et al.*, 2016; Diaz & Plummer, 2018; Diaz *et al.*, 2018; Diaz *et al.*, 2019) and cyanobacteria (Hansel *et al.*, 2016; Diaz & Plummer, 2018). Because biotic H_2O_2 production was higher in light exposed bottles, this may indicate that H_2O_2 production in western Lake Erie is the result of extracellular superoxide production by phytoplankton cells in the < 105 μm size fraction.

While only measurements of dark O_2^- production for *Microcystis* exist currently (Fujii *et al.*, 2011), published O_2^- production rates by *Trichodesmium* exposed to light cannot explain the H_2O_2 production in the bottle experiments (Appendix 6). However, diatoms produce more O_2^- than cyanobacteria (Sutherland *et al.*, 2020), and if we assume that superoxide production in Lake Erie equals the maximum dark O_2^- production rates by diatoms reported in Sutherland et al. 2020, and that superoxide production by diatoms and cyanobacteria increases by a factor of 2-8 with light exposure as reported previously (Schneider *et al.*, 2016), direct O_2^- production by diatoms could account for the H_2O_2 production on some dates in 2017 and 2018 when diatom

abundance was high (Kharbush *et al.*, 2019). However, these estimates assume no oxidative loss of superoxide in western Lake Erie, which does not result in H_2O_2 formation (Lee-Ruff, 1977; Petasne & Zika, 1987; Fujii *et al.*, 2010; Heller & Croot, 2010) and can be a significant proportion of total superoxide decay in aquatic environments (Petasne & Zika, 1987; Andrews *et al.*, 2000). Increasing O_2^- production with light exposure only occurred at low colony densities in *Trichodesmium* (Hansel *et al.*, 2016) and O_2^- production rates decrease with increasing cell densities (Diaz *et al.*, 2019; Hansel *et al.*, 2019), which is in contrast to the relationship between H_2O_2 production rates and chlorophyll *a* concentration observed during the experiments. While some of the H_2O_2 production in Lake Erie is likely derived from extracellular O_2^- production by both phytoplankton and bacteria, our data suggests other potential sources of H_2O_2 during western Lake Erie cyanobacterial blooms. Future studies that quantify light and dark superoxide production in *Microcystis,* freshwater diatoms*,* and natural western Lake Erie communities, H_2O_2 production from respiration of phytoplankton exudates, and the relationship between superoxide production, superoxide dismutation and hydrogen peroxide production during Lake Erie cyanobacterial blooms are required to fully understand the relative importance of biotic O_2^- production as a source of H_2O_2 in Lake Erie.

5.5.3 H_2O_2 Production is Related to Microbial Community Composition

The PCoA axis with the most robust correlations with H_2O_2 production and decay rates explained a relatively low amount of the community dissimilarity (Tables 5.2 & 5.3), which suggests that H_2O_2 dynamics do not shift as strongly with microbial community composition when compared with other factors such as pH and chlorophyll *a* concentration. However, the correlations between net H_2O_2 production rates, H_2O_2 decay rates, and maximum H_2O_2 concentrations with microbial community dissimilarity along PCoA3 and OTU abundances

supports that H_2O_2 dynamics influence, or are influenced by, microbial community composition. The relationship between microbial community dissimilarity and H_2O_2 production rate must be attributed to shifts in the populations of multiple bacterial taxa rather than a few select species, because no single OTU had a large impact on the random forest model performance (Tables 5.5 and 5.6).

While the data support that different microbial communities are associated with different H_2O_2 production and decay dynamics, it is impossible to determine whether the effect is due to shifts in taxa with differing sensitivities to H_2O_2 or due to shifts in taxa with different H_2O_2 production and decay rates with this data. There are large variations in the production and decay rates of both H_2O_2 and O_2^- between microbial taxa (Bayer *et al.*, 2019; Bond *et al.*, 2020; Diaz *et al.*, 2013; Diaz & Plummer, 2018) and within a single taxon at different growth phases (Diaz *et al.*, 2019; Gonzalez-Flecha & Demple, 1997; Hansel *et al.*, 2019). However, there are also large differences in sensitivities between microbial taxa due to differences in the presence and efficiency of genes that decompose H_2O_2 (Kim *et al.*, 2016; M. Kim *et al.*, 2019; S. Kim *et al.*, 2019; Morris *et al.*, 2008). The abundances of two of the more important OTUs in the random forest models (Unclassified Comamonadaceae OTU 123 and *Flavobacterium* OTU 311) were significantly correlated with gross biotic H_2O_2 production rates (Figure 5.9), suggesting that they may be high H_2O_2 producing organisms. Information on the capacity of these taxa for H_2O_2 production is lacking, but H_2O_2-producing enzymes have been isolated from *Flavobacterium* species (Koga *et al.*, 1997). Many of the important OTUs that were positively correlated with H_2O_2 production during the experiments are from the phyla Bacteroidetes and Proteobacteria, which were more resistant to large additions of H_2O_2 representative of H_2O_2 additions used to control harmful cyanobacterial blooms (Lusty & Gobler, 2020). In addition, several OTUs were

negatively correlated with H_2O_2 production rates, indicating that these taxa are more sensitive to H_2O_2 and that the growth of these organisms is disfavored when H_2O_2 production is high (Figure 5.10), which supports the hypothesis that the relationship between H_2O_2 production and microbial community structure is due in part to the differing sensitivities of microbes to H_2O_2. While further experiments are required to determine the exact mechanisms behind the association between natural H_2O_2 production and decay dynamics and microbial community composition and the abundances of specific bacteria species, this study is the first to show that natural H_2O_2 production and decay rates are related to microbial community composition.

5.5.4 Absolute Decay Rate Constants are Correlated With Gross H_2O_2 Production

Absolute decay rate constants were significantly correlated with total gross H_2O_2 production rates (Figure 5.4), as previously observed in dark incubations with sea water (Vermilyea *et al.*, 2010b), which indicates that microbial decomposition of H_2O_2 increases with H_2O_2 production rates. This may suggest that microbes increase their production of catalase and peroxidase enzymes, and by extension their H_2O_2 degradation capability, as a defense against stress caused by elevated H_2O_2 production. Supporting this interpretation, diel regulation of genes encoding catalase and peroxidase enzymes has been observed in marine microbial communities (Morris *et al.*, 2016), as well as up-regulation of catalase and peroxidase genes in response to increasing concentrations of intracellular H_2O_2 concentrations (Gonzalez-Flecha & Demple, 1997) or additions of H_2O_2 to bacteria cultures (Loewen *et al.*, 1985; Daniel *et al.*, 2019). Alternatively, if the relationship between H_2O_2 production rates and microbial community composition is underpinned by changes in the sensitivity of the microbial communities to H_2O_2, increasing H_2O_2 decay rates with H_2O_2 production rate could be attributed to higher H_2O_2 production rates favoring bacteria taxa that are more efficient H_2O_2 degraders. Indeed, the ability

to degrade H_2O_2 varies widely across microbial taxa (Morris *et al.*, 2011; Kim *et al.*, 2019a; Kim *et al.*, 2019b). To test these hypotheses, future studies should examine how the abundance and expression of catalase and peroxidase genes changes with total H_2O_2 production rates. Regardless of the mechanism, the data support that increasing H_2O_2 production rates lead to higher H_2O_2 decomposition rates in order to mitigate oxidative stress from H_2O_2 accumulation.

5.6 Conclusions

In summary, the data indicate that biological H_2O_2 production is an important source of H_2O_2 during western Lake Erie cyanobacterial blooms. In addition, this work provides evidence that biological H_2O_2 production is related to photosynthesis, which could be explained by respiration of phytoplankton exudates by free-living bacteria or direct production by nano- and microplankton cells smaller than 105 µm diameter. Differences in H_2O_2 production are explained by shifts in the abundance of multiple bacteria taxa.

Because filtration of large *Microcystis* colonies, which contained a large proportion of *Microcystis* cells during the experiments, did not impact H_2O_2 production rates, the H_2O_2 produced cannot be attributed to large *Microcystis* colonies. Therefore, *Microcystis* may not only be impacted by H_2O_2 decomposition by the surrounding bacterial community as discussed in Chapter 2 and elsewhere (Kim *et al.*, 2019a) but also by community-wide H_2O_2 production. Indeed, H_2O_2 producing taxa are thought to influence the proliferation of other microbes in the human microbiome (Eschenbach *et al.*, 1989). Furthermore, the high rates of net H_2O_2 production despite increases in net H_2O_2 decay rates indicates that changes in H_2O_2 concentration are largely due to differences in H_2O_2 production rates, which can sometimes outpace microbial decay. Thus, community-wide decay is unable to mitigate stress to sensitive organisms from H_2O_2 in some waters. Any negative impacts to H_2O_2-sensitive *Microcystis*

would be highest when rates of primary production, respiration, and perhaps exudate excretion are highest, which may maximize growth advantages of *Microcystis* strains that are relatively H_2O_2-resistant. However, the impact of the H_2O_2 fluxes measured here on growth of *Microcystis* relative to other factors such as water temperature, light availability, and nutrient concentrations remains unknown. In Chapter 2, H_2O_2 concentrations observed in the cultures were representative of the highest H_2O_2 concentrations measured in these experiments, which suggests that the effect of H_2O_2 production on *Microcystis* may be minor; however, gross H_2O_2 fluxes in the *Microcystis* cultures where not quantified. Therefore, how the total H_2O_2 exposure in the cultivation experiments relate to the fluxes observed here is uncertain.

Failed model assumptions in some experiments led to increased uncertainty in the gross H_2O_2 production and indicates a need for a revised model to quantify biological production in light exposed waters. While photochemical production can be modelled using CDOM and irradiance data (Cory *et al.*, 2016; Powers & Miller, 2014; Ueki *et al.*, 2020), the relationship between light-dependent biological H_2O_2 production and time over a diel cycle unknown, which prevents creating a model of biotic H_2O_2 production in the light that includes variables with biological or chemical meaning. Previous models included biotic H_2O_2 production by altering the model used here with curve fitting parameters and assuming that PH_2O_2 increases nonlinearly with time (Dixon *et al.*, 2013). However, only the portion of the curve when PH_2O_2 is increasing was modeled in this study, which is not sufficient for the time frame of a full diel curve where light-dependent H_2O_2 is expected to decrease with solar zenith angle in the afternoon or with increasing cloud cover. A better characterization of how light-dependent biological H_2O_2 production changes with light intensity and other environmental parameters is ultimately required to model biological H_2O_2 production *in situ*.

5.7 Figures and Tables

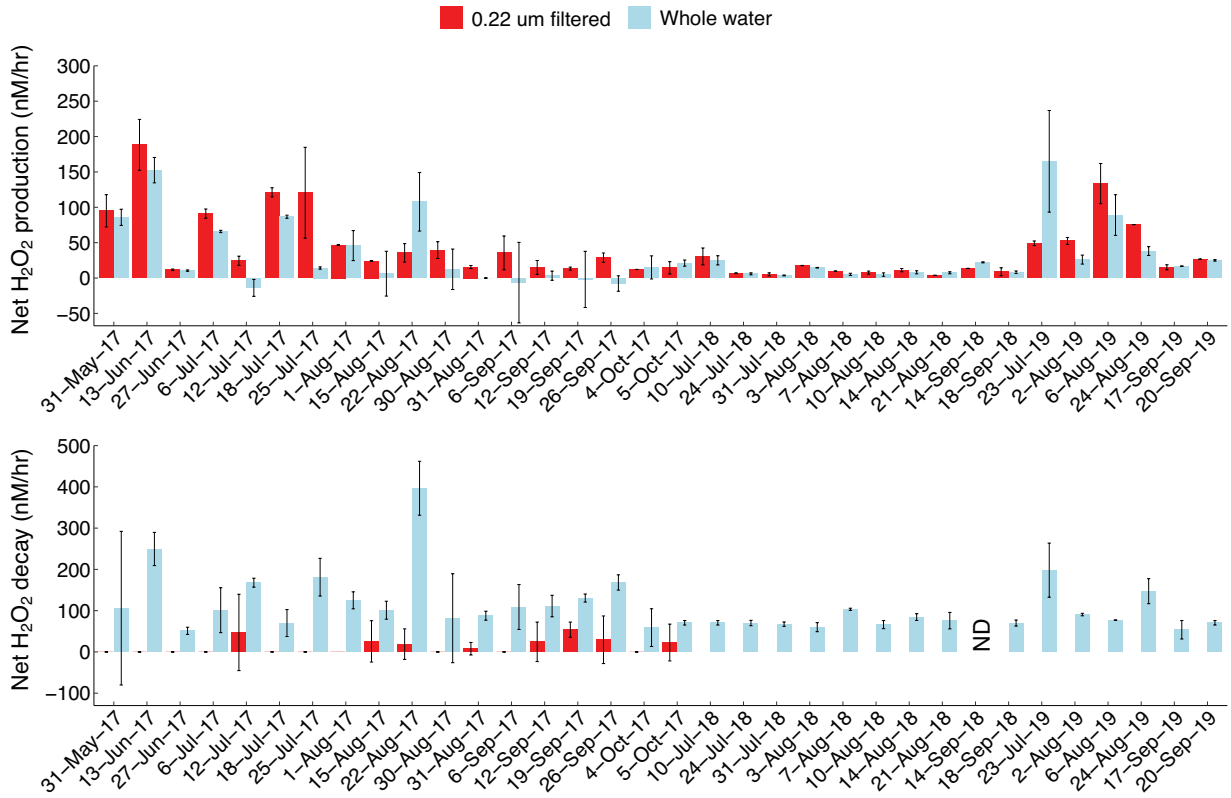

Figure 5.1: Net H_2O_2 production and decay rates in whole (blue) and 0.22 µm filtered water (red) exposed to light. A: Net H_2O_2 production rates in unamended bottles. B: Net H_2O_2 decay rates in spiked bottles exposed to light. Net decay in spiked 0.22 µm filtered water was only measured in 2017. ND: no data in both whole and filtered water. Error bars show upper and lower bounds determined by 95 % confidence intervals.

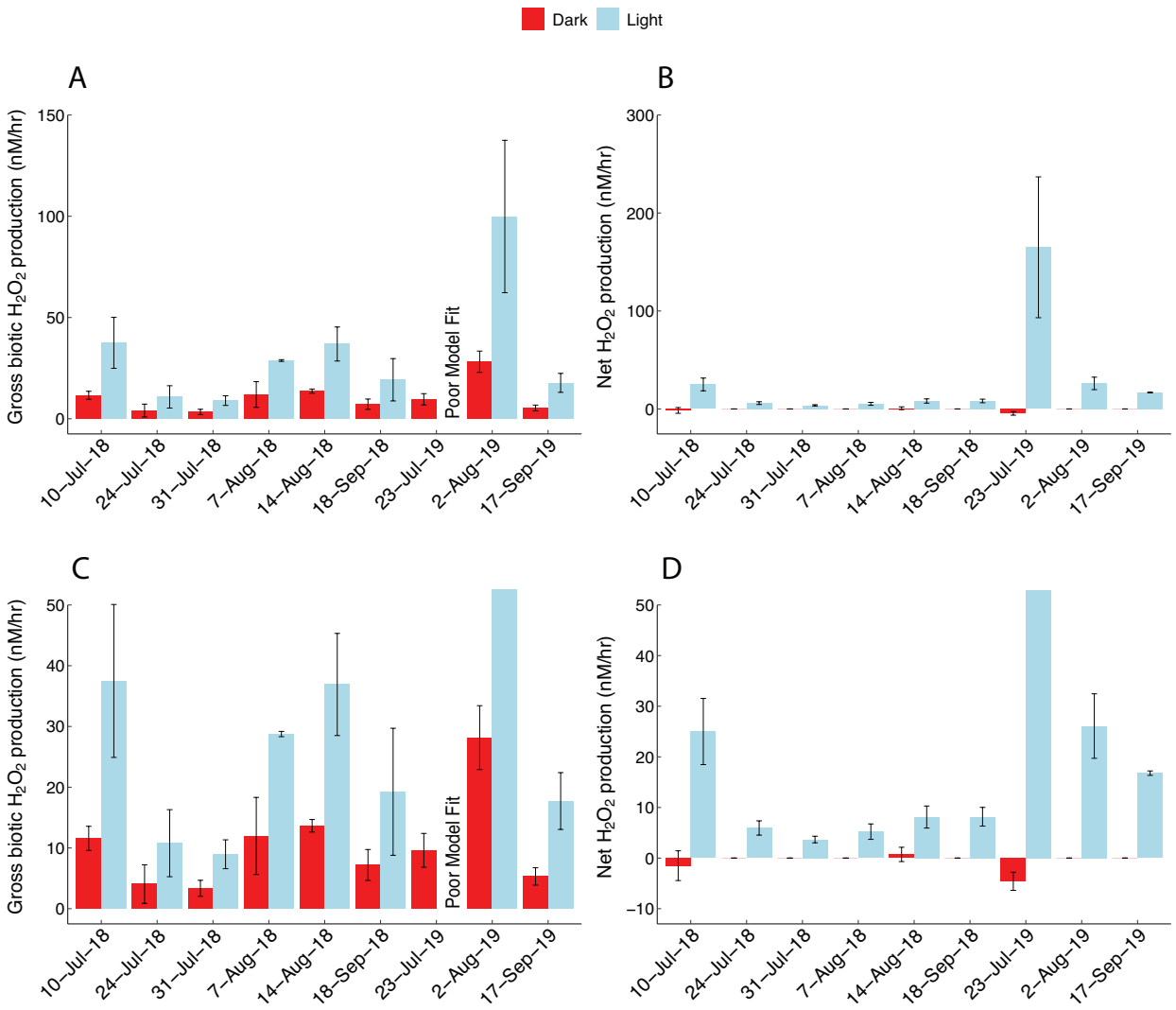

Figure 5.2: H_2O_2 production in whole water incubated in light (blue) and dark (red) bottles. A: Estimated gross biotic H_2O_2 production rates, showing the full range of data. B: Measured net H_2O_2 production rates in unamended whole water, showing the full range of data. C: Estimated gross biotic H_2O_2 production rates, zooming in on smaller rates. D: Measured net H_2O_2 production rates in unamended whole water, zooming in on smaller dates. Error bars show upper and lower bounds determined by 95 % confidence intervals. Gross production rates could not be calculated from light exposed bottles on 23-Jul-19.

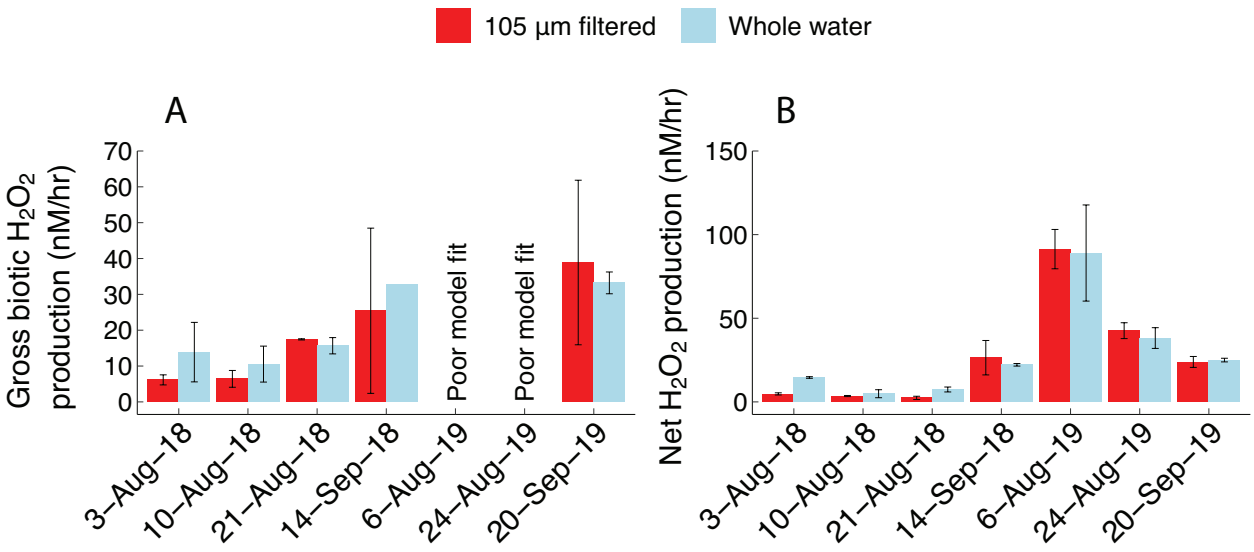

Figure 5.3: H_2O_2 production in whole (blue) and 105 µm filtered (red) water. A: Estimated gross biotic H_2O_2 production rates. Gross production rates could not be calculated from bottles on 6-Aug-19 and 24-Aug-19. B: Measured net H_2O_2 production rates. Error bars show upper and lower bounds determined by 95 % confidence intervals.

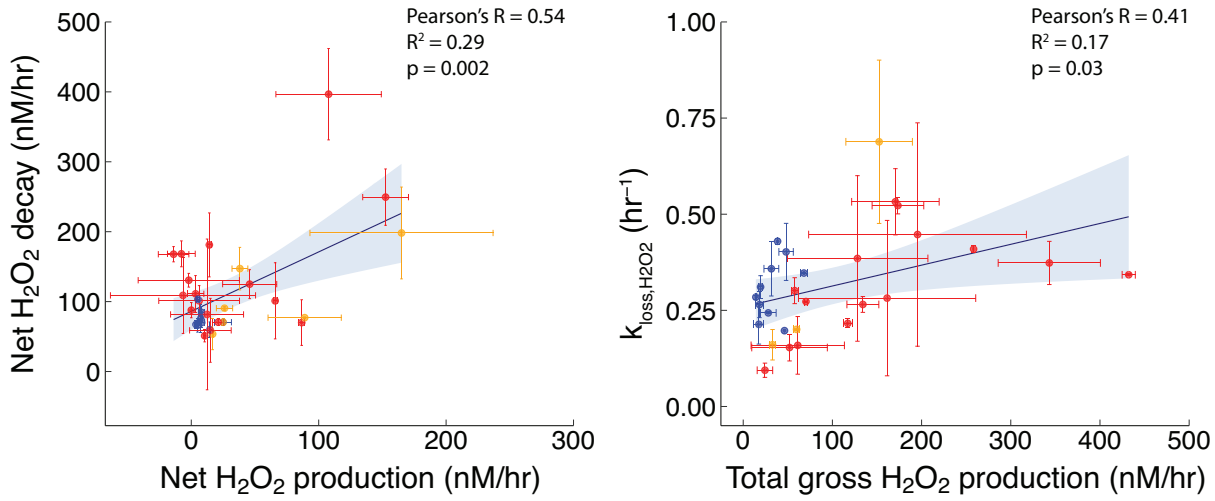

Figure 5.4: Linear regressions with net H_2O_2 production and net H_2O_2 decay rates (A) and with absolute decay constants and total gross H_2O_2 production (B).

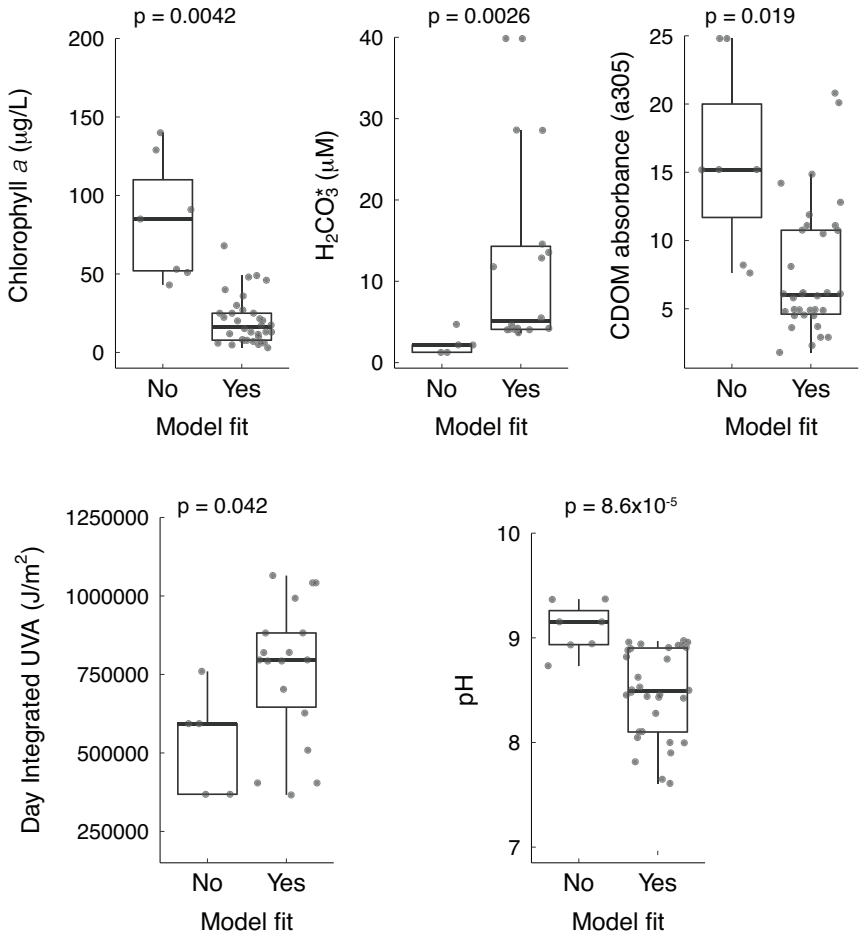

Figure 5.5: Significant differences in chlorophyll *a*, $H_2CO_3^*$, CDOM concentrations, pH, and day integrated UVA were detected between experiments on dates where the model did and did not fit the data. All p-values were calculated using a Welch's two-sided T-test.

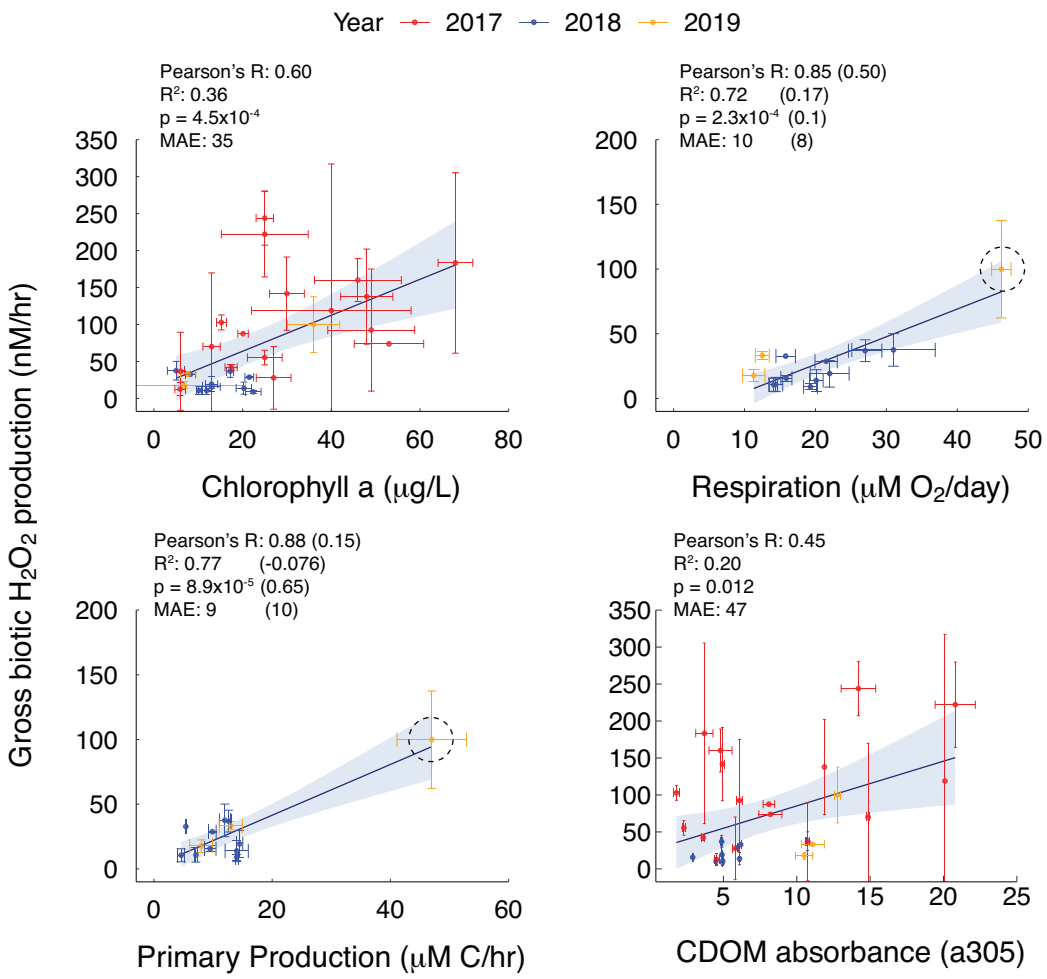

Figure 5.6: Linear regressions of gross biotic H_2O_2 production rates and chlorophyll *a* concentration, respiration rate, primary production rates, and CDOM absorbance. Only values from experiments where the model fit the data are included. Statistics in parenthesis were calculated excluding the outlier point in the dashed circle. Error bars show upper and lower bounds determined by 95% confidence intervals.

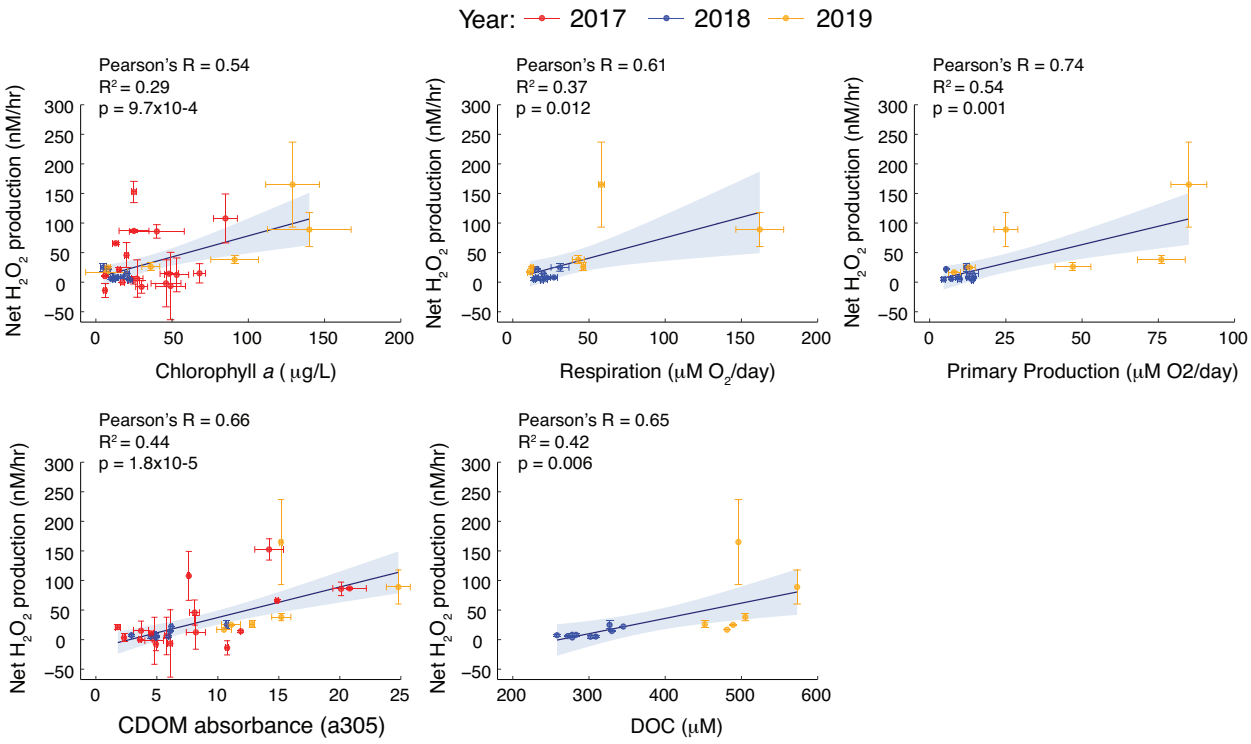

Figure 5.7: Linear regressions of net H_2O_2 production rates and chlorophyll *a* concentration, respiration rate, primary production rate, CDOM absorbance, and DOC concentration. Error bars show upper and lower bounds determined by 95% confidence intervals.

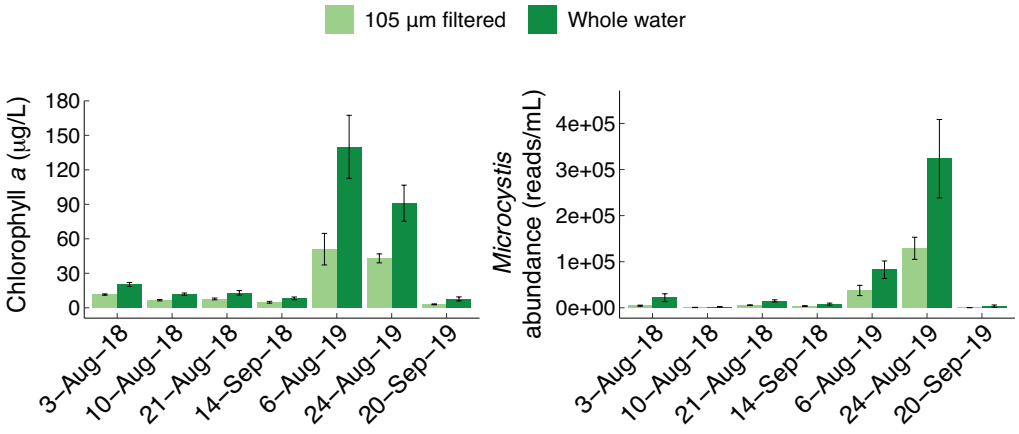

Figure 5.8: Reductions in *Microcystis* abundance and chlorophyll *a* concentration in 105 µm filtered water compared to whole water. Differences in both *Microcystis* abundance and chlorophyll *a* concentrations had p-values < 0.05 on all dates (Welch's one-sided T-test).

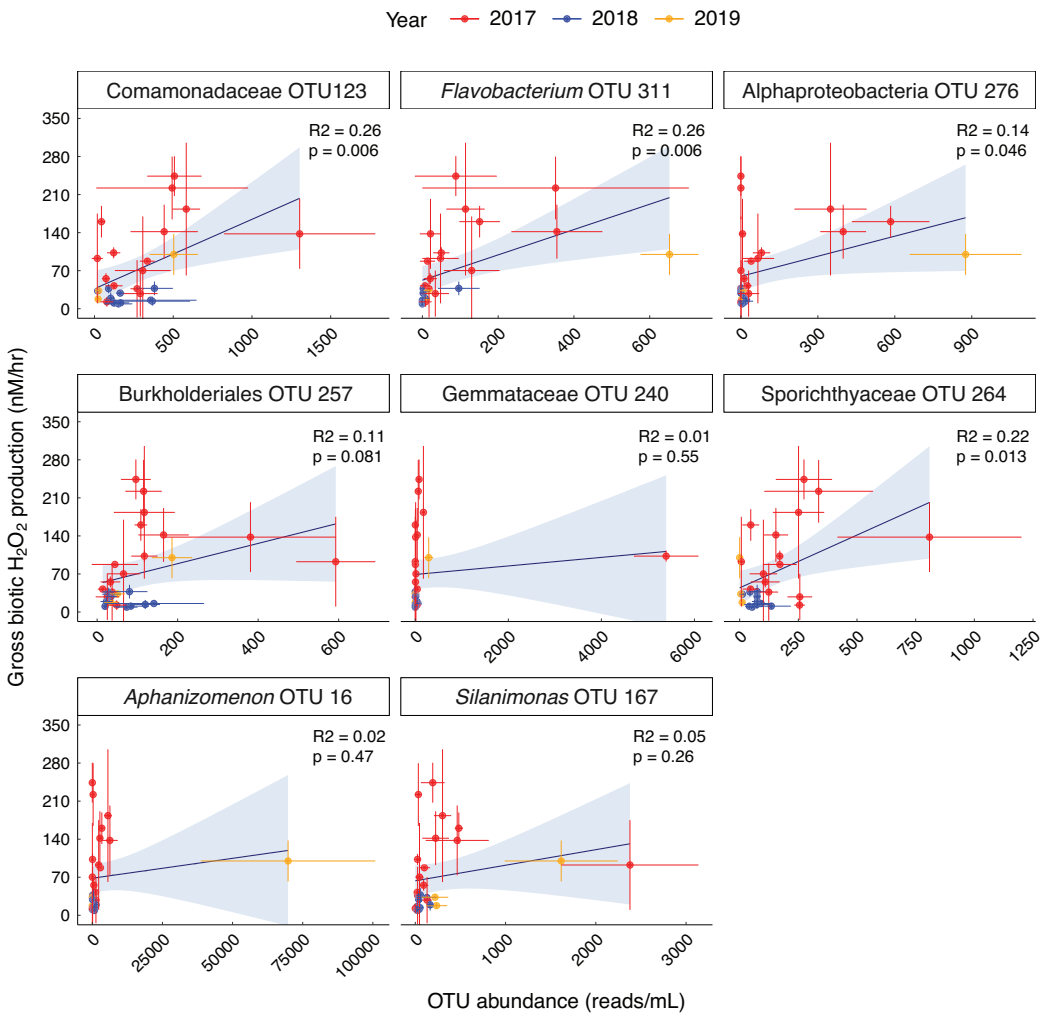

Figure 5.9: Linear regression of gross biotic H_2O_2 production rate and abundance of important OTUs in random forest models.

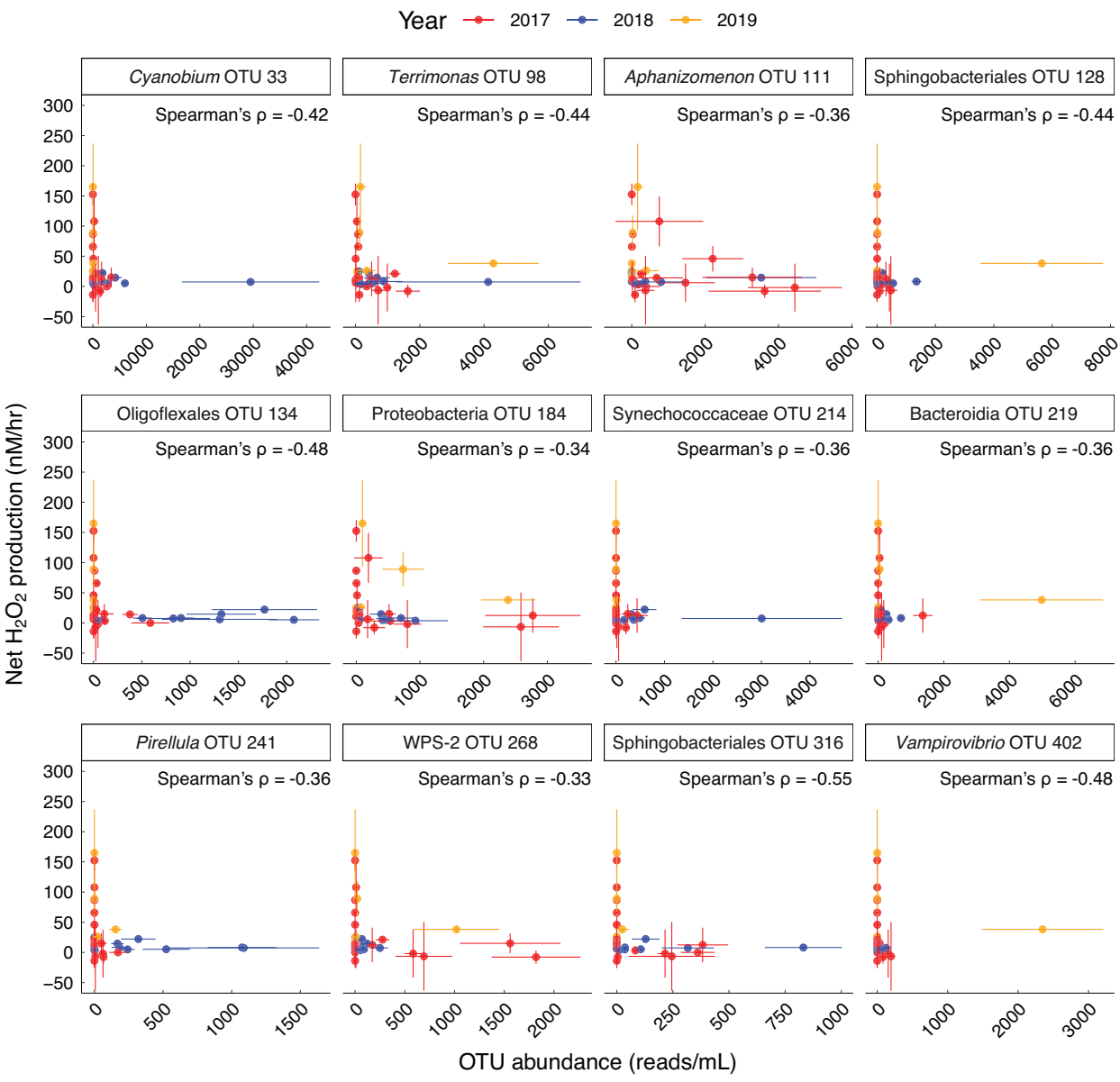

Figure 5.10: The 12 OTUs with the highest negative correlation with net H_2O_2 production rate according to a Spearman's rank-order correlation.

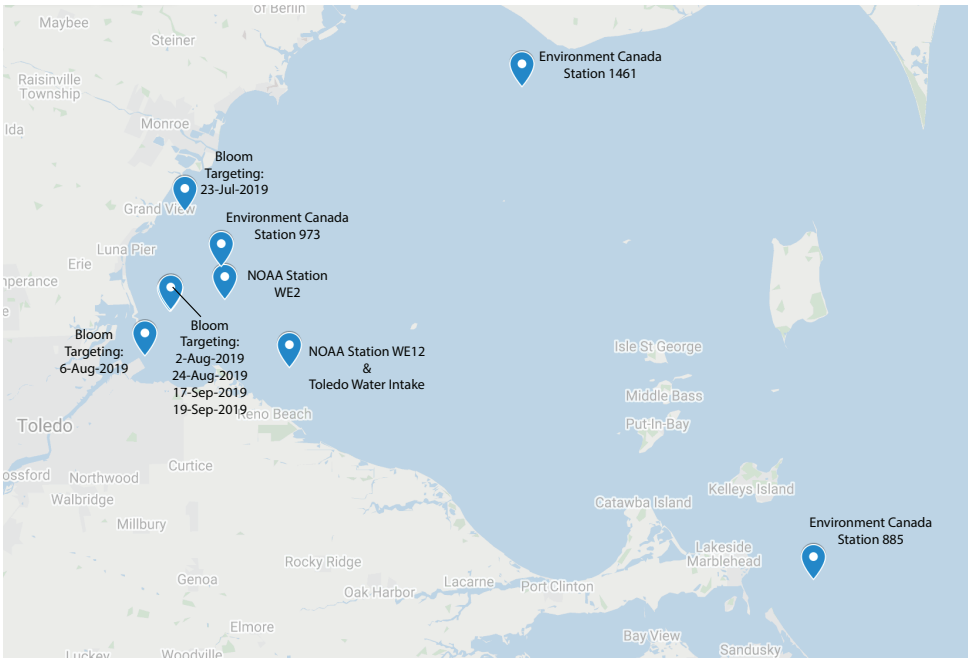

Figure S 5.1: Sites of water collection in western Lake Erie.

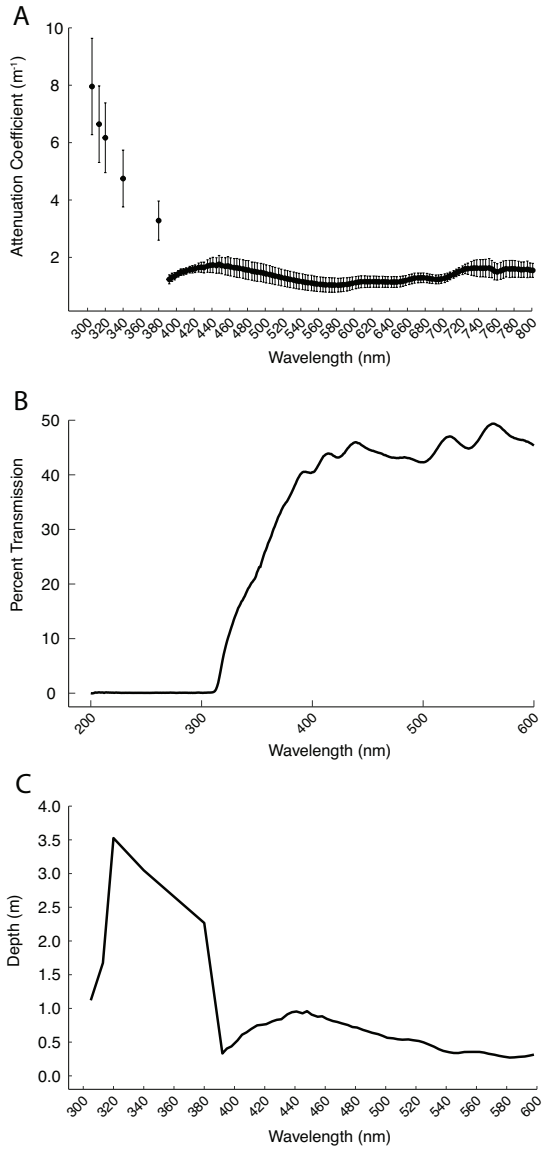

Figure S 5.2: Light attenuation in Lake Erie water column and bottle experiments. A: Spectral attenuation coefficients calculated from UV and PAR profiles measured in western Lake Erie. Error bars represent the upper and lower bound determined from 95% confidence intervals. B: The percent of light transmitted through neutral density screening and plastic bottles used during the experiments. C: The average depth in western Lake Erie at which the fraction of light transmission equals the fraction of light transmission in the experimental bottles.

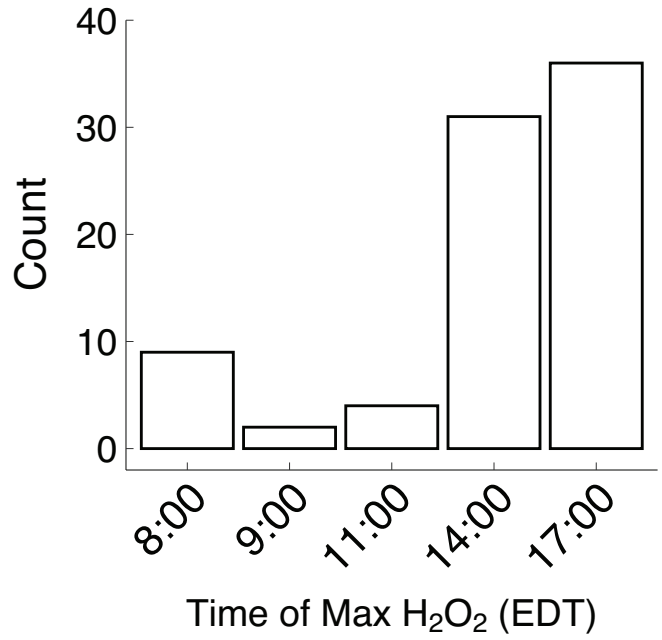

Figure S 5.3: Histogram of the time of maximum H_2O_2 in unamended whole water bottles.

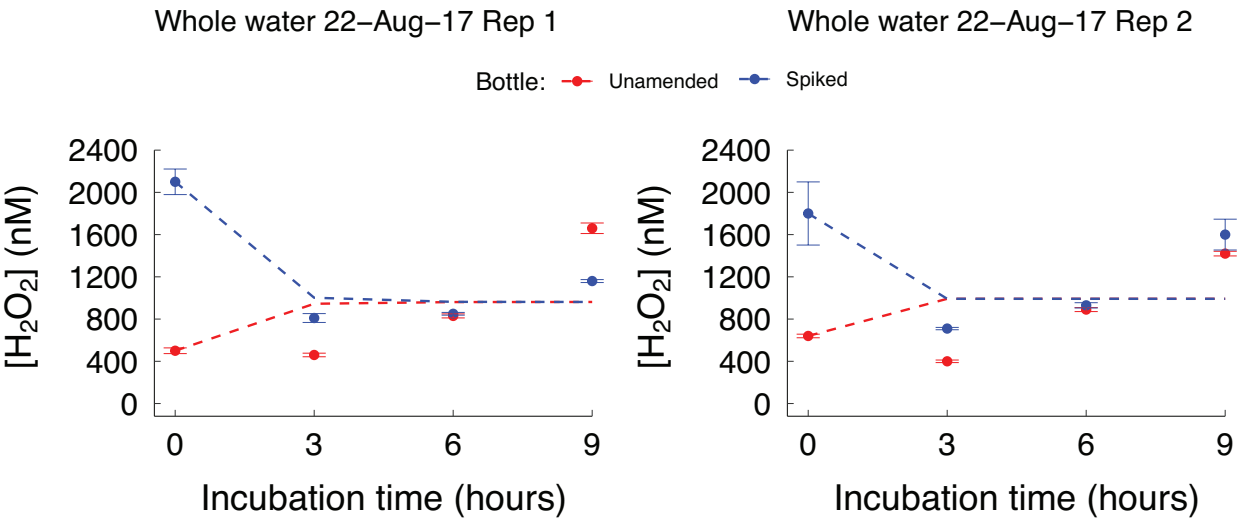

Figure S 5.4: Measured and modeled H_2O_2 concentrations from experiments with poor fit on 22-Aug-2017 with whole water.

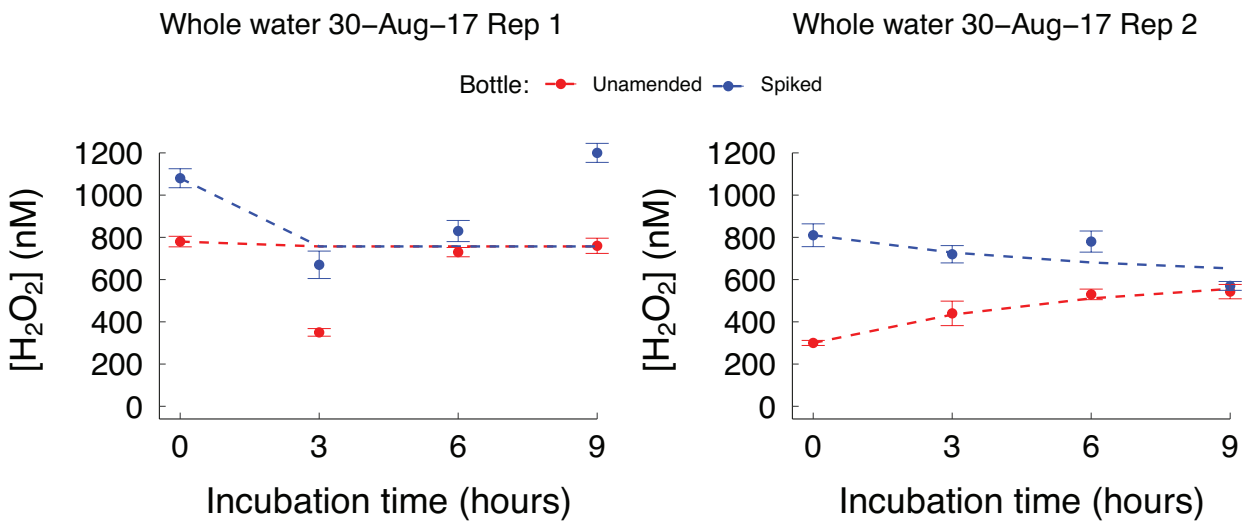

Figure S 5.5: Measured and modeled H_2O_2 concentrations from experiments with poor fit on 30-Aug-2017 with whole water.

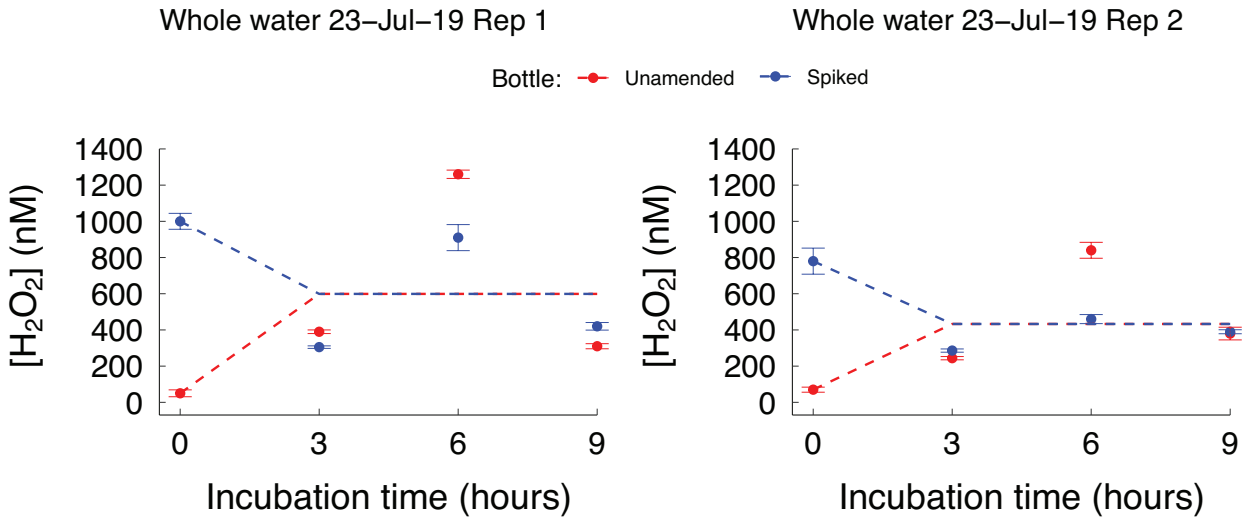

Figure S 5.6: Measured and modeled H_2O_2 concentrations from experiments with poor fit on 23-Jul-2019 with whole water.

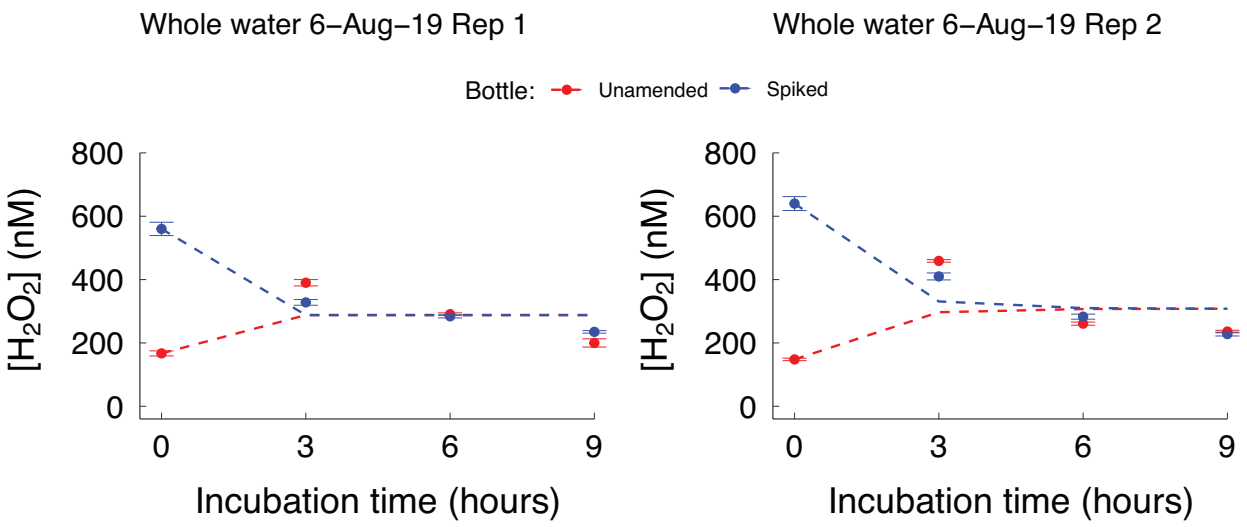

Figure S 5.7: Measured and modeled H_2O_2 concentrations from experiments with poor fit on 6-Aug-2019 with whole water.

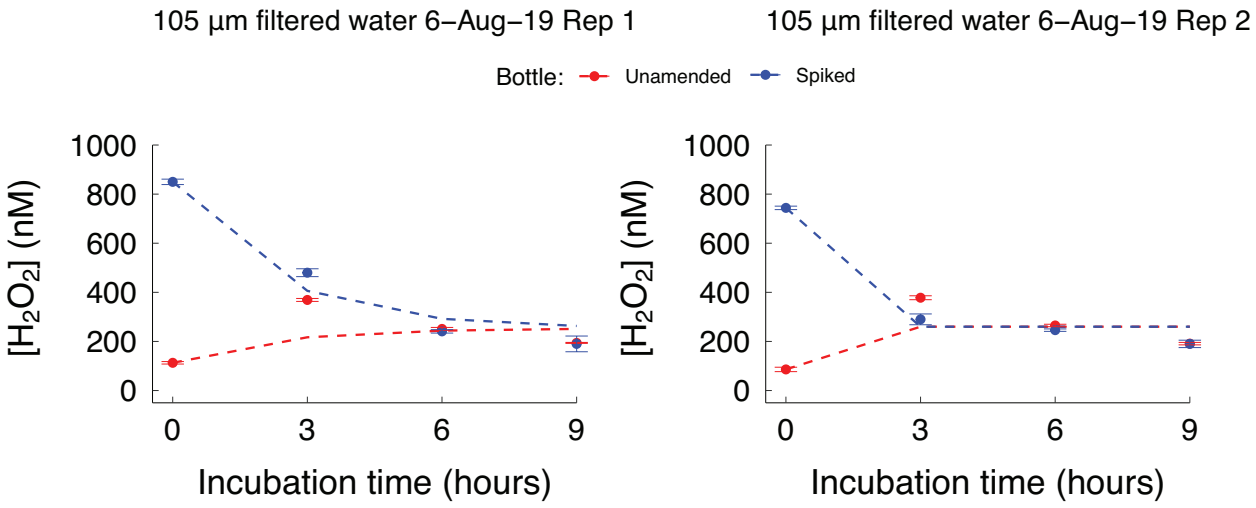

Figure S 5.8: Measured and modeled H_2O_2 concentrations from experiments with poor fit on 6-Aug-2019 with 105 µm filtered water.

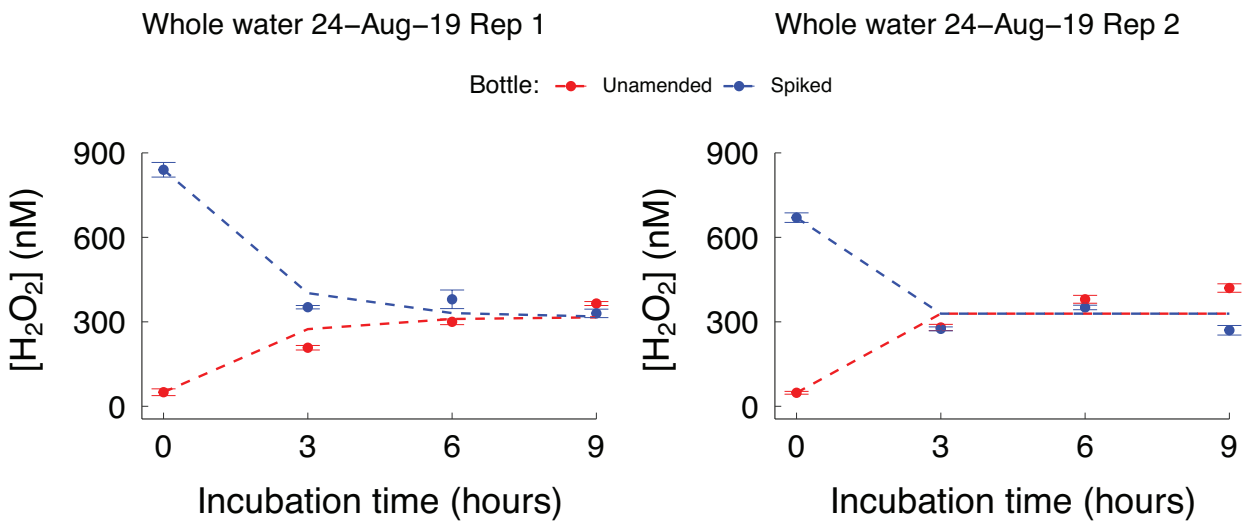

Figure S 5.9: Measured and modeled H_2O_2 concentrations from experiments with poor fit on 24-Aug-2019 with whole water.

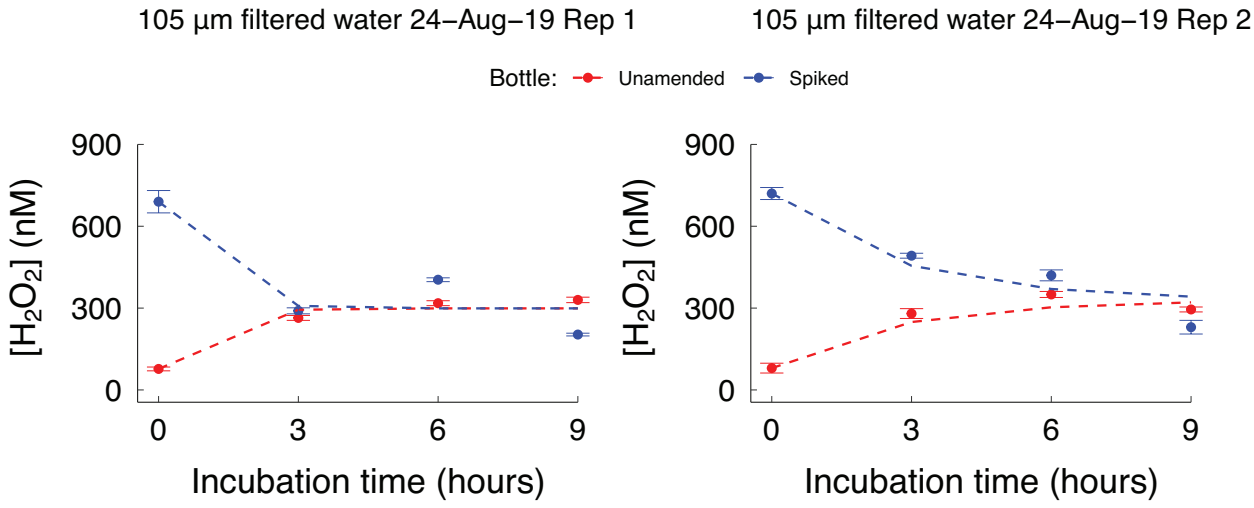

Figure S 5.10: Measured and modeled H_2O_2 concentrations from experiments with poor fit on 24-Aug-2019 with 105 µm filtered water.

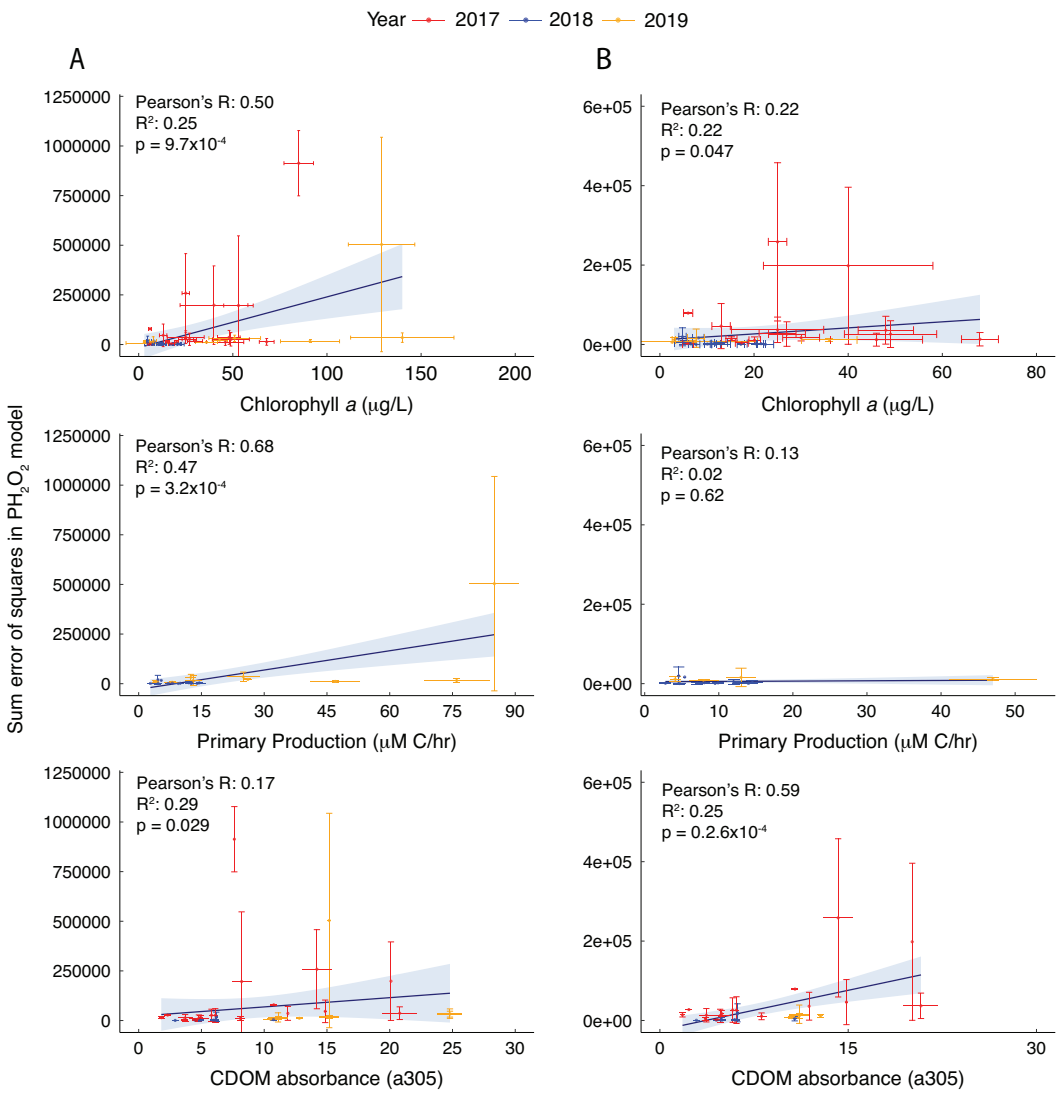

Figure S 5.11: Correlation with model error sum of squares and chlorophyll *a* concentrations and primary production rates. Column A contains regression with all experiments, and column B contains regressions excluding the experiments with poor fit to the model. Error bars show upper and lower bounds determined by 95% confidence intervals.

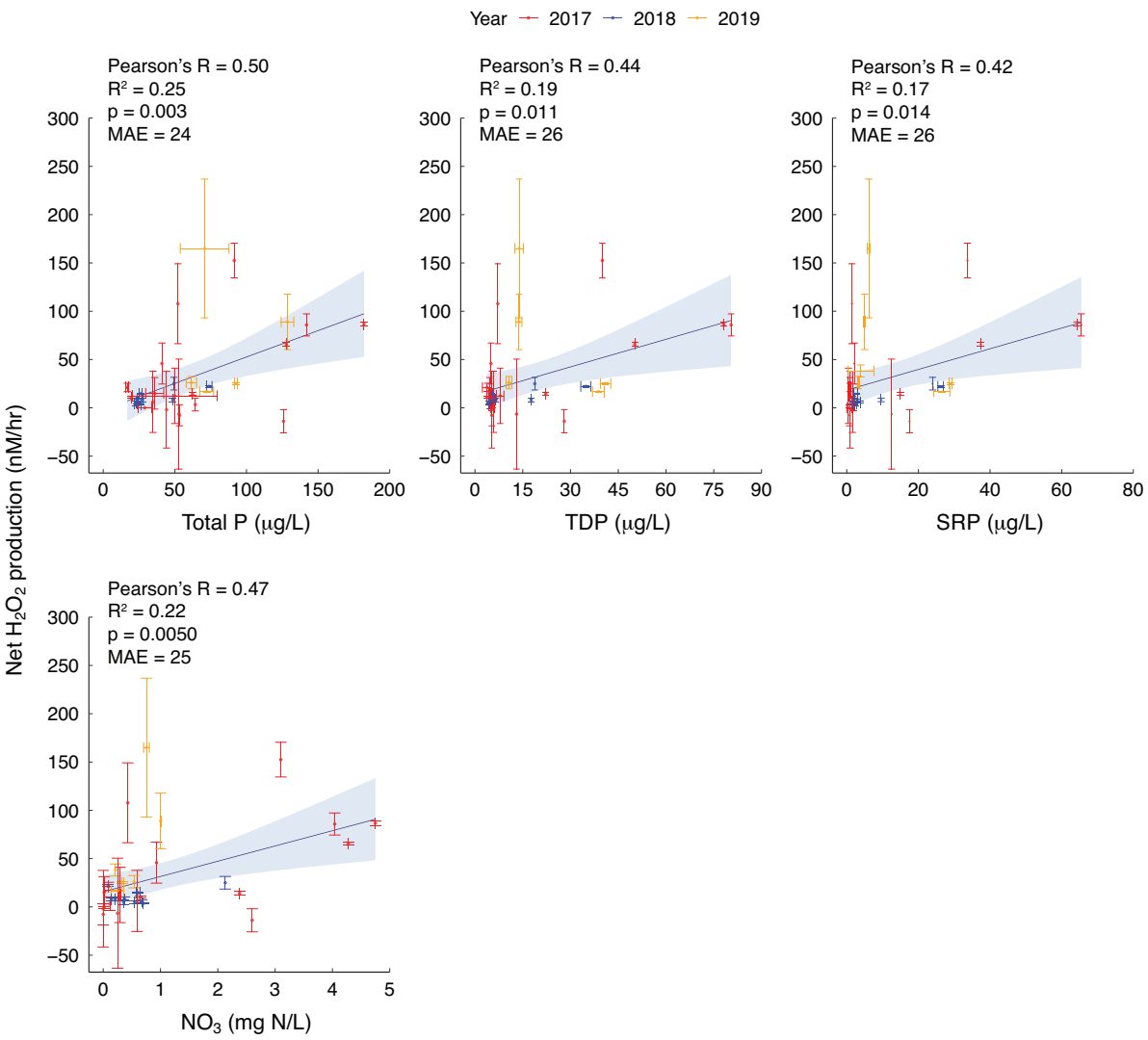

Figure S 5.12: Significant correlations between net H_2O_2 production, total phosphorus (P), total dissolved phosphorus (TDP), soluble reactive phosphorus (SRP), and nitrate (NO_3) concentrations in bottle experiments. Error bars show upper and lower bounds determined by 95% confidence intervals.

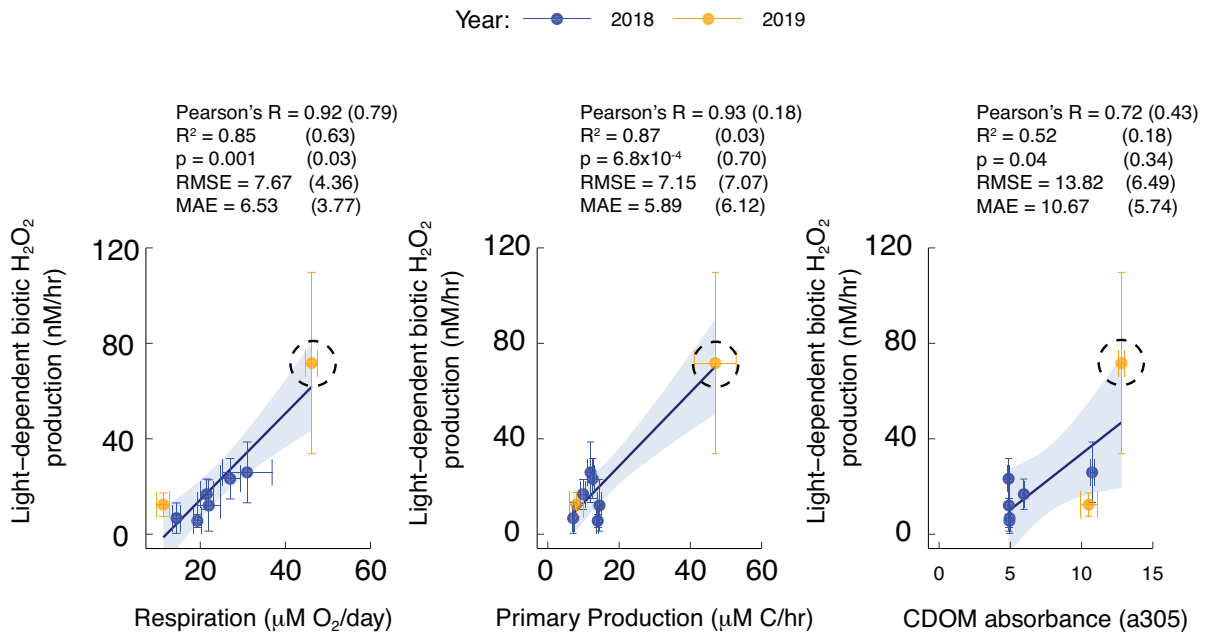

Figure S 5.13: Correlations between the difference in whole water gross biotic H_2O_2 production rate in the light and dark and respiration rates, primary production rates, and CDOM absorbance. Statistics in parenthesis were calculated excluding the outlier point in the dashed circle. Error bars show upper and lower bounds determined by 95% confidence intervals.

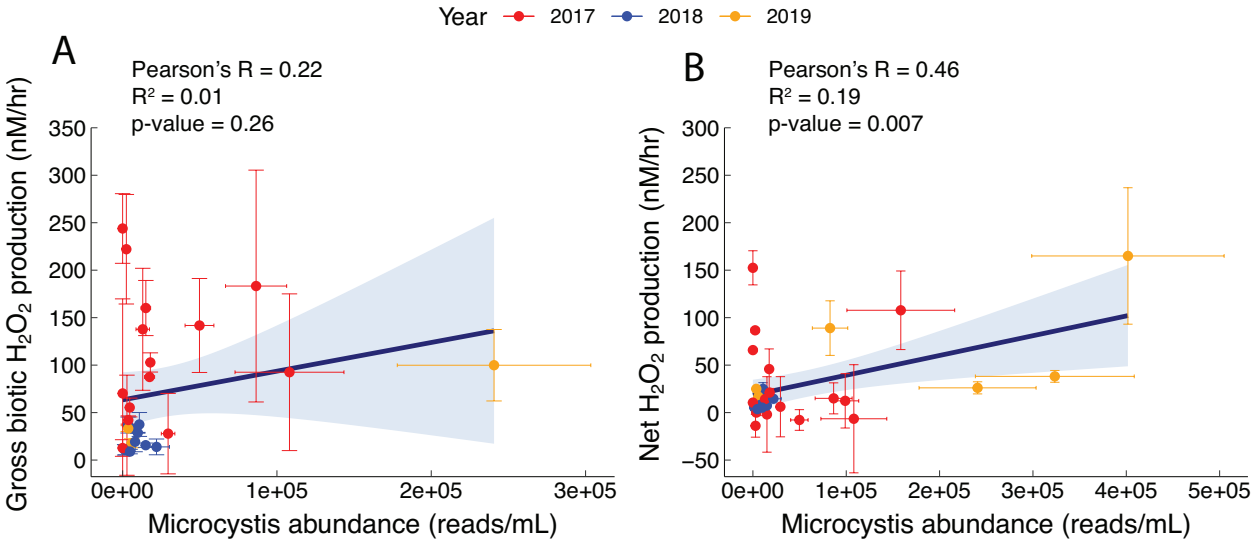

Figure S 5.14: Correlations between *Microcystis* abundance and gross biotic H_2O_2 production rates (A) and net H_2O_2 production rates (B). Error bars show upper and lower bounds determined by 95% confidence intervals.

Table 5.1: Comparison of total gross H_2O_2 production and net H_2O_2 production in experiments where gross H_2O_2 production rates could be calculated. Fold differences between gross and net production rates were only calculated for dates when net production was observed (23/28 observations).

Experiment date	*Total gross H_2O_2 production (nM/hr)*	*95 % CI (nM/hr)*	*Net H_2O_2 production (nM/hr)*	*95 % CI (nM/hr)*	*Fold difference (Gross:net)*
2017-06-13	432	7	153	18	2.8
2017-06-27	24	9	11	1	2.2
2017-07-06	160	99	66	2	2.4
2017-07-12	60	52	-10	12	NA
2017-07-18	340	57	87	2	3.9
2017-07-25	258	0.4	14	2	18
2017-08-01	130	18	50	21	2.6
2017-08-15	50	42	6	32	8.3
2017-08-31	58	4	0	0	NA
2017-09-06	130	79	-7	57	NA
2017-09-12	70	1	3	7	23
2017-09-19	170	29	-2	40	NA
2017-09-26	170	49	-8	11	NA
2017-10-04	200	122	20	16	10
2017-10-05	117	5	21	4	5.6
2018-07-10	68	4	25	7	2.7
2018-07-24	18	5	6	1	3.0
2018-07-31	14	1	4	1	3.5
2018-08-03	32	8	15	0.5	2.1
2018-08-07	39	0.02	5	2	7.8
2018-08-10	18	5	5	2	3.6
2018-08-14	48	8	8	2	6.0
2018-08-21	19	2	7	1	2.7
2018-09-14	46	-	22	1	2.1
2018-09-18	28	9	8	2	3.5
2019-08-02	150	37	26	6	5.8
2019-09-17	33	3	17	0.4	1.9
2019-09-20	60	3	25	1	2.4

Table 5.2: Bootstrap support and p-values of chemical and biological variables (rows) in stepwise linear regression models generated with ordination of microbial community dissimilarities on PCoA axes (columns). Only samples with values for gross H_2O_2 production were included in stepwise regression. All p-values were calculated with an F-test. Significant p-values are in bold print. Bootstrap support was calculated with 300 replicates.

	PCoA1 (35 %)			**PCoA2 (18 %)**			**PCoA3 (7.7 %)**			**PCoA4 (6.9 %)**		
Predictors	*Bootstrap*	*p*	*df*	*Bootstrap*	*p*	*df*	*Bootstrap*	*p*	*df*	*Bootstrap*	*p*	*df*
K_{loss}	0.89	**<0.001**	16	0.81	**0.015**	16	0.78	0.054	20	0.86	**0.011**	14
Net H_2O_2 prod.	0.76	**0.035**	16									
Max. H_2O_2 conc.	0.79	0.058	16				0.84	**0.006**	20	0.84	**0.019**	14
Gross biotic H_2O_2 prod.	0.91	**0.003**	16	0.70	0.064	16				0.82	0.055	14
pH	0.74	0.058	16							0.89	**0.014**	14
Chl *a*	0.91	**0.002**	16	0.77	0.054	16	0.76	**0.005**	20			
Nitrate	0.91	**0.001**	16	0.75	0.135	16				0.86	**0.013**	14
NH_4^+	0.75	0.079	16	0.76	0.133	16				0.83	**0.006**	14
Temp	0.90	**0.007**	16	0.75	**0.017**	16				0.94	**0.001**	14
CDOM				0.85	**0.009**	16				0.89	**0.043**	14
TP				0.81	**0.032**	16	0.77	0.063	20	0.91	**<0.001**	14
TDP				0.78	**0.002**	16	0.85	**0.012**	20	0.85	**0.020**	14
SRP										0.82	**0.042**	14
n	26			26			26			26		
R^2 / R^2 adjusted	0.875 / 0.805			0.821 / 0.721			0.734 / 0.667			0.875 / 0.777		
BIC	-42.752			-31.489			-53.518			-54.978		

Table 5.3: Bootstrap support and p-values of variables in stepwise linear regression models generated with stepAIC of chemical and biological parameters (rows) vs ordination of microbial

community dissimilarities on PCoA axes (columns). Gross H_2O_2 production and decay rates were not considered as model features during stepwise regression. Four samples with missing values in nutrient, pH, or net decay data were excluded. All p-values were calculated with an F-test. Significant p-values are in bold print. Bootstrap support was calculated with 300 replicates.

	PCoA1 (35 %)			**PCoA2 (18 %)**			**PCoA3 (7.7 %)**			**PCoA4 (6.9 %)**		
Predictors	*Boot-strap*	*p*	*df*	*Boot-strap*	*p*	*df*	*Boot-strap*	*p*	*df*	*Boot-strap*	*p*	*df*
Chl *a*	0.87	**<0.001**	26	0.94	**0.003**	22				0.77	0.066	24
pH	0.66	**0.001**	26	0.71	**0.001**	22						
Net H_2O_2 prod.				0.70	**<0.001**	22	0.75	**<0.001**	24			
CDOM				0.82	**<0.001**	22						
SRP				0.70	**0.001**	22						
Temp				0.81	0.068	22				1.0	**0.007**	24
Net H_2O_2 decay							0.94	**<0.001**	24			
Max H_2O_2 conc.							0.95	**<0.001**	24			
TDP							0.82	**0.001**	24			
Nitrate										0.87	**<0.001**	24
TP										0.91	**<0.001**	24
n	29			29			29			29		
R^2 / R^2 adjusted	0.745 / 0.726			0.749 / 0.681			0.783 / 0.747			0.693 / 0.641		
BIC	-28.271			-35.201			-68.092			-55.582		

Table 5.4: Comparison of R^2 values and mean absolute errors (MAE) in models for predicting gross biotic and net H_2O_2 production rates. Two R^2 values are reported for the random forest

models; the first value is the fit to all data points, and the second value is the average R^2 across the held-out datasets during the k-fold cross validation (k=4).

Statistic	*OTU random forest*	*Chlorophyll a regression*	*CDOM regression*
Gross biotic H_2O_2 production R^2	0.89 / 0.43	0.36	0.20
Gross biotic H_2O_2 production MAE	15	35	47
Net H_2O_2 production R^2	0.86 / 0.31	0.29	0.44
Net H_2O_2 production MAE	10	27	21

Table 5.5: OTUs in the random forest model for gross biotic H_2O_2 production with importance lower bounds above 0.01.

Importance rank	*OTU number*	*Lowest Taxonomic Assignment*	*Model Importance*	*Importance 95 % CI*
1	OTU 123	Comamonadaceae	0.18	0.046
2	OTU 311	*Flavobacterium*	0.08	0.025
3	OTU 276	Alphaproteobacteria	0.024	0.003
4	OTU 257	Burkholderiales; TRA3-20	0.022	0.006
5	OTU 240	Gemmataceae	0.014	0.006
6	OTU 264	Sporichthyaceae; hgcI_clade	0.013	0.005
7	OTU 16	*Aphanizomenon*	0.013	0.003
8	OTU 167	*Silanimonas*	0.012	0.003

Table 5.6: OTUs in the random forest model for net H_2O_2 production with importance lower bounds above 0.01.

Importance rank	*OTU number*	*Lowest Taxonomic Assignment*	*Model Importance*	*Importance 95 % CI*
1	OTU 822	*Lacihabitans*	0.09	0.02
2	OTU 579	*Runella*	0.045	0.009
3	OTU 378	Spirosomaceae	0.03	0.006
4	OTU 323	*Lacibacter*	0.029	0.007
5	OTU 258	Alcaligenaceae; GKS98 freshwater group	0.029	0.006
6	OTU 123	Comamonadaceae	0.017	0.005
7	OTU 433	*Candidatus Aquiluna*	0.017	0.004

5.8 References

Aboelmy, M. H., & Peterhansel, C. (2014). Enzymatic characterization of *Chlamydomonas reinhardtii* glycolate dehydrogenase and its nearest proteobacterial homologue. *Plant Physiol Biochem, 79*: 25-30.

Andeer, P. F., Learman, D. R., McIlvin, M., Dunn, J. A., & Hansel, C. M. (2015). Extracellular haem peroxidases mediate Mn (II) oxidation in a marine *Roseobacter* bacterium via superoxide production. *Environ Microbiol, 17*(10): 3925-3936.

Andrews, S. S., Caron, S., & Zafiriou, O. C. (2000). Photochemical oxygen consumption in marine waters: A major sink for colored dissolved organic matter? *Limnol Oceanogr, 45*(2): 267-277.

Anesio, A. M., Granéli, W., Aiken, G. R., Kieber, D. J., & Mopper, K. (2005). Effect of humic substance photodegradation on bacterial growth and respiration in lake water. *Appl Environ Microbiol, 71*(10): 6267-6275.

Barchewitz, T., Guljamow, A., Meissner, S., Timm, S., Henneberg, M., Baumann, O. *et al.* (2019). Non-canonical localization of RubisCO under high-light conditions in the toxic cyanobacterium Microcystis aeruginosa PCC7806. *Environ Microbiol, 21*(12): 4836-4851.

Bateson, M. M., & Ward, D. M. (1988). Photoexcretion and fate of glycolate in a hot spring cyanobacterial mat. *Appl Environ Microbiol, 54*(7): 1738-1743.

Bayer, B., Pelikan, C., Bittner, M. J., Reinthaler, T., Könneke, M., Herndl, G. J., & Offre, P. (2019). Proteomic Response of Three Marine Ammonia-Oxidizing Archaea to Hydrogen Peroxide and Their Metabolic Interactions with a Heterotrophic Alphaproteobacterium. *mSystems, 4*(4): e00181-00119.

Beliaev, A. S., Romine, M. F., Serres, M., Bernstein, H. C., Linggi, B. E., Markillie, L. M. *et al.* (2014). Inference of interactions in cyanobacterial-heterotrophic co-cultures via transcriptome sequencing. *ISME J, 8*(11): 2243-2255.

Bond, R. J., Hansel, C. M., & Voelker, B. M. (2020). Heterotrophic Bacteria Exhibit a Wide Range of Rates of Extracellular Production and Decay of Hydrogen Peroxide. *Front Mar Sci*.

Briand, E., Escoffier, N., Straub, C., Sabart, M., Quiblier, C., & Humbert, J.-F. (2009). Spatiotemporal changes in the genetic diversity of a bloom-forming Microcystis aeruginosa (cyanobacteria) population. *ISME J, 3*(4): 419-429.

Bushnell, B. (2018). BBTools: a suite of fast, multithreaded bioinformatics tools designed for analysis of DNA and RNA sequence data: Joint Genome Institute.

Cheng, K., Miller, A., & Colman, B. (1972). An investigation of glycolate excretion in two species of blue-green algae. *Planta, 103*(2): 110-116.

Codd, G., Lord, J., & Merrett, M. (1969). The glycollate oxidising enzyme of algae. *FEBS Lett, 5*(5): 341-342.

Cooper, W. J., & Zika, R. G. (1983). Photochemical formation of hydrogen peroxide in surface and ground waters exposed to sunlight. *Science, 220*(4598): 711-712.

Cooper, W. J., Zika, R. G., Petasne, R. G., & Plane, J. M. (1988). Photochemical formation of hydrogen peroxide in natural waters exposed to sunlight. *Environ Sci Technol, 22*(10): 1156-1160.

Cooper, W. J., Shao, C., Lean, D. R., Gordon, A. S., & Scully Jr, F. E. (1994). Factors affecting the distribution of H_2O_2 in surface waters. In: ACS Publications.

Cory, R. M., Ward, C. P., Crump, B. C., & Kling, G. W. (2014). Sunlight controls water column processing of carbon in arctic fresh waters. *Science, 345*(6199): 925-928.

Cory, R. M., Davis, T. W., Dick, G. J., Johengen, T., Denef, V. J., Berry, M. A. *et al.* (2016). Seasonal dynamics in dissolved organic matter, hydrogen peroxide, and cyanobacterial blooms in Lake Erie. *Front Mar Sci, 3*: 54.

Cory, R. M., Davis, T., Dick, G., Johengen, T., Denef, V. J., Berry, M. *et al.* (2017). Corrigendum: Seasonal dynamics in dissolved organic matter, hydrogen peroxide, and cyanobacterial blooms in Lake Erie. *Front Mar Sci, 4*: 377.

Cosgrove, K., Coutts, G., Jonsson, M., Tarkowski, A., Kokai-Kun, J. F., Mond, J. J., & Foster, S. J. (2007). Catalase (*KatA*) and alkyl hydroperoxide reductase (*AhpC*) have compensatory roles in peroxide stress resistance and are required for survival, persistence, and nasal colonization in *Staphylococcus aureus*. *J Bacteriol, 189*(3): 1025-1035.

Daniel, E., Weiss, G., Murik, O., Sukenik, A., Lieman-Hurwitz, J., & Kaplan, A. (2019). The response of *Microcystis aeruginosa* strain MGK to a single or two consecutive H2O2 applications. *Environ Microbiol Rep, 11*(5): 621-629.

Davis, T. W., Berry, D. L., Boyer, G. L., & Gobler, C. J. (2009). The effects of temperature and nutrients on the growth and dynamics of toxic and non-toxic strains of *Microcystis* during cyanobacteria blooms. *Harmful Algae, 8*(5): 715-725.

de Duve, C. (1969). The peroxisome: a new cytoplasmic organelle. *Proc R Soc Lond, 173*(1030): 71-83.

Diaz, J. M., Hansel, C. M., Voelker, B. M., Mendes, C. M., Andeer, P. F., & Zhang, T. (2013). Widespread production of extracellular superoxide by heterotrophic bacteria. *Science, 340*(6137): 1223-1226.

Diaz, J. M., & Plummer, S. (2018). Production of extracellular reactive oxygen species by phytoplankton: past and future directions. *J Plankton Res, 40*(6): 655-666.

Diaz, J. M., Plummer, S., Tomas, C., & Alves-de-Souza, C. (2018). Production of extracellular superoxide and hydrogen peroxide by five marine species of harmful bloom-forming algae. *J Plankton Res*: fby043-fby043. doi:10.1093/plankt/fby043

Diaz, J. M., Plummer, S., Hansel, C. M., Andeer, P. F., Saito, M. A., & McIlvin, M. R. (2019). NADPH-dependent extracellular superoxide production is vital to photophysiology in the marine diatom *Thalassiosira oceanica*. *Proc Natl Acad Sci, 116*(33): 16448-16453.

Dixon, T. C., Vermilyea, A. W., Scott, D. T., & Voelker, B. M. (2013). Hydrogen peroxide dynamics in an agricultural headwater stream: Evidence for significant nonphotochemical production. *Limnol Oceanogr, 58*(6): 2133-2144.

Dziallas, C., & Grossart, H.-P. (2011). Increasing oxygen radicals and water temperature select for toxic *Microcystis* sp. *PLoS One, 6*(9): e25569.

Eisenhut, M., Kahlon, S., Hasse, D., Ewald, R., Lieman-Hurwitz, J., Ogawa, T. *et al.* (2006). The plant-like C2 glycolate cycle and the bacterial-like glycerate pathway cooperate in phosphoglycolate metabolism in cyanobacteria. *Plant Physiol, 142*(1): 333-342.

Eschenbach, D. A., Davick, P. R., Williams, B. L., Klebanoff, S. J., Young-Smith, K., Critchlow, C., & Holmes, K. K. (1989). Prevalence of hydrogen peroxide-producing *Lactobacillus* species in normal women and women with bacterial vaginosis. *J Clin Microbiol, 27*(2): 251-256.

Fujii, M., Rose, A. L., Omura, T., & Waite, T. D. (2010). Effect of Fe (II) and Fe (III) transformation kinetics on iron acquisition by a toxic strain of *Microcystis aeruginosa*. *Environ Sci Technol, 44*(6): 1980-1986.

Fujii, M., Dang, T., Rose, A. L., Omura, T., & Waite, T. (2011). Effect of light on iron uptake by the freshwater cyanobacterium *Microcystis aeruginosa*. *Environ Sci Technol, 45*(4): 1391-1398.

Garg, S., Rose, A. L., & Waite, T. D. (2011). Photochemical production of superoxide and hydrogen peroxide from natural organic matter. *Geochim Cosmochim Acta, 75*(15): 4310-4320.

Geueke, B., & Hummel, W. (2002). A new bacterial L-amino acid oxidase with a broad substrate specificity: purification and characterization. *Enzyme Microb Tech, 31*(1-2): 77-87.

Goldstone, J. V., & Voelker, B. M. (2000). Chemistry of superoxide radical in seawater: CDOM associated sink of superoxide in coastal waters. *Environ Sci Technol, 34*(6): 1043-1048.

Gonzalez-Flecha, B., & Demple, B. (1997). Homeostatic regulation of intracellular hydrogen peroxide concentration in aerobically growing *Escherichia coli*. *J Bacteriol, 179*(2): 382-388.

Hackenberg, C., Kern, R., Hüge, J., Stal, L. J., Tsuji, Y., Kopka, J. *et al.* (2011). Cyanobacterial lactate oxidases serve as essential partners in N2 fixation and evolved into photorespiratory glycolate oxidases in plants. *Plant Cell, 23*(8): 2978-2990.

Häkkinen, P. J., Anesio, A. M., & Granéli, W. (2004). Hydrogen peroxide distribution, production, and decay in boreal lakes. *Can J Fish Aquat Sci, 61*(8): 1520-1527.

Han, T.-W., & Eley, J. (1973). Glycolate excretion by Anacystis nidulans: effect of HCO_3^- concentration, oxygen concentration and light intensity. *Plant Cell Physiol, 14*(2): 285-291.

Hansel, C., Buchwald, C., Diaz, J., Ossolinski, J., Dyhrman, S., Van Mooy, B., & Polyviou, D. (2016). Dynamics of extracellular superoxide production by *Trichodesmium* colonies from the Sargasso Sea. *Limnol Oceanogr, 61*(4): 1188-1200.

Hansel, C. M., Diaz, J. M., & Plummer, S. (2019). Tight Regulation of Extracellular Superoxide Points to Its Vital Role in the Physiology of the Globally Relevant *Roseobacter* Clade. *mBio, 10*(2): e02668-02618.

Hansel, C. M., & Diaz, J. M. (2020). Production of Extracellular Reactive Oxygen Species by Marine Biota. *Annual Review of Marine Science, 13*.

Harke, M. J., Steffen, M. M., Gobler, C. J., Otten, T. G., Wilhelm, S. W., Wood, S. A., & Paerl, H. W. (2016). A review of the global ecology, genomics, and biogeography of the toxic cyanobacterium, *Microcystis* spp. *Harmful Algae, 54*: 4-20.

Hellebust, J. A. (1965). Excretion Of Some Organic Compounds By Marine Phytoplankton. *Limnol Oceanogr, 10*(2): 192-206.

Heller, M., & Croot, P. (2010). Kinetics of superoxide reactions with dissolved organic matter in tropical Atlantic surface waters near Cape Verde (TENATSO). *J Geophys Res Oceans, 115*(C12).

Imlay, J. A. (2003). Pathways of oxidative damage. *Annu Rev Microbiol, 57*(1): 395-418.

Ivančič, I., & Degobbis, D. (1984). An optimal manual procedure for ammonia analysis in natural waters by the indophenol blue method. *Water Res, 18*(9): 1143-1147.

Kardinaal, W. E. A., Janse, I., Kamst-van Agterveld, M., Meima, M., Snoek, J., Mur, L. R. *et al.* (2007). *Microcystis* genotype succession in relation to microcystin concentrations in freshwater lakes. *Aquat Microb Ecol, 48*(1): 1-12.

Kern, R., Bauwe, H., & Hagemann, M. (2011). Evolution of enzymes involved in the photorespiratory 2-phosphoglycolate cycle from cyanobacteria via algae toward plants. *Photosynth Res, 109*(1-3): 103-114.

Kharbush, J. J., Smith, D. J., Powers, M., Vanderploeg, H. A., Fanslow, D., Robinson, R. S. *et al.* (2019). Chlorophyll nitrogen isotope values track shifts between cyanobacteria and eukaryotic algae in a natural phytoplankton community in Lake Erie. *Org Geochem, 128*: 71-77.

Kim, J.-G., Park, S.-J., Damsté, J. S. S., Schouten, S., Rijpstra, W. I. C., Jung, M.-Y. *et al.* (2016). Hydrogen peroxide detoxification is a key mechanism for growth of ammonia-oxidizing archaea. *Proc Natl Acad Sci, 113*(28): 7888-7893.

Kim, M., Shin, B., Lee, J., Park, H. Y., & Park, W. (2019a). Culture-independent and culture-dependent analyses of the bacterial community in the phycosphere of cyanobloom-forming *Microcystis aeruginosa*. *Sci Rep, 9*(1): 1-13.

Kim, S., Kang, I., Seo, J.-H., & Cho, J.-C. (2019b). Culturing the ubiquitous freshwater actinobacterial acI lineage by supplying a biochemical 'helper' catalase. *ISME J, 13*: 2252-2263.

King, D. W., Cooper, W. J., Rusak, S. A., Peake, B. M., Kiddle, J. J., O'Sullivan, D. W. *et al.* (2007). Flow injection analysis of H2O2 in natural waters using acridinium ester chemiluminescence: method development and optimization using a kinetic model. *Anal Chem, 79*(11): 4169-4176.

Knap, A., Michaels, A., Close, A., Ducklow, H., & Dickson, A. (1996). Protocols for the joint global ocean flux study (JGOFS) core measurements. In.

Kozich, J. J., Westcott, S. L., Baxter, N. T., Highlander, S. K., & Schloss, P. D. (2013). Development of a Dual-Index Sequencing Startegy and Curation Pipeline for Analyzing

Amplicon Sequence Data on the MiSeq Illumina Sequencing Platform. *Appl Environ Microbiol, 79*(17): 5112-5120.

Lau, W., & Armbrust, E. (2006). Detection of glycolate oxidase gene glcD diversity among cultured and environmental marine bacteria. *Environ Microbiol, 8*(10): 1688-1702.

Lau, W. W., Keil, R. G., & Armbrust, E. V. (2007). Succession and diel transcriptional response of the glycolate-utilizing component of the bacterial community during a spring phytoplankton bloom. *Appl Environ Microbiol, 73*(8): 2440-2450.

Lee-Ruff, E. (1977). The organic chemistry of superoxide. *Chemical Society Reviews, 6*(2): 195-214.

Lin, L., Shan, K., Xiong, Q., Zhou, Q., Li, L., Gan, N., & Song, L. (2018). The ecological risks of hydrogen peroxide as a cyanocide: its effect on the community structure of bacterioplankton. *J Oceanol Limnol, 36*(6): 2231-2242.

Lin, Y., Gifford, S., Ducklow, H., Schofield, O., & Cassar, N. (2019). Towards Quantitative Microbiome Community Profiling Using Internal Standards. *Appl Environ Microbiol, 85*(5): e02634-02618.

Loewen, P. C., Switala, J., & Triggs-Raine, B. L. (1985). Catalases HPI and HPII in *Escherichia coli* are induced independently. *Arch Biochem Biophys, 243*(1): 144-149.

Lord, J. (1972). Glycolate oxidoreductase in *Escherichia coli*. *BBA-Bioenergetics, 267*(2): 227-237.

Lucas-Elío, P., Gómez, D., Solano, F., & Sanchez-Amat, A. (2006). The antimicrobial activity of marinocine, synthesized by *Marinomonas mediterranea*, is due to hydrogen peroxide generated by its lysine oxidase activity. *J Bacteriol, 188*(7): 2493-2501.

Lusty, M. W., & Gobler, C. J. (2020). The Efficacy of Hydrogen Peroxide in Mitigating Cyanobacterial Blooms and Altering Microbial Communities across Four Lakes in NY, USA. *Toxins, 12*(7): 428.

Ma, L., Calfee, B. C., Morris, J. J., Johnson, Z. I., & Zinser, E. R. (2018). Degradation of hydrogen peroxide at the ocean's surface: the influence of the microbial community on the realized thermal niche of *Prochlorococcus*. *ISME J, 12*(2): 473-484.

Marsico, R. M., Schneider, R. J., Voelker, B. M., Zhang, T., Diaz, J. M., Hansel, C. M., & Ushijima, S. (2015). Spatial and temporal variability of widespread dark production and decay of hydrogen peroxide in freshwater. *Aquat Sci, 77*(4): 523-533.

Matthijs, H. C., Visser, P. M., Reeze, B., Meeuse, J., Slot, P. C., Wijn, G. *et al.* (2012). Selective suppression of harmful cyanobacteria in an entire lake with hydrogen peroxide. *Water Res, 46*(5): 1460-1472.

Moffett, J. W., & Zafiriou, O. C. (1990). An investigation of hydrogen peroxide chemistry in surface waters of Vineyard Sound with $H_2{}^{18}O_2$ and $^{18}O_2$. *Limnol Oceanogr, 35*(6): 1221-1229.

Morris, J. J., Kirkegaard, R., Szul, M. J., Johnson, Z. I., & Zinser, E. R. (2008). Facilitation of robust growth of *Prochlorococcus* colonies and dilute liquid cultures by "helper" heterotrophic bacteria. *Appl Environ Microbiol, 74*(14): 4530-4534.

Morris, J. J., Johnson, Z. I., Szul, M. J., Keller, M., & Zinser, E. R. (2011). Dependence of the cyanobacterium *Prochlorococcus* on hydrogen peroxide scavenging microbes for growth at the ocean's surface. *PloS one, 6*(2): e16805.

Morris, J. J. (2015). Black Queen evolution: the role of leakiness in structuring microbial communities. *Trends Genet, 31*(8): 475-482.

Morris, J. J., Johnson, Z. I., Wilhelm, S. W., & Zinser, E. R. (2016). Diel regulation of hydrogen peroxide defenses by open ocean microbial communities. *J Plankton Res, 38*(4): 1103-1114.

Murphy, J., & Riley, J. P. (1962). A modified single solution method for the determination of phosphate in natural waters. *Anal Chim Acta, 27*: 31-36.

Nelson, E. B., & Tolbert, N. (1970). Glycolate dehydrogenase in green algae. *Arch Biochem Biophys, 141*(1): 102-110.

Oksanen, J., Blanchet, F. G., Kindt, R., Legendre, P., Minchin, P. R., O'hara, R. *et al.* (2013). Package 'vegan'.

Paerl, H. W., & Otten, T. G. (2013). Blooms bite the hand that feeds them. *Science, 342*(6157): 433-434.

Palenik, B., & Morel, F. M. (1990). Comparison of cell-surface L-amino acid oxidases from several marine phytoplankton. *Mar Ecol Prog Ser, 59*: 195-201.

Pedregosa, F., Varoquaux, G., Gramfort, A., Michel, V., Thirion, B., Grisel, O. *et al.* (2011). Scikit-learn: Machine learning in Python. *J Mach Learn Res, 12*: 2825-2830.

Petasne, R. G., & Zika, R. G. (1987). Fate of superoxide in coastal sea water. *Nature, 325*(6104): 516-518.

Powers, L. C., & Miller, W. L. (2014). Blending remote sensing data products to estimate photochemical production of hydrogen peroxide and superoxide in the surface ocean. *Environ Sci Process Impact, 16*(4): 792-806.

Pruesse, E., Quast, C., Knittel, K., Fuchs, B. M., Ludwig, W., Peplies, J., & Glöckner, F. O. (2007). SILVA: a comprehensive online resource for quality checked and aligned ribosomal RNA sequence data compatible with ARB. *Nucleic Acids Res, 35*(21): 7188-7196.

Renström, E., & Bergman, B. (1989). Glycolate metabolism in cyanobacteria: I. Glycolate excretion and phosphoglycolate phosphatase activity. *Physiol Plant, 75*(2): 137-143.

Rizopoulos, D. (2009). Package 'bootStepAIC'. In.

Rojas, C. M., Senthil-Kumar, M., Wang, K., Ryu, C.-M., Kaundal, A., & Mysore, K. S. (2012). Glycolate oxidase modulates reactive oxygen species–mediated signal transduction during nonhost resistance in *Nicotiana benthamiana* and *Arabidopsis*. *Plant Cell, 24*(1): 336-352.

Rose, A. L., & Waite, T. D. (2006). Role of superoxide in the photochemical reduction of iron in seawater. *Geochim Cosmochim Acta, 70*(15): 3869-3882.

Rose, A. L., Webb, E. A., Waite, T. D., & Moffett, J. W. (2008). Measurement and implications of nonphotochemically generated superoxide in the equatorial Pacific Ocean. *Environ Sci Technol, 42*(7): 2387-2393.

Schloss, P. D., & Bishop, L. (2019). MiSeq Wet Lab SOP. Retrieved from https://github.com/SchlossLab/MiSeq_WetLab_SOP/blob/master/MiSeq_WetLab_SOP.md

Schmitz, J., Srikanth, N. V., Hüdig, M., Poschmann, G., Lercher, M. J., & Maurino, V. G. (2017). The ancestors of diatoms evolved a unique mitochondrial dehydrogenase to oxidize photorespiratory glycolate. *Photosynth Res, 132*(2): 183-196.

Schneider, R. J., Roe, K. L., Hansel, C. M., & Voelker, B. M. (2016). Species-level variability in extracellular production rates of reactive oxygen species by diatoms. *Front Chem, 4*: 5.

Schuurmans, J. M., Brinkmann, B. W., Makower, A. K., Dittmann, E., Huisman, J., & Matthijs, H. C. (2018). Microcystin interferes with defense against high oxidative stress in harmful cyanobacteria. *Harmful Algae, 78*: 47-55.

Seaver, L. C., & Imlay, J. A. (2001). Alkyl hydroperoxide reductase is the primary scavenger of endogenous hydrogen peroxide in *Escherichia coli*. *J Bacteriol, 183*(24): 7173-7181.

Seki, M., Iida, K.-i., Saito, M., Nakayama, H., & Yoshida, S.-i. (2004). Hydrogen peroxide production in *Streptococcus pyogenes*: involvement of lactate oxidase and coupling with aerobic utilization of lactate. *J Bacteriol, 186*(7): 2046-2051.

Sutherland, K. M., Wankel, S. D., & Hansel, C. M. (2020). Dark biological superoxide production as a significant flux and sink of marine dissolved oxygen. *Proc Natl Acad Sci, 201912313*. doi:10.1073/pnas.1912313117

Tolar, B. B., Powers, L. C., Miller, W. L., Wallsgrove, N. J., Popp, B. N., & Hollibaugh, J. T. (2016). Ammonia oxidation in the ocean can be inhibited by nanomolar concentrations of hydrogen peroxide. *Front Mar Sci, 3*: 237.

Tolbert, N. (1979). Glycolate metabolism by higher plants and algae. In *Photosynthesis II* (pp. 338-352): Springer.

Tong, H., Chen, W., Merritt, J., Qi, F., Shi, W., & Dong, X. (2007). *Streptococcus oligofermentans* inhibits *Streptococcus mutans* through conversion of lactic acid into inhibitory H2O2: a possible counteroffensive strategy for interspecies competition. *Mol Microbiol, 63*(3): 872-880.

Tong, H., Chen, W., Shi, W., Qi, F., & Dong, X. (2008). SO-LAAO, a novel L-amino acid oxidase that enables *Streptococcus oligofermentans* to outcompete *Streptococcus mutans* by generating H2O2 from peptone. *J Bacteriol, 190*(13): 4716-4721.

Trusiak, A., Treibergs, L. A., Kling, G. W., & Cory, R. M. (2018). The role of iron and reactive oxygen species in the production of CO2 in arctic soil waters. *Geochim Cosmochim Acta, 224*: 80-95.

Ueki, R., Imaizumi, Y., Iwamoto, Y., Sakugawa, H., & Takeda, K. (2020). Factors controlling the degradation of hydrogen peroxide in river water, and the role of riverbed sand. *Sci Total Environ, 716*: 136971.

Vermilyea, A. W., Dixon, T. C., & Voelker, B. M. (2010a). Use of H218O2 to measure absolute rates of dark H2O2 production in freshwater systems. *Environ Sci Technol, 44*(8): 3066-3072.

Vermilyea, A. W., Paul Hansard, S., & Voelker, B. M. (2010b). Dark production of hydrogen peroxide in the Gulf of Alaska. *Limnol Oceanogr, 55*(2): 580-588.

Voelker, B. M., Sedlak, D. L., & Zafiriou, O. C. (2000). Chemistry of superoxide radical in seawater: Reactions with organic Cu complexes. *Environ Sci Technol, 34*(6): 1036-1042.

Wang, Q., Garrity, G. M., Tiedje, J. M., & Cole, J. R. (2007). Naive Bayesian classifier for rapid assignment of rRNA sequences into the new bacterial taxonomy. *Appl Environ Microbiol, 73*(16): 5261-5267.

Weinbauer, M. G., & Suttle, C. A. (1999). Lysogeny and prophage induction in coastal and offshore bacterial communities. *Aquat Microb Ecol, 18*(3): 217-225.

Westcott, S. L., & Schloss, P. D. (2017). OptiClust, an improved method for assigning amplicon-based sequence data to operational taxonomic units. *MSphere, 2*(2): e00073-00017.

Wood, E. D., Armstrong, F., & Richards, F. A. (1967). Determination of nitrate in sea water by cadmium-copper reduction to nitrite. *J Mar Biolog, 47*(1): 23-31.

Wuttig, K., Heller, M. I., & Croot, P. L. (2013). Reactivity of inorganic Mn and Mn desferrioxamine B with O2, O2–, and H2O2 in Seawater. *Environ Sci Technol, 47*(18): 10257-10265.

Wynne, T. T., Stumpf, R. P., Tomlinson, M. C., Fahnenstiel, G. L., Dyble, J., Schwab, D. J., & Joshi, S. J. (2013). Evolution of a cyanobacterial bloom forecast system in western Lake Erie: development and initial evaluation. *J Great Lakes Res, 39*: 90-99.

Xenopoulos, M. A., & Bird, D. F. (1997). Effect of acute exposure to hydrogen peroxide on the production of phytoplankton and bacterioplankton in a mesohumic lake. *Photochem Photobiol, 66*(4): 471-478.

Xie, H., Zafiriou, O. C., Cai, W.-J., Zepp, R. G., & Wang, Y. (2004). Photooxidation and its effects on the carboxyl content of dissolved organic matter in two coastal rivers in the southeastern United States. *Environ Sci Technol, 38*(15): 4113-4119.

Xu, P., Yano, T., Yamamoto, K., Suzuki, H., & Kumagai, H. (1996). Characterization of a lactate oxidase from a strain of gram negative bacterium from soil. *Appl Biochem Biotechnol, 56*(3): 277-288.

Zafiriou, O. (1990). Chemistry of superoxide ion-radical (O_2^-) in seawater. I. pK_{asw}^*(HOO) and uncatalyzed dismutation kinetics studied by pulse radiolysis. *Mar Chem, 30*: 31-43.

Zika, R. G., Moffett, J. W., Petasne, R. G., Cooper, W. J., & Saltzman, E. S. (1985). Spatial and temporal variations of hydrogen peroxide in Gulf of Mexico waters. *Geochim Cosmochim Acta, 49*(5): 1173-1184.

Zinser, E. R. (2018a). The microbial contribution to reactive oxygen species dynamics in marine ecosystems. *Environ Microbiol Rep, 10*(4): 412-427.

Zinser, E. R. (2018b). Cross-protection from hydrogen peroxide by helper microbes: the impacts on the cyanobacterium *Prochlorococcus* and other beneficiaries in marine communities. *Environ Microbiol Rep, 10*(4): 399-411.

Chapter 6 Conclusions

6.1 Overview and Summary

In this chapter, the major conclusions of the research in this dissertation are discussed along with remaining research gaps to be addressed in future work. In this section, an overview and summary of the research questions is given, and following sections expand on specific conclusions and future work. In Chapter 2, the hypothesis that hydrogen peroxide (H_2O_2) concentrations in lakes may favor microcystin producing ("toxic") and non-microcystin producing ("nontoxic") strains of the harmful cyanobacterium *Microcystis* (Paerl & Otten, 2013) was tested using two approaches. First, the genes and organisms that participate in hydrogen peroxide (H_2O_2) decomposition during cyanobacteria blooms in western Lake Erie were identified. Second, the response of toxic and nontoxic *Microcystis* strains that lack catalase genes to an exogenous H_2O_2 scavenger was measured. While some published genomes of the harmful bloom forming cyanobacterium *Microcystis* have catalase genes, most do not, which suggests that *Microcystis* strains vary in their ability to resist damage from H_2O_2. While expression of *katG* by *Microcystis* was detected during blooms, *katG* transcripts in phytoplankton seston were dominated by other non-cyanobacteria, which may indicate that community wide decomposition of H_2O_2 by bacteria in the phycosphere benefits the growth of *Microcystis* strains lacking catalase genes. Although all *Microcystis* strains degraded H_2O_2 without catalase, which suggests that *ahpC* activity is sufficient to degrade and detoxify H_2O_2 in *Microcystis* under the experimental conditions tested here, the study found that some *Microcystis* strains benefit from

help decomposing extracellular H_2O_2. However, maximum growth rates of both toxic and nontoxic *Microcystis* strains were unimpacted by the H_2O_2 scavenger, which suggests that other genotypic and phenotypic differences apart from microcystin production determine how H_2O_2 affects *Microcystis* growth. Thus, changes in H_2O_2 concentrations and H_2O_2 decomposition by phycosphere bacteria may favor some *Microcystis* strains over others although not along a toxic versus nontoxic dichotomy.

Chapter 3 identified which bacteria in bulk phytoplankton seston are specifically associated with *Microcystis* colonies, and characterized how bacterial community composition in the *Microcystis* phycosphere varies across colony oligotypes and seasonally over *Microcystis* bloom development. Several bacteria species were found to be frequent members of individual *Microcystis* colonies. However, no bacteria species were present on every *Microcystis* colony, and phycosphere community composition was significantly more similar between colonies that shared a sampling date and *Microcystis* oligotype. The significant differences between sampling date and colony oligotype suggests that phycosphere communities change over time and that different *Microcystis* strains harbor characteristic microbiomes; however, future experimental work is required to test the extent to which time of sampling and strain identity explain differences in phycosphere community composition.

Chapter 4 described the genome sequences of two novel Acidobacteria assembled from metagenomic sequences collected from phytoplankton seston during western Lake Erie cyanobacterial blooms. These organisms were of interest because they comprised a large proportion of *katG* transcripts during peak *katG* metatranscriptomic abundance in Chapter 2. The metabolism and potential interactions with *Microcystis* or other phytoplankton were inferred from the assembled genome sequences and gene functional annotations. The genome sequences

involved in the uptake and processing of oligopeptides, including cyanobacterial-derived peptides, amino acids, and known algal exudates suggests that these bacteria derive organic carbon and nitrogen from cell lysis or organic carbon excretion by phytoplankton. Efflux of amino acids during oligopeptide degradation may regenerate amino acids for phytoplankton growth. Both Acidobacteria lack B_{12} synthesis pathways yet express genes that require B_{12}, suggesting that they are auxotrophs and may also derive vitamins from phytoplankton or other bacteria in the phycosphere. Both organisms were detected in amplicon datasets from *Microcystis* blooms, including *Microcystis* colony phycosphere communities in Chapter 3. However, they were not specific to or found in all bloom datasets. Both Acidobacteria were present in some non-bloom samples, and were not present in every sample that contained *Microcystis*. Their irregular and non-specific presence in cyanobacteria blooms suggests that the Acidobacteria may only be associated with some *Microcystis* species or strains under certain conditions, and may also be attached to other phytoplankton taxa or inorganic and detrital particles.

Chapter 5 characterized the nature of H_2O_2 production and decay and tested the hypothesis that microbial community composition is related to H_2O_2 production rates in western Lake Erie cyanobacterial blooms. Net H_2O_2 production in whole water was similar to net H_2O_2 production in 0.22 μm filtered water despite higher net H_2O_2 decay in unfiltered water and no decay in 0.22 μm filtered water, which suggests a particle-dependent source of H_2O_2 that is attributed to microorganisms. This particle dependent source was found to be the predominant source in the experiments on average, although complications with estimating gross H_2O_2 production in light exposed bottles and the light wavelengths included in the experiment preclude a quantitative assessment of biological H_2O_2 production relative to photochemical

production of H_2O_2 *in situ*. H_2O_2 production increased with chlorophyll *a* concentrations, respiration rate, and primary production rate, suggesting that biological production of H_2O_2 increases with phytoplankton biomass and microbial growth. Microbial community similarity and OTU abundances were also correlated with H_2O_2 production rates, with OTU abundances explaining more of the variation in H_2O_2 production than chlorophyll *a* concentration or CDOM absorbance. However, future work is required to determine to what extend variable H_2O_2 sensitivities or variable H_2O_2 production rates between taxa can explain the observed relationships between H_2O_2 production rates and microbial community composition. In addition, a large portion of biotic H_2O_2 production was light-dependent, and filtration of large phytoplankton assemblages, including *Microcystis* colonies, did not significantly change H_2O_2 production rates. The results from filtration of phytoplankton assemblages >105 μm together with the light-dependency of biotic H_2O_2 production and the correlations between biotic H_2O_2 production and chlorophyll *a* concentration and primary production rates suggest that biotic H_2O_2 production in western Lake Erie is related to photosynthesis, but cannot be attributed to large phytoplankton assemblages and large *Microcystis* colonies.

6.2 Variable *katG* Distribution Across *Microcystis* Strains and its Importance for H_2O_2 Resistance

An investigation of the catalase and peroxidase genes in published *Microcystis* genomes revealed that most isolated *Microcystis* strains to date lack catalase genes, including *katG*, the primary scavenger of high concentrations of exogenous H_2O_2 in bacteria (Seaver & Imlay, 2001a; Perelman *et al.*, 2003; Cosgrove *et al.*, 2007). High sensitivity to H_2O_2 has been attributed to the absence of catalases in the cyanobacterium *Prochlorococcus* (Morris *et al.*, 2008; Morris *et al.*, 2011; Morris *et al.*, 2012) and in some species of Thaumarchaeota (Kim *et al.*, 2016; Bayer *et al.*, 2019). In addition, some strains of abundant freshwater bacterial clades require

removal of H_2O_2 in growth media for successful cultivation, which was attributed to the presence of a low efficiency *katG* in these bacteria (Kim *et al.*, 2019b). These H_2O_2-sensitive organisms require catalase producing helpers to tolerate naturally occurring H_2O_2 concentrations in media (Morris *et al.*, 2008; Kim *et al.*, 2016; Bayer *et al.*, 2019; Kim *et al.*, 2019b) and the environment (Morris *et al.*, 2011; Tolar *et al.*, 2016). Therefore, the variable distribution of *katG* in *Microcystis* may indicate that some strains are better equipped to degrade H_2O_2 than others. However, this hypothesis assumes that *katG* in *Microcystis* is comparable to the high activity catalases present in "helper" bacteria. Thus, comparisons of the catalase activity in *Microcystis* *katG* with those of efficient catalases is required to assess the role of *katG* in H_2O_2 detoxification in *Microcystis*.

Despite the absence of *katG*, several strains of *Microcystis* could degrade and tolerate H_2O_2 concentrations in growth media that inhibited the growth of other *katG*-lacking microbes (Morris *et al.*, 2011; Kim *et al.*, 2016). Because *Microcystis* could tolerate H_2O_2 concentrations in culture that are representative of some of the higher concentrations observed during blooms (Cory *et al.*, 2016; Cory *et al.*, 2017), KatG activity may not be essential for *Microcystis*, unlike other organisms. The H_2O_2 degradation by the *Microcystis* cultures is likely attributed to AhpC activity, which can compensate for the loss of *katG* in some bacteria at submicromolar H_2O_2 concentrations (Tichy & Vermaas, 1999; Seaver & Imlay, 2001a; Perelman *et al.*, 2003; Cosgrove *et al.*, 2007). However, *ahpC* genes in *Prochlorococcus* (Kim *et al.*, 2019a) could not compensate for the absence of *katG* at comparable H_2O_2 concentrations (Morris *et al.*, 2011). The data in the literature together with the results in this dissertation suggests that AhpC activity only compensates for a lack of *katG* in cyanobacteria under certain conditions or in certain organisms.

Several mechanisms could perhaps explain how *Microcystis* is less dependent on *katG* than other aquatic microbes. Because *Microcystis* grows in eutrophic waters with higher CDOM concentrations than those in the open ocean, it is likely that *Microcystis* has evolved to tolerate the higher H_2O_2 concentrations that would be produced. For example, AhpC in *Microcystis* may be more efficient at H_2O_2 degradation than in sensitive organisms such as *Prochlorococcus*. Indeed, AhpC protein in bacteria are less prone to over-oxidation and deactivation by H_2O_2 than their eukaryotic homologs**,** which is attributed to insertion sequences in the eukaryotic homologs that are absent in bacterial *ahpC* (Wood et al., 2003). Insertion sequences in *ahpC* that are unique to certain cyanobacteria and proteobacteria have also been observed (Wood *et al.*, 2003), but the significance of the insertion sequences in these organisms to protein function and the resistance of the organism to exogenous H_2O_2 are currently unknown.

Second, the ability for *ahpC* to compensate for the loss of *katG* may depend on the availability of NADPH and reduced thioredoxin, which are required electron donors for AhpC activity (Tichy & Vermaas, 1999; Hosoya-Matsuda *et al.*, 2005; Pérez-Pérez *et al.*, 2009). Thioredoxins have a variety of target enzymes (Wolosiuk & Buchanan, 1978; Buchanan, 1980; Schürmann & Jacquot, 2000; Kumar *et al.*, 2004) that may compete with AhpC for electron donor. AhpC activity may also change with nutrient status of the cell, as intracellular NAD(P)H concentrations in *Microcystis* change with the form and availability of nitrogen (Steffen *et al.*, 2014). Light availability may also determine AhpC activity, as the regeneration of reduced thioredoxin can occur through a light-dependent ferredoxin:thioredoxin reductase system in cyanobacteria (Buchanan *et al.*, 1971; Wolosiuk & Buchanan, 1978). Indeed, *katG* mutants of cyanobacteria require light to decompose H_2O_2 (Tichy & Vermaas, 1999; Perelman *et al.*, 2003);

however, how H_2O_2 degradation rates change as a function of light intensity in the mutant strains or in cyanobacteria that naturally lack *katG* is unknown.

Third, the sensitivity of *Microcystis* toward H_2O_2 may change with environmental conditions independent of AhpC activity. For instance, while *Prochlorococcus* strains did not vary in their ability to degrade H_2O_2, whether or not a given *Prochlorococcus* strain relied on catalase-producing helpers to grow was dependent on light intensity (Morris *et al.*, 2011) and deviation from optimal growth temperature (Ma *et al.*, 2018). Furthermore, the effectiveness of H_2O_2 treatments in suppressing *Microcystis* growth depended on the wavelength and intensity of light (Piel *et al.*, 2020) and nutrient availability (Sandrini *et al.*, 2020). Changes in exopolysaccharide production (Gao *et al.*, 2015) or cell surface structures (Bayer *et al.*, 2019) with environmental conditions may also alter the ability of a strain to tolerate H_2O_2 by changing the amount of H_2O_2 that diffuses into the cell. This suggests that KatG activity (either from helper bacteria or within its own cells) may be essential for some *Microcystis* strains only under a specific set of environmental conditions. In addition, the H_2O_2 concentrations present in growth media may select for *Microcystis* strains that are more tolerant to high H_2O_2 concentrations, as observed in other bacteria (Tanaka *et al.*, 2014; Kawasaki & Kamagata, 2017). Therefore, H_2O_2 may also more widely impair *Microcystis* growth than indicated by the experiments in this dissertation. To test if *Microcystis* strains become more sensitive to H_2O_2 under certain environmental conditions, the experiments conducted in Chapter 2 of this dissertation should be repeated under a wider range of culturing conditions.

6.3 Increased H_2O_2 Concentrations do not Favor Microcystin-Producing *Microcystis* Strains *per se*

Some evidence suggests that microcystin may protect cyanobacteria from oxidative stress caused by H_2O_2. Previous studies have showed that toxic *Microcystis* strains have lower

decreases in chlorophyll *a* concentrations when treated with H_2O_2 (Dziallas & Grossart, 2011; Zilliges *et al.*, 2011) and that microcystin binds to proteins at areas sensitive to H_2O_2 damage (Zilliges *et al.*, 2011), which lead to the hypothesis that higher concentrations of H_2O_2 during *Microcystis* blooms favor the proliferation of toxic *Microcystis* over nontoxic *Microcystis* strains. However, other studies have presented contradicting evidence, that toxic strains are more susceptible to H_2O_2 (Schuurmans *et al.*, 2018). Neither hypothesis is supported by the results of this dissertation in that 1) several toxic and nontoxic *Microcystis* strains were unimpacted by the addition of an H_2O_2 scavenger to the growth medium, which should have improved the growth of strains that were impaired by H_2O_2, and 2) the only strain with improved growth rates in the presence of a scavenger was toxic. Therefore, the ability of a strain to produce microcystin does not inherently make it more or less resistant to H_2O_2 than a naturally nontoxic strain. This suggests that other genotypic and phenotypic differences between *Microcystis* strains determine their sensitivity to H_2O_2. However, this interpretation may be impacted by the caveat that the *Microcystis* strains tested here may become sensitive to H_2O_2 under different growth conditions than those tested in this dissertation. Therefore, a comparison of growth impairments from H_2O_2 in toxic and nontoxic *Microcystis* strains over a wider range of culturing conditions is warranted.

6.4 The Impact of Community Wide H_2O_2 Decomposition on the Composition of *Microcystis* Strains During Blooms

Despite the ability of all the *Microcystis* strains tested to degrade H_2O_2, one of the strains had improved growth rates when cultured with a scavenger of H_2O_2 and thus was sensitive to H_2O_2 in the growth medium. This result demonstrates that 1) *Microcystis* strains can have variable sensitivities to H_2O_2 in spite of having similar H_2O_2 degradation capabilities, and 2) the presence of *ahpC* and H_2O_2 degradation does not preclude a microorganism from benefitting from H_2O_2 decomposition by other H_2O_2 scavengers. Therefore, H_2O_2 decomposition by bacteria

in the phycosphere could impact growth of some *Microcystis* under certain conditions. While this dissertation does not support that changes in H_2O_2 concentrations favor nontoxic or toxic *Microcystis* strains specifically, it does indicate that changes in H_2O_2 concentrations can differently impact growth rates of *Microcystis* strains. The differential impact of changing H_2O_2 concentrations on *Microcystis* strain growth could impact the composition of *Microcystis* strains during blooms, albeit not along a toxic and nontoxic dichotomy as previously hypothesized (Paerl & Otten, 2013; Schuurmans *et al.*, 2018). However, it is still uncertain at what H_2O_2 concentration thresholds *Microcystis* strains begin to experience negative outcomes on growth, and how these concentration thresholds may change as a function of other environmental conditions as described above. Future work should better characterize under which environmental conditions and concentrations H_2O_2 effects various *Microcystis* strains. Furthermore, competition experiments between various *Microcystis* strains at a range of H_2O_2 concentrations are ultimately required to explicitly demonstrate that H_2O_2 concentrations can impact *Microcystis* strain composition during blooms.

Although *katG* expression by *Microcystis* was detected in western Lake Erie cyanobacterial blooms, *katG* expression in phytoplankton seston was dominated by attached non-cyanobacteria (nc-bacteria). Additionally, because phycosphere bacteria colonize the perimeter of *Microcystis* colonies (Parveen *et al.*, 2013), they likely are exposed to more exogenous H_2O_2 than *Microcystis* cells on the colony interior and may act as a first line of defense against exogenous H_2O_2 for colonial *Microcystis* cells. However, the H_2O_2 decomposition rates of many of the enzymes and organisms identified in western Lake Erie are unknown and thus require biochemical validation in order to identify which organisms are likely important "helpers" for H_2O_2 degradation in cyanobacterial colonies.

6.5 *Microcystis* Phycosphere Bacterial Communities are Distinct From Bacterial Communities in Bulk Whole Water and Phytoplankton Seston

In Chapter 2, the organisms that express catalases and peroxidases in phytoplankton seston were identified. While *Microcystis* dominates colonial cyanobacteria in western Lake Erie blooms (Berry *et al.*, 2017), other phytoplankton such as diatoms (Kharbush *et al.*, 2019) can also be a substantial portion of the phytoplankton community during western Lake Erie blooms. Therefore, the bacteria identified in bulk phytoplankton seston may not necessarily be associated with *Microcystis* nor could their gene expression or abundance patterns be related to *Microcystis* physiology. The results in Chapter 3 demonstrate that bacterial communities associated with *Microcystis* colonies are distinct from total water column communities and bulk phytoplankton communities and suggests that the *Microcystis* phycosphere is a microenvironment that harbors a specific subset of the bacteria present in bulk seston. This characterization of the communities physically associated with *Microcystis* is important for understanding their interactions, which are limited to small spatial scales when the uptake rates of molecules exchanged between community members is fast compared to their diffusion rates (Dal Co *et al.*, 2020). However, rates of metabolite uptake and leakage in *Microcystis* colonies have yet to be measured, thus the spatial scale of interactions between nc-bacteria and *Microcystis* is uncertain.

6.6 *Microcystis* Phycosphere Community Composition Varies With Sampling Date and *Microcystis* Oligotype

Although *Microcystis* phycosphere communities were found to be distinct from bulk communities, they varied by both sampling date and *Microcystis* oligotype, which suggests that phycosphere communities of different *Microcystis* strains have characteristic microbiomes and that the phycosphere communities change over time. However, due to limitations in the sampling of *Microcystis* colonies and the resolution of oligotyping to identify *Microcystis* strains, we

cannot determine the mechanism that drives the observed taxonomic divergence in phycosphere community composition, nor can we infer whether temporal effects or genotypic and phenotypic differences between *Microcystis* are more important in determining phycosphere community composition. However, the relative abundance patterns of specific OTUs identified in the *Microcystis* phycosphere suggest that both mechanisms likely play a role for different bacterial species in the phycosphere. Colonization experiments are required to test the hypotheses emerging from the results of Chapter 3.

The observation that different bacterial communities occupy the *Microcystis* phycosphere at different times and are associated with different *Microcystis* strains suggests that the impact associated bacteria have on *Microcystis* fitness also changes by time and strain. Indeed, bacterial isolates can have strain specific impacts on phytoplankton growth, and the same isolate can be beneficial, neutral, or harmful to different phytoplankton taxa, which includes species or strains of the same genus (Sison-Mangus *et al.*, 2014; Amin *et al.*, 2015; Agha *et al.*, 2016). As there is experimental evidence that bacteria can influence competition between *Microcystis* and other phytoplankton groups (Schmidt *et al.*, 2020), such strain specific impacts on growth may influence successions in phytoplankton taxa during cyanobacteria blooms. However, taxonomically divergent *Microcystis* phycosphere communities in enrichment cultures converged in their functional potential (Jackrel *et al.*, 2019), and host-specific recruitment of bacterial communities does not always translate into host-specific outcomes on phytoplankton fitness (Jackrel *et al.*, 2020). Therefore, the significance of taxonomically distinct microbiomes over time and between *Microcystis* genotypes on the growth of different *Microcystis* strains is uncertain. Measurements of the impact that taxonomically distinct microbiomes have on growth

of various *Microcystis* strains is required to assess their importance in affecting bloom development and *Microcystis* strain successions.

6.7 Genomic Analysis Highlights Potential Peptide, Amino Acid, and Vitamin Exchange Within the *Microcystis* Phycosphere

In Chapter 4, analysis of gene expression in two Acidobacteria genomes that had high *katG* expression relative to their abundance in phytoplankton seston from *Microcystis* blooms suggested that a bacterium in the *Microcystis* phycosphere (a novel *Bryobacter* sp.) uptakes oligopeptides, amino acids, nucleosides, and organic acid exudates from phytoplankton. Furthermore, there was metatranscriptomic evidence that *Bryobacter* regenerates ammonia from amino acids with amino acid oxidases and may export and regenerate amino acids during oligopeptide decomposition. The regeneration of these nitrogen containing compounds may fuel phytoplankton growth during blooms (Davis *et al.*, 2010; Paerl *et al.*, 2011), especially during periods when dissolved inorganic nitrogen is depleted. Another unclassified Acidobacterium showed expression of genes with similar functional annotations, but its absence from the *Microcystis* phycosphere communities described in Chapter 3 and its presence in datasets where *Microcystis* is absent suggests that it associates with other phytoplankton or other particles. Because the specific particle types that the unclassified Acidobacterium associates with are unknown, and both Acidobacteria genomes have high sequence dissimilarity from known organisms, their role in affecting phytoplankton growth remains uncertain. Cultivation of these organisms and biochemical characterization of their proteins is required to assess their impact on and dependence on phytoplankton growth.

6.8 Biotic H_2O_2 Production can be an Important Source of H_2O_2 During *Microcystis* Blooms

In Chapter 5, H_2O_2 production rates in the summer-fall in western Lake Erie were correlated with chlorophyll *a* concentration, respiration rates, primary production rates, OTU abundances, microbial community dissimilarity and CDOM absorbance, suggesting that both biological and photochemical sources of H_2O_2 are important during western Lake Erie cyanobacterial blooms. Further supporting this, observed net H_2O_2 production in whole water was comparable to observed H_2O_2 production in 0.22 μm filtered water (which removes most microorganisms) despite increased decay of H_2O_2 in whole water, which indicates increased total gross H_2O_2 production in whole water due to an additional particle-dependent source. The most parsimonious source in freshwaters is currently production from microorganisms (Vermilyea *et al.*, 2010; Diaz *et al.*, 2013; Marsico *et al.*, 2015; Diaz & Plummer, 2018), which is supported in that bacterial OTU abundances could explain more of the variation in gross particle dependent H_2O_2 production than both chlorophyll *a* concentration (a proxy of phytoplankton biomass) and CDOM absorbance.

Although it was not always the predominate source, estimated biotic production was consistently a substantial portion (> 40 %) of total H_2O_2 production during the experiments. However, error in the model used to derive gross biotic production rates increased with increasing CDOM absorbance, which may indicate that experiments with high photochemical production confounded estimates of biological production in the light. In addition, UV light, which has the highest H_2O_2 yield per mol photon (Powers & Miller, 2014), during the experiments was lower than those experienced by surface waters in Lake Erie. Therefore, the results in Chapter 5 may bias biological production over photochemical production, and the relative importance of the two sources *in situ* remains uncertain. Despite this shortcoming, it is

clear from the reduced UV conditions in the experiments and the differences in whole and 0.22 μm filtered water that biological production is a substantial source of H_2O_2 in Lake Erie waters.

6.9 Biotic H_2O_2 Production in Western Lake Erie is Related to Photosynthesis but not Attributed to Large Phytoplankton Assemblages and *Microcystis* Colonies

Results from Chapter 5 provide evidence that biotic H_2O_2 is related to photosynthesis yet is not related to large *Microcystis* colonies and other large phytoplankton assemblages. Light-dependent biotic H_2O_2, and significant correlations between biotic H_2O_2 production, chlorophyll *a* concentration, and primary production rates support that H_2O_2 production is related to phytoplankton growth, but filtration of *Microcystis* colonies and phytoplankton assemblages > 105 μm diameter did not changes H_2O_2 production rates. Respiration of algal exudates by heterotrophic bacteria could be a potential source of H_2O_2, as excretion of photosynthates by phytoplankton is light dependent (Hellebust, 1965; Han & Eley, 1973; Bateson & Ward, 1988; Renström & Bergman, 1989), and microbial oxidation of some organics in photosynthate, such as glycolate, amino acids, and lactate and produces H_2O_2 (Xu *et al.*, 1996; Tong *et al.*, 2008; Hackenberg *et al.*, 2011). Alternatively, small micro- and nanophytoplankton may be sources of H_2O_2 during Lake Erie blooms (Schneider *et al.*, 2016; Diaz & Plummer, 2018; Diaz *et al.*, 2019). While future experimental work is required to determine which microbial species and pathways are most important for H_2O_2 production during western Lake Erie cyanobacterial blooms, the results from this dissertation support that *Microcystis* may not only be impacted by H_2O_2 decomposition by the surrounding bacterial community as discussed in Chapter 2 and elsewhere (Kim *et al.*, 2019a) but also by community-wide H_2O_2 production. Because biotic H_2O_2 increases with primary production rates and chlorophyll *a* concentrations in western Lake Erie, potential negative impacts to H_2O_2-sensitive *Microcystis* would be highest when rates of primary production, respiration, and perhaps exudate excretion are highest, which may maximize

growth advantages of *Microcystis* strains that are relatively H_2O_2-resistant. However, the impact of the H_2O_2 fluxes measured here on growth of *Microcystis* relative to other factors such as water temperature, light availability, and nutrient concentrations remains unknown.

6.10 Phytoplankton Assemblages do not Impact Whole Water H_2O_2 Decomposition Rates

In Chapter 5, filtration of phytoplankton assemblages and large *Microcystis* colonies also had no significant impact on H_2O_2 decay rates, suggesting that large *Microcystis* colonies have little or no impact on whole water H_2O_2. This result suggests that free-living or smaller particles are responsible for the majority of whole water H_2O_2 decomposition, which brings to question the significance of the *katG* expressing bacteria attached to phytoplankton seston identified in Chapter 2. It is uncertain whether the lack of importance of *Microcystis* colonies and their phycospheres for whole water H_2O_2 decomposition rates means that H_2O_2 decomposition in the phycosphere is unimportant for *Microcystis* growth and physiology. Previous work has demonstrated that community-wide H_2O_2 decomposition is important in determining the response of a given microbe to H_2O_2 (Morris *et al.*, 2011; Bayer *et al.*, 2019). However, this work was performed strictly in single-cell batch cultures. Therefore, how the benefits of potential H_2O_2 interactions across various degrees of physical association and interaction scales is unknown. Previous work determined that interactions underpinned by metabolite exchange occur on the scale of a few cell lengths when the uptake rates of the exchanged metabolites are fast compared to metabolite excretion rates (Dal Co *et al.*, 2020). Because H_2O_2 diffuses in and out of cells rapidly (Seaver & Imlay, 2001b), and H_2O_2 production and decay can also be rapid (Seaver & Imlay, 2001b; Marsico *et al.*, 2015), interactions based on H_2O_2 decomposition may also be limited to short interaction ranges. Therefore, while unimportant for measured H_2O_2 concentrations in whole water, H_2O_2 decomposition of attached bacteria in the phycosphere may

be important for fitness of H_2O_2-sensitive *Microcystis* strains. However, interaction ranges of the organisms must then also vary between organisms with different H_2O_2 decomposition rates, which varies widely (Bond *et al.*, 2020). Future work that quantifies the interaction ranges of H_2O_2 decomposition of microbes in the phycosphere is required to assess their importance to *Microcystis* growth and physiology.

6.11 H_2O_2 Production Rates are Correlated With Microbial Community Composition and OTU Abundances

H_2O_2 production rates in western Lake Erie were correlated with microbial community dissimilarity and OTU abundances, however it is difficult to determine from the results presented in this dissertation whether this is due to increasing H_2O_2 production favoring the proliferation of resistant microbes or a proliferation of high H_2O_2 producing species that cause increasing H_2O_2 production. Production of H_2O_2 and its precursor superoxide radical anion (O_2^-) varies widely across bacterial and phytoplankton taxa (Diaz *et al.*, 2013; Diaz & Plummer, 2018; Bayer *et al.*, 2019; Bond *et al.*, 2020; Sutherland *et al.*, 2020), as does the sensitivity of microbes to H_2O_2 (Morris *et al.*, 2008; Zinser, 2018; Lusty & Gobler, 2020), so it is likely that both mechanisms are at play, although this hypothesis remains speculative at this point. The abundance of most OTUs had a low overall importance in predicting observed total and estimated biotic H_2O_2 production rates, which indicates that the response to H_2O_2 is a community-wide response (or at least a response of multiple populations) rather than a response in a few key species. Therefore, if a change in the abundance of H_2O_2 producing species explains the correlation between microbial community composition and H_2O_2 production rates, it may be due to changes in community-wide H_2O_2 production rates or the abundances of specific H_2O_2 producing genes and metabolisms that are distributed across multiple taxonomic groups. While the mechanism behind the correlation between microbial community composition and H_2O_2 production is uncertain, the

results presented here are the first to show that microbial community composition is related to natural H_2O_2 production rates in aquatic ecosystems, and is an important advance in understanding the relationship between reactive oxygen species production and microbial communities.

6.12 Future Directions

Overall, this dissertation has advanced our understanding of the role of H_2O_2 on impacting *Microcystis* fitness and the relative proportions of toxic and nontoxic *Microcystis* strains, the nature of H_2O_2 production during harmful cyanobacterial blooms, the composition of bacterial communities associated with the *Microcystis* phycosphere, and how microbial interactions underpin the effects that H_2O_2 have on CHAB ecology. This dissertation has provided the first evidence suggesting that H_2O_2 concentrations relevant to natural systems impact CHABs, rather than the large H_2O_2 treatments that are used to mitigate CHABs (Matthijs *et al.*, 2012; Schuurmans *et al.*, 2018; Daniel *et al.*, 2019; Lusty & Gobler, 2020; Piel *et al.*, 2020), and that other genotypic and phenotypic differences in *Microcystis* strains determine their sensitivity to H_2O_2. Thus, future work should place less emphasis on strains being toxic versus nontoxic strains when comparing *Microcystis* H_2O_2-sensitivities, and perhaps also differences in other traits. However, how differences between strains and changing environmental conditions lead to different sensitivities to H_2O_2 across *Microcystis* strains is unknown and requires further investigation.

In addition, this dissertation provides the first evidence that bacteria associated with *Microcystis* colonies may impact growth and physiology of some *Microcystis* strains under certain conditions. However, how H_2O_2 decomposition rates in the phycosphere bacteria compare to those in various *Microcystis* strains is still unknown and requires future

characterization. Furthermore, the relative importance of H_2O_2 decomposition by free-living and *Microcystis* attached bacteria remains uncertain, and future work that identifies the interaction range of H_2O_2 degradation is also needed to assess the importance of H_2O_2 decomposition in the phycosphere.

This dissertation also is the first to characterize natural H_2O_2 production and decay rates during freshwater CHABs. Evidence was provided that suggests biological production is an important source of H_2O_2 during CHABs and that the production is related to photosynthesis yet not directly attributed to *Microcystis* colonies. These results suggest that free-living microbes produce more H_2O_2 as photosynthesis increases, although the specific populations and pathways behind H_2O_2 production in CHABs could not be identified. Combined with the results of chapter 2, this suggests that community-wide H_2O_2 production and decay may impact *Microcystis* physiology as well as H_2O_2 decay. This dissertation also provides the first direct measurement of how microbial community composition and bacterial species abundance relate to natural production and decay rates of H_2O_2. However, the data presented here are not adequate to determine the mechanism behind the identified correlations. Future experimental work is necessary to pinpoint the cause of the significant relationships between H_2O_2 production rates and microbial community composition as well as to identify which pathways are important sources of H_2O_2 during CHABs.

This dissertation provides the first characterization of bacterial communities in the *Microcystis* phycosphere in individual colonies collected in a time series, thus allowing comparisons of how *Microcystis* phycosphere communities vary both with time and between different colonies and *Microcystis* strains. *Microcystis* phycosphere community composition varied by both sampling date and *Microcystis* oligotype. While the relative importance of time

and *Microcystis* oligotype on *Microcystis* phycosphere community composition could not be quantified, evidence suggests that both are important drivers in determining the abundance of certain OTUs on *Microcystis* colonies. However, limitations on identifying *Microcystis* strains by 16S rRNA oligotyping may confound interpretation of phycosphere community dissimilarity by sampling date and *Microcystis* oligotype. Therefore, further sampling of larger colony datasets with better resolution of *Microcystis* strains is warranted. Furthermore, the functional significance of taxonomically distinct phycosphere communities is also unknown, and should be a focus of future work.

Last, novel Acidobacteria genomes identified in the phycosphere of *Microcystis* and other particles were described. This work represents the first description of Acidobacteria genomes from aquatic environments and identifies putative interactions with phytoplankton. However, cultivation of the Acidobacteria and experimental verification of the putative interactions inferred here are required from future work.

6.13 References

Agha, R., del Mar Labrador, M., de los Ríos, A., & Quesada, A. (2016). Selectivity and detrimental effects of epiphytic *Pseudanabaena* on *Microcystis* colonies. *Hydrobiologia, 777*(1): 139-148.

Amin, S. A., Hmelo, L. R., van Tol, H. M., Durham, B. P., Carlson, L. T., Heal, K. R. *et al.* (2015). Interaction and signalling between a cosmopolitan phytoplankton and associated bacteria. *Nature, 522*(7554): 98-101. doi:10.1038/nature14488

Bateson, M. M., & Ward, D. M. (1988). Photoexcretion and fate of glycolate in a hot spring cyanobacterial mat. *Appl Environ Microbiol, 54*(7): 1738-1743.

Bayer, B., Pelikan, C., Bittner, M. J., Reinthaler, T., Könneke, M., Herndl, G. J., & Offre, P. (2019). Proteomic Response of Three Marine Ammonia-Oxidizing Archaea to Hydrogen Peroxide and Their Metabolic Interactions with a Heterotrophic Alphaproteobacterium. *mSystems, 4*(4): e00181-00119.

Berry, M. A., Davis, T. W., Cory, R. M., Duhaime, M. B., Johengen, T. H., Kling, G. W. *et al.* (2017). Cyanobacterial harmful algal blooms are a biological disturbance to Western Lake Erie bacterial communities. *Environ Microbiol, 19*(3): 1149-1162.

Bond, R. J., Hansel, C. M., & Voelker, B. M. (2020). Heterotrophic Bacteria Exhibit a Wide Range of Rates of Extracellular Production and Decay of Hydrogen Peroxide. *Front Mar Sci*.

Buchanan, B. B., Schürmann, P., & Kalberer, P. P. (1971). Ferredoxin-activated Fructose Diphosphatase of Spinach Chloroplasts. Resolution Of The System, Properties of the Alkaline Fructose Diphosphatase Compenent, and Physiological Significance of the Ferredoxin-Linked Activation. *J Biol Chem, 246*(19): 5952-5959.

Buchanan, B. B. (1980). Role of light in the regulation of chloroplast enzymes. *Ann Rev Plant Physiol, 31*(1): 341-374.

Cory, R. M., Davis, T. W., Dick, G. J., Johengen, T., Denef, V. J., Berry, M. A. *et al.* (2016). Seasonal dynamics in dissolved organic matter, hydrogen peroxide, and cyanobacterial blooms in Lake Erie. *Front Mar Sci, 3*: 54.

Cory, R. M., Davis, T., Dick, G., Johengen, T., Denef, V. J., Berry, M. *et al.* (2017). Corrigendum: Seasonal dynamics in dissolved organic matter, hydrogen peroxide, and cyanobacterial blooms in Lake Erie. *Front Mar Sci, 4*: 377.

Cosgrove, K., Coutts, G., Jonsson, M., Tarkowski, A., Kokai-Kun, J. F., Mond, J. J., & Foster, S. J. (2007). Catalase (*KatA*) and alkyl hydroperoxide reductase (*AhpC*) have compensatory roles in peroxide stress resistance and are required for survival, persistence, and nasal colonization in *Staphylococcus aureus*. *J Bacteriol, 189*(3): 1025-1035.

Dal Co, A., van Vliet, S., Kiviet, D. J., Schlegel, S., & Ackermann, M. (2020). Short-range interactions govern the dynamics and functions of microbial communities. *Nat Ecol Evol, 4*(3): 366-375.

Daniel, E., Weiss, G., Murik, O., Sukenik, A., Lieman-Hurwitz, J., & Kaplan, A. (2019). The response of *Microcystis aeruginosa* strain MGK to a single or two consecutive H2O2 applications. *Environ Microbiol Rep, 11*(5): 621-629.

Davis, T. W., Harke, M. J., Marcoval, M. A., Goleski, J., Orano-Dawson, C., Berry, D. L., & Gobler, C. J. (2010). Effects of nitrogenous compounds and phosphorus on the growth of toxic and non-toxic strains of *Microcystis* during cyanobacterial blooms. *Aquat Microb Ecol, 61*(2): 149-162.

Diaz, J. M., Hansel, C. M., Voelker, B. M., Mendes, C. M., Andeer, P. F., & Zhang, T. (2013). Widespread production of extracellular superoxide by heterotrophic bacteria. *Science, 340*(6137): 1223-1226.

Diaz, J. M., & Plummer, S. (2018). Production of extracellular reactive oxygen species by phytoplankton: past and future directions. *J Plankton Res, 40*(6): 655-666.

Diaz, J. M., Plummer, S., Hansel, C. M., Andeer, P. F., Saito, M. A., & McIlvin, M. R. (2019). NADPH-dependent extracellular superoxide production is vital to photophysiology in the marine diatom *Thalassiosira oceanica*. *Proc Natl Acad Sci, 116*(33): 16448-16453.

Dziallas, C., & Grossart, H.-P. (2011). Increasing oxygen radicals and water temperature select for toxic *Microcystis* sp. *PLoS One, 6*(9): e25569.

Gao, L., Pan, X., Zhang, D., Mu, S., Lee, D.-J., & Halik, U. (2015). Extracellular polymeric substances buffer against the biocidal effect of H2O2 on the bloom-forming cyanobacterium *Microcystis aeruginosa*. *Water Res, 69*: 51-58.

Hackenberg, C., Kern, R., Hüge, J., Stal, L. J., Tsuji, Y., Kopka, J. *et al.* (2011). Cyanobacterial lactate oxidases serve as essential partners in N2 fixation and evolved into photorespiratory glycolate oxidases in plants. *Plant Cell, 23*(8): 2978-2990.

Han, T.-W., & Eley, J. (1973). Glycolate excretion by Anacystis nidulans: effect of HCO3− concentration, oxygen concentration and light intensity. *Plant Cell Physiol, 14*(2): 285-291.

Hellebust, J. A. (1965). Excretion Of Some Organic Compounds By Marine Phytoplankton. *Limnol Oceanogr, 10*(2): 192-206.

Hosoya-Matsuda, N., Motohashi, K., Yoshimura, H., Nozaki, A., Inoue, K., Ohmori, M., & Hisabori, T. (2005). Anti-oxidative Stress System in Cyanobacteria: Significance Of Type II Peroxiredoxin and the Role of 1-Cys Peroxiredoxin in *Synechocystis* sp. strain PCC 6803. *J Biol Chem, 280*(1): 840-846.

Jackrel, S. L., White, J. D., Evans, J. T., Buffin, K., Hayden, K., Sarnelle, O., & Denef, V. J. (2019). Genome Evolution and Host Microbiome Shifts Correspond with Intraspecific Niche Divergence within Harmful Algal Bloom-Forming *Microcystis aeruginosa*. *Mol Ecol, 28*(17): 3994-4011.

Jackrel, S. L., Yang, J. W., Schmidt, K. C., & Denef, V. J. (2020). Host specificity of microbiome assembly and its fitness effects in phytoplankton. *ISME J*: 1-15.

Kawasaki, K., & Kamagata, Y. (2017). Phosphate-catalyzed hydrogen peroxide formation from agar, gellan, and κ-carrageenan and recovery of microbial cultivability via catalase and pyruvate. *Appl Environ Microbiol, 83*(21): e01366-01317.

Kharbush, J. J., Smith, D. J., Powers, M., Vanderploeg, H. A., Fanslow, D., Robinson, R. S. *et al.* (2019). Chlorophyll nitrogen isotope values track shifts between cyanobacteria and eukaryotic algae in a natural phytoplankton community in Lake Erie. *Org Geochem, 128*: 71-77.

Kim, J.-G., Park, S.-J., Damsté, J. S. S., Schouten, S., Rijpstra, W. I. C., Jung, M.-Y. *et al.* (2016). Hydrogen peroxide detoxification is a key mechanism for growth of ammonia-oxidizing archaea. *Proc Natl Acad Sci, 113*(28): 7888-7893.

Kim, M., Shin, B., Lee, J., Park, H. Y., & Park, W. (2019a). Culture-independent and culture-dependent analyses of the bacterial community in the phycosphere of cyanobloom-forming *Microcystis aeruginosa*. *Sci Rep, 9*(1): 1-13.

Kim, S., Kang, I., Seo, J.-H., & Cho, J.-C. (2019b). Culturing the ubiquitous freshwater actinobacterial acI lineage by supplying a biochemical 'helper' catalase. *ISME J, 13*: 2252-2263.

Kumar, J. K., Tabor, S., & Richardson, C. C. (2004). Proteomic analysis of thioredoxin-targeted proteins in Escherichia coli. *Proc Natl Acad Sci, 101*(11): 3759-3764.

Lusty, M. W., & Gobler, C. J. (2020). The Efficacy of Hydrogen Peroxide in Mitigating Cyanobacterial Blooms and Altering Microbial Communities across Four Lakes in NY, USA. *Toxins, 12*(7): 428.

Ma, L., Calfee, B. C., Morris, J. J., Johnson, Z. I., & Zinser, E. R. (2018). Degradation of hydrogen peroxide at the ocean's surface: the influence of the microbial community on the realized thermal niche of *Prochlorococcus*. *ISME J, 12*(2): 473-484.

Marsico, R. M., Schneider, R. J., Voelker, B. M., Zhang, T., Diaz, J. M., Hansel, C. M., & Ushijima, S. (2015). Spatial and temporal variability of widespread dark production and decay of hydrogen peroxide in freshwater. *Aquat Sci, 77*(4): 523-533.

Matthijs, H. C., Visser, P. M., Reeze, B., Meeuse, J., Slot, P. C., Wijn, G. *et al.* (2012). Selective suppression of harmful cyanobacteria in an entire lake with hydrogen peroxide. *Water Res, 46*(5): 1460-1472.

Morris, J. J., Kirkegaard, R., Szul, M. J., Johnson, Z. I., & Zinser, E. R. (2008). Facilitation of robust growth of *Prochlorococcus* colonies and dilute liquid cultures by "helper" heterotrophic bacteria. *Appl Environ Microbiol, 74*(14): 4530-4534.

Morris, J. J., Johnson, Z. I., Szul, M. J., Keller, M., & Zinser, E. R. (2011). Dependence of the cyanobacterium *Prochlorococcus* on hydrogen peroxide scavenging microbes for growth at the ocean's surface. *PloS one, 6*(2): e16805.

Morris, J. J., Lenski, R. E., & Zinser, E. R. (2012). The Black Queen Hypothesis: evolution of dependencies through adaptive gene loss. *MBio, 3*(2): e00036-00012.

Paerl, H. W., Xu, H., McCarthy, M. J., Zhu, G., Qin, B., Li, Y., & Gardner, W. S. (2011). Controlling harmful cyanobacterial blooms in a hyper-eutrophic lake (Lake Taihu, China): the need for a dual nutrient (N & P) management strategy. *Water Res, 45*(5): 1973-1983.

Paerl, H. W., & Otten, T. G. (2013). Blooms bite the hand that feeds them. *Science, 342*(6157): 433-434.

Parveen, B., Ravet, V., Djediat, C., Mary, I., Quiblier, C., Debroas, D., & Humbert, J. F. (2013). Bacterial communities associated with *Microcystis* colonies differ from free-living communities living in the same ecosystem. *Environ Microbiol Rep, 5*(5): 716-724.

Perelman, A., Uzan, A., Hacohen, D., & Schwarz, R. (2003). Oxidative stress in *Synechococcus* sp. strain PCC 7942: various mechanisms for H_2O_2 detoxification with different physiological roles. *J Bacteriol, 185*(12): 3654-3660.

Pérez-Pérez, M. E., Mata-Cabana, A., Sánchez-Riego, A. M., Lindahl, M., & Florencio, F. J. (2009). A comprehensive analysis of the peroxiredoxin reduction system in the cyanobacterium *Synechocystis* sp. strain PCC 6803 reveals that all five peroxiredoxins are thioredoxin dependent. *J Bacteriol, 191*(24): 7477-7489.

Piel, T., Sandrini, G., White, E., Xu, T., Schuurmans, J. M., Huisman, J., & Visser, P. M. (2020). Suppressing Cyanobacteria with Hydrogen Peroxide Is More Effective at High Light Intensities. *Toxins, 12*(18): 2-20. doi:10.3390/toxins12010018

Powers, L. C., & Miller, W. L. (2014). Blending remote sensing data products to estimate photochemical production of hydrogen peroxide and superoxide in the surface ocean. *Environ Sci Process Impact, 16*(4): 792-806.

Renström, E., & Bergman, B. (1989). Glycolate metabolism in cyanobacteria: I. Glycolate excretion and phosphoglycolate phosphatase activity. *Physiol Plant, 75*(2): 137-143.

Sandrini, G., Piel, T., Xu, T., White, E., Qin, H., Slot, P. C. *et al.* (2020). Sensitivity to hydrogen peroxide of the bloom-forming cyanobacterium *Microcystis* PCC 7806 depends on nutrient availability. *Harmful Algae, 99*: 101916.

Schmidt, K. C., Jackrel, S. L., Smith, D. J., Dick, G. J., & Denef, V. J. (2020). Genotype and host microbiome alter competitive interactions between *Microcystis aeruginosa* and *Chlorella sorokiniana*. *Harmful Algae, 99*(101939).

Schneider, R. J., Roe, K. L., Hansel, C. M., & Voelker, B. M. (2016). Species-level variability in extracellular production rates of reactive oxygen species by diatoms. *Front Chem, 4*: 5.

Schürmann, P., & Jacquot, J.-P. (2000). Plant thioredoxin systems revisited. *Annu Rev Plant Biol, 51*(1): 371-400.

Schuurmans, J. M., Brinkmann, B. W., Makower, A. K., Dittmann, E., Huisman, J., & Matthijs, H. C. (2018). Microcystin interferes with defense against high oxidative stress in harmful cyanobacteria. *Harmful Algae, 78*: 47-55.

Seaver, L. C., & Imlay, J. A. (2001a). Alkyl hydroperoxide reductase is the primary scavenger of endogenous hydrogen peroxide in *Escherichia coli*. *J Bacteriol, 183*(24): 7173-7181.

Seaver, L. C., & Imlay, J. A. (2001b). Hydrogen peroxide fluxes and compartmentalization inside growing *Escherichia coli*. *J Bacteriol, 183*(24): 7182-7189.

Sison-Mangus, M. P., Jiang, S., Tran, K. N., & Kudela, R. M. (2014). Host-specific adaptation governs the interaction of the marine diatom, *Pseudo-nitzschia* and their microbiota. *ISME J, 8*(1): 63-76.

Steffen, M. M., Dearth, S. P., Dill, B. D., Li, Z., Larsen, K. M., Campagna, S. R., & Wilhelm, S. W. (2014). Nutrients drive transcriptional changes that maintain metabolic homeostasis but alter genome architecture in *Microcystis*. *ISME J, 8*(10): 2080-2092.

Sutherland, K. M., Wankel, S. D., & Hansel, C. M. (2020). Dark biological superoxide production as a significant flux and sink of marine dissolved oxygen. *Proc Natl Acad Sci, 201912313*. doi:10.1073/pnas.1912313117

Tanaka, T., Kawasaki, K., Daimon, S., Kitagawa, W., Yamamoto, K., Tamaki, H. *et al.* (2014). A hidden pitfall in the preparation of agar media undermines microorganism cultivability. *Appl Environ Microbiol, 80*(24): 7659-7666.

Tichy, M., & Vermaas, W. (1999). In Vivo Role of Catalase-Peroxidase in *Synechocystis* sp. Strain PCC 6803. *J Bacteriol, 181*(6): 1875-1882.

Tolar, B. B., Powers, L. C., Miller, W. L., Wallsgrove, N. J., Popp, B. N., & Hollibaugh, J. T. (2016). Ammonia oxidation in the ocean can be inhibited by nanomolar concentrations of hydrogen peroxide. *Front Mar Sci, 3*: 237.

Tong, H., Chen, W., Shi, W., Qi, F., & Dong, X. (2008). SO-LAAO, a novel L-amino acid oxidase that enables *Streptococcus oligofermentans* to outcompete *Streptococcus mutans* by generating H2O2 from peptone. *J Bacteriol, 190*(13): 4716-4721.

Vermilyea, A. W., Dixon, T. C., & Voelker, B. M. (2010). Use of H218O2 to measure absolute rates of dark H2O2 production in freshwater systems. *Environ Sci Technol, 44*(8): 3066-3072.

Wolosiuk, R. A., & Buchanan, B. B. (1978). Activation of chloroplast NADP-linked glyceraldehyde-3-phosphate dehydrogenase by the ferredoxin/thioredoxin system. *Plant Physiol, 61*(4): 669-671.

Wood, Z. A., Poole, L. B., & Karplus, P. A. (2003). Peroxiredoxin evolution and the regulation of hydrogen peroxide signaling. *Science, 300*(5619): 650-653.

Xu, P., Yano, T., Yamamoto, K., Suzuki, H., & Kumagai, H. (1996). Characterization of a lactate oxidase from a strain of gram negative bacterium from soil. *Appl Biochem Biotechnol, 56*(3): 277-288.

Zilliges, Y., Kehr, J.-C., Meissner, S., Ishida, K., Mikkat, S., Hagemann, M. *et al.* (2011). The cyanobacterial hepatotoxin microcystin binds to proteins and increases the fitness of *Microcystis* under oxidative stress conditions. *PloS one, 6*(3): e17615.

Zinser, E. R. (2018). Cross-protection from hydrogen peroxide by helper microbes: the impacts on the cyanobacterium *Prochlorococcus* and other beneficiaries in marine communities. *Environ Microbiol Rep, 10*(4): 399-411.

Appendices

Appendix 1

Appendix Table 1: Blastn Results of Acidobacteria Hypothetical Protein Sequences Against NCBI nr Database

Query	Database Subject	Shared ANI (%)	Alignment Length (bp)	E-value	Bit Score
2807003360_Acidobacteria_CoA2_BinC42	CP063849.1	71.91	267	4.83E-27	136
2807003360_Acidobacteria_CoA2_BinC42	CP063849.1	76.423	123	1.80E-13	92.4
2807003360_Acidobacteria_CoA2_BinC42	CP020715.1	83.673	49	0.045	53.6
2807006060_Bryobacter	CP039252.1	91.724	145	7.22E-50	208
2807006060_Bryobacter	CP059256.1	91.034	145	3.07E-48	204
2807006060_Bryobacter	CP059256.1	91.034	145	3.07E-48	204
2807006060_Bryobacter	CP039252.1	90.345	145	3.74E-47	199
2807006060_Bryobacter	CP059256.1	90.345	145	3.74E-47	199
2807006060_Bryobacter	CP059256.1	90.345	145	3.74E-47	199
2807006060_Bryobacter	CP059256.1	90.345	145	3.74E-47	199
2807006060_Bryobacter	LR134356.1	89.041	146	5.55E-45	192
2807006060_Bryobacter	CP039252.1	90.58	138	1.94E-44	191
2807006060_Bryobacter	CP020046.1	88.966	145	1.94E-44	190
2807000547_Acidobacteria_CoA2_BinC42	No Hits	NA	NA	NA	NA
2807000092_Acidobacteria_CoA2_BinC42	No Hits	NA	NA	NA	NA
2807002401_Acidobacteria_CoA2_BinC42	No Hits	NA	NA	NA	NA
2807005264_Bryobacter	No Hits	NA	NA	NA	NA
2807006953_Bryobacter	No Hits	NA	NA	NA	NA

Appendix 2

Appendix Table 2: Total Gross H_2O_2 Production, Absolute Decay Constants, Maximum H_2O_2 Concentrations, and Model Fit in H_2O_2 Production and Decay Experiments

Experiment Date	Rep	Site	Condition	Model Fit	Sum Error Squares	PH_2O_2 (nM/hr)	K_{loss} (hr^{-1})	Max H_2O_2 (nM)	0.22 µm filt. Max H_2O_2 (nM)
31-May-17	1	WE2	Whole water light	Yes	299193.59	314	0.31	940	1330
31-May-17	2	WE2	Whole water light	Yes	97350.8	113	0.08	890	1040
13-Jun-17	1	WE2	Whole water light	Yes	360172.55	428	0.34	1550	2600
13-Jun-17	2	WE2	Whole water light	Yes	156842.25	436	0.34	1340	2730
27-Jun-17	1	WE2	Whole water light	Yes	1774.58	20	0.08	186	250
27-Jun-17	2	WE2	Whole water light	Yes	2524.2	29	0.10	240	250
6-Jul-17	1	WE2	Whole water light	Yes	75294.79	111	0.18	610	1010
6-Jul-17	2	WE2	Whole water light	Yes	17354.75	212	0.38	600	1000
12-Jul-17	1	WE2	Whole water light	Yes	78393.5	88	0.20	500	530
12-Jul-17	2	WE2	Whole water light	Yes	79862.86	34	0.12	650	560
18-Jul-17	1	WE2	Whole water light	Yes	53309.84	372	0.40	1060	1270
18-Jul-17	2	WE2	Whole water light	Yes	20617.85	314	0.34	910	1340
25-Jul-17	1	WE2	Whole water light	Yes	18032.86	259	0.41	600	1600
25-Jul-17	2	WE2	Whole water light	Yes	53819.79	258	0.40	730	980
1-Aug-17	1	WE2	Whole water light	Yes	14912.53	143	0.28	540	NA
1-Aug-17	2	WE2	Whole water light	Yes	6183.06	125	0.25	430	940
15-Aug-17	1	WE2	Whole water light	Yes	42008.79	30	0.14	470	940
15-Aug-17	2	WE2	Whole water light	Yes	10478.11	74	0.17	421	590
22-Aug-17	1	WE2	Whole water light	No	829377.27	NA	NA	1660	610
22-Aug-17	2	WE2	Whole water light	No	997084.69	NA	NA	1420	530
30-Aug-17	1	EC 973	Whole water light	No	177080.68	NA	NA	780	520

30-Aug-17	2	EC 973	Whole water light	Yes	2340.81	142	0.25	543	400
31-Aug-17	1	EC 885	Whole water light	Yes	5885.21	56	0.32	200	240
31-Aug-17	2	EC 885	Whole water light	Yes	2415.38	60	0.28	220	220
6-Sep-17	1	WE2	Whole water light	Yes	8932.13	168	0.49	383	600
6-Sep-17	2	WE2	Whole water light	Yes	43336.22	88	0.28	680	300
12-Sep-17	1	WE2	Whole water light	Yes	27637.99	71	0.27	300	270
12-Sep-17	2	WE2	Whole water light	Yes	27213.12	70	0.27	320	180
19-Sep-17	1	WE2	Whole water light	Yes	20372.59	159	0.51	550	380
19-Sep-17	2	WE2	Whole water light	Yes	3755.82	188	0.53	360	280
26-Sep-17	1	WE2	Whole water light	Yes	21266.02	146	0.49	440	1000
26-Sep-17	2	WE2	Whole water light	Yes	12921.99	196	0.58	400	540
4-Oct-17	1	EC 973	Whole water light	Yes	21839.35	258	0.60	460	310
4-Oct-17	2	EC 973	Whole water light	Yes	4610.08	133	0.30	420	280
5-Oct-17	1	EC 1461	Whole water light	Yes	16832.28	115	0.21	610	360
5-Oct-17	2	EC 1461	Whole water light	Yes	11462.6	120	0.22	540	290
10-Jul-18	1	WE2	Whole water dark	Yes	1640.9	13	0.38	50	410
10-Jul-18	2	WE2	Whole water dark	Yes	408.28	11	0.34	60	244
10-Jul-18	1	WE2	Whole water light	Yes	1705.84	70	0.35	210	380
10-Jul-18	2	WE2	Whole water light	Yes	7312.16	66	0.35	220	480
24-Jul-18	1	WE2	Whole water dark	Yes	2915	2	0.18	30	51
24-Jul-18	2	WE2	Whole water dark	Yes	1083.5	6	0.21	40	40
24-Jul-18	1	WE2	Whole water light	Yes	26.36	20	0.24	80	95
24-Jul-18	2	WE2	Whole water light	Yes	2321.25	15	0.19	80	100
31-Jul-18	1	WE2	Whole water dark	Yes	1056.7	3	0.24	24	27
31-Jul-18	2	WE2	Whole water dark	Yes	299.93	4	0.26	30	25
31-Jul-18	1	WE2	Whole water light	Yes	681.02	15	0.29	60	60
31-Jul-18	2	WE2	Whole water light	Yes	196.83	14	0.28	50	80
3-Aug-18	1	TWI	105 µm filtered light	Yes	1931.28	25	0.31	97	178
3-Aug-18	2	TWI	105 µm filtered light	Yes	2632.73	23	0.32	91	170
3-Aug-18	1	TWI	Whole water light	Yes	1465.27	36	0.39	102	178
3-Aug-18	2	TWI	Whole water light	Yes	2266.79	27	0.32	105	170

7-Aug-18	1	WE2	Whole water dark	Yes	165.23	15	0.37	36	58
7-Aug-18	2	WE2	Whole water dark	Yes	1398.76	9	0.31	40	74
7-Aug-18	1	WE2	Whole water light	Yes	1278.16	39	0.43	104	131
7-Aug-18	2	WE2	Whole water light	Yes	2680.03	39	0.43	90	140
10-Aug-18	1	TWI	105 µm filtered light	Yes	1907.42	14	0.22	72	79
10-Aug-18	2	TWI	105 µm filtered light	Yes	431.6	15	0.26	50	99
10-Aug-18	1	TWI	Whole water light	Yes	234.78	21	0.28	76	79
10-Aug-18	2	TWI	Whole water light	Yes	758.96	16	0.25	70	99
14-Aug-18	1	WE2	Whole water dark	Yes	1689.98	14	0.32	61	62
14-Aug-18	2	WE2	Whole water dark	Yes	2123.16	13	0.30	60	63
14-Aug-18	1	WE2	Whole water light	Yes	1004.6	44	0.36	133	150
14-Aug-18	2	WE2	Whole water light	Yes	291.97	52	0.44	120	161
21-Aug-18	1	WE12	105 µm filtered light	Yes	262.3	17	0.29	69	31
21-Aug-18	2	WE12	105 µm filtered light	Yes	165	18	0.30	60	25
21-Aug-18	1	WE12	Whole water light	Yes	626.31	18	0.30	70	60
21-Aug-18	2	WE12	Whole water light	Yes	671.89	21	0.33	79	70
14-Sep-18	1	TWI	105 µm filtered light	Yes	7774.53	51	0.23	240	175
14-Sep-18	2	TWI	105 µm filtered light	Yes	30915.96	27	0.12	172	153
14-Sep-18	1	TWI	Whole water light	Yes	16656.98	46	0.20	233	175
14-Sep-18	2	TWI	Whole water light	Yes	NA	NA	NA	226	153
18-Sep-18	1	WE2	Whole water dark	Yes	887.7	8	0.25	60	54
18-Sep-18	2	WE2	Whole water dark	Yes	1315.41	6	0.22	60	49
18-Sep-18	1	WE2	Whole water light	Yes	2744.23	24	0.24	115	103
18-Sep-18	2	WE2	Whole water light	Yes	5568.06	33	0.24	139	160
23-Jul-19	1	Bloom Chase	Whole water dark	Yes	173.38	11	0.79	45	32
23-Jul-19	2	Bloom Chase	Whole water dark	Yes	206.23	8	0.64	40	37
23-Jul-19	1	Bloom Chase	Whole water light	No	779320.84	NA	NA	1260	350
23-Jul-19	2	Bloom	Whole water light	No	228365.33	NA	NA	840	337

		Chase							
2-Aug-19	1	Bloom Chase	Whole water dark	Yes	524.49	34	0.53	80	124
2-Aug-19	2	Bloom Chase	Whole water dark	Yes	91.71	28	0.45	76	120
2-Aug-19	1	Bloom Chase	Whole water light	Yes	13151.39	133	0.58	248	572
2-Aug-19	2	Bloom Chase	Whole water light	Yes	9656.31	171	0.80	220	620
6-Aug-19	1	Bloom Chase	105 µm filtered light	No	39762.17	NA	NA	369	2040
6-Aug-19	2	Bloom Chase	105 µm filtered light	No	24706.12	NA	NA	378	1490
6-Aug-19	1	Bloom Chase	Whole water light	No	22582.2	NA	NA	390	2040
6-Aug-19	2	Bloom Chase	Whole water light	No	46950.85	NA	NA	459	1490
24-Aug-19	1	Bloom Chase	105 µm filtered light	No	22745.38	NA	NA	318	770
24-Aug-19	2	Bloom Chase	105 µm filtered light	No	20302.03	NA	NA	350	770
24-Aug-19	1	Bloom Chase	Whole water light	No	11853.13	NA	NA	365	NA
24-Aug-19	2	Bloom Chase	Whole water light	No	20163.48	NA	NA	420	770
17-Sep-19	1	Bloom Chase	Whole water dark	Yes	4094.8	5	0.14	35	40
17-Sep-19	2	Bloom Chase	Whole water dark	Yes	2145.42	6	0.13	50	48
17-Sep-19	1	Bloom Chase	Whole water light	Yes	5604.18	34	0.18	179	160

17-Sep-19	2	Bloom Chase	Whole water light	Yes	8929.47	31	0.14	187	177
20-Sep-19	1	Bloom Chase	105 µm filtered light	Yes	14905.63	77	0.25	280	290
20-Sep-19	2	Bloom Chase	105 µm filtered light	Yes	7821.71	54	0.18	250	300
20-Sep-19	1	Bloom Chase	Whole water light	Yes	27564.68	58	0.20	260	290
20-Sep-19	2	Bloom Chase	Whole water light	Yes	3949.34	61	0.20	260	300

Appendix 3

Appendix Table 3: Time Point When $[H_2O_2]_{spike} \approx [H_2O_2]_{unamended}$ in Light-Exposed H_2O_2 Production and Decay Experiments

Experiment_Date	Rep	Site	Condition	Time after spike (hours)
31-May-17	1	WE2	Whole water light	9
31-May-17	2	WE2	Whole water light	NA
13-Jun-17	1	WE2	Whole water light	9
13-Jun-17	2	WE2	Whole water light	9
27-Jun-17	1	WE2	Whole water light	NA
27-Jun-17	2	WE2	Whole water light	NA
6-Jul-17	2	WE2	Whole water light	6
6-Jul-17	1	WE2	Whole water light	9
12-Jul-17	1	WE2	Whole water light	NA
12-Jul-17	2	WE2	Whole water light	NA
18-Jul-17	1	WE2	Whole water light	6
18-Jul-17	2	WE2	Whole water light	6
25-Jul-17	2	WE2	Whole water light	6
25-Jul-17	1	WE2	Whole water light	9
1-Aug-17	1	WE2	Whole water light	9
1-Aug-17	2	WE2	Whole water light	9
15-Aug-17	1	WE2	Whole water light	NA
15-Aug-17	2	WE2	Whole water light	NA
22-Aug-17	1	WE2	Whole water light	6
22-Aug-17	2	WE2	Whole water light	6
30-Aug-17	1	EC 973	Whole water light	6
30-Aug-17	2	EC 973	Whole water light	9
31-Aug-17	1	EC 885	Whole water light	9
31-Aug-17	2	EC 885	Whole water light	9
6-Sep-17	1	WE2	Whole water light	6
6-Sep-17	2	WE2	Whole water light	6
12-Sep-17	1	WE2	Whole water light	9
12-Sep-17	2	WE2	Whole water light	9
19-Sep-17	1	WE2	Whole water light	6
19-Sep-17	2	WE2	Whole water light	6
26-Sep-17	1	WE2	Whole water light	6
26-Sep-17	2	WE2	Whole water light	6
4-Oct-17	1	EC 973	Whole water light	6
4-Oct-17	2	EC 973	Whole water light	6
5-Oct-17	1	EC 1461	Whole water light	9
5-Oct-17	2	EC 1461	Whole water light	9
10-Jul-18	1	WE2	Whole water light	9
10-Jul-18	2	WE2	Whole water light	9
24-Jul-18	1	WE2	Whole water light	9
24-Jul-18	2	WE2	Whole water light	9

31-Jul-18	1	WE2	Whole water light	9
31-Jul-18	2	WE2	Whole water light	9
3-Aug-18	1	TWI	105 µm filtered light	6
3-Aug-18	2	TWI	105 µm filtered light	6
3-Aug-18	1	TWI	Whole water light	6
3-Aug-18	2	TWI	Whole water light	6
7-Aug-18	1	WE2	Whole water light	9
7-Aug-18	2	WE2	Whole water light	9
10-Aug-18	1	TWI	105 µm filtered light	9
10-Aug-18	2	TWI	105 µm filtered light	9
10-Aug-18	1	TWI	Whole water light	9
10-Aug-18	2	TWI	Whole water light	9
14-Aug-18	1	WE2	Whole water light	9
14-Aug-18	2	WE2	Whole water light	9
21-Aug-18	1	WE12	105 µm filtered light	9
21-Aug-18	2	WE12	105 µm filtered light	9
21-Aug-18	1	WE12	Whole water light	9
21-Aug-18	2	WE12	Whole water light	9
14-Sep-18	1	TWI	105 µm filtered light	9
14-Sep-18	2	TWI	105 µm filtered light	9
14-Sep-18	1	TWI	Whole water light	NA
18-Sep-18	1	WE2	Whole water light	9
18-Sep-18	2	WE2	Whole water light	9
23-Jul-19	1	Bloom Targeting	Whole water light	3
23-Jul-19	2	Bloom Targeting	Whole water light	3
2-Aug-19	1	Bloom Targeting	Whole water light	6
2-Aug-19	2	Bloom Targeting	Whole water light	6
6-Aug-19	1	Bloom Targeting	105 µm filtered light	3
6-Aug-19	2	Bloom Targeting	105 µm filtered light	3
6-Aug-19	1	Bloom Targeting	Whole water light	3
6-Aug-19	2	Bloom Targeting	Whole water light	3
24-Aug-19	1	Bloom Targeting	105 µm filtered light	3
24-Aug-19	2	Bloom Targeting	105 µm filtered light	6
24-Aug-19	1	Bloom Targeting	Whole water light	6
24-Aug-19	2	Bloom Targeting	Whole water light	6
17-Sep-19	1	Bloom Targeting	Whole water light	9
17-Sep-19	2	Bloom Targeting	Whole water light	9
20-Sep-19	1	Bloom Targeting	105 µm filtered light	9
20-Sep-19	2	Bloom Targeting	105 µm filtered light	9
20-Sep-19	1	Bloom Targeting	Whole water light	9
20-Sep-19	2	Bloom Targeting	Whole water light	9

Appendix 4

Appendix Table 4: Correlation and Regression Statistics Between Gross Biotic H_2O_2 Production in Dark Bottles and Measured Biological and Chemical Parameters.

Independent Variable	Pearson's R	F-test p-value	R^2
$k_{loss,H2O2}$	0.49	0.18	0.24
chlorophyll *a*	0.13	0.74	0.016
dissolved inorganic carbon	-0.31	0.42	0.096
carbonic acid	-0.52	0.15	0.27
bicarbonate	-0.36	0.34	0.13
carbonate	0.56	0.11	0.32
dissolved organic carbon	0.34	0.37	0.12
respiration rate	0.59	0.096	0.35
primary production rate	0.37	0.33	0.13
CDOM	0.44	0.24	0.19
Day Integrated UVA	0.35	0.36	0.12
Day Integrated UVB	0.59	0.097	0.34
UVA + UVB	0.36	0.34	0.13
pH	0.58	0.11	0.33
total phosphorus	0.25	0.52	0.061
total dissolved phosphorus	-0.16	0.69	0.025
nitrate	0.042	0.91	0.002
ammonium	0.014	0.97	2.00E-04
soluble reactive phosphorus	-0.21	0.58	0.046
incubation temperature	0.41	0.27	0.17
incubation temperature standard deviation	0.041	0.92	0.0017

Appendix 5

Appendix Table 5: Welch's T-Test Results Testing the Hypothesis That the Mean Abundance of Important OTUs in Random Forest Models in Whole Water and 105 µm Filtered Water are Significantly Different.

Otu #	Experiment Date	T-stat	p-value
Otu00016	26-Jul-19	3.46094809	0.02639031
Otu00016	6-Aug-19	2.87452294	0.03433594
Otu00016	3-Aug-18	2.78633619	0.03690915
Otu00016	24-Aug-19	2.1738578	0.0921491
Otu00016	14-Sep-18	-0.9891138	0.38679893
Otu00016	10-Aug-18	0.13616709	0.89871516
Otu00016	21-Aug-18	-0.1321111	0.90061407
Otu00016	20-Sep-19	NaN	NaN
Otu00123	24-Aug-19	2.37320612	0.05686578
Otu00123	24-Aug-19	2.37320612	0.05686578
Otu00123	14-Sep-18	-2.7531918	0.05820877
Otu00123	14-Sep-18	-2.7531918	0.05820877
Otu00123	3-Aug-18	1.08790057	0.34755301
Otu00123	3-Aug-18	1.08790057	0.34755301
Otu00123	6-Aug-19	0.81860297	0.44908353
Otu00123	6-Aug-19	0.81860297	0.44908353
Otu00123	21-Aug-18	0.74431534	0.50335837
Otu00123	21-Aug-18	0.74431534	0.50335837
Otu00123	26-Jul-19	0.53673679	0.61208646
Otu00123	26-Jul-19	0.53673679	0.61208646
Otu00123	10-Aug-18	-0.3660297	0.72984789
Otu00123	10-Aug-18	-0.3660297	0.72984789
Otu00123	20-Sep-19	0.05272989	0.95989179
Otu00123	20-Sep-19	0.05272989	0.95989179
Otu00167	6-Aug-19	3.73895163	0.02205341
Otu00167	20-Sep-19	2.51302239	0.08578314
Otu00167	26-Jul-19	2.02668144	0.11940833
Otu00167	24-Aug-19	1.79783098	0.15056155
Otu00167	10-Aug-18	1.76179202	0.15566474
Otu00167	3-Aug-18	1.49165818	0.20930052
Otu00167	14-Sep-18	0.43878546	0.68445464
Otu00167	21-Aug-18	-0.1382628	0.89458756
Otu00240	24-Aug-19	2.9339608	0.03652298
Otu00240	6-Aug-19	-1.9183395	0.12252249
Otu00240	14-Sep-18	1.20996629	0.31293537
Otu00240	20-Sep-19	-1	0.39100222
Otu00240	3-Aug-18	-0.8096838	0.4490413
Otu00240	21-Aug-18	0.81772648	0.45008538
Otu00240	26-Jul-19	-0.7408805	0.49850033
Otu00240	10-Aug-18	0.44237415	0.68294873

Otu00257	24-Aug-19	3.71041006	0.02788177
Otu00257	3-Aug-18	2.28170853	0.07051078
Otu00257	10-Aug-18	-2.5850203	0.08058608
Otu00257	6-Aug-19	2.10499405	0.10546948
Otu00257	20-Sep-19	1.64979287	0.15125812
Otu00257	21-Aug-18	1.47631677	0.23365846
Otu00257	26-Jul-19	0.63188045	0.5607405
Otu00257	14-Sep-18	-0.2241863	0.83162395
Otu00258	10-Aug-18	-1.1982585	0.27827775
Otu00258	6-Aug-19	1.22527833	0.28092214
Otu00258	24-Aug-19	0.85265878	0.43119169
Otu00258	14-Sep-18	0.65549893	0.54719557
Otu00258	21-Aug-18	0.60445274	0.57806073
Otu00258	26-Jul-19	0.26217381	0.80227616
Otu00258	20-Sep-19	0.25306519	0.8086801
Otu00258	3-Aug-18	-0.0327012	0.97544367
Otu00264	10-Aug-18	-2.3337871	0.07806454
Otu00264	6-Aug-19	-1	0.39100222
Otu00264	14-Sep-18	-0.8197738	0.44395055
Otu00264	26-Jul-19	0.32619934	0.76339169
Otu00264	3-Aug-18	0.19121289	0.85636096
Otu00264	20-Sep-19	0.16527507	0.8783814
Otu00264	21-Aug-18	-0.034552	0.97357909
Otu00264	24-Aug-19	NaN	NaN
Otu00276	24-Aug-19	6.44523413	0.00449844
Otu00276	21-Aug-18	3.09717568	0.0215151
Otu00276	20-Sep-19	0.99671527	0.38910406
Otu00276	10-Aug-18	1	0.39100222
Otu00276	14-Sep-18	-1	0.39100222
Otu00276	3-Aug-18	0.74773221	0.50280115
Otu00276	6-Aug-19	0.66524157	0.54024662
Otu00276	26-Jul-19	-0.0978861	0.92522343
Otu00311	24-Aug-19	2.11111111	0.09631356
Otu00311	21-Aug-18	-2.3176518	0.10330558
Otu00311	14-Sep-18	-1.6220396	0.17317494
Otu00311	20-Sep-19	1.09913864	0.32681592
Otu00311	26-Jul-19	0.95674849	0.37703318
Otu00311	6-Aug-19	0.31658592	0.76844576
Otu00311	3-Aug-18	NaN	NaN
Otu00311	10-Aug-18	NaN	NaN
Otu00323	6-Aug-19	1.8565517	0.12665289
Otu00323	20-Sep-19	-1.7154308	0.18477397
Otu00323	26-Jul-19	1.11134806	0.34290819
Otu00323	10-Aug-18	-1	0.39100222
Otu00323	24-Aug-19	0.71556283	0.52022484
Otu00323	3-Aug-18	NaN	NaN
Otu00323	21-Aug-18	NaN	NaN
Otu00323	14-Sep-18	NaN	NaN
Otu00378	24-Aug-19	-1.7315076	0.18178997
Otu00378	26-Jul-19	1.32542122	0.26310421
Otu00378	21-Aug-18	1	0.39100222
Otu00378	6-Aug-19	-0.0500974	0.96288875
Otu00378	3-Aug-18	NaN	NaN
Otu00378	10-Aug-18	NaN	NaN
Otu00378	14-Sep-18	NaN	NaN
Otu00378	20-Sep-19	NaN	NaN

Otu00433	26-Jul-19	-1.5297883	0.17878761
Otu00433	20-Sep-19	1.07612413	0.34618148
Otu00433	3-Aug-18	1	0.39100222
Otu00433	10-Aug-18	1	0.39100222
Otu00433	21-Aug-18	-1	0.39100222
Otu00433	6-Aug-19	1	0.39100222
Otu00433	24-Aug-19	-1	0.39100222
Otu00433	14-Sep-18	NaN	NaN
Otu00579	20-Sep-19	-1.5571122	0.2173135
Otu00579	26-Jul-19	0.90832935	0.41277727
Otu00579	6-Aug-19	0.32686054	0.759251
Otu00579	3-Aug-18	0.00626362	0.995236
Otu00579	10-Aug-18	NaN	NaN
Otu00579	21-Aug-18	NaN	NaN
Otu00579	14-Sep-18	NaN	NaN
Otu00579	24-Aug-19	NaN	NaN
Otu00822	6-Aug-19	1.73173929	0.18174737
Otu00822	26-Jul-19	1.04018513	0.34933681
Otu00822	20-Sep-19	-0.5487788	0.61256392
Otu00822	14-Sep-18	0.05453215	0.95829184
Otu00822	3-Aug-18	NaN	NaN
Otu00822	10-Aug-18	NaN	NaN
Otu00822	21-Aug-18	NaN	NaN
Otu00822	24-Aug-19	NaN	NaN

Appendix 6

Appendix Table 6: Estimates of Biotic O_2^- Production in Western Lake Erie From Literature Values

Ref.	Lake Erie organisms and scenario considered	Date	*Trichodesmium*/*Microcystis* O_2^- Prod. (nM/cell)	*Synechococcus* O_2^- Prod. (nM/cell)	Diatom O_2^-Prod. (nM/cell)	*Cyanobium* abund (cells/L)	*Microcystis* abund. (cells/L)	Hypothetical Diatom abund. (cells/L)	Est. O_2^-Prod. rate (nM/hr)	Est. H_2O_2 from O_2^- (nM/hr)	Obs. biotic H_2O_2 prod. (nM/hr)
Sutherland et al. 2020	Microcystis and Cyanobium (approximately equal abundance)	1-Aug-17	1.5e-6	5.5e-7	-	9728000	8727000	-	18	9	87
Sutherland et al. 2020	Microcystis, Cyanobium, Diatoms (date of approximately equal fluoroprobe fluorescence)	19-Sep-17	1.5e-6	5.5e-7	1.3e-5	3339000	7525000	10864000	154	77	160
Sutherland et al. 2020; Schneider et al. 2016	Microcystis, Cyanobium, Diatoms (date of approximately equal fluoroprobe fluorescence)	19-Sep-17	1.5e-6	5.5e-7	1.3e-5	3339000	7525000	10864000	296	148	160
Sutherland et al. 2020; Schneider et al. 2016	Microcystis, Cyanobium, Diatoms (date of approximately equal fluoroprobe	19-Sep-17	1.5e-6	5.5e-7	1.3e-5	3339000	7525000	10864000	1143	571	160

	fluorescence)										
Fujii et al. 2011, Sutherland et al. 2020	Microcystis and Cyanobium (approximately equal abundance)	1-Aug-17	1.20E-09	5.5e-7	-	9728000	8727000	-	5	3	87
Fujii et al. 2011, Sutherland et al. 2020	Microcystis and Cyanobium (approximately equal abundance)	1-Aug-17	1.20E-09	5.5e-7	-	9728000	8727000	-	43	21	87
Fujii et al. 2011, Sutherland et al. 2020	Microcystis and Cyanobium (approximately equal abundance)	1-Aug-17	1.20E-09	5.5e-7	-	9728000	8727000	-	11	5	87
Sutherland et al. 2020; Schneider et al. 2016	Microcystis, Cyanobium, Diatoms (date of highest biotic H2O2 production)	13-Jun-17	1.5e-6	5.5e-7	-	25000	2000	-	0.0275048	0.0137524	290
Sutherland et al. 2020; Schneider et al. 2016	Microcystis, Cyanobium, Diatoms (date of highest biotic H2O2 production)	13-Jun-17	1.5e-6	5.5e-7	-	25000	2000	-	0.0275048	0.0137524	290